1994

Waves, currents and sand transport predictors on a macro-tidal beach

Foote, Yolanda Lucy Margaret

WAVES, CURRENTS AND SAND TRANSPORT PREDICTORS ON A MACRO-TIDAL BEACH

by

Yolanda Lucy Margaret Foote

A thesis submitted to the University of Plymouth
in partial fulfilment for the degree of
Doctor of Philosophy

Institute of Marine Studies
Faculty of Science
January 1994

DECLARATION

At no time during the registration for the degree of Doctor of Philosophy has the author been registered for any other University award.

This study was financed with the aid of a CASE Studentship from the Science and Engineering Research Council (SERC) in collaboration with British Maritime Technology Ltd. (Ceemaid Division), Southampton.

During the course of the present study the author attended lunch time research seminars for the Ocean and Fisheries Science Group and presented work on a number of occasions. A poster was presented at UK Oceanography '92 at Liverpool University and a paper was presented at the 23rd International Conference on Coastal Engineering (October 1992) in Venice. A further two papers based on this work were presented by Professor Huntley at Euromech (Le Havre) and Coastal Dynamics '94 (Barcelona).

Signed .....

Date 31.1.94

Aerial photograph of the tip of Spurn Head, Humberside
(Courtesy of Chris Gomersall, RSPB).

The people along the sand
All turn and look one way.
They turn their back on the land.
They look at the sea all day.

As long as it takes to pass
A ship keeps raising its hull;
The wetter ground like glass
Reflects a standing gull.

The land may vary more;
But wherever the truth may be —
The water comes ashore,
And the people look at the sea.

They cannot look out far.
They cannot look in deep.
But when was that ever a bar
To any watch they keep?

Robert Frost (1936)
'Neither Out Far Nor In Deep'.

WAVES, CURRENTS AND SAND TRANSPORT PREDICTORS ON A MACRO-TIDAL BEACH

by
YOLANDA LUCY MARGARET FOOTE

ABSTRACT

A field experiment was carried out at Spurn Head, Humberside as part of the British Beach And Nearshore Dynamics (B-BAND) project. The B-BAND measurements at Spurn Head were obtained over 10 tidal cycles during April 1991. Three tidal cycles are described in the present work which encompass a spectrum of conditions from storm to calm. The beach at the field site comprised a veneer of sand and shingle overlying a glacial till shore plug. The beach was characterised by a macro-tidal (3-7m tidal range) intermediate morphodynamic regime which fluctuated between dissipative at low water, and reflective at mid to high water.

A square array of four sensor stations was deployed extending to approximately 200 metres offshore of the high water level. The sensor rigs comprised on average, 3 electromagnetic current meters, 3 optical backscatter sensors at varying heights above the bed, plus 1 pressure sensor. Large-scale changes in beach profile were recorded by regular levelling surveys at each low tide. Measurements of sea surface elevation, current velocity and suspended sediment concentration were made in order to examine the relative importance of short wave, long wave and mean flow components of the local flow field to the nearshore hydrodynamic regime and sediment response.

Incident waves travelling towards the shoreline are known to have a groupy structure, with an alternating sequence of high waves and low waves. Associated with this incident wave 'groupiness' are gradients in the radiation stress generating a forced long wave, of long wave period, where a depression of mean sea level corresponds with groups of high waves and a rise in mean sea level corresponds with groups of low waves. Incident wave groupiness contributes significantly to the nearshore wave field and has been incorporated into models of long wave generation both in the offshore and nearshore zones and nearshore sediment transport, and through its effect on coastal and marine structures.

Energetics-based predictors of cross-shore suspended sand transport (*e.g.* Bailard, 1981; Guza and Thornton, 1985a) relate the behaviour of the nearshore velocity field to the movement of sand near the sea bed, whereby the energy needed to move the sediment is equated with a fixed proportion of the available energy supplied by the water movement. Such energetics models provide moments for the bedload and suspended load transports, which are related to moments of the local velocity field. Comparison between energetics-based predictions of suspended sand transport and observations of suspended sand fluxes allows some indication of the usefulness of such physically-based models.

The present work is based around the investigation of these two areas of interest. This research has shown that firstly, wave groupiness does not decay immediately at the breakpoint, instead there is a persistence of groupiness through the surf zone up to the shoreline. Cross-correlation between the incident wave envelope and long period wave motion is relatively insensitive to depth variations across the nearshore, at the breakpoint the correlation decreases towards zero, whilst in the inner surf zone a positive correlation occurs. Modelling the response of sediment in the nearshore should incorporate some groupiness factor.

Secondly, the examination of Guza and Thornton's (1985a) cross-shore transport equation reveals two dominant moments which describe suspended load and bedload transport. Accurate estimation of these transports requires a knowledge of the spatial distributions of the relative magnitudes of the relevant moments, which we call spatial 'shape functions'. Comparison between the velocity moment shape function predictors and observed sand fluxes indicates that these energetics-based models do not accurately predict the conditions which exist on this macro-tidal beach. A noticeable asymmetry exists between flood and ebb stages of the tidal cycle which may be a contributory factor to the differences seen between velocity moment predictions and sand flux observations. Physically-based models do not realistically represent the conditions which occur on macro-tidal intermediate beaches such as Spurn Head.

ACKNOWLEDGEMENTS

It is difficult to know where to begin thanking the people who have helped me during the last three years. Undoubtedly, it is the person who has persevered in helping me grasp a few of the concepts of beach processes, my supervisor, David Huntley, who deserves not only my gratitude, but also my admiration for his patience.

Peter Sims took on the role of second supervisor half way through this project and since that time, has helped and encouraged me constantly. Peter has always been enthusiastic, translating the more difficult ideas and problems into words that I can understand.

The B-BAND post-docs., Mark Davidson and Paul Russell, whom I have pestered throughout the last three years, have always given their support and scientific expertise when ever approached, they are also to be thanked for generating the vast quantity of data from the various B-BAND field experiments. Similarly, I should like to thank Tim O'Hare who taught me a thing or two about wave groups. I am also grateful to Jack Hardisty, my third supervisor, who has been involved with the collaborative B-BAND project since its start.

Of course, this work would not have passed as pleasurably without the presence of the infamous IMS Coffee Club who have provided me with copious volumes of coffee, a smattering of most excellent parties and their undying wit and tasteless sense of humour. Not forgetting the Civ. Eng. coastal chaps Phlax and Adam (for his northern charm).

My former Bangor associates should also be thanked for making me want to continue in research. Vikky, who I have known for six years, managed to share a flat with me, even whilst I was writing up. Willie ought also be mentioned for being a true Scot.

Last, but by no means least, there is my family who have supported me untiringly during the last three years. Thanks to my sister, Caroline, and Guy who provided me with a most brilliant niece, Lottie. Many thanks to my step-father, Roger, and his family who have shown me so much kindness. My most special thanks go to my mother, Jean, a remarkable person. I should like finally to mention Gordon, my father, who was an engineer in the Navy, and the inspiration for my interest in oceanography.

LIST OF CONTENTS

LIST OF ILLUSTRATIONS

LIST OF PLATES

LIST OF TABLES

LIST OF SYMBOL NOTATION

a	Wave amplitude (m)
a_b	Breaking wave amplitude (m)
c	Suspended sediment concentration (gl^{-1})
c_p	Phase velocity (ms^{-1})
c_g	Group velocity (ms^{-1})
$\overline{c' u'}$	Flux coupling ($gl^{-1}ms^{-1}$)
e	Exponential function
f_s	Shear of offshore face of longshore current (Hz)
f_w	Wave friction factor
g	Acceleration due to gravity (ms^{-2})
h	Water depth (m)
h_b	Breakpoint depth (m)
i	Total immersed weight sediment transport rate ($kgm^{-1}s^{-1}$)
$\hat{\imath}$	Unit vector in the x direction
i_B	Bedload immersed weight transport rate ($kgm^{-1}s^{-1}$)
i_S	Suspended load immersed weight transport rate ($kgm^{-1}s^{-1}$)
i_θ	Time-averaged immersed weight sediment transport rate per unit width in the θ direction ($kgm^{-1}s^{-1}$)
$\hat{\jmath}$	Unit vector in the y direction
k	Wavenumber (m^{-1})
k_o	Deep water wavenumber (m^{-1})
k_v	Wavenumber of free gravity waves (m^{-1})
n	Model number
p^{+max}	Excess pressure (Nm^{-2})
Δp	Amplitude of pressure oscillations (Nm^{-2})
t	Independent variable, usually time (s)
Δt	Sampling frequency (s)
u	Cross-shore flow component (ms^{-1})
$\bar{u}$	Mean cross-shore velocity (ms^{-1})
$\tilde{u}$	Cross-shore oscillatory velocity (ms^{-1})
u_m	Maximum near-bed orbital velocity (ms^{-1})
u_θ	Steady current in the θ direction (ms^{-1})
$\bar{u}_t$	Total instantaneous velocity vector (ms^{-1})
$(u3)^*$	Dimensionless third even moment of velocity
$(u5)^*$	Dimensionless fifth even moment of velocity
v	Longshore flow component (ms^{-1})
x	Cross-shore co-ordinate (m)
x_v	Numerical value(s) of a random variable for a particular number of degrees of freedom
y	Longshore co-ordinate (m)
z	Vertical axis with origin at the sea surface (m)
A	Asymmetry
B_o	Breaker coefficient
C	Energy dissipated during offshore phase of sediment flow/energy dissipated during onshore phase of sediment flow (J/m^2s)
C_f	Drag coefficient
D_{50}	Median grain size of a sediment distribution (mm)
H	Wave height (m)
H_b	Breaking wave height (m)
H_s	Significant wave height (m)
K'	Dimensionless constant
L	Wavelength (m)
L_n	Laguerre polynomials of order n
L_o	Deep water wavelength (m)
N	Number of segments

Nd	Number of disjoint segments
P	Number of data points in each segment
S	Skewness
S_{xx}	Onshore component of radiation stress (J/m^2)
T	Wave period (s)
U_r	Ursell number (dimensionless)
W	Fall velocity (ms^{-1})
α	Probability associated with a critical region
α_n	Angle between wave orthogonal and onshore direction (rad)
β	Angle of bed (deg)
β_e	Relative location of ideal edge of passband (Hz)
χ	Offshore distance (m)
δ	Dimensionless steady flow ($= \bar{u}_T/u_m$)
δ_w	Relative width of filter transition band (Hz)
ε	Surf scaling parameter
ε_B	Bedload efficiency factor
ε_S	Suspended load efficiency factor
ϕ	Angle of internal friction (rad)
γ	Auto-suspension factor
η	Sea surface elevation (m)
λ	Stopband loss (dB)
ν	Number of degrees of freedom
π	Pi
θ	Mean current angle (deg)
θ_∞	Deep water wave direction (deg)
ρ	Water density (kgm^{-2})
σ	Radian frequency ($\approx 2\pi/T$)
σ^2	Total variance of the oscillatory velocity (m^2s^{-2})
τ	Shear stress (Nm^{-2})
ω	Rate of energy production of stream (Js^{-1})
ζ	Mean water level under wave groups (m)
$\phi(x)$	Dimensionless offshore structure of waveform
Θ	Represents x or y for cross-correlation coefficient
Ω	Dimensionless sediment fall velocity
Ω_f	Incident wave radian frequency ($\approx 2\pi/T$)
ψ_1	Dimensionless first odd moment of velocity
ψ_2	Dimensionless second odd moment of velocity
$tan\beta$	Beach slope (m/m)
~	Fluctuating component
-	Mean component
< >	Time-averaging

CHAPTER 1
MACRO-TIDAL BEACH PROCESSES - AN INTRODUCTION

Classification of beach environments is often achieved through examination of the tidal range; micro-tidal (< 2m tidal range); meso-tidal (2-4m) and macro-tidal (> 4m). These three beach types are produced by the same combination of wave and sediment interactions, but the difference is the impact of increasing tidal range and tide-induced shoreline mobility on morphodynamics. To-date, macro-tidal beach studies (*e.g.* Short, 1991) have tended to lag those concerning micro-tidal regimes (*e.g.* Wright and Short, 1984), although macro-tidal beach environments are characteristic of the shorelines which frame the British Isles and constitute a significant proportion of the world's beaches. Although features of the macro-tidal beach profile differ considerably from those of micro-tidal systems (*e.g.* the formation of an intertidal terrace between the high- and low-tide beach faces), comparatively little research has been concerned with the understanding of the hydrodynamic processes which drive sediment transport and beach profile change.

A number of predictors have been developed for sand transport on beaches (*e.g.* Inman and Bagnold, 1963; Bowen, 1980a; Bailard, 1981; Bailard and Inman, 1981; Guza and Thornton, 1985a; Roelvink and Stive, 1989). These energetics-based models, which follow on from earlier stream flow sediment transport theories (*e.g.* Bagnold, 1963, 1966), lead to reasonable estimates of the local longshore and cross-shore sediment transport rates as well as the equilibrium beach slope, for micro-tidal

environments (*e.g.* Doering and Bowen, 1985, 1988; Russell, 1990). Energetics modelling describes sediment transport through the behaviour of the nearshore velocity field. The energy needed to move the sediment is equated with a fixed proportion of the available energy supplied by the water movement (Foote *et al.*, 1993). Such energetics-based sediment transport models can yield both bedload and suspended load components, which are related to moments of the local velocity field. The application of energetics-based sand transport models to the macro-tidal beach system is not well documented.

Development of fast-response bi-axial electromagnetic current meters for deployment on natural beach environments has enabled the reliable monitoring of the local velocity field and, therefore, the estimation of the moment terms which describe the cross-shore transport rates of sand on beaches. Examination of these velocity moments is a useful approach towards quantifying the magnitude of the various nearshore hydrodynamic forces (*e.g.* stirring and transporting agents). A knowledge of the relative importance of these processes could enable the development of more realistic parameterisations and predictors of the processes which drive cross-shore sand transport on beaches. A means of verifying such moment-derived predictors of cross-shore sand transport is equally important if the relative flow contributions are to be taken as pointers of the dominant transport mechanisms.

Instrument development has proved more fruitful for recording suspended load movement of sediment, rather than that of bedload, owing to the complexity and difficulty of collecting measurements at the bed. Acoustic (*e.g.* Vincent *et al.*, 1991; Thorne *et al.*, 1993) and optical (Jaffe *et al.*, 1984; Hanes and Huntley, 1986) sampling techniques have proved the most successful methods for monitoring sediment fluxes in the nearshore region, so far. Optical backscatter sensors, developed by Downing *et al* (1981), allow the continuous measurement of suspended sediment concentration profiles in the nearshore zone, providing the opportunity to examine the response of the near-bed suspended sediment concentrations to the local velocity fields and rough bottom boundaries, as well as the ability to estimate local sediment fluxes (Osborne, 1990). Sampling suspended sand concentrations, under a variety of wave and bottom-

current conditions, in conjunction with simultaneous current velocity measurements allows analysis of the cross-shore fluxes of sand which arise: in other words, it is possible to attribute the sediment response to the mechanisms responsible for stirring and transporting the sand. The relative contributions of the low and high frequency motions and mean flows to sand transport can be estimated through use of co-spectra (Hanes and Huntley, 1986; Huntley and Hanes, 1987) or through the adaptation of cross-shore sediment flux analyses (*e.g.* Jaffe *et al.*, 1984). For example, some studies have revealed the dominance of infragravity oscillations (Russell *et al.* (1991) found suspended sediment events to be well correlated with infragravity frequency flows), whilst other investigations have indicated the dominance of gravity wave energy over the long period wave contributions (*e.g.* Davidson *et al.*, 1993). Similarly, Hanes and Huntley (1986) observed the occurrence of wave groups in the nearshore and found the passage of a group of high waves to coincide with the suspension event high in the water column. Hanes (1990) later observed the intermittence of these near-bed suspension events within and beyond the surf zone, and the occurrence of events was again correlated with periods of higher velocity associated with groups of larger waves. Coupling between the incoming wave groups and bound long wave motions over an erodible bed is known to cause suspension of sediments under high waves (*e.g.* Shi and Larsen, 1984). However, the important implications of wave groupiness for modelling sediment response have not yet been fully considered.

Despite these advances in both theories of beach sediment transport and field measurements, direct attempts to link theory and field measurements are very limited, especially on macro-tidal beaches. This research will incorporate field measurements of cross-shore current velocity, suspended sediment concentration and sea surface elevation data in order to examine firstly, the nature of wave groupiness variations across the nearshore zone; secondly, the relative importance of the various hydrodynamic processes which drive cross-shore sediment transport; and thirdly, the usefulness of certain sand transport predictors on a macro-tidal beach.

CHAPTER 2
MACRO-TIDAL BEACH PROCESSES - A REVIEW OF EXISTING KNOWLEDGE

2.1 INTRODUCTION

Cornaglia (1889), over a century ago, discussed the movement of beach sediments, observing that the sea accumulates and distributes material through the action of waves and the impulse of the moving fluid touching the bottom, ultimately generating sediment transport. Bascom (1964) wrote about beaches,

> "The surf changes from moment to moment, day to day, and beach to beach. The waves are influenced by the bottom and the bottom is changed by the waves. And since the waves arriving at a beach are highly variable in height, period, and direction, each wave creates a slightly different bottom configuration for the ones that come after it. The water level changes with the tide and the waves change as the storms at sea develop, shift position, and die out again. The result is that the sand bottom is forever being rearranged."

On beaches, the net effect of sediment transport can lead to three-dimensional changes in the shape of the beach and, in turn, the resultant beach changes will influence the surrounding coastal environments.

Man has utilised the littoral zone for centuries for not only recreational purposes (*e.g.* swimming, sailing, surfing) but also for economic means (*e.g.* exploitation of valuable minerals, acquisition of sand and gravel) and also the disposal of waste products and seaward defence of the country. In addition, there is, of course, the most vital role played by the coastal zone - that of the beach as a natural buffer

between the ocean and the land (Komar, 1976). Destruction of these natural buffers will eventually lead to the vulnerability of the surrounding coastal region open to the full force of the elements. The beach is a valuable natural resource which requires careful and thorough investigation if a better understanding and knowledge of the environment is to be attained.

Within the coastal region, three basic phenomena influence nearshore processes: the wind, waves and currents. Wind can generate waves, induce currents and also transport sand directly; incident wave energy is dissipated or reflected over the shallowing waters and generates currents and turbulence which, together with drift currents bring about complicated sediment transport patterns; interaction of the various hydrodynamic forces can generate a range of beach morphologies and environments.

Our knowledge of the processes that drive nearshore sediment transport is, as yet, insufficient for solving the problems which occur along the coastal zone, let alone those problems which will occur in the future. If the predicted effects of global warming and associated rise in sea-level are realistic, then the need to understand the coastal environment is imperative.

2.2 THE COASTAL ZONE

One estimate of the length of the coastline of England and Wales, is about 2, 750 miles or 4.4×10^2 km. The coastline is the broad region that is the meeting place of the land and the sea. It can be carved into many kinds of shapes; wide low beaches, crescents of small beaches in small bays alternating with rocky headlands, wide sweeping sandy tidal flats or steep rocky cliffs (Press and Siever, 1986). Coastlines around the world can, however, comprise rias (drowned river valleys), deltas, fjords, estuaries, drumlins, barrier islands, cuspate forelands, mangrove, coral atoll, volcanic- and fault-related environments. Coasts are produced both by terrestrial and marine processes, Shepard (1973) divided all coastlines into primary or secondary types according to the mode of formation (*i.e.* tectonic, erosional and depositional). Primary coastlines owe their character and appearance to processes that occur at the land-air boundary, whilst secondary coastlines owe their character and appearance to processes that are primarily

of marine origin (Duxbury and Duxbury, 1991).

Defining the 'coastal zone' is not particularly simple, nor is it clear-cut. For instance, Beer (1983) describes this region as "the land and waters extending inland for 1km from the high water mark on the foreshore extending seawards to the 30m depth contour line, also including the water, beds and banks of all rivers, estuaries, inlets, creeks, bays or lakes subject to the ebb and flow of the tide". The term 'littoral zone' is often used instead of 'coastal zone', yet it describes a region which extends across the beach and into the water to a depth at which the sediment is less actively transported by surface waves, a 'coastal zone' is, therefore, a more inclusive label. An additional terminology which is often applied to this environment is the 'nearshore zone' reaching seawards from the shoreline to just beyond the region of wave breaking (Komar, 1976). Focusing more specifically upon the beach environment, Komar (1976) describes the beach as the "accumulation of unconsolidated sediment extending shorewards from the mean low-tide limit to some physiographical change such as a sea cliff or dune field, or to a point where permanent vegetation is established". Beaches are composed of whatever coarser material occurs locally in greatest abundance or was abundant in past geological times (Beer, 1983), the provenance of beach and nearshore sediments can be fluvial, terrestrial (material from sea cliffs, for example), biogenic or mechanical (eroded by wave action), in origin.

Basinski (1989) suggested a division of the coastal zone according to the dynamic behaviour of the waves upon the shore profile and the variations in beach topography and morphology. The effect of the seabed upon the transformation of waves in the nearshore zone is assumed to occur from a depth of half the wave length, which results in wave refraction from these depths, shorewards. The region offshore of the limit of wave contact with the sea floor is referred to as the 'offshore zone', the seaward boundary of the offshore zone being dependent upon random wave parameters. The waves approaching the shoreline do not differ from their equilibrium state until breaking occurs. Depending upon wave steepness and bed slope, the process of breaking can take a range of forms. The breaker line marks the offshore boundary of the breaker zone and whilst some of the waves (the highest) break at considerable

distances from the shoreline, most of the wave spectrum components break more gradually as the depth decreases. Subsequent to the last wave breaking on the beach, wave energy is entirely dissipated. The classification and definition of the various coastal sub-zones, as suggested by the CERC (1973), are illustrated in Figures 2.1 and 2.2 which include the terminology used to describe the beach profile according to the various hydrodynamic and the morphologic features, respectively.

Wright and Short (1983, 1984) further classified the beach profile according to the morphodynamic variability of surf zones and beaches. Their model described plan and profile configurations of six major beach states. The two extreme states were fully dissipative and highly reflective; morphologically these states correspond to flat, shallow beaches with relatively large sub-aqueous sand storage and steep beaches with small sub-aqueous sand storage, respectively. Between the two extreme cases were a range of intermediate states which possess both dissipative and reflective elements. Dissipative beaches are associated with persistent high waves and abundant find sand to create wide, low gradient beaches and surf zones. Dissipative beach regimes are stable, possessing low spatial and temporal variability. Reflective beaches, on the other hand, represent low energy environments with low modal wave heights. Intermediate beaches, conversely, are spatially and temporally the most dynamic beach types. Their characteristics include rip circulation, dynamic bar forms, abundant sediments and moderate waves and they can undergo rapid reversals in cross-shore and longshore sediment transport with significant wave height fluctuations. Intermediate beaches have the highest mobility of the three beach states. They are often favoured by bi-modal sediment populations with coarser fractions accumulating in the form of a steep sub-aerial beach face, with finer materials being located over the surf zone and forming bars (Wright and Short, 1983).

The beach state model proposed by Wright and Short (1983, 1984) provided a spatial classification, enabling prediction of beach change and equilibrium beach state. Each model beach state describes wave and sediment characteristics in terms of a dimensionless fall velocity, $\Omega = H_b/WT$, where H_b is the breaking wave height, W is

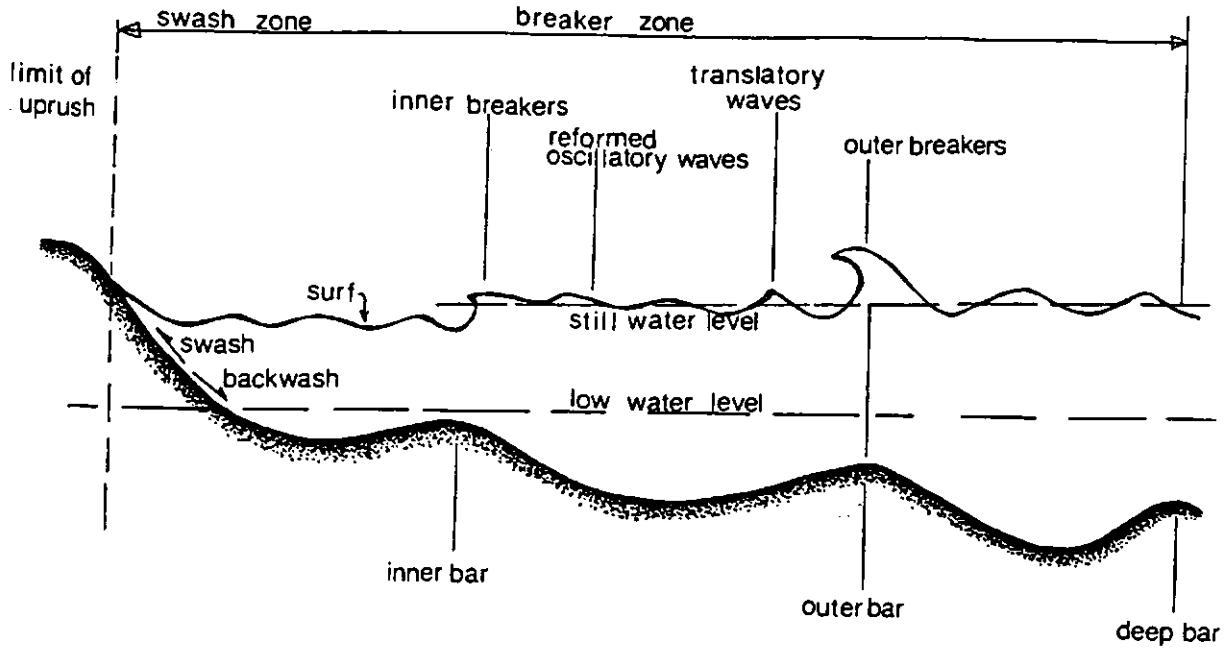

FIGURE 2.1 Characterising the beach profile according to the hydrodynamics of the system (from CERC, 1973).

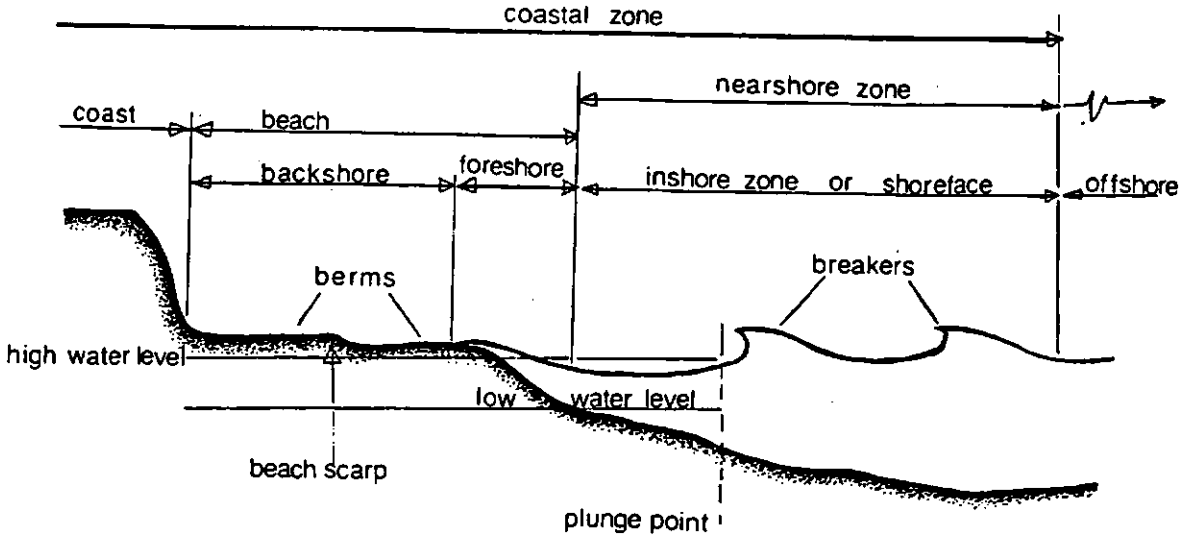

FIGURE 2.2 Characterising the beach profile according to the morphology of the system (from CERC, 1973).

the sediment fall velocity and T is the wave period. Where values of $\Omega < 1$ occur, Wright and Short (1984) suggested that a reflective beach state resulted, for Ω values of 1-6 the beaches are characterised by intermediate conditions and for $\Omega > 6$ the beach is thought to be dissipative. Intermediate beach states are grouped into four types with increasing Ω values into low tide terrace (LTT), transverse bar and rip (TBR), rhythmic bar and beach (RBB) and longshore bar trough (LBT).

As Masselink and Short (1993) point out, the beach state model put forward by Wright and Short (1984) was developed on and for the conditions of a micro-tidal beach environment without any consideration of the influence of the tidal range. Short (1991) then included the tide into his conceptual beach model by tentatively grouping together macro- to micro-tidal beach and tidal flat systems. Masselink and Short (1993) combined and extended the work by Wright and Short (1984) and Short (1991), examining the relative contribution made by breaking wave height and tidal range through studying the relative effects of waves and tides on beach morphology. Their model describes beach state as a function of dimensionless fall velocity, Ω, and the relative tide range (RTR). Figure 2.3 shows the conceptual model proposed by Masselink and Short (1993) based upon micro- and macro-tidal literature and field measurements. In Figure 2.3 we can see that as both Ω and RTR increase, a logical sequence of change in beach morphodynamics occurs from the reflective to the ultra-dissipative beach types.

2.3 COASTAL HYDRODYNAMICS

The processes which affect a coastline were reviewed by Cooke and Doornkamp (1974) and included the waves, tides and winds which act as process variables on beach materials to influence the response variables which are, in turn, the forms of both beach and coast in profile and plan. Understanding nearshore wave dynamics is, therefore, an essential component of any coastal protection or engineering study.

Waves are considered the most important 'process element' on the majority of, although not all, coastlines and have been extensively studied. However, our understanding of the mechanism of wave formation is far from complete. This

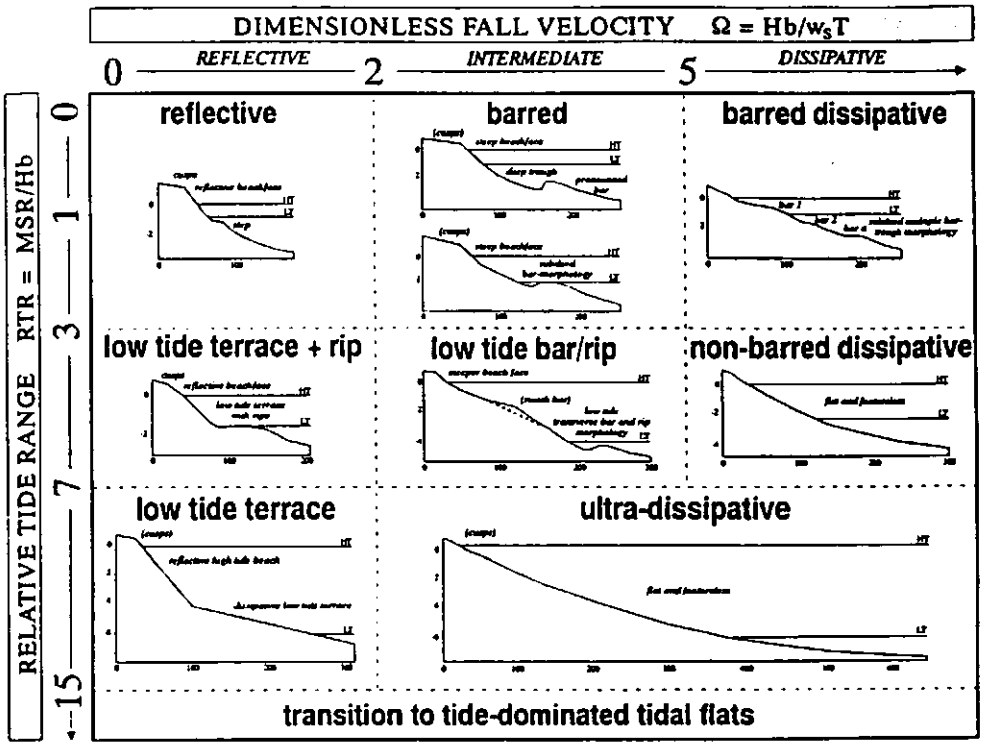

FIGURE 2.3 Conceptual beach model and classification of beach state based upon the dimensionless fall velocity, Ω, and the relative tide range (RTR), where mean high tide and mean low tide levels are denoted by HT and LT, respectively (from Masselink and Short, 1993).

inadequate understanding is partly due to the difficulty in observing wave characteristics at sea and because numerical models of wave behaviour relate to the dynamics of idealised fluids, and the ocean does not of course act as an ideal medium (Brown *et al.*, 1989).

Oceans and coastal waters display water level variations which fall into three broad categories depending upon period or time scale: short period waves (wave period, T < 30s), comprising wind waves and swell; long period wave motions (30s <T< hours) comprising, for example, tsunamis and surf beat; and thirdly, tides and storm surges (T > hours to days) which consist, for example, of the gravitational action of the moon and sun (Svendsen and Jonsson, 1980).

Whilst the short-period incident waves which approach the shoreline from deep water are a vital force acting upon the beach profile and coastal system, it has been known for several years that nearshore wave motions with periods substantially greater than those of incident waves, are present and in some cases can dominate the velocity field near to the shoreline. Bowen and Huntley (1984) determined through extensive data analysis, that these 'long wave' motions can occur in the form of progressive edge waves or forced wave motion or standing edge waves or even as free waves propagating away from the shoreline, all of which might also contribute to the nearshore wave energy. It is the short-period gravity band and longer-period infragravity band motions (surf beat) which are of primary concern in this study.

2.3.1 WIND-GENERATED WAVES

Short period waves, typically wind waves and swell, are generally defined to include waves of periods of less than 20-30s. Wind waves ('sea' waves or chop) are the short bumpy, sharp-crested waves which appear in the open sea under windy conditions. 'Swell' describes the slow, gently rolling waves that impinge on exposed shorelines even on calm days and is storm-generated some distance from the area of observation. Swell experienced on the Californian coast, for example, may have originated near New Zealand, whilst the sea waves are generally induced by strong wind conditions, being primarily of local generation.

A wave 'spectrum' may be analysed through Fourier techniques whereby the energy assigned to particular wave periods can be determined and the wave spectrum is separated into its constituent wave forms. Under deep water conditions it is possible to predict certain wave characteristics, but what actually happens to these properties as the incoming water is transformed across the decreasing water depths of the nearshore zone? Shoaling describes the process of waves entering shallower water. When the waves begin to feel the bottom, they slow, shorten and steepen. In this area, energy dissipation and wave height reduction, due to bottom friction, becomes increasingly important, whilst internal viscous dissipation and percolation losses are generally less significant factors (Svendsen and Jonsson, 1980).

The direction of a wave front as it propagates through the shallow water depths alters through 'depth refraction' and then, as the water becomes progressively shallower, the effect of the bottom slope increases, causing the deformation or asymmetry of the wave profile. Prior to wave breaking, mean water level is depressed (wave set-down). Then, as the wave reaches a height near to the water depth, the wave becomes unstable and breaking occurs. Wave height increases near the breakpoint through the opposing effects of shoaling and bottom friction, and the waves themselves develop more peaked crests and flatter troughs (Svendsen and Jonsson, 1980).

Airy (1845) developed a theory (commonly referred to as "linear wave theory") for irrotational waves travelling over a horizontal bottom in any depth of water. In this surface wave theory a number of assumptions are applied; namely, that wave shapes are sinusoidal, wave amplitudes are small with respect to wavelength and depth, viscosity and surface tension are negligible, as are Coriolis force and vorticity, depth is uniform and the bed is planar, waves are not constrained or deflected by obstructions (Komar, 1976). According to linear wave theory, where $1/2 > h/L > 1/20$, the general expression for phase velocity may be used,

$$c_p = \sqrt{\frac{gT}{2\pi}\tanh\left(\frac{2\pi h}{L}\right)} \qquad (2.1)$$

and the general expression for wavelength is given by

$$L = \frac{gT^2}{2\pi}\tanh\frac{2\pi h}{L} \qquad (2.2)$$

where L is wavelength, h is water depth, T is wave period and *tanh* is the hyperbolic

tangent. Commonly accepted limits for the deep and shallow water approximations are h/L > 1/2 and h/L < 1/20, respectively. The deep water limit is, therefore, described as h/L > 1/2, where the group velocity is half the phase velocity and phase velocity is:

$$c_p = \sqrt{\frac{gT}{2\pi}} = \sqrt{\frac{g}{\sigma}} \tag{2.3}$$

where g is the acceleration due to gravity, T is the wave period and σ is the radian frequency. Once the ratio of water depth to wave length approaches 1/20 then the approximation below is used:

$$\tanh\left(\frac{2\pi h}{L}\right) \cong \frac{2\pi h}{L} \tag{2.4}$$

This approximation is substituted into Eqn. (2.2) to produce expressions for the shallow water wavelength and phase velocity,

$$L = T\sqrt{gh} \tag{2.5}$$

$$c_p = \frac{L}{T} \text{ and } c_p = \sqrt{gh} \tag{2.6}$$

in which, c_p is the wave speed, or celerity of propagation, and $c_p = \sigma/k$, (where k is wave number ($=2\pi/L$) and σ ($=2\pi/T$) the radian frequency). When linear wave theory requirements become invalid, other wave theories (*e.g.* Stokes, Gerstner or cnoidal) may be more appropriate for the conditions being examined. Dean and Dalrymple (1984) examined the validity of non-linear wave theories to establish, for example, if linear wave theory is suitable for a particular situation, or whether 'cnoidal theory' must be used. Dean (1974) examined the analytical validity of many wave theories. Figure 2.4 shows the results of the comparison of the theories, denoting the regions for which each theory provides the 'best fit' to the dynamic free surface boundary condition. The cnoidal wave theory does well in shallow water, while in deeper water the Stokes V wave theory proved to be more applicable. In Figure 2.4 linear (Airy) wave theory is suitable for a considerable range of water depths, especially the intermediate depths. Surprisingly, Davidson (1992) found linear wave theory adequate for characterising the conditions found in the surf zone of a natural beach.

Linear wave relationships are important and enable prediction of the transformations undergone by a wave across the breaker zone. Such transformations are most apparent in long period swell waves which 'feel' the bottom first and tend to

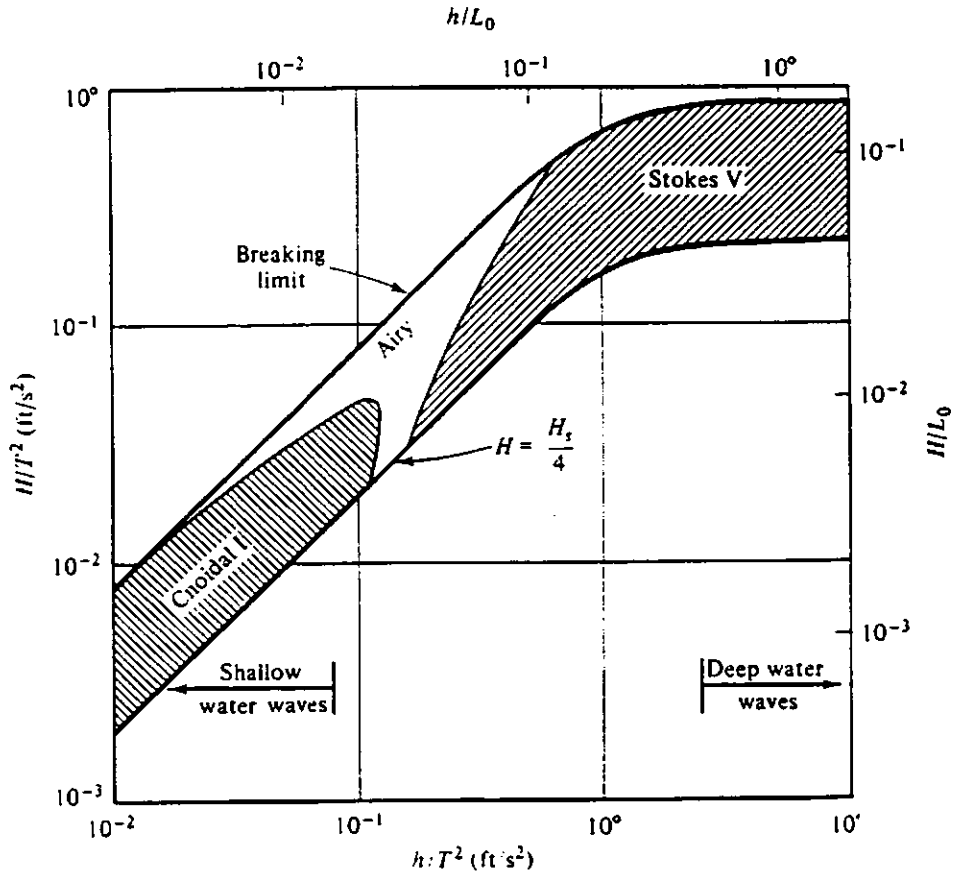

FIGURE 2.4 Comparison of the analytical validity of wave theories (from Dean and Dalrymple, 1984).

be most near-sinusoidal initially. The wave steepness (a ratio of wave height-to-wavelength, *H/L*) varies for shoaling waves. Wave steepness drops marginally below the deep water value temporarily, as the waves pass through intermediate water depths and then increases rapidly in shallower water. The sudden increase in wave steepness, together with the increase in wave height in the shallow water, is probably the most striking feature of the shoaling waves, and the steepness increases until a point is reached where the waves become unstable and break.

2.3.2 BREAKING WAVES

Battjes (1988) discusses how the 'surf zone' is characterised by the irreversible and almost complete transformation 'of the organised motion of the incident wind-generated waves into motions of different types and scales, including small-scale turbulence, larger-scale coherent vertical motions, low-frequency waves, and steady flows'. Wave breaking, one of the most important nearshore processes, promotes the re-distribution of energy and momentum throughout the spectrum. The turbulence injected into the water column, by breaking, is vital to the support of a suspended load and vertical variability in the breaking process and probably contributes to the generation of undertow (Nearshore Processes Workshop, 1990).

Waves approaching a beach generally break before arriving at the shoreline. The fluid dynamics of wave breaking have been well researched by Peregrine (1983), whilst Kobayashi (1988) provides a reference-rich review of incident wave transformation processes. Two types of motion are distinguished by Battjes (1988) in the evolution of breakers. First is the irrotational motion during wave steepening, overturning and jet formation, and the second is that following jet impingement, leading to the gradual development of a turbulent bore. The early work of Carrier and Greenspan (1958), who derived an exact standing wave solution to the inviscid, non-linear shallow water equations, Keller (1963), who carried out similar analysis for arbitrary relative depth, and Miche (1944) and Munk and Wimbush (1969), are also discussed in the review of surf zone dynamics by Battjes (1988).

The differences in the velocity fields which occur between steep and shallow

beaches were examined by Huntley and Bowen (1975b) and Wright and Short (1984). On a steep beach, waves will steepen rapidly to form plunging breakers and then collapse to dissipate their energy over a narrow surf zone. Observations seem to suggest that, within this narrow surf zone, the swash plays an important role by interacting with incoming breakers, whilst the collapse of the breaker itself is a violent process, often involving the rebound of the plunging face. On a shallow beach, changes to the breaker waveform occur much more slowly as the waves traverse a much wider surf zone. In reality a continuum of breaker types occurs (shown in Figures 2.5 and 2.6) which grade from one type to the next, and consequently application of a definite breaker type classification is not easy. Breaker types are, however, usually classified into three or four breaking wave forms (Galvin, 1968; Komar, 1976).

Foam, bubbles and turbulent water appearing at the wave crest and eventually covering the front face of a wave can signify a spilling breaker, for which the wave shape as a whole remains initially more or less symmetric. Spilling begins at the crest with the faster forward motion of a small tongue of water compared with the motion of the entire waveform. Spilling breakers are often associated with beaches of low slope.

The term 'plunging' is usually applied to the steepening and overturning of the whole wave front face, where the wave crest curls over and a large splash occurs at the point of crest impact. Generally speaking, plunging waves are identified with steeper beach slopes and with waves of intermediate steepness.

Where the front face and crest of a wave remain relatively smooth, the term 'surging' breaker is used as the wave proceeds up the beach with small amounts of foam and bubbles, not dissimilar to a standing wave. Surging breaker waveforms tend to form on beaches with steep gradients and with waves of low steepness.

Figures 2.5 and 2.6 illustrate these breaker types. Battjes (1988) suggests that the distinction between plunging and spilling breakers refers to the phase of initial breaking, while onshore both types develop turbulent bores which eventually collapse to form swash.

Considerable interest and research has been devoted to quantifying breaking

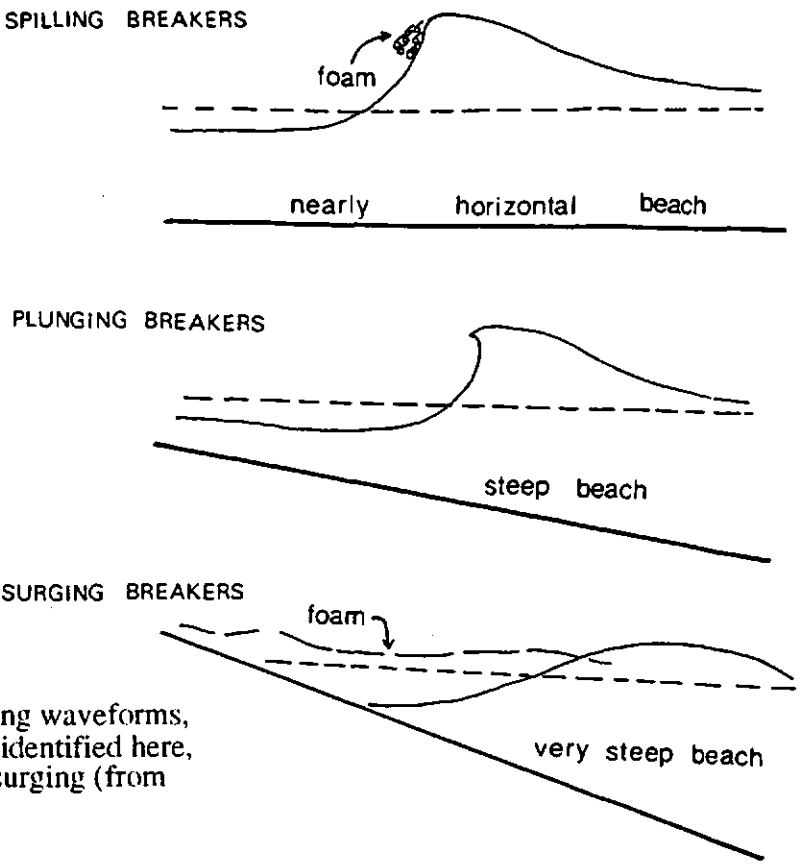

FIGURE 2.5
Classification of breaking waveforms, three breaker types are identified here, spilling, plunging and surging (from Komar, 1976).

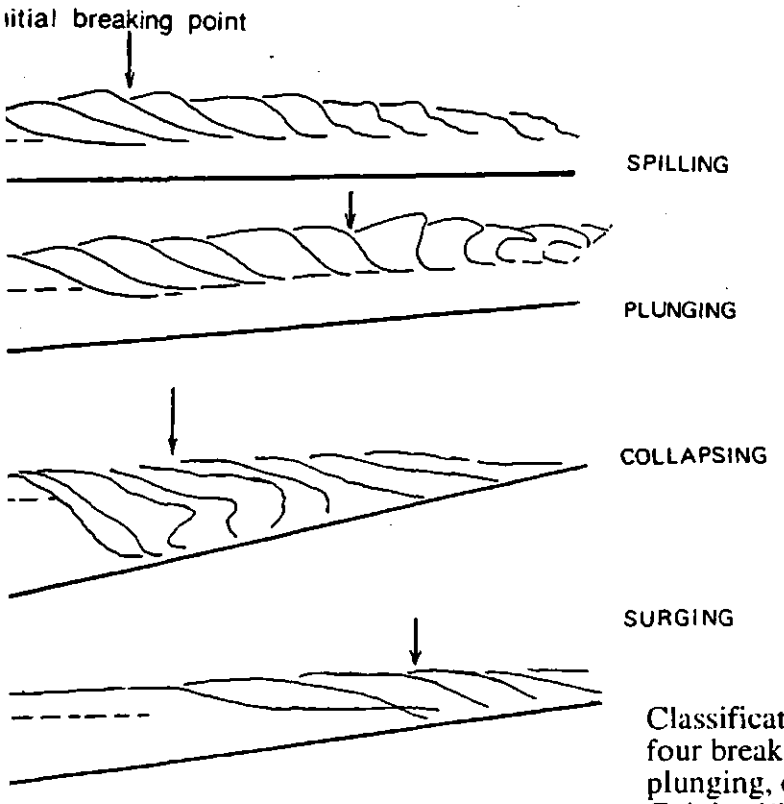

FIGURE 2.6
Classification of breaking waveforms, four breaker types are shown, spilling, plunging, collapsing and surging (from Galvin, 1968).

wave processes and to formulating numerical ranges for the classification of breakers. Galvin (1968) developed a breaker coefficient, B_o:

$$B_o = \frac{H_b}{gT^2 \tan\beta} \tag{2.7}$$

where H_b is breaking wave height, g is the acceleration due to gravity, T is wave period and $tan\beta$ is the beach slope. Breaker types are classified according to calculated values of B_o. If B_o is less than 10^{-1} or greater than 10^{-1} the breaker types will be plunging or spilling, respectively. There are concomitant changes, therefore, in the breaking waves transgressing the surf zone with changes in the beach profile. Guza and Inman (1975) proposed a surf scaling parameter whereby,

$$\varepsilon = \frac{a_b \Omega_f^{\,2}}{g \tan^2\beta} \tag{2.8}$$

where a_b is the breaking wave amplitude, Ω_f is the incident wave radian frequency ($\approx 2\pi/T$), g is the acceleration due to gravity, and β is the angle of the bed. Wright and Short (1983) explain how the surf zone widens and turbulent dissipation of incident wave energy increases with increasing ε. Complete reflection is to be expected where $\varepsilon < 1.0$, and when $\varepsilon \leq 2.0$-2.5 strong reflection will continue to allow standing wave motion, surging breakers and resonance. For values of $\varepsilon > 2.5$ the waves will begin to plunge and dissipate their energy until the point where values of $\varepsilon > 20$ occur, and spilling plungers result.

Owing to the important contribution of breaking waves to coastal processes, the properties of breaking waves have been studied extensively through recent years (*e.g.* Peregrine, 1983; Battjes and Stive, 1985; Mizuguchi, 1987). However, relating the hydrodynamic properties of breaking waves to sediment dynamics is mostly qualitative or empirical at present. The Nearshore Processes Workshop (1990) highlighted areas where further research associated with breaking waves is required, including: the initiation and type of wave breaking as a function of incident wave conditions and nearshore topography; prediction of wave statistics for random waves across the nearshore; and vertical gradients in turbulence generated by, and buoyancy effects of, bubble entrainment caused by wave breaking.

2.3.3 LOW FREQUENCY MOTIONS

The existence of low-frequency motions was realised some time ago. Munk (1949) observed long waves outside the surf zone and suggested an association with wave groups and the beating of several incident frequencies. Tucker (1950) also observed low frequency variations of the sea surface close to the shoreline.

What are long waves? Long waves are low frequency motions generated by the transfer of energy from modulated high frequency waves (short waves) when they propagate into shallow water (Hamm *et al.*, 1993). The period of these 'surf beats' (also referred to as low frequency motions, infragravity motions or long waves) is generally considered to be greater than 20-30s. Longuet-Higgins and Stewart (1964) described the process of generation of long waves, occurring through the variations in the short-wave momentum flux, or radiation stress, as the short waves of varying amplitude propagate over shallow water.

Determination of the long wave source was not possible with the early measurements, as it was difficult to know if the observed infragravity energy was first propagated from deep water towards the shoreline and then reflected back out to sea (leaky waves), or if the infragravity motions were generated in shallow water then trapped by refraction in the nearshore (topographic edge waves), or whether the long waves were generated locally in response to incoming groupy wind waves. More recent field measurements have established that long period motion exists on natural beaches and within the surf zone infragravity variance can grow in a shorewards direction in association with a decrease of incident and harmonic variance (*e.g.* Holman, 1981; Guza and Thornton, 1982; Holman and Sallenger, 1985; Russell *et al* , 1991). Some recent studies have shown, however, the opposite case whereby the infragravity energy plays a subordinate role to the short wave energy contribution on intermediate beaches (*e.g.* Wright *et al.*, 1982; Davidson *et al.*, 1993). Figure 2.7 shows the key elements of momentum transfer across the nearshore, whereby, as the incident waves travel into the shallow nearshore waters, energy is non-linearly transferred to both lower frequency motions (*e.g.* mean flows and infragravity waves) and higher frequency motions (*e.g.* harmonics of the incident waves and turbulence).

It is worth considering the possible effect, if any, of these long period motions on the nearshore sediment transport regime. Holman (1983) discussed the interesting, yet obvious, phenomenon of the effect of long waves on beach sediments stating,

> "Storm waves incident on a beach have their maximum energy at the breakpoint and their minimum at the shoreline, particularly on shallow beaches. It is therefore somewhat paradoxical that storms often result in tremendous erosion and the rearrangement of sediment in the inner surf and swash zones, just where the incident waves have their least expression. Clearly, there must be some other processes acting which may not be as apparent to the eye but whose effect is weighted toward the shoreline."

In this case, the processes were edge waves, but the importance of long wave motions, generally, to the nearshore morphology is also implied.

Formation of crescentic bars on long, straight beaches was explained by Bowen and Inman (1971) through the existence of standing edge waves, low frequency wave motions with periods of 30-60s and significant amplitude. The association between nearshore morphology and the infragravity band motions has been known for several years (*e.g.* Bowen and Inman, 1969; Guza and Inman, 1975; Huntley and Bowen, 1975a; Short, 1975; Wright *et al.*, 1978). The fact that the typical length scales of many morphological features on natural beaches are similar to the length scales of long waves, does seem to suggest that surf beat has an important effect on beach profiles (Roelvink, 1993). Huntley *et al.* (1993) present a thorough and clear report of the results from field measurements of long period motions and associated sediment transport on beaches (see also Section 2.4 for a fuller discussion).

The existence of long period motion is generally most clearly seen at the shoreline. Measured shoreline oscillations are generally separated into mean vertical elevation, known as set-up, and varying swash components. Properties of beach swash have evoked considerable research interest. The run-up at the shoreline has been determined through application of run-up meters, wave staffs positioned parallel to the shore, and time-lapse photography (Holman and Guza, 1984). Of the swash oscillations on natural beaches, swash can be thought to comprise 'saturated' high frequency and 'unsaturated' lower frequencies which correspond approximately to the incident wave and infragravity bands, respectively (Huntley *et al.*, 1977, Guza and Thornton, 1982). These observations have shown the high frequency saturation of the

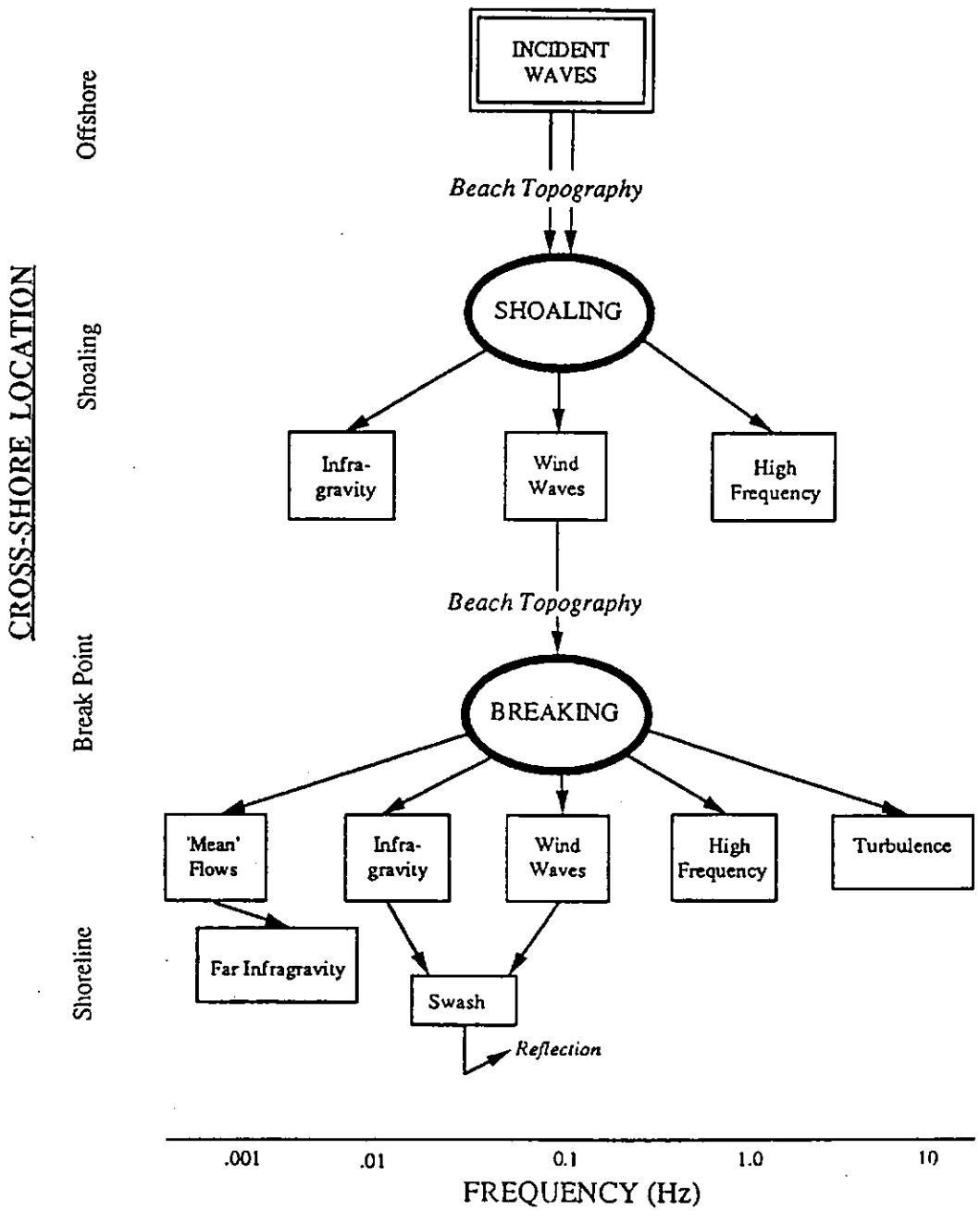

FIGURE 2.7 Flow-chart of the important nearshore processes showing how the incident wave energy that drives the system, evolves as the waves progress from offshore to the shoreline (top to bottom of the diagram). Beach topography provides the bottom boundary condition for flow, in turn waves move sediment and the profile alters accordingly (from Nearshore Processes Workshop, 1990).

swash spectrum and, as Battjes (1988) infers, the saturation of the higher frequencies allows a predominance of low frequency motions in the surf zone. Low frequency motions have been found to be of particular importance to the swash zone on beaches with gentle slopes (*e.g.* Guza and Thornton, 1985a). Guza *et al.*. (1984), using data collected at California and North Carolina, similarly showed that low frequency motions tended to dominate the swash spectrum on these two dissipative beaches.

Holman and Sallenger (1985) observed a dependence of the swash measurements upon the surf scaling parameter (see Eqns. 2.7 and 2.8), which decreases with a decreasing foreshore slope and increasing incident wave steepness. On beaches with steep gradients, run-up comprises significant energy at the sub-harmonic frequency (period twice that of the incident waves). On beaches with shallower gradients, the frequencies were generally found to be much lower and appeared unrelated to the incoming wave frequencies.

Modes of low frequency motion fall naturally into two categories, according to Battjes (1988) and Huntley *et al.* (1993), those propagating cross-shore and those propagating alongshore. The latter are edge waves, trapped at the shoreline, and the former are leaky waves, radiating energy between the shore and deeper water. This classification of long period motion includes :

(a) free waves (i) edge waves - progressive or standing,
(ii) leaky modes;
and (b) forced waves.

Waves in the infragravity band, consequently, maybe either freely propagating *edge waves* (trapped to the shoreline by wave refraction) and either *progressive* or *standing waves* in the alongshore direction, in addition to untrapped *leaky waves* (standing in the cross-shore direction) or *bound modes* (forced secondary waves non-linearly coupled to groups of incident waves (Longuet-Higgins and Stewart, 1962; Huntley *et al.*, 1981, Elgar *et al.*, 1992). The review by Kobayashi (1988) provides a reasonably comprehensive investigation of these different modes of low frequency motions.

The relative importance of forced waves, edge waves and leaky waves is not well known. Seawards of the surf zone, relative contributions to the total energy by the different types of infragravity motions tends to vary with distance offshore (Elgar *et al.*,

1992). Elgar *et al.* (1992) studied pressure records from 8m and 8-13m depth along the Pacific and Atlantic coastlines, respectively. The observed infragravity motions in 8-13m water depth were dominated by free waves with a dominant bound long wave contribution occurring only in very energetic swell conditions. Investigations using measurements taken far offshore have revealed that the bound long waves can dominate the infragravity band (*e.g.* Sand, 1982). Pressure data from 8-13m mean water depth were examined by Okihiro *et al.* (1992) who estimated that the bound long wave component contributed, at most, 50% of the observed infragravity energy. On the other hand, Huntley and Kim (1984) estimated that 80% of the observed energy in the infragravity band, on a natural beach, was associated with bound long wave energy.

Huntley *et al.* (1981) and Oltman-Shay and Guza (1987) established that a considerable (although not well quantified) proportion of the long wave energy can actually occur as edge waves. Analysing two days of field measurements obtained in the NSTS fieldwork at Torrey Pines Beach (NSTS or Nearshore Sediment Transport Study was a large-scale field experiment which took place on a range of Californian beaches during 1978-1980) Huntley *et al.* (1981) estimated that at least 30% of the total longshore current energy is progressive edge waves. Oltman-Shay and Guza (1987) on the other hand, estimated that more than 50%, and up to 88%, of the total variance in the longshore current, near the shoreline within the surf zone, at low frequencies could be low mode (0 to 3) edge wave motions. Low mode edge wave motions are considered to be less significant to the cross-shore velocity field than higher mode edge waves or reflected forced waves. The role played by low-mode edge waves is most likely to become less important with increasing offshore distance as they are trapped close to the shoreline by refraction.

Huntley (1988) found that co-spectra between alongshore and cross-shore velocities are particularly sensitive to *phase coupling* between a low mode edge wave, which dominates the longshore velocity, and higher mode edge waves, which dominate the cross-shore velocity. Other sources of energy than progressive low mode edge waves therefore appear more important to the cross-shore flow in the surf zone, including forced and free (leaky and/or high-mode energy edge) waves (Huntley *et al.*,

1981, Huntley and Kim, 1984, Elgar and Guza, 1985).

(a) EDGE WAVES

Edge waves, unlike leaky waves, cannot radiate energy out to deeper water, nor can they propagate away from shallow water. Suhayda (1974) described edge waves as trapped modes with longshore wavelengths at the same scale as offshore wavelengths. Unlike leaky modes, their longshore wavelengths for a given frequency and bottom slope have a discrete spectrum. Edge wave energy can only be dissipated through friction or interaction with currents and other waves, existing equally well along straight or gently curving shores and on either uniformly sloping, concavely- or convexly- curving offshore depth profiles.

Edge waves are known to play an important role in a variety of nearshore processes (*e.g.* Howd *et al.*, 1992), including mean circulation patterns (Bowen and Inman, 1969), the generation of nearshore morphology (Holman and Bowen, 1982) and wave momentum and energy transfer across the nearshore zone (Elgar and Guza, 1985). They have been the focus of many research projects not least because their length scales appear similar to those of sand bar systems, both in the cross-shore (*e.g.* Short, 1975; Bowen and Huntley, 1984) and in the longshore directions (*e.g.* Bowen and Inman, 1971; Holman and Bowen, 1982). Superimposed upon the incident waves at the shoreline, edge waves are free modes of water motion trapped in the 'waveguide of a sloping beach' (Oltman-Shay and Howd, 1993) by refraction offshore and reflection at the shoreline, the energy decreasing asymptotically to zero with distance offshore (Huntley, 1976).

Modelling edge waves should, in theory, be easier than forced wave modelling since their amplitude is considered to be decoupled from the changes of incident wave amplitude over the time scale of wave groups (Huntley *et al.*, 1993). Naturally, however, modelling edge wave interactions in the nearshore zone does rely upon the development of a good understanding and realistic parameterisation of the dynamics and properties of edge waves.

Edge wave dynamics have been the subject of several investigations (*e.g.*

Gallagher, 1971; Bowen and Guza, 1978; Holman, 1981; Huntley, 1976; Huntley *et al.*, 1981). Holman (1983) provides a clear explanation of the form and behaviour of edge waves and relates these properties in Eqns. 2.9-2.12 below. Figure 2.8 illustrates the motion of a progressive mode 0 edge wave along the shoreline. The waveform, η, is largest at the shoreline, sinusoidal in the longshore direction, and with an exponential offshore decay and can be described as:

$$\eta\,(x,y,t) \;=\; \mathrm{a}\, e^{-kx} \cos\,(ky - \sigma t) \qquad (2.9)$$

where a is the amplitude at the shoreline, x and y are the cross-shore and longshore co-ordinates, respectively, and k and σ are the wavenumber and radian frequency of the edge wave ($k = 2\pi/L$ and $\sigma = 2\pi/T$, here L is wavelength, T, the wave period).

Modelling edge waves must also include a knowledge of the mode number (Huntley *et al.*, 1993). Figure 2.9 shows a mode 1 ($n = 1$) edge wave, which differs from the mode 0 wave because of its offshore structure, the mode 1 wave having one crossing of mean sea level in its cross-shore elevation profile. In fact, a range of edge wave modes exist, and the cross-shore shapes of edge wave modes 0-3 are illustrated in Figure 2.10. Offshore behaviour of edge waves becomes increasingly complex with increasing model number, n, the number which determines the number of zero (mean sea level) crossings in the cross-shore direction before ultimate decay of edge wave energy occurs (Holman, 1983). The cross-shore structure can be written in terms of a 'velocity potential', $\phi(x)$, assuming a planar beach with uniform slope, $\tan\beta$ (Eckart, 1951; Ursell, 1952). The offshore waveforms in shallow water can be expressed as the product of polynomials and the exponential decay,

$$\phi\,(x) \;=\; L_n(2kx)\, e^{-kx} \qquad (2.10)$$

in this expression, L_n, represents the Laguerre polynomials of order n. Huntley and Bowen (1973, 1975a) studied the cross-shore and longshore horizontal components of the velocity field and found the ratio of cross-shore to longshore current amplitudes to be approximately constant, independent of offshore position. The observed phase and amplitude ratios between onshore and longshore current components indicated the presence of a standing zero mode sub-harmonic edge wave. The edge wave dispersion relation, derived by Ursell (1952), is an important expression for linking the wave-

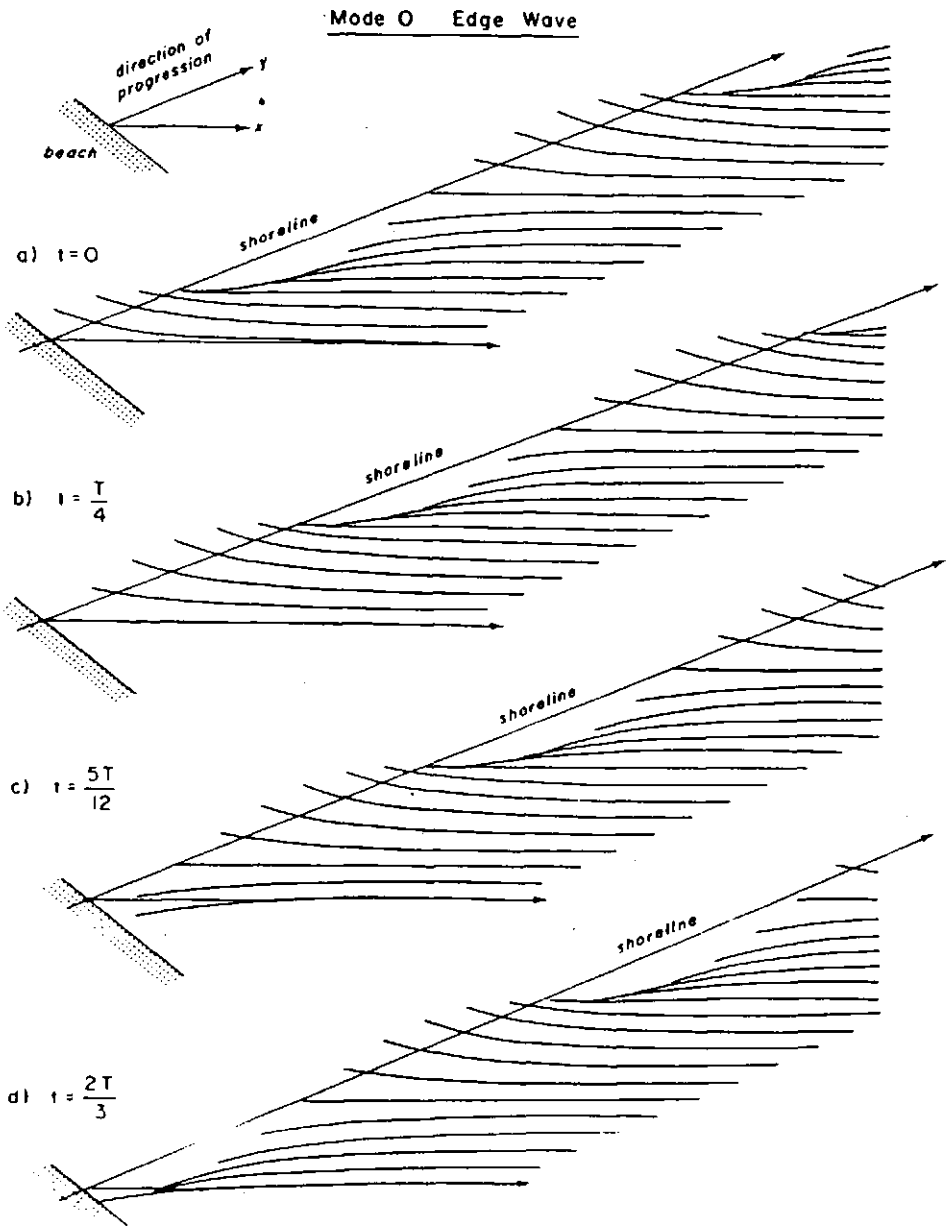

FIGURE 2.8 Progressive edge wave (mode 0) viewed obliquely from offshore. Offshore is to the right of the diagram, onshore to the left. The shoreline reaches from the lower left corner to the upper right corner. Time progression of the waves is shown by the four figures (from Holman, 1983).

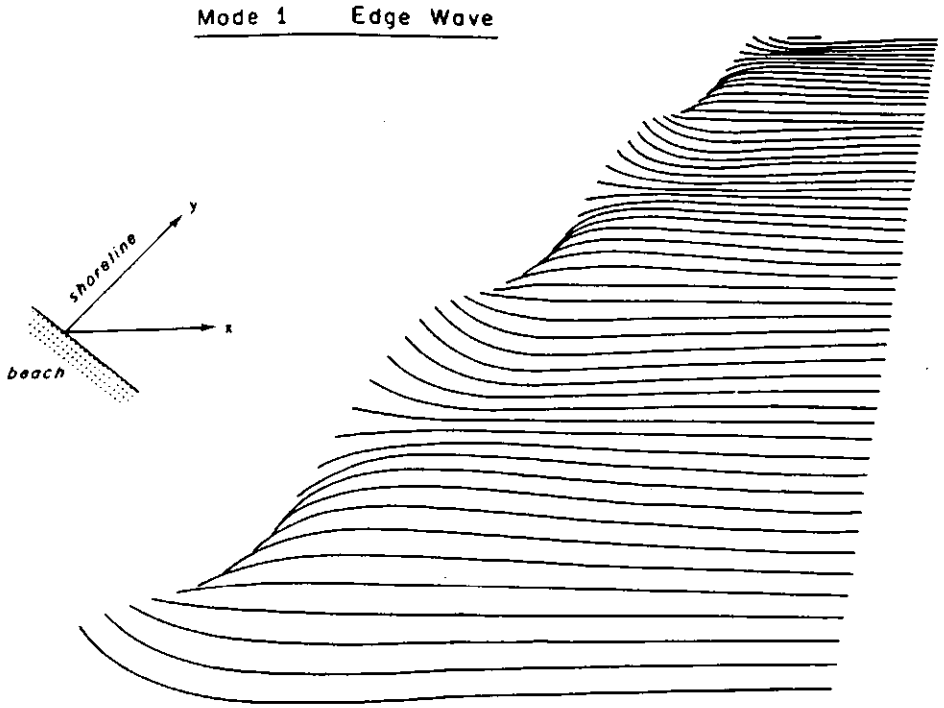

FIGURE 2.9 Edge wave (mode 1), viewed obliquely from offshore. The wave is also sinusoidal in the longshore, but showing an offshore anti-node. The structure equates well with the features of nearshore bar formation.

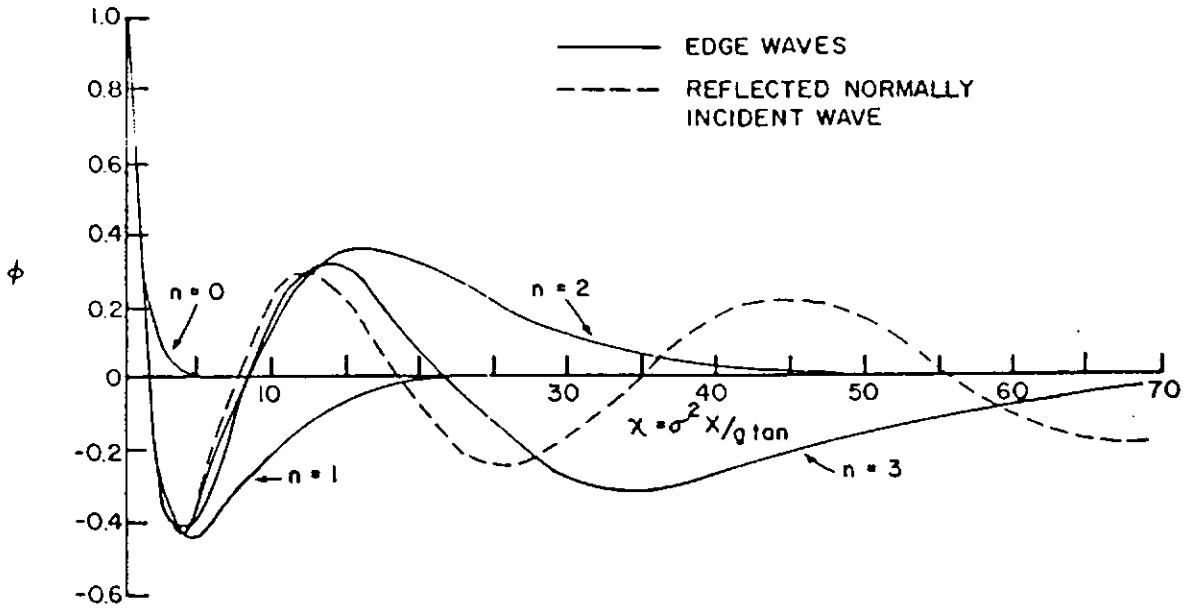

FIGURE 2.10 Offshore structure of edge wave modes (0 to 3) plotted in terms of a non-dimensional offshore distance, χ. The similarity which exists between edge wave modes and also the standing incident wave, an example of a leaky wave, makes distinguishing between modes, quite difficult (from Holman, 1983).

length and period of an edge wave. Thus, for a planar beach,

$$L = \frac{gT^2}{2\pi} \sin\left[(2n + 1)\beta\right] \tag{2.11}$$

Wavelength is dependent upon mode number as well as the period and beach slope. From the dispersion relation (Eqn. 2.11), the dimensionless offshore distance, χ, can be written,

$$\frac{x}{L} = \frac{x}{g2\pi/\sigma^2(2n+1)\beta} = \frac{\sigma^2 x}{(2n + 1)g\beta}\frac{1}{2\pi}; \tag{2.12}$$

the expression above can also be used as a non-dimensionalisation factor.

The existence of edge waves on natural beaches was originally inferred from the formation of beach cusps and crescentic bars, and from the periodic spacing of rip currents. Laboratory experiments carried out by Bowen and Inman (1971) suggested that standing edge waves (at sub-harmonic frequencies) provided a satisfactory explanation for the formation of crescentic bars. Huntley and Bowen (1973), however, described their *field* results from a steep beach in South Devon and their measurements of current velocities close to the shoreline suggested the existence of a sub-harmonic, zero-order edge wave. Guza and Bowen (1976) showed similarly the formation of sub-harmonic edge waves on steep beaches. Guza and Davis (1974) illustrated theoretically how surface waves incident on a beach from deep water can excite edge waves, also that viscous effects suggest that a zero-mode edge wave with a frequency half that of the incident wave (*i.e.* sub-harmonic) is preferentially excited. In other words, only the mode zero edge wave is forced instead of a combination of modes. Sub-harmonic edge waves are effectively isolated in the spectrum, and are therefore easier to distinguish than infragravity edge waves (Holman, 1983).

Field evidence of infragravity edge waves has, therefore, come about more slowly than that of sub-harmonic edge waves. The non-linear interaction of the incident waves of slightly different periods and possibly different angles of incidence may result in low-frequency edge waves on gentle dissipative beaches (*e.g.* Gallagher, 1971; Huntley, 1976; Bowen and Guza, 1978). Similarity, between the offshore structure of edge wave modes and a standing incident wave, reflected from the shoreline, creates some difficulty in the observation of infragravity edge waves. For instance, the cross-shore structure of leaky waves and high mode edge waves are

almost indistinguishable for the first few zero crossings (Guza and Davis, 1974). A further distinction was provided by Huntley (1976) through examination of the amplitude of the components of flow. To first order approximation, the ratios of longshore current (v) and cross-shore current (u) amplitudes at the shoreline will be given by,

Reflected incident waves $$\left(\frac{v}{u}\right)_{x=0} = \beta \sin\theta_\infty \qquad (2.13)$$

Progressive edge waves $$\left(\frac{v}{u}\right)_{x=0} = \frac{1}{(2n+1)} \qquad (2.14)$$

where θ_∞ is the deep water wave direction. The ratio will be greater for edge waves unless the mode number becomes sufficiently large. However, in the absence of independent knowledge of edge wave mode numbers use of Eqns. 2.13 and 2.14 cannot confirm the existence of edge waves definitively.

It was through the examination of the longshore variation of the waveform by Huntley *et al.* (1981) that definitive evidence for the existence of progressive edge wave motions (at infragravity frequencies) was provided. Katoh (1981) examined a beach located near a breakwater and similarly obtained convincing measurements of infragravity edge waves in the natural environment. More recently, Oltman-Shay and Guza (1987) observed a dominance of progressive low mode ($n \leq 2$) edge waves in the longshore current variance with the cross-shore current variance characterised by high mode and/or leaky waves, for current velocity measurements made on two Californian beaches. Since these early investigations, substantial research has been carried out into the nature of infragravity edge waves on beaches and the possible importance of edge waves to modelling nearshore hydrodynamics and sediment transport (*e.g.* Bauer and Greenwood, 1990; Davidson, 1990; Howd *et al.*, 1991; Oltman-Shay and Howd, 1993).

(i) Progressive Edge Waves

Eckart (1951) used the shallow water equations and established the edge wave dispersion relationship between the angular frequency, $\sigma(=2\pi/T$ where T is wave period), and the longshore wavenumber, k ($=2\pi/L$ where L is longshore wavelength), where: $$\sigma^2 = gk(2n+1)\beta, \quad \text{where } n = 0, 1, 2.... \qquad (2.15)$$

where β is the beach slope and n is the edge wave mode number. The mathematical expressions for progressive edge waves are described by Huntley (1976) through the forms of the cross-shore *(u)* and longshore *(v)* velocities, as

$$u(x,y,t) = \left(\frac{a_n gk}{\sigma}\right) u.(x) cos(ky - \sigma t) \tag{2.16}$$

$$v(x,y,t) = \left(\frac{-a_n gk}{\sigma}\right) v.(x) sin(ky - \sigma t) \tag{2.17}$$

where,

$$u.(x) = \left[\frac{\delta}{\delta(kx)}\right].\left[L_n(2kx)e^{-kx}\right] \tag{2.18}$$

$$v.(x) = L_n(2kx)e^{-kx} \tag{2.19}$$

Here, x is the co-ordinate perpendicular to the shoreline, y is the co-ordinate parallel to the shoreline, a_n is the amplitude of the mode 'n' edge wave at the shoreline and L_n is the Laguerre polynomial of order n.

Ursell (1952) demonstrated the principle of a 'cut-off' period, whereby waves with larger periods than the specified cut-off will be untrapped, radiating energy away from the nearshore. Ursell stated that, at any given frequency, edge waves occur only in conjunction with longshore wave numbers greater than the cut-off, which increases with increasing frequency. Free waves can take any longshore wave number in a continuum of values, whilst edge waves can only occur at distinct frequency values.

Bowen and Huntley (1984) showed schematically the relationship between, σ, and the longshore wavenumber, k, for a beach of slope $\beta = 0.12$ (Figure 2.11). In Figure 2.11, the solid lines denotes a set of edge wave modes ($n = 0, 1, 2, 3$ *etc.*) whose amplitude is largest at the shoreline, decreasing with distance seawards, so that the wave is trapped to the shoreline. The trapped modes have a discrete set of eigenvalues in the range $\sigma^2 \leq gk$ given by Eqn. (2.15). If $(2n + 1)\beta > \pi/2$, then no trapped solutions exist and any waves with such (σ, k) values will, subsequently, be leaky modes (including the normal incident waves). Between the edge wave modes are combinations of (σ, k) values which do not satisfy the dispersion relationship (Eqn. (2.15)). Motion in this sector is termed 'forced', with a response that will in theory be weaker than at the free modes. Bowen and Huntley (1984) describe this range of forced modes which do not satisfy the dispersion relation for free modes in the cross-

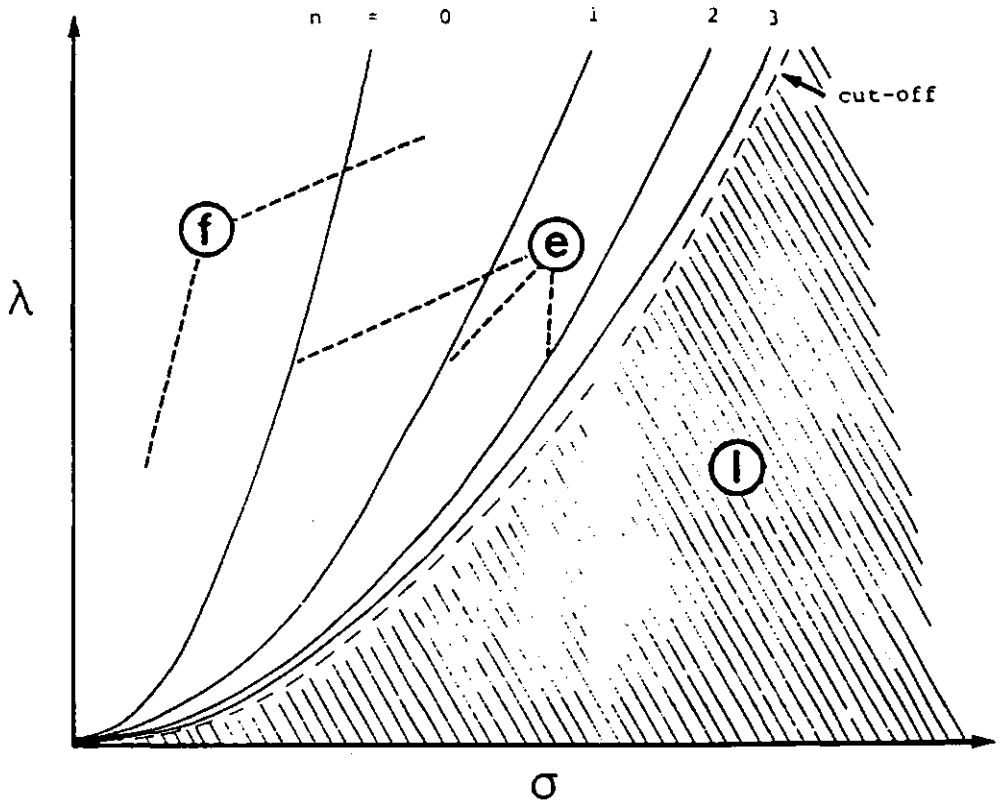

FIGURE 2.11 Dispersion relationship between wave frequency, σ, and longshore wavenumber, λ, for a beach slope where $\beta = 0.12$, n is the modal number of the edge waves denoted by, e, leaky modes are represented by, l, and forced modes by, f (from Bowen and Huntley, 1984).

shore direction; their (σ, k) values do not satisfy the normal conditions for surface gravity waves. In Figure 2.11, leaky mode waves are described by the region denoted by '*l*' they can take any value of σ provided that $\sigma^2 > g\lambda$. As Bowen and Huntley (1984) illustrate, these leaky waves occupy a continuum in frequency-longshore wavenumber space as shown in Figure 2.11. Ursell (1952) illustrated that for a given frequency, edge waves can occur only with (σ, k) values greater than the cut-off wavenumber which increases with increasing frequency. Physically the cut-off period of an edge wave mode occurs when the longshore wave number of the edge wave, k_v, equals the wavenumber of a free gravity wave, k_o, in deep water, therefore, $k_v < k_o$. If $k_v > k_o$ then the only free waves which can occur are edge waves trapped to the shoreline, conversely, waves with $k_v < k_o$ longshore wavenumbers, will be leaky and radiate energy seawards, being no longer trapped.

In the previous section, it was noted that only through the examination of the longshore variation of the waveform could definitive evidence for the existence of progressive edge waves be obtained. A large longshore array of instruments is, therefore, necessary to separate modes if a number of different modes, trapped and leaky, occur at the same frequency (Bowen and Huntley, 1984). Figure 2.12 from Huntley *et al.* (1981) shows contours of energy in the longshore component of velocity plotted on a (σ, k) diagram in which most of the energy occurs as progressive edge waves, with one mode dominating at any particular frequency, mode 0 dominated between 0.006-0.0011 Hz.

(ii) Standing Edge Waves

The edge waves measured by Munk *et al.* (1964) were progressive, with almost equal amounts of energy propagating north and south alongshore. It is probable, however, that an obstruction or topographic change in the sea floor could reflect these longshore propagating waves, and initiate *standing* edge wave motion with both nodes and antinodes occurring at regular intervals along the shoreline (Huntley *et al.*, 1981).

Tatavarti (1989) examined previous studies of edge waves; they appear to have followed two main routes. The first line of edge wave investigations were generally

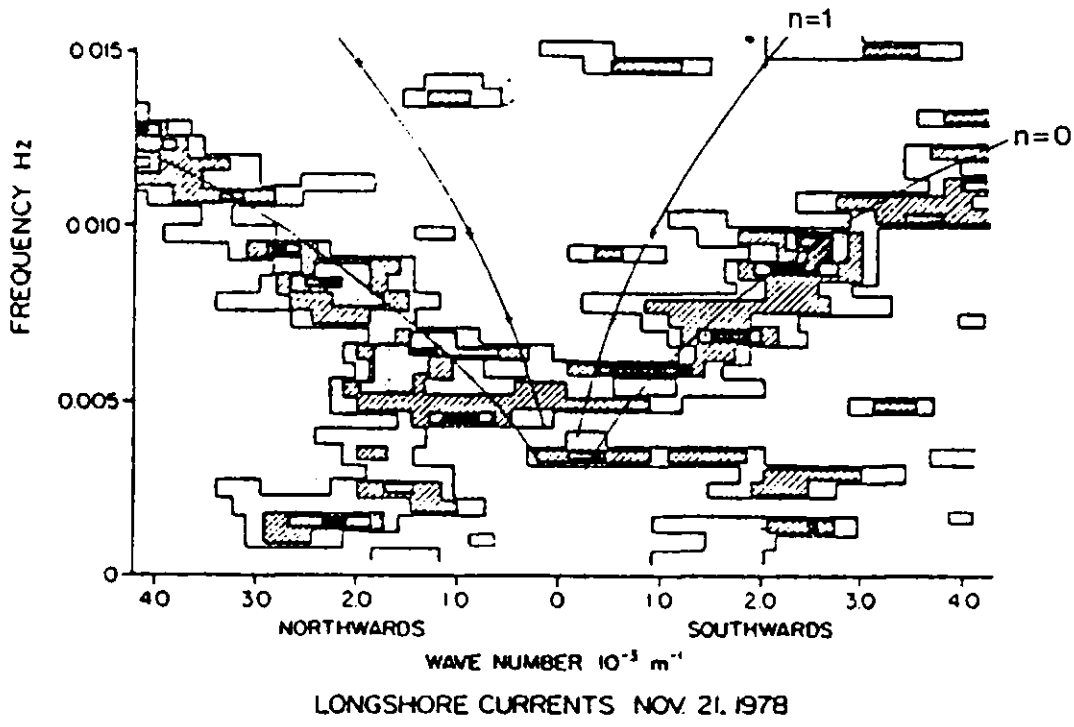

FIGURE 2.12 Part of the longshore current spectrum. Curves are for $n = 0$ and $n = 1$ assuming a plane beach slope $\beta = 0.023$. Showing energy propagation south and north along the shoreline (from Huntley *et al*, 1981).

two-dimensional in nature with no longshore dependence (Munk, 1949; Tucker, 1950 and Longuet-Higgins and Stewart, 1964). The second line of edge wave investigation dealt with the analysis of three-dimensional theories, involving longshore modulation of the incident waves (Guza and Bowen, 1976; Bowen and Guza, 1978). Guza and Inman (1975), however, highlighted the difficulty and problems in distinguishing between the standing incident and standing edge waves which occur at the shoreline, owing to the similarity of both types of offshore profiles. Huntley (1976) showed how in Eqns. 2.16 and 2.17 for progressive edge waves, the cosine and sine terms can be replaced by ($cos\ kx\ cos\ \sigma t$) and ($sin\ kx\ cos\ \sigma t$) respectively for standing edge waves.

(b) LEAKY WAVES

Leaky modes are waves incident from deep water or waves progressing seawards after either reflection from the beach, or generation in the nearshore region by non-linear interactions (Tatavarti, 1989). Long period leaky mode waves, primarily in the on-offshore direction, are considered to play an important role in the formation of shore-parallel features (*e.g.* longshore bars) owing to the similarity between the length scales of the leaky modes and nearshore morphology (Bowen and Inman, 1971; Sonu, 1972; Lau and Travis, 1973; Bowen, 1980a; Bowen and Huntley, 1984).

The mechanism for leaky mode generation (or low frequency motions generally) in the surf zone, is not well known. Several models have, however, been proposed for the mechanism of generation. For example, Symonds *et al.* (1982) related the presence of leaky mode waves to time variation of the breakpoint for incident waves. The model proposed by Symonds *et al.* predicted a bound long wave that is released through the breaking region and reflected from near the shoreline as a free long wave. Longuet-Higgins and Stewart (1962, 1964) suggested that a bound long wave, arriving at the breakpoint with an incident wave group, could be released to travel seawards or shorewards as a free wave. Watson and Peregrine (1992) examined model and laboratory data of runs using idealised wave groups; their results illustrated the generation of low frequency waves by forcing within the surf zone and swash zone, contrary to the breakpoint forcing (*e.g.* Symonds *et al.*, 1982; Schäffer, 1993) or bound

wave reflection mechanisms (*e.g.* Longuet-Higgins and Stewart, 1962). In order to study the location of long wave reflection, the approach adopted by Tatavarti *et al.* (1988) involved the decomposition of sea surface elevation and velocity data to separate incoming and outgoing waves close to the shoreline. Observations of the time lags between the incoming and outgoing long waves suggested that considerable reflection or generation of long waves occurred at the breakpoint and at the shoreline. Further, the relative phase between the incoming and outgoing waves near the breakpoint corresponded well with breakpoint generation of seawards propagating long waves.

Suhayda (1974) examined the behaviour of standing (in the cross-shore direction) waves on beaches, concentrating mainly on leaky modes, rather than trapped modes. When untrapped leaky waves, standing in the cross-shore direction, occur at the same frequency as trapped modes, then it can be difficult to separate the two (Huntley, 1976; Holman *et al.*, 1978; Holman, 1981; Oltman-Shay and Guza, 1987). Extensive arrays of instruments in both the longshore and cross-shore directions should provide the means to distinguish between the different waveforms in the nearshore. Using a cross-shore array of measurements, the array would have to extend some distance beyond the last antinode of the highest possible mode of the edge wave that can be trapped (Oltman-Shay and Guza, 1987). In addition, the possibility of partial reflection at the shoreline and the possible presence of several modes, makes cross-shore arrays generally unsatisfactory for distinguishing edge wave modes and leaky waves (Snodgrass *et al.*, 1962). Alongshore arrays of electromagnetic current meters, for example at NSTS and SUPERDUCK (a large-scale sand transport study which took place at Duck, North Carolina during 1986) field sites, enabled estimation of the longshore wavenumber-frequency spectrum of infragravity motions in the nearshore zone. Examination of longshore wavenumber-frequency spectra allows differentiation between high wavenumber edge waves trapped at the shoreline, and the leaky modes which escape offshore. Oltman-Shay and Guza (1987) examined data from two alongshore arrays of bi-directional current meters, deployed on two Californian beaches. The measurements provided the opportunity to estimate the longshore

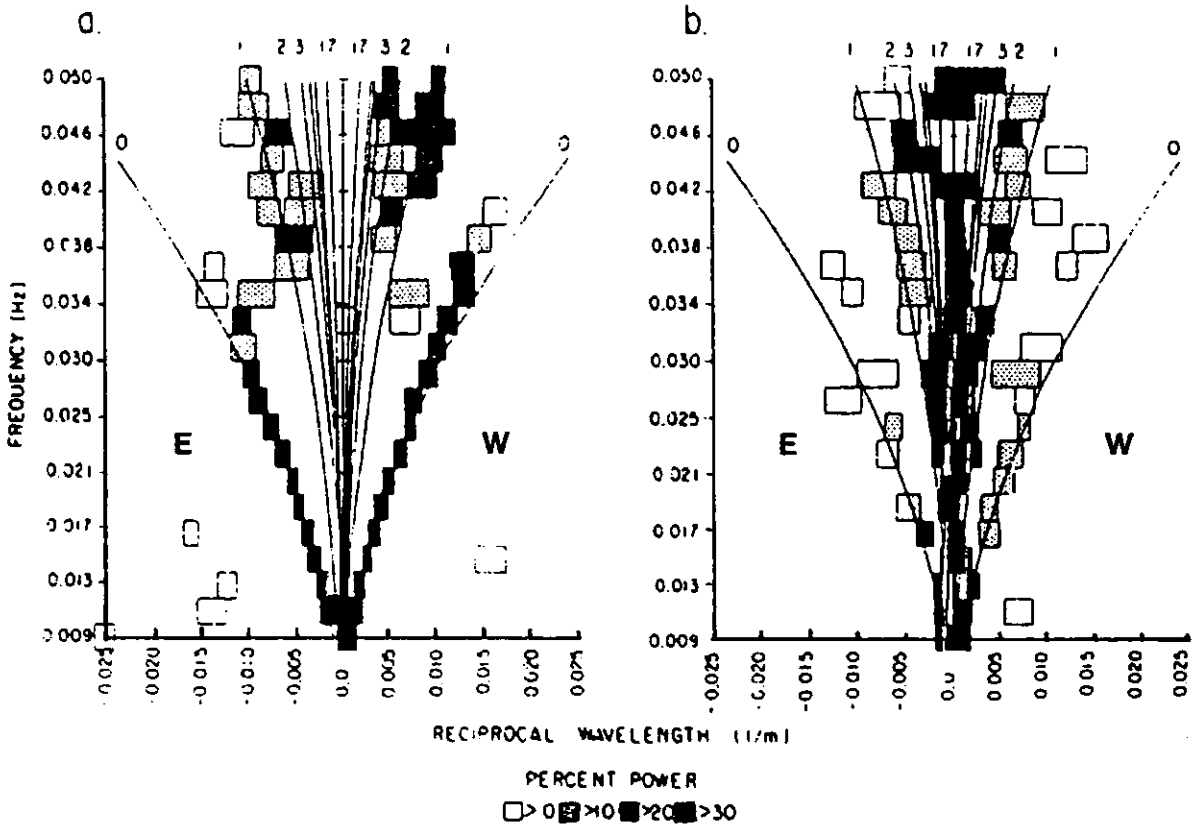

FIGURE 2.13 The longshore (a) and cross-shore (b) current IMLE (iterative maximum likelihood estimator) wavenumber-frequency spectra (with 42 degrees of freedom). The first four and cut-off mode dispersion curves are drawn for $\beta = 0.053$ (from Oltman-Shay and Guza, 1987).

wavenumber-frequency spectrum of motions in the very nearshore. Figure 2.13 shows some of the results from this field experiment, indicating the important contribution made by low mode edge waves to the run-up and longshore component of the infragravity wave velocity field. The low mode signal in the cross-shore velocity field, however, is thought to be masked by either high mode edge, leaky or locally-forced, waves (Huntley *et al.*, 1981; Oltman-Shay and Guza, 1987), or by phase-locking between modes (Huntley, 1988).

Tatavarti (1989) discussed the development of a method for fitting dynamical modes (edge waves and leaky modes) to observed data and describing the infragravity field in terms of the edge and leaky wave motions. Theoretical problems with this work included the choice of topographic smoothing scales both in the long- and cross-shore directions, modelling the spatial forms of the different modes and the incompletely reflected waves and also, the possibility of some forcing of surf beat within, and outside, the surf zone.

(c) FORCED WAVES

Research by Munk (1949) and Tucker (1950) provided some early observations of, and a theory for, the forced oscillation of the sea surface associated with incident wave groups. These oscillations, observed approximately 300m offshore, were well correlated with modulations in the height and period of the incoming short waves. Tucker (1950) established correlation between the low frequency motions and incident waves, with a time lag similar to the required time for the propagation of incident waves to the surf zone, and for the subsequent long wave to be reflected back as a free wave (Figures 2.14 and 2.15).

Incident waves travelling towards the shoreline are known to have a groupy structure, with an alternating sequence of high waves and low waves. Longuet-Higgins and Stewart (1962, 1964), Larsen (1982) and Shi and Larsen (1984) proposed that associated with this incident wave "groupiness" are gradients in the radiation stress and mass flux generating a forced long wave (of infragravity frequency) where a depression of mean sea surface is correlated with groups of high waves and a rise in mean sea

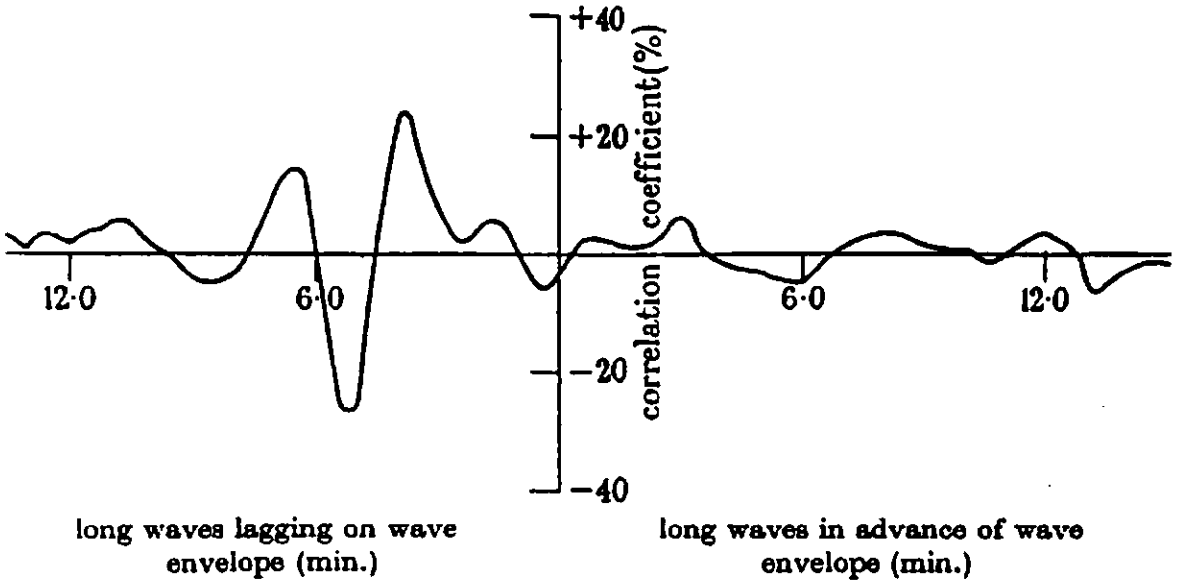

FIGURE 2.14 Correlogram representing correlation between the short wave envelope and the long wave elevation, at different time lags (from Tucker, 1950).

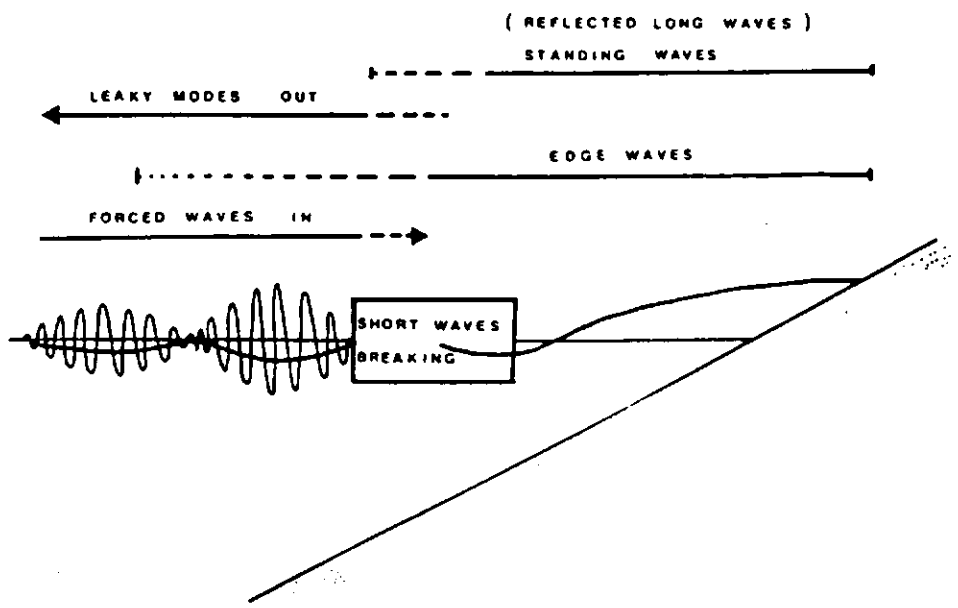

FIGURE 2.15 The various forms of long wave motion on sloping beaches. The top three lines represent free waves, the bottom line represents the forced wave motion (from Huntley and Kim, 1984).

surface corresponds to groups of low waves. Ottesen Hansen (1978) showed theoretically the amplitude of the bound long wave to be proportional to the product of the amplitudes of the corresponding primary waves. Experimental evidence provided by Kostense (1984) confirmed the amplitude of the bound long wave to be of second order in the short wave amplitude.

The mechanism proposed by Longuet-Higgins and Stewart (1964) relates, $\overline{\zeta}$, the mean water level under wave groups, to S_{xx} the onshore component of radiation stress,

$$\overline{\zeta} = \frac{-S_{xx}}{\rho\left(gh - c_g^2\right)} + constant \qquad (2.20)$$

where h is a uniform water depth, c_g is the group velocity and ρ and g are the water density and acceleration due to gravity, respectively. The radiation stress, S_{xx}, is proportional to the square of the amplitude of the incident waves. Eqn. (2.20) is valid when the wave group wavelength is long compared to the water depth, however, at small Ursell numbers ($U_r = ak/(kh)^3$) when the incident waves travel into shallow water c_g tends to c_p, and the shallow water form of Eqn. (2.20) is used,

$$\overline{\zeta} \approx -\frac{3}{4}\frac{ga^2}{\sigma^2 h^2} \qquad (2.21)$$

here, a is wave amplitude, σ is radian frequency. Unfortunately, as Kim (1985) pointed out, the large mean water level changes predicted by this formula as h decreases are not appropriate in the nearshore zone.

Numerous field observations have illustrated the existence of long waves bound to the incoming wave groups (*e.g.* Guza *et al.*, 1984; Huntley and Kim, 1984; Abdelrahman and Thornton, 1987; List, 1986, 1991; Okihiro *et al.*, 1992). Previous field experiments have revealed, as discussed by Battjes (1988), a more or less linear dependence of the low frequency wave amplitude on the incident, short wave amplitude; observed outside the surf zone (Munk, 1949; Tucker, 1950) as well as inside the surf zone (Holman, 1981; Guza and Thornton, 1982).

Techniques for the examination of the incident wave envelope generally follow one of two lines of investigation. Goda (1970) introduced the concept of a 'run' or group of waves, defined as a sequence of waves exceeding a specified value of the wave height without falling below that height. Studies relating the statistical properties

of groups of ocean waves to spectral shape have been conducted by Rye (1974), Goda (1976), Kimura (1980), Elgar *et al.* (1984a,b), Battjes and Van Vledder (1984), Medina and Hudspeth (1990). Elgar *et al.* (1984b) established that such theoretical models which predict wave group statistics, given only the power spectral density, are not appropriate for the majority of ocean spectra, although certain wave group statistics can be predicted by a linear numerical simulation from the energy spectrum. Elgar *et al.* (*op. cit.*) illustrated that such linear simulations can predict wave group statistics adequately until shallower water depths of 2-3m are reached. Beyond these depths, non-linearities become significant and the linear simulation technique becomes invalid for shallow water conditions. This study emphasised the problem concerning the examination of wave groupiness since the majority of wave group analyses have involved the deep water environment. Variation of **wave groupiness** across the surf zone is not well investigated.

An alternative approach that examines the entire envelope function was adopted by Funke and Mansard (1979), Sand (1982), Sobey and Liang (1986), Yasuda *et al.* (1986), Mase (1989) and List (1991). Funke and Mansard (1979) introduced the SIWEH or Smoothed Instantaneous Wave Energy History whereby, the SIWEH is the squared sea-surface time series, smoothed using a Bartlett filter with a width equal to the peak spectral period of the incident waves. List (1991) estimated a **groupiness factor** based upon a similar hypothesis, with the exception that a filter cut-off related to the spectral division between short and long wave components was applied. List (*op. cit.*) examined the variation in his new groupiness factor in both deep water unbroken waves and across the surf zone. He observed that through a wide range of spectral shapes, from storm to swell waves, the groupiness did not vary significantly, also whilst the groupiness decreased through the surf zone a considerable degree of wave height variability persisted even through a saturated surf zone.

The model described by Symonds *et al.* (1988) provides a mechanism for long wave generation by temporal variations of the breakpoint and wave set-up by normally incident wave groups. Energy is transferred to low frequency waves in the nearshore, predicting the same linear dependence of long wave amplitude on incident short wave

amplitude. Schäffer and Svendsen (1988) extended the work by Symonds *et al.* by including long wave forcing outside the surf zone in their model. The long wave forcing/incident wave groupiness decreases across the surf zone, but does not decay completely; their model did not assume the inner surf zone to be saturated. List (1992a, b) extended his wave groupiness research (List, 1986; 1991), by computing a model for the generation of two-dimensional surf beat. The model incorporates an incident wave model providing time-varying radiation stress gradients across the nearshore, and a long wave model which describes the forcing mechanism of the incident waves. In List's model, the wave groups propagate across the nearshore, the bound long wave progressively lags the short wave groups, breaking occurs, the bound long wave is released as a free wave and is then reflected at the shoreline.

Battjes (1988) considered there to be no group structure in the inner surf zone, where the wave field is more or less fully saturated and, subsequently, no forcing occurs at group frequencies. However, recent field measurements have shown that in the nearshore zone of a macro-tidal intermediate beach the wave groupiness can actually persist inside the breaking region and through the surf zone (Foote *et al.*, 1992). Cross-correlating the incident wave envelope with the long wave motion (Figure 2.16) provides a test of the theory that long waves are forced outside the surf zone and that the short waves are modulated by long waves inside the surf zone (*e.g.* Huntley and Kim, 1984; Abdelrahman and Thornton, 1987; List, 1986, 1991; Roelvink and Stive, 1989; Roelvink, 1991).

Abdelrahman and Thornton (1987) examined sea surface elevation time series from the NSTS deployments. Their findings indicated a positive correlation between the incident wave envelope and long period motion *inside* the surf zone, with negative correlation coefficients occurring *outside* the surf zone in deeper water, indicating forced long wave motion (Figure 2.17). Modelling this incident wave group/long wave forcing mechanism was carried out by Roelvink and Stive (1989); their model results were compared with laboratory measurements for two types of beach profile under a range of incident wave conditions. In this work, they included a simple bi-chromatic incident wave field generating a monochromatic forced long wave. For the

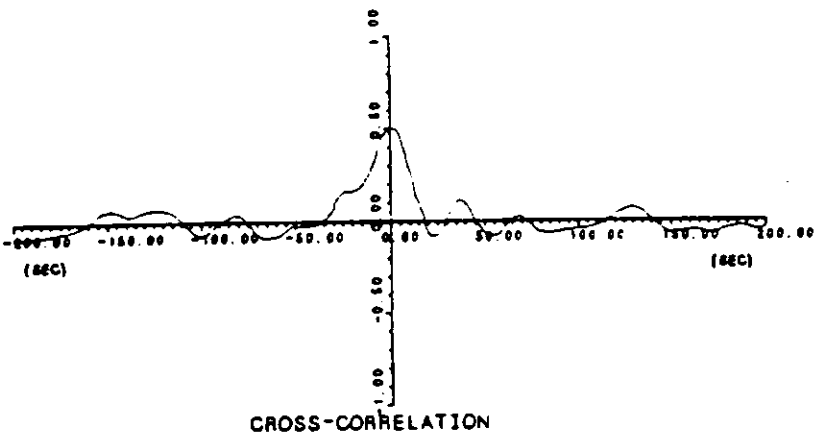

FIGURE 2.16 Cross-correlations between the incident wave envelope and the long period motion have been calculated for time lags up to ± 200 seconds. A positive lag implies that the wave envelope leads the long period motion (from Huntley and Kim, 1984).

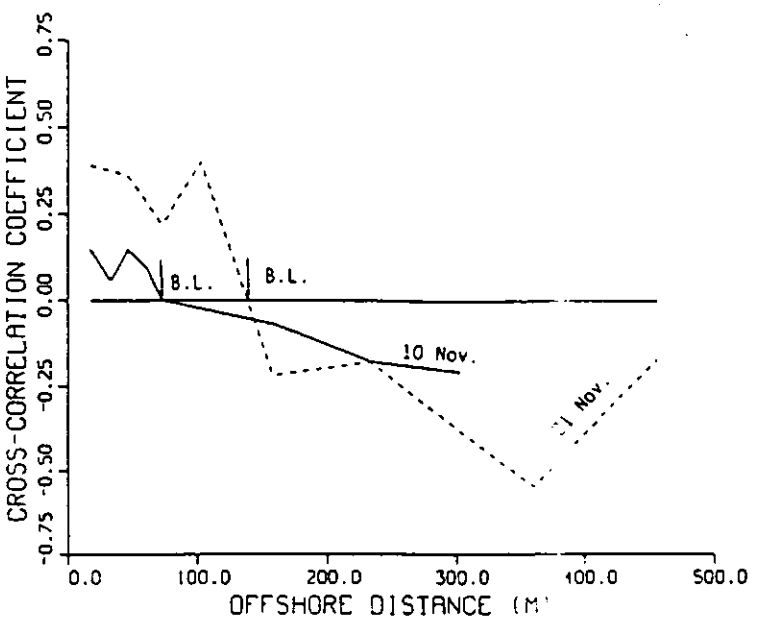

FIGURE 2.17 Spatial distribution of cross-correlation coefficients calculated from measurements obtained at Torrey Pines Beach, California as part of the NSTS. The zero correlation is found to coincide with the approximate location of the breaker line (B.L.), negative values occur consistently outside the surf zone, and positive values occur closer to the shoreline (from Abdelrahman and Thornton, 1987).

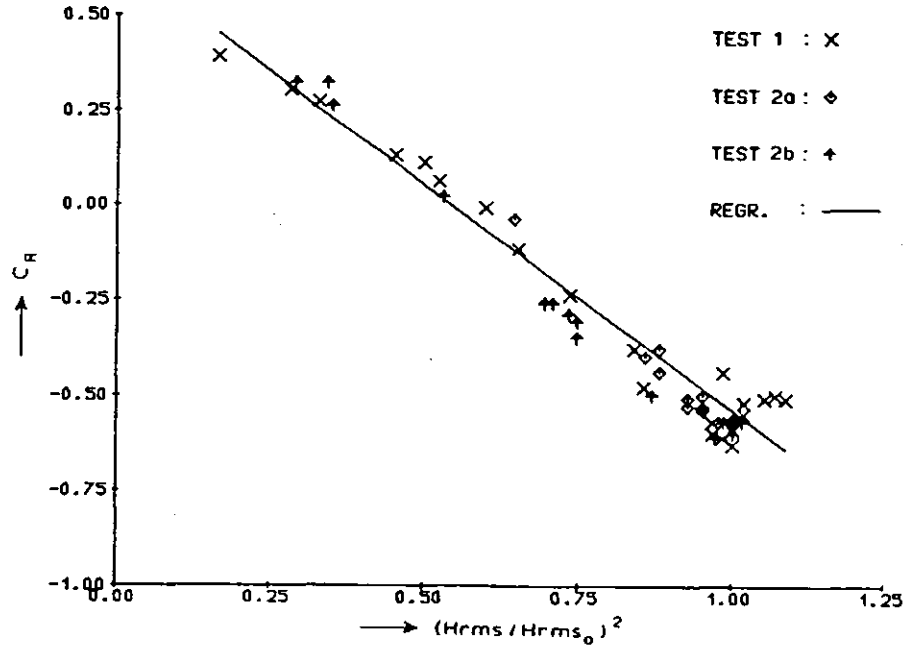

FIGURE 2.18 Laboratory measurements of the correlation coefficient (C_R) between the wave envelope and long wave surface variation, versus the ratio of actual and incident wave energy (from Roelvink and Stive, 1989).

range of conditions examined they observed a linear relationship between wave height and the cross-correlation coefficient (Figure 2.18). Thus, Roelvink and Stive obtained similar results to those of Abdelrahman and Thornton (1987), with positive correlations upon entering the surf zone and high negative correlations offshore. Roelvink (1991) improved this work by developing a time-dependent hydrodynamic model for the dissipation and propagation of wave groups and the bound long waves over an arbitrary profile.

Shi and Larsen (1984) suggested that the passage of a wave group and bound long wave over an erodible bed causes the re-suspension of sediments under high waves which, in conjunction with a negative long wave flow, result in net reverse sediment transport. Hanes (1988) observed the suspension of sand at both the incident wave frequency and at frequencies corresponding to wave groups. Whilst few studies have examined the variations in wave groupiness across the surf zone, where waves are radically transformed, the groupiness of ocean waves is known to be an important characteristic of the climatology of waves both within and beyond the surf zone. Incident wave groupiness contributes significantly to the nearshore wave field. This is demonstrated through the use of groupiness as a driving mechanism in models of long wave generation both in the offshore and nearshore zones (List, 1991), through its role in nearshore bar formation (O'Hare and Huntley, 1994), through its influence on nearshore sediment transport (Vincent *et al.*, 1991; Sato, 1992), and through its effect on coastal and marine structures (Johnson *et al.*, 1978).

2.3.4 FAR INFRAGRAVITY MOTIONS

Whilst the largest part of nearshore zone research has involved the investigation of mean currents and gravity and infragravity motions, recent studies have revealed the phenomenon of 'Far Infragravity Motions' (*e.g.* Bowen and Holman, 1989; Oltman-Shay *et al.*, 1989; Church *et al.*, 1992). Analysis of cross-shore and longshore velocity from the bar-trough region during the SUPERDUCK field experiment revealed energetic, coherent motions with time-scales of hundreds of seconds and wavelengths of hundreds of metres, termed the 'far infragravity (FIG) band' (Figure 2.19). Oltman-

(a)

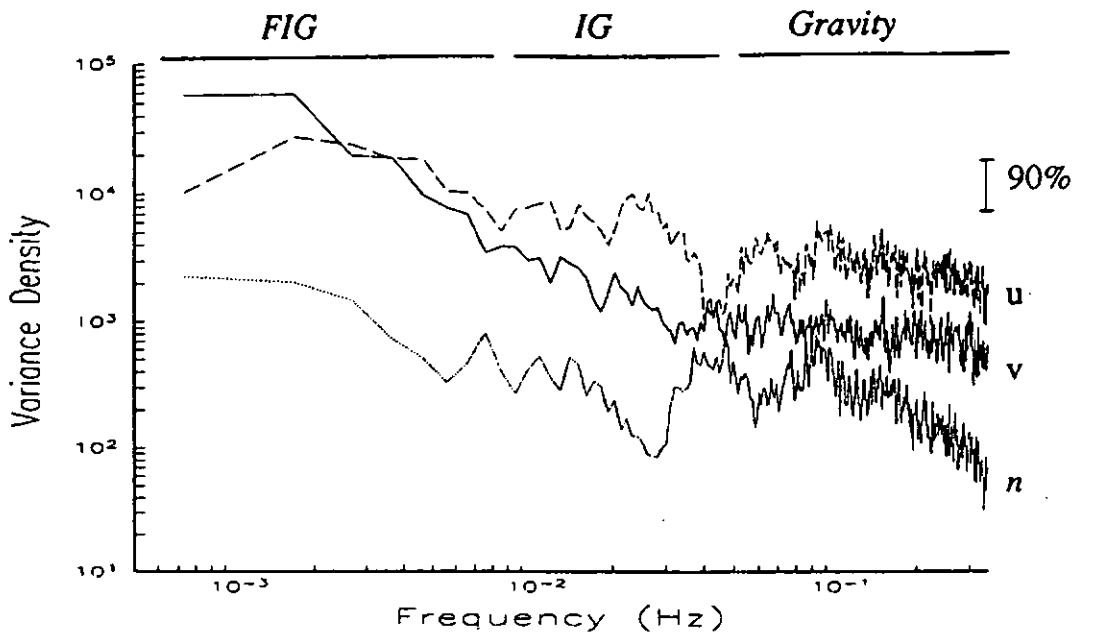

(b)

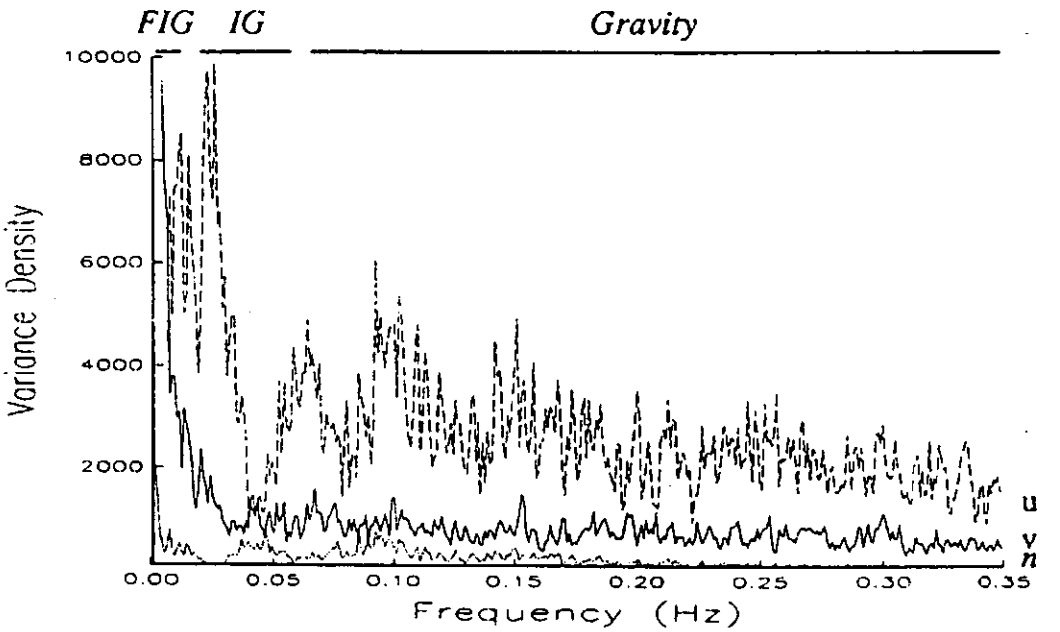

FIGURE 2.19 (a) Log-scaled and (b) variance conserving, linear-scaled variance density-frequency spectrum of longshore (solid, cm^2s^{-1}), cross-shore (dashed, cm^2s^{-1}) velocity and surface displacement (dot, cm). Frequency bands were identified as gravity, infragravity (IG) and far-infragravity (FIG). The vertical line represents the 90% confidence interval (from Oltman-Shay *et al.*, 1989).

Shay *et al.* (1989) describe bi-directional current measurements, which were utilised in order to examine the longshore wavenumber spectrum of sub-incident frequency band motions in the surf zone and show the existence of this far infragravity motion. This new form of nearshore wave, distinct in its kinematics from surface gravity waves, is based upon the shear instability of a steady longshore current (Bowen and Holman, 1989) where the representative frequency is given by 0.07 f_s (f_s is the shear of the seaward face of the longshore current), typically in the range of 10^{-3} to 10^{-2} Hz. Typically, these FIG band motions are characterised by longshore wavelengths and periods of the order of 10^2m and s, respectively, with rms. horizontal velocity amplitudes of at least 30 cms^{-1}. The longshore phase speeds of these motions increase with increasing mean longshore current velocity. They occur only in the presence of a mean longshore current, being uni-directional in behaviour. Bowen and Holman (1989) developed a model for the propagation of FIG band waves, and their results suggest that this shear instability is likely to be more of importance to barred, rather than planar beach environments as a result of the stronger shears expected over a bar crest. Putrevu and Svendsen (1992) conducted a numerical study of shear instabilities over a range of bottom topographies and established that a weak shear in the longshore current is capable of generating significant mixing. Similarly, Church *et al.* (1992) used model generated stream functions to investigate the role of shear instabilities of the longshore current as a source of mixing within the surf zone. Excellent agreement was found between the predicted range of shear instabilities and observations.

An alternative explanation for weak motions in this frequency band, using data from the NSTS field deployment on the planar beach at Torrey Pines, California, was provided by Tang and Dalrymple (1988) who modelled the low frequency signals in terms of a migrating rip current system, driven by a slowly beating incident wave field.

2.4 MODELLING CROSS-SHORE SEDIMENT TRANSPORT ON BEACHES

> "The transport of granular material, such as silt, sand and gravel, by the flow of air or water, in short the transport of sediment, occurs under a variety of natural and man-made conditions. It determines the evolution of river-beds, estuaries and coastlines, and consequently it exerts a considerable influence on the formation of the topography and stratification of the Earth's surface. In the field of civil engineering it is important because it affects the functioning and determines the life span of many hydraulic structures and sea defence works", Yalin (1977).

Despite its importance, understanding sediment transport dynamics is one of the most difficult problems in nearshore process studies. A number of research areas were identified by the Nearshore Processes Workshop (1990) which still require investigation, including developing governing equations for initiation of sediment motion, the role of pore water motion and pressure gradients, the effects of grain size distribution and transport under a range of random waves combined with mean flows. The present study examines cross-shore sediment transport on a macro-tidal intermediate beach, under a spectrum of wave and current conditions.

Beach profile change is reversible. Unlike erosion of cliffs and cohesive shorelines, beach erosion and deposition takes place in response to external forces exerted by waves and currents, fluctuations in water level, and variations in sediment source (Kraus and Horikawa, 1990). Beach profile morphology can change on time scales that range from a single wave period, to daily and seasonal cycles and, ultimately, to long term profile changes over the duration of years.

How can changes in shoreline position and shape be recorded? Bowen and Inman (1966) introduced the analysis of the 'budget of littoral sediments' which occur on beaches, which essentially is the application of the principle of conservation of mass to the littoral sediments. Komar (1983) explains this approach, whereby the various contributions (credits) and losses (debits) are assessed and equated to the net gain or loss (balance of sediments) in a given sedimentary compartment or stretch of coast. The sediment balance relates to the net erosion or deposition of the shoreface. Unfortunately, it is very difficult to quantify the various components of the budget (*e.g.* the losses or gains from the offshore region). As Komar (*op. cit.*) states, the best known component of the budget is the balance itself which is estimated through monitoring rates of erosion or deposition over a period of time. Deposition and erosion

of the shoreface requires that local gradients in the net sediment transport rate occur. The equilibrium condition is satisfied when gradients in the net transport rate are zero everywhere (Osborne, 1990).

In a water column in which sediment concentrations are small, momentum fluxes are caused primarily by fluid turbulence and the weight of sediment is supported by this turbulence. Under these conditions, sediment transport is termed **suspended load**. With increasing depth and increasing proximity to the seabed, sediment concentrations increase until volume concentrations become greater than 9% (Bagnold, 1963) and inter-granular collisions, saltation and creep, become the primary mechanism for vertical momentum flux. Transport promoted by such collisions is termed **bedload**. Other transport mechanisms include, the mass movement of the surface grains, on the seabed, as a fluidised layer (**sheet flow**), and the transport of sediment grains by fluid vortices, formed over and shed from, sand ripples (**vortex load**).

Owing to the complexity and difficulty involved with monitoring these processes, our understanding of sediment transport processes has lagged that of nearshore fluid dynamics (Nearshore Processes Workshop, 1990). Furthermore, greater success has been made in measuring the relevant variables of suspended load transport than those of bedload transport. For instance, the development of such techniques as optical backscatter sensors (*e.g.* Downing *et al.*, 1981), acoustic concentration measuring devices (*e.g.* Thorne *et al.*, 1991; Vincent and Osborne, 1993) and laser techniques (*e.g.* Thornton, 1977) has allowed sampling at the temporal and spatial scales of the turbulence that supports suspended load transport, but no equivalent sensors are available for bedload.

The relationship between sediment transport and beach profile response has been studied extensively over the last couple of decades (*e.g.* Sonu, 1973; Short, 1978; Wright *et al.*, 1978; Dally and Dean, 1984). Nearshore sediment transport studies are usually separated into investigations of **longshore** sediment transport for models of coastal plan shape and on-offshore or **cross-shore** sediment transport for the shore-normal seabed profile. The two studies can then be united in order to examine the full

three-dimensional bathymetry (Hardisty, 1989). Longshore sediment transport processes have generally been more extensively investigated and are, consequently, relatively well understood: cross-shore or orthogonal sediment transport processes, on the other hand, are generally poorly understood. Cross-shore transport is mainly produced by the wave orbital motion, whereas longshore transport is primarily associated with wave-induced longshore currents. In this study, cross-shore sediment transport processes are considered.

2.4.1 CROSS-SHORE SEDIMENT TRANSPORT RATES - THE ENERGETICS APPROACH

Early models for nearshore sediment transport employed bulk empirical formulae based upon the general properties of the incident waves. Existing transport models are generally extensions to these theories, developed originally for the uni-directional conditions of aeolian or fluvial transport (*e.g.* Bagnold, 1963, 1966); such models examine either bedload or suspended load transport. The analysis of sediment transport under the action of waves and currents is generally separated into bedload and suspended load.

Osborne (1990) separates sediment transport models into those which describe force-balance and those which describe energy-balance. The models of force-balance behaviour describe the resisting forces as a function of local sediment and bed characteristics, and the driving forces as a function of the fluid properties. The energy-balance models are Bagnold-type energetics models, which include the effect of beach slope. Local sediment transport rates include expressions for both the driving forces (*e.g.* a function of fluid properties and the hydrodynamics) and the resisting forces (*e.g.* a function of local sediment and bed characteristics). Examples of force-balance models include the work of Einstein (1972), Madsen and Grant (1976), Nielsen *et al.* (1978, 1979, 1988), Hallermeier (1982) and Dally and Dean (1984), which examine either sediment in suspension or bottom sediment. Einstein (1972), for example, assumed a statistical approach in analogy to the bedload transport in uniform flow, incorporating the concepts of particle pick-up and step length. Statistical approaches,

such as Einstein's, need to be supplemented by a description of the suspended load transport, such as the diffusion equation concept of Hom-ma and Horikawa (1963). Conversely, there have been numerous studies which have preferred to adopt the power or energetics model approach. Examples of energetics-based approaches include derivations of the work by Bagnold (1963, 1966), comprising models by Bowen (1980a), Bailard (1981), Bailard and Inman (1981), Guza and Thornton (1985a), Roelvink and Stive (1989). Such models are usually formulated for a time-varying flow field, where waves mobilise the sediment to be transported by currents.

Bagnold (1954) concluded that a fluid energetics or power approach was more fruitful than a force-balance approach. Consequently, Bagnold formulated expressions for the rates of both bedload and suspended load transport, in terms of the power available to displace and transport the sediment (Bagnold, 1963). One primary advantage of the energetics models over the force-balance theories is inclusion of the beach slope in the transport equations. Beach slope can affect sand transport in a variety of manners. The slope may influence local flow conditions; it may alter the threshold conditions and/or it might promote or hinder sediment transport rates, once the grains are in motion, (Whitehouse and Hardisty, 1988). Whitehouse and Hardisty (1988) conducted an experimental assessment of two theories for the effect of beach slope on the threshold of bedload transport. Their experimental results suggested that a marked decrease in threshold velocities occurred on increasingly steeper, negative slopes (downslope) and a general increase for the positive (upslope) case.

Authors such as Bowen (1980a) and Bailard and Inman (1981) include beach slope in their models, suggesting that equilibrium cross-shore transport can be a balance between wave asymmetry and beach slope. Their theoretical results suggested a marked decrease in threshold velocities on increasingly steeper negative slopes (downslope) and a general increase for the positive (upslope) case. King (1991) assessed the possible effect of beach slope on oscillatory flow bedload transport by comparison of laboratory measurements with the models of Bagnold (1963) and Kobayashi (1982). King found that his data supported Bagnold's sloping bed development. His observations gave an order of magnitude support to the hypothesis

that equilibrium cross-shore transport in the bedload regime could be a balance between wave asymmetry and beach slope.

The most detailed development of an energetics model is that of Bailard (1981; Bailard and Inman, 1981), so we will now review this model in more detail. Bailard (1981) developed Bagnold's (1963, 1966) equation for total load sediment transport equation for two-dimensional stream flow where:

$$i = i_B + i_S = \left(\frac{\varepsilon_B}{\tan\phi - \tan\beta} + \frac{\varepsilon_S}{(W/\bar{u})} \right) \omega \qquad (2.22)$$

Here, i is the total immersed weight sediment transport rate, i_B is the bedload transport, i_S is the suspended load transport, ε_B and ε_S are the bedload and suspended load efficiencies, respectively, ϕ is the angle of sediment repose, $\tan\beta$ is the slope of the bed, W is the fall velocity, $\bar{u}$ is the mean velocity and ω is the rate of energy production of the stream. Bagnold (1963) studied stream flow conditions and found $\varepsilon_B \approx 0.13$ and $\varepsilon_S \approx 0.01$.

This energetics-approach describes qualitatively various fundamental morphological phenomena, for example, the 'null-point hypothesis', where coarser particles move onshore and finer grains move offshore (Bowen, 1980a) and the existence of equilibrium beach slopes (Bowen, 1980a; Bailard, 1981). For oscillatory flows, such as those found in the surf zone, another related transport expression was developed by Inman and Bagnold (1963), who defined local slope as a function of the angle of internal friction of the sediment and the ratio of offshore to onshore energy dissipation rates under oscillatory flows,

$$\tan\beta = \tan\phi \left(\frac{1-C}{1+C} \right) \qquad (2.23)$$

where the sediment friction coefficient $\tan\phi$ is a constant (since $\phi \approx$ angle of repose of the material) and C is the ratio of the amount of energy dissipated during the seaward sediment flow divided by the amount of energy dissipated during the shoreward sediment flow. The energy dissipation ratio (C) is assumed to be represented by the horizontal asymmetry in the cross-shore velocity field (*e.g.* Inman and Frautschy, 1966). In this expression, the importance of an asymmetrical velocity distribution to cross-shore bedload transport is illustrated for an equilibrium beach slope, where the horizontal asymmetry in the cross-shore velocity field is assumed to be represented by the

energy dissipation ratio (C). Osborne (1990) suggests that an offshore asymmetry (values of $C > 1.0$) results in a negative gradient or shorewards slope, observed on barred beach profiles.

Also using Inman and Bagnold's (1963) basic ideas, Bailard and Inman (1981) derived the following equation for the equilibrium beach slope

$$\tan \beta = \tan \phi \frac{\langle \tilde{u}^3 \rangle}{\langle |\tilde{u}|^3 \rangle} \tag{2.24}$$

where $\tilde{u}$ is the cross-shore oscillatory velocity and it is assumed that bedload transport occurs without any mean flows, <> denote time-averaging and || denotes the magnitude of $\tilde{u}$. In deriving this expression, the quadratic stress law is assumed to apply to the instantaneous velocity (where τ is shear stress),

$$\tau = \rho f_w \tilde{u}_t |\tilde{u}_t| \tag{2.25}$$

where f_w is the wave friction factor for fully turbulent flows (Jonsson, 1966), ρ is water density, $u_t = u_m \cos \sigma t$, where $\tilde{u}_t$ is the total instantaneous velocity vector, u_m is the maximum near-bed orbital velocity and σ is angular frequency. Guza and Thornton (1985a) point out that the quantity $<\tilde{u}^3>/<|\tilde{u}|^3>$ in Eqn. (2.24) does not represent skewness, which is usually represented by $(<\tilde{u}^3>/<\tilde{u}^2>^{3/2})$.

Bagnold (1963) superimposed a steady current, of arbitrary strength, on the wave-induced oscillatory motion which results in transport of the sediment in the direction of the steady current, and the following total load sediment transport model

$$i_\theta = K' \omega \frac{u_\theta}{u_m} \tag{2.26}$$

where i_θ is the time-averaged immersed weight sediment transport rate per unit width in the θ direction, u_θ is the steady current in the θ direction and u_m is the maximum orbital velocity, ω is the local rate of energy dissipation and K' is a dimensionless constant.

Equation (2.26) has been incorporated, in some form, into several models for longshore transport, including the work by Inman and Bagnold (1963), Komar (1971), Bailard and Inman (1981) and Guza and Thornton (1985a). Guza and Thornton (1985a) discuss how such models, for example Eqn. (2.24), show an explicit dependence on the first three velocity field moments (*i.e.* averages of the velocity,

velocity squared and cubed) but they are not technically Bagnold-derived expressions, which is assumed to be their source. One problem here is that the time-averaged sediment transport rate should be obtained by time-averaging the instantaneous transport rate, and this is not included in such models. Consequently, Guza and Thornton (1985a) carried out more accurate time-averaging to obtain a further set of transport equations which are discussed here. Guza and Thornton (1985a) examined the transport equations derived by Bowen (1980a,b) and Bailard (1981) which are, in turn, systematically derived from the work by Bagnold (1963, 1966) for total load sediment transport under stream flow conditions. The predictor for the total time-averaged immersed weight sediment transport, given by Bailard, is written as:

$$\left\langle \vec{i}_t \right\rangle = \rho C_f \frac{\varepsilon_B}{\tan\phi}\left[\left\langle |\vec{u}_t|^2 \vec{u}_t \right\rangle + \frac{\tan\beta}{\tan\phi}\left\langle |\vec{u}_t|^3 \right\rangle \hat{i}\right] + \rho C_f \frac{\varepsilon_S}{W}\left[\left\langle |\vec{u}_t|^3 \vec{u}_t \right\rangle + \frac{\varepsilon_S}{W}\tan\beta \left\langle |\vec{u}_t|^5 \right\rangle \hat{i}\right] \tag{2.27}$$

In this expression, ρ is the mass density of the water, C_f is a drag coefficient, ε_B and ε_S are the bedload and suspended load efficiencies, $tan\phi$ is the sediment friction coefficient, $\vec{u}_t$ is the total instantaneous velocity vector, $tan\beta$ is the local bed slope, $\hat{i}$ is the unit vector in the onshore direction, W is the fall velocity of the sediment and <> denotes a time-averaged quantity. Bagnold's stream-based total load sediment transport model (Eqn. (2.27)) is a special case of Eqn. (2.22), since both equations are equal when $\tan\beta << 1$ and $\vec{u}_t = -\vec{u}\hat{i}$. The velocity, $\vec{u}_t$ may have contributions from several fluid motions, including short-period incident waves, a steady current such as the wave-induced longshore current, the return flow under wave action (undertow), and long-period waves.

Although they are similar, one important difference between the Bowen and Bailard models are the equations, adopted by the two authors, to describe instantaneous suspended load transport and, more specifically, the expressions used to predict auto-suspension (γ). Bailard's expression for suspended load transport (Eqn. 2.28), differs from that of Bowen (Eqn. 2.29), by the inclusion of the factor ε_S in the denominator of Bailard's equation for the magnitude of the suspended sediment transport rate,

Bailard

$$\left|\vec{i}_s\right| = \frac{\varepsilon_s \omega}{\left[(W/\bar{u}) - \varepsilon_s \tan \beta\right]}, \quad \omega = \rho C_f |\vec{u}|^3 \text{ and } \gamma = \varepsilon_s \beta / W \tag{2.28}$$

Bowen

$$i_s = \frac{\varepsilon_s C_f \rho}{W(1 - \gamma u)} \cdot u^3 |u|, \text{ and } \gamma = \beta / W \tag{2.29}$$

The expression derived by Bailard means that auto-suspension does not occur. Subsequent expansion of the denominator, in his instantaneous suspended load equation, and time-averaging provides a further expression for the suspended sediment transport. Only the first two terms of this expansion are used by Bailard in the suspended load part of his total sediment transport model. Auto-suspension conditions can occur relatively frequently when using a model such as Bowen's, however, which is in agreement with Bagnold's equations. This, as Bailard points out, leads to momentary infinite offshore suspended sediment transport rates, where the expansion of the denominator in the instantaneous suspended load transport formula will not converge, and the suspended load transport model proposed by Bowen (1980a,b) will be inappropriate. The difference between the Bagnold/Bowen suspended load transport models, and that of Bailard, should prove negligible for the small bed slopes normally found in stream flow conditions, however, it becomes more potentially important, with respect to real beach slopes. The existence or otherwise of auto-suspension has not yet been resolved.

Guza and Thornton (1985a, hereafter GT85) considered the two proposals and concluded that Bailard's workings to be more appropriate when tested with field data. Extending this analysis, GT85 decomposed the total velocity field into oscillatory (˜) and mean (¯) components, and cross-shore (x) and longshore (y) directed components

$$\vec{u}_t = (\tilde{u} + \bar{u})\,\hat{i} + (\tilde{v} + \bar{v})\,\hat{j} \tag{2.30}$$

and $\hat{i}, \hat{j}$ are unit vectors in the x and y directions, respectively. The next step taken by GT85 is the substitution of Eqn. (2.30) into Eqn. (2.27) which generates equations for the average cross- and longshore sediment transport rates,

$$\langle i_x \rangle = \rho C_f \frac{\varepsilon_B}{\tan \phi} \left(\begin{array}{l} \langle \tilde{u}^3 \rangle + \langle \tilde{u}\tilde{v}^2 \rangle + \langle \tilde{u}^2 + \tilde{v}^2 \rangle \bar{u} + 2\langle \tilde{u}^2 \rangle \bar{u} + 2\langle \tilde{u}\tilde{v} \rangle \bar{v} + \bar{u}\bar{v}^2 + \bar{u}^3 \\ \quad + \dfrac{\tan \beta}{\tan \phi} \langle |\tilde{u}_t|^3 \rangle \end{array} \right)$$

$$+ \rho C_f \varepsilon_S W^{-1} \left(\langle |\tilde{u}_t|^3 \tilde{u} \rangle + \langle |\tilde{u}_t|^3 \bar{u} \rangle + \varepsilon_S \tan \beta W^{-1} \langle |\tilde{u}_t|^5 \rangle \right) \quad (2.31)$$

$$\langle i_y \rangle = \rho C_f \frac{\varepsilon_B}{\tan \phi} \left(\langle \tilde{v}^3 \rangle + \langle \tilde{u}^2 \tilde{v} \rangle + \langle \tilde{u}^2 + \tilde{v}^2 \rangle \bar{v} + 2\langle \tilde{v}^2 \rangle \bar{v} + 2\langle \tilde{u}\tilde{v} \rangle \bar{u} + \bar{u}^2 \bar{v} + \bar{v}^3 \right)$$

$$+ \rho C_f \varepsilon_S W^{-1} \left(\langle |\tilde{u}_t|^3 \tilde{v} \rangle + \langle |\tilde{u}_t|^3 \bar{v} \rangle \right) \quad (2.32)$$

In this expression $|\tilde{u}_t| = \left[\tilde{u}^2 + \tilde{v}^2 + \bar{u}^2 + \bar{v}^2 + 2(\tilde{u}\bar{u} + \tilde{v}\bar{v}) \right]^{1/2}$.

Bailard (1987) simplified the time-averaged cross-shore sediment transport rate, $\langle i_x \rangle$, assuming weak mean currents and small incident wave angles, as

$$\langle i_x \rangle = \rho C_f u_m^3 \left\{ \begin{array}{l} \dfrac{\varepsilon_B}{\tan \phi} \left[\psi_1 + \dfrac{3}{2} \delta_u - \dfrac{\tan \beta}{\tan \phi} (u3)^* \right] \\ \quad + \varepsilon_S \dfrac{u_m}{W} \left[\psi_2 + 4(u3)^* \delta_u - \varepsilon_S \dfrac{u_m}{W} \tan \beta \, (u5)^* \right] \end{array} \right\} \quad (2.33)$$

GT85 defined the various moments in this transport equation as

$$u_m^2 = 2\langle \tilde{u}^2 \rangle \qquad \psi_1 = \langle \tilde{u}^3 \rangle / u_m^3 \qquad \psi_2 = \langle |\tilde{u}|^3 \tilde{u} \rangle / u_m^4$$

$$\delta_u = \bar{u}/u_m \qquad (u3)^* = \langle |\tilde{u}|^3 \rangle / u_m^3 \qquad (u5)^* = \langle |\tilde{u}|^5 \rangle / u_m^5$$

Bailard (1987) examined the behaviour of surf zone wave velocity moments using data collected at Torrey Pines and Leadbetter Beaches, as part of the NSTS experiment. Spatially-averaged moments were substituted into the cross-shore sediment transport equation (Eqn. 2.31) along with representative values for each free parameter (*e.g.* water density, sediment fall velocity, transport efficiencies *etc.*). Bailard estimated cross-shore sediment transport rate as a function of the significant wave height and average beach slope (Figure 2.20), finding the energetics-based estimations of cross-shore sediment transport rate to exhibit several realistic characteristics. For example, for a given beach slope, the cross-shore sediment transport rate was weakly onshore for small wave heights and strongly offshore for large wave heights. He concluded that the surf zone velocity moments played an important role in controlling cross-shore transport processes.

GT85 examined the case of sediment transport under monochromatic uni-

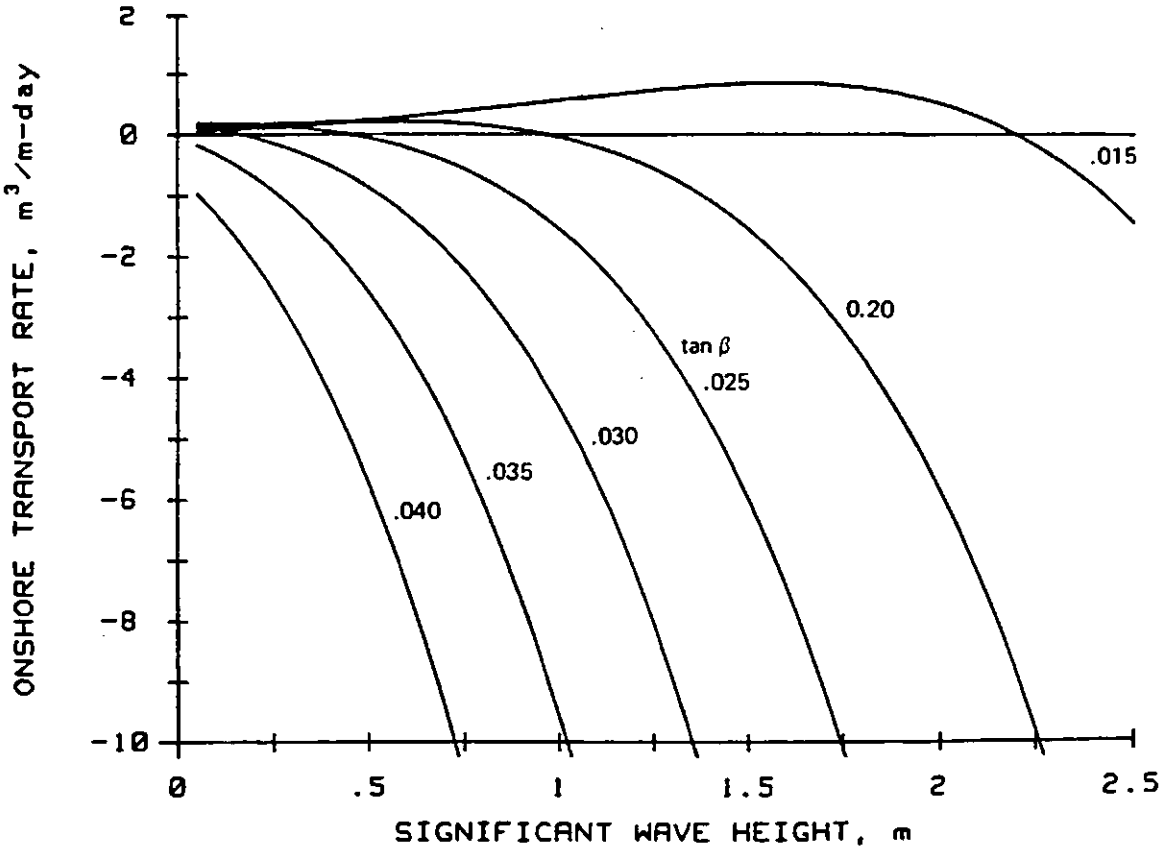

FIGURE 2.20 Onshore sediment transport rate versus the significant wave height and average beach slope. The cross-shore sediment transport rate was estimated using spatially-averaged velocity moments and representative values for each of the free parameters (from Bailard, 1987).

directional wave conditions, and also for random seas. They considered the special case of only cross-shore oscillatory velocities with no longshore transport, where the resulting cross-shore transport rate is described by,

$$\langle i_x \rangle = \left[\rho C_f \frac{\varepsilon_B}{\tan \phi} \left\{ \langle \tilde{u}^3 \rangle + \frac{\tan \beta}{\tan \phi} \langle |\tilde{u}|^3 \rangle \right\} \right] \text{Bedload}$$

$$+ \left[\rho C_f \frac{\varepsilon_S}{W} \left\{ \langle |\tilde{u}|^3 \tilde{u} \rangle + \frac{\varepsilon_S}{W} \sin \beta \langle |\tilde{u}|^5 \rangle \right\} \right] \text{Suspended Load} \qquad (2.34)$$

In this expression, even moments do not critically depend upon cross-shore velocity asymmetry, either because they are even powers ($\tilde{u}^2$) or odd powers of absolute values ($|\tilde{u}|^3$, $|\tilde{u}|^5$). As Osborne (1990) states, these even moments do not influence the directionality of the sediment transport; however, as the terms are non-zero for symmetric velocities, they do influence the magnitude of the transport. Odd moments ($<\tilde{u}^3>$, $<|\tilde{u}^3|\tilde{u}>$) in the expression above, are zero for symmetric motions but can be non-zero for asymmetric (non-linear) motions, and it is these terms which control the direction of net transport.

GT85 compared Gaussian and monochromatic wave moments. Modelling the nearshore velocity field as a linear, Gaussian, random process resulted in reasonably accurate predictions of some normalised moments, and poor predictions of others. No moments were accurately given by the monochromatic, uni-directional wave model. Monochromatic, uni-directional transport equations (GT85) were compared to the unsimplified forms (Eqns. 2.29 and 2.30) which were re-expressed in a generalised form,

$$\langle i_x \rangle = \rho C_f u_m^3 \left\{ \frac{\varepsilon_B}{\tan \phi} \left[\psi_1 \cos \alpha_1 + \delta_u^3 + \delta_u \left(\frac{1}{2} + \cos^2 \alpha_2 + \delta_v^2 \right) + \delta_v \sin \alpha_3 \cos \alpha_3 + \frac{\tan \beta}{\tan \phi} (u3)^* \right] + \frac{u_m}{W} \varepsilon_S \left[\psi_2 \cos \alpha_5 + \delta_u (u3)^* \right] + \frac{u_m^2}{W^2} \varepsilon_S^2 \tan \beta (u5)^* \right\} \qquad (2.35)$$

where the relative steady current strengths, δ, δ_u , and δ_v are,

$$\delta = \bar{u}_T/u_m \qquad \delta_u = \bar{u}_T/u_m \cos\theta \qquad \delta_v = \bar{u}_T/u_m \sin\theta$$

and the angles of incidence α_n, are equal for monochromatic, uni-directional plane wave conditions, where $\bar{u} = (\bar{u}^2 + \bar{v}^2)$ and θ, the mean current angle is defined as $\tan\theta$

= $\bar{v}/\bar{u}$ whilst the monochromatic velocity amplitude, u_m, is related to total oscillatory variance,

$$u_m^2 = 2\,(\langle\tilde{u}^2\rangle + \langle\tilde{v}\rangle) \qquad (2.36)$$

Field data from the NSTS experiment were used to examine the relevant moments and identify which terms were largest in this cross-shore sediment transport equation. From their observations, GT85 concluded that both oscillatory asymmetries, and combined mean flow-wave variance terms, to be important to cross-shore sediment transport. Asymmetries in the oscillatory wave field tended to transport sediment *onshore*, while the interaction of the offshore mean flow with waves, produced an *offshore* sediment flux. (Note, that Table 3 in this paper (GT85) which describes the relative magnitudes of the velocity terms, representing the largest terms in the cross-shore transport equation, has the terms describing suspended load transport inadvertently juxtaposed with those terms representing the bedload transport. Mismatching of terms and labels in this way provides a plausible explanation as to why Guza and Thornton found the net *bedload* transport to be several times greater than the *suspended load* transport when in reality the reverse is likely to be true).

Energetics-based models are considered to offer a promising 'meso-scale' approach to describing sediment transport (*e.g.* Kraus and Horikawa, 1990). Disadvantages of the Bailard approach to sand transport modelling include, the use of empirical coefficients (*e.g.* constant bedload and suspended load efficiency factors) and the definition of the near-bottom velocity. The use of time- and depth-averaged flow and sediment load parameters denies any input of a knowledge of the vertical variations which occur in the cross-shore flows and suspended sediment flux, which can cause phase differences between the sediment response and the flow. Furthermore, using vertically-integrated equations, sediment transport is assumed to respond to the near-bottom water velocity in an instantaneous, quasi-steady manner. Guza and Thornton (1985a) also found that the higher the moment, the greater the differences between model predictions of the moment values. A planar bed is assumed in the Bailard model, which is not always suitable for certain natural beach environments. Inman and Bowen (1963), for example, observed in their laboratory experiment, complex phase-

dependent behaviour associated with vortex-induced sediment suspension over ripple crests, in the present of waves and currents. A model such as Bailard's is, therefore, more likely to be accurate if used to describe sediment transport within the surf zone, where plane bed conditions exist.

2.4.2 MOMENTS OF THE CROSS-SHORE VELOCITY FIELD

A small amplitude wave progressing over a horizontal bed can be described by linear wave theory which predicts a purely sinusoidal orbital velocity above the bed. Where the wave has finite amplitude, non-linear effects arise whereby the wave profile is no longer symmetrical about the mean water level. The parameter **skewness** is defined statistically as the degree of asymmetry of a distribution.

Cornish (1898) recognised that an asymmetry of the orbital velocity field, described in terms of the higher harmonics of the fundamental motion, could become important as the waves shoaled. Stokes (1847) had even earlier proposed that the onshore velocity associated with the wave crest, to be stronger and of shorter duration than the offshore velocity associated with the wave trough. Models such as the one proposed by Bailard (1981) allow prediction of the instantaneous (time-varying) rate of sediment transport from which the net (time-averaged) rate of sediment transport, can be calculated. Needless-to-say, the problem is to obtain both predictions and measurements of the net rate of cross-shore sediment transport. Net sediment transport in a wave-dominated environment arises from the differences in the rate at which sediment is transported back and forth with the oscillatory wave motion. Such differences occur with the second order effects such as wave asymmetry, wave-induced mass transport currents and superimposed tidal or wind-induced currents and the bottom slope.

Calculation of the moments of the statistical distribution of the local velocity components (u, v) is an informative procedure in the investigation of the nearshore velocity field (*e.g.* Doering, 1988) and, as seen previously, velocity moments are often incorporated into sediment transport formulae. Various sediment transport models describe transport as proportional to u^n, where n has a range of values, usually between

3 (Inman and Bagnold, 1963) and 6 (Madsen and Grant, 1976). Hanes and Huntley (1986) state that, if such models are valid, then the amount of material in suspension in the water column must be proportional to u^{n-1} (but were unable to determine n due to scatter in their data). Other workers have conducted a similar line of research. For example, Russell (1994) scrutinised time series of suspended sediment concentrations obtained on a macro-tidal beach. Instantaneous near-bed SSC's during major suspension events were found to be predicted reasonably well by the cube of the offshore directed velocities, well above the threshold for sediment suspension.

The moments most often applied to sediment transport modelling are the mean, variance (a measure of wave energy) and skewness (a measure of wave asymmetry). The mean component, $\langle u \rangle$, of cross-shore current velocities indicates the direction and magnitude of the mean flows. Variance of the cross-shore orbital velocity, defined as $\langle u^2 \rangle$, provides a measure of the wave activity such as, for example, the ability to move sediment; it is directly related to the local wave height. Second-order statistics, such as the variance, provide no details of the wave shape, and cannot be incorporated into cross-shore sediment transport models that are sensitive to velocity or acceleration skewness and asymmetry (Elgar *et al.*, 1990). It is the skewness of the orbital velocity field, defined as $\langle u^3 \rangle / \langle u^2 \rangle^{3/2}$, which provides some measure of the non-linearity of the system (Doering and Bowen, 1985). Cross-shore sediment transport theories such as those by Bowen (1980a) and Bailard (1981, 1987), discussed previously, generate various moments, of which the relative magnitudes and distributions across the nearshore region are not well known.

Skewness, asymmetry and other higher-order moments are intrinsically non-linear properties, where linear finite depth theory is invalid for describing their variation across the nearshore zone (Elgar and Guza, 1985; Elgar *et al.*, 1990). Asymmetry of the surface profile is witnessed in the near-bed velocity which has a greater forward velocity of shorter duration under the wave crests, and smaller backward velocity of longer duration under the troughs, than is predicted by small amplitude wave theory (Madsen and Grant, 1976). Asymmetry of the wave orbital velocity field is created by a saw tooth-shaped elevation waveform, which may or may

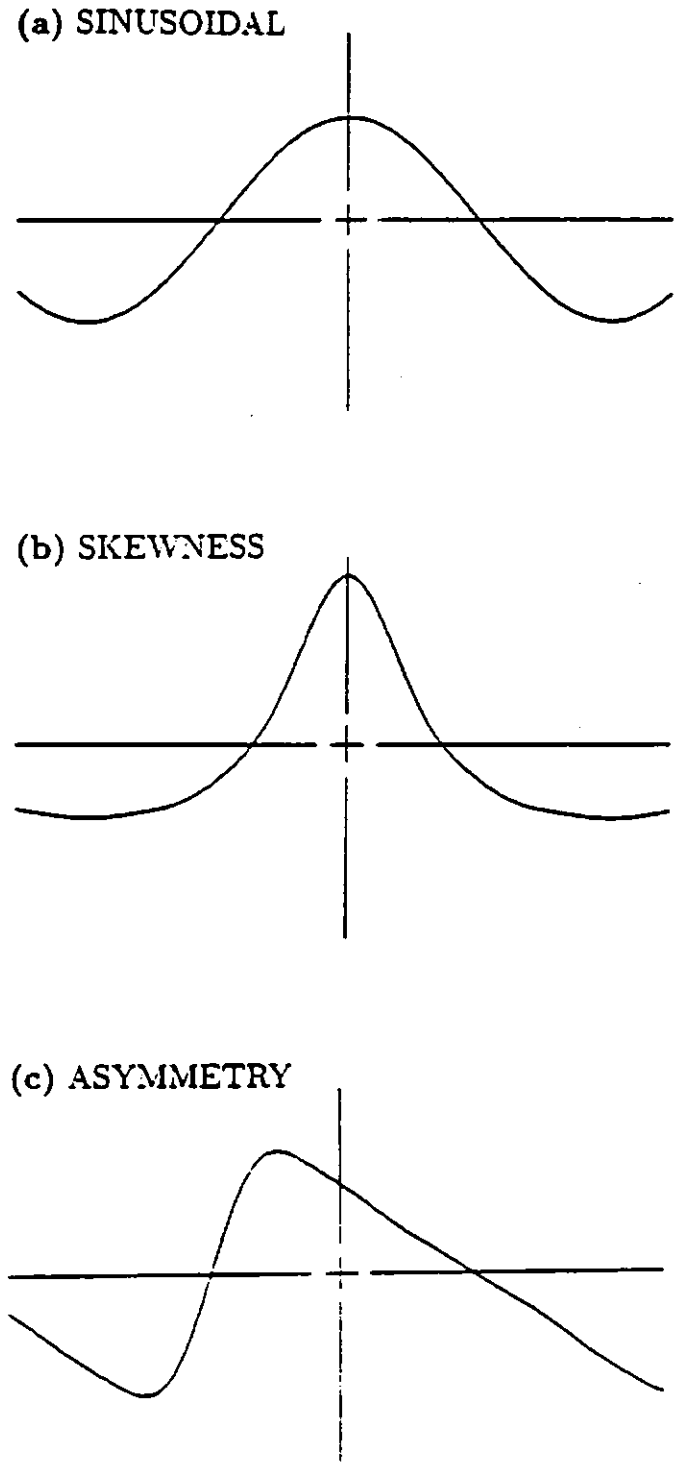

FIGURE 2.21 (a) Schematic showing a sinusoidal profile that is symmetric, with respect to both the horizontal and vertical. (b) A skewed profile, that lacks symmetry with respect to the horizontal, and is vertically symmetric. (c) An asymmetric profile, that lacks symmetry with respect to the vertical, and is horizontally symmetric (from Doering, 1988).

not possess skewness.

The variance of shoaling gravity waves is known to increase towards the shoreline, wave profiles are also known to evolve from sinusoids (Figure 2.21), in deeper water, to positively skewed shapes and then to vertically asymmetrical, saw tooth shapes just before breaking occurs. This transformation can be described by the evolution of third moments, skewness S and asymmetry A, which reflect the deviations from symmetry about the horizontal and vertical axes, respectively. A saw tooth shape (steep front faces and gently sloping rear faces, but crests and troughs of equal amplitudes) has $S=0$, and $A\neq0$, whereas, a Stokes-type wave shape (broad, low troughs and narrow, tall crests, but has both symmetric front and back faces) has $S\neq0$, but $A=0$ (Elgar *et al.*, 1990). Asymmetry refers, therefore, to the difference between the front and rear wave-face profiles. Skewness, on the other hand, describes the difference between the wave crest and trough profiles (Figure 2.21).

Skewness of the flow is often associated with the mobilisation, suspension and transport of sediment, in line with the suggestion that cross-shore variation of skewness might lead to the convergence and divergence of sediment in the nearshore (Doering and Bowen, 1988). It should be noted that for sediment transport, it is the skewness of the velocity which is important, not the surface shape of the wave. Roelvink and Stive (1989) conducted laboratory experiments towards understanding the cross-shore flow mechanisms which promote bar formation. They suggested that a transport formulation employing some near-bed flow property such as the asymmetry of the acceleration, in order to include a non-instantaneous property, might be a successful approach. Previously, Bowen (1980a) also realised the need for a sediment transport model which included various non-linear hydrodynamic factors such as the mass transport (drift) velocity, the wave orbital characteristics including the higher harmonics, and any additional flow patterns due to, for example, wave-induced nearshore circulation. Since the net sediment transport, and undoubtedly the existence of the beach itself, are critically dependent on the small departures from symmetry in the on-offshore velocity field, it is difficult to test the adequacy of any sediment transport model without a reasonable knowledge of the hydrodynamics.

The relatively recent design and construction of fast-response instrumentation, such as electro-magnetic current meters, has enabled the collection of extensive, accurate sets of flow speed data, in the nearshore zone. Presently, it is the velocity field, in the water column, which can be determined more accurately than any parameter directly related to sediment transport. Examination of the spatial distribution and magnitude of such parameters is, therefore, a more fruitful research pathway. Doering and Bowen (1988) analysed data collected as part of the Canadian Coastal Sediment Study. The field measurements showed sediment response to correlate well with both individual waves and wave groups. Sediment concentration responded strongly to the onshore flow associated with wave crests, but very weakly to the offshore flow associated with a wave trough. Their field measurements indicate the behaviour of sediment concentration and sediment transport to be dependent upon a high power of the velocity with very little time lag. Several experiments have examined the variation of velocity skewness across the nearshore (*e.g.* Bailard, 1981; 1987; Bowen, 1980a,b; Guza and Thornton, 1985a; Bowen and Doering, 1984; Doering, 1988; Roelvink and Stive, 1989; Elgar *et al.*, 1990; Roelvink, 1991; 1993; Greenwood and Osborne, 1991). Doering and Bowen (1985) used NSTS (Nearshore Sediment Transport Study) field data to examine the spatial distribution of some moments of the nearshore velocity field. Skewness is plotted as a function of depth, and in deep water, the skewness tends to be small, increasing slightly only when the wave shoals (Figure 2.22). Doering and Bowen compared their C^2S^2 results, with NSTS field measurements (see Bowen and Doering, 1984), which showed skewness values increasing from zero at the shoreline to a maximum value at the breaker region with skewness values decreasing again offshore (Figure 2.23). The skewness and asymmetry were parameterised in terms of the local depth and the Ursell number. Both moments showed some functional dependence on the two parameters but with considerable scatter in the data. Doering and Bowen found the parameterisation of these velocity moments to be a difficult process.

Most often, such studies of velocity skewness using current meter data, consider <u>total</u> skewness estimates, which include the contributions from all resolvable

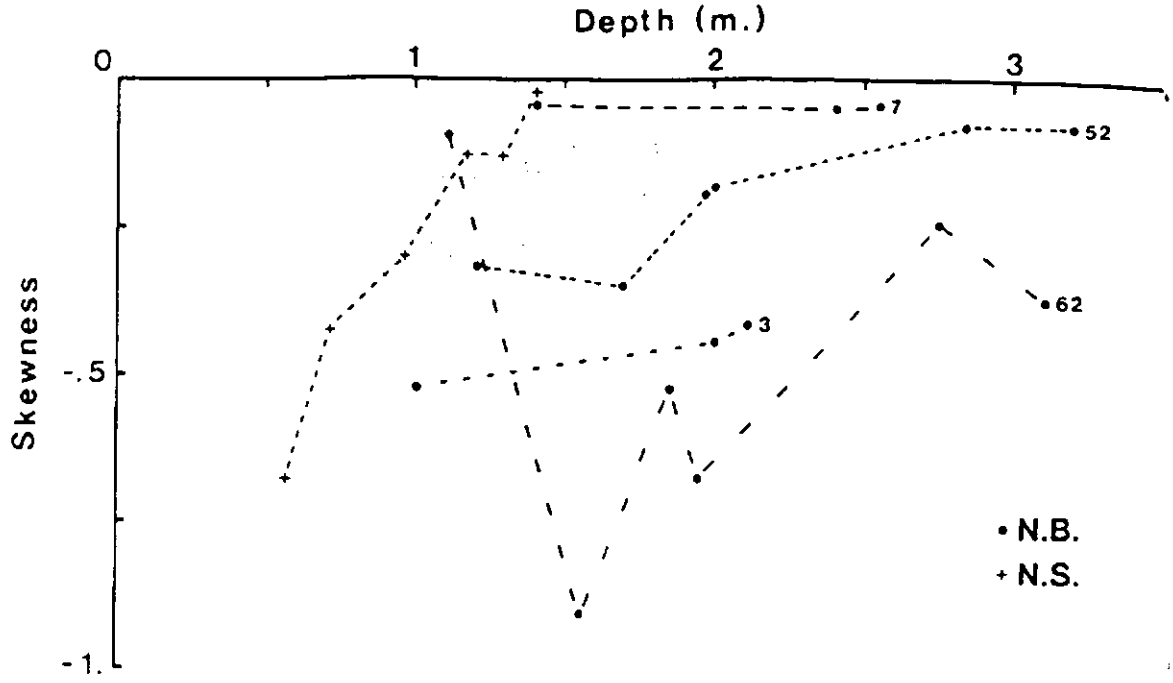

FIGURE 2.22 Skewness is plotted as a function of depth. The skewness is small in deep water, tending to increase as the wave shoals, N.B. is New Brunswick, N.S. is Nova Scotia (from Doering and Bowen, 1985).

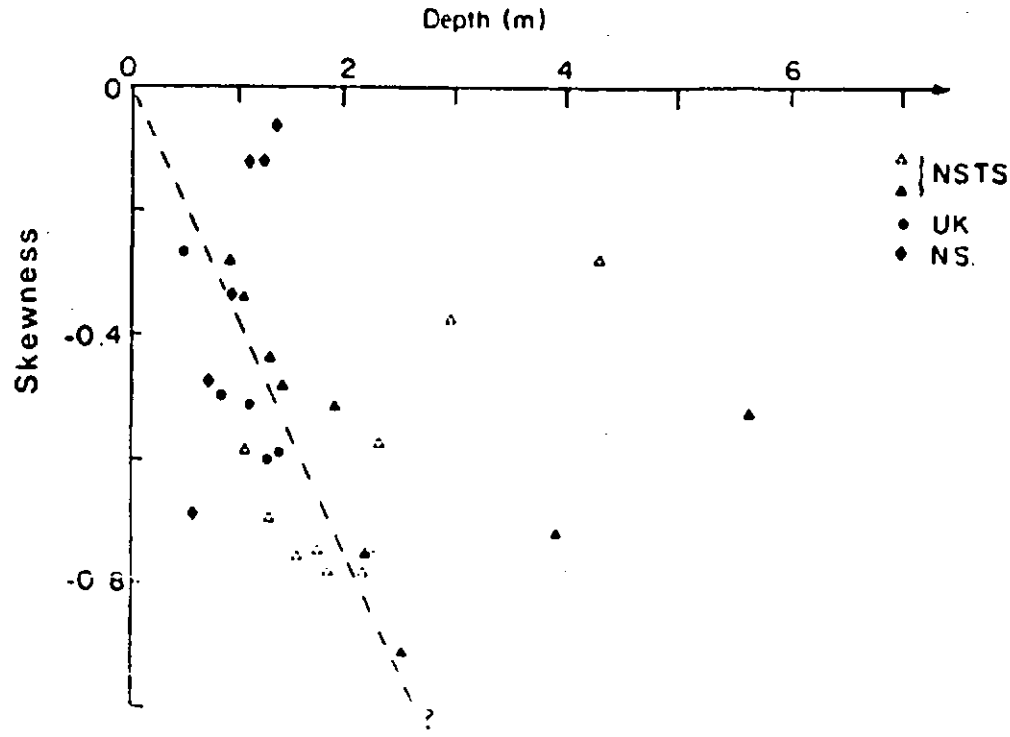

FIGURE 2.23 Skewness as a function of depth for data from NSTS, U.K. and Queensland, Nova Scotia. Where skewness is defined in the normal statistical sense as $\langle u^3 \rangle / \langle u^2 \rangle^{3/2}$. The data from inside the surf zone on the NSTS and U.K. beaches, lie on a straight line increasing from zero at the shoreline to a maximum value in the breaking region with skewness decreasing offshore. The Queensland data, however, cuts across the general trend, but does increase onshore to a maximum close to the breakpoint (from Bowen and Doering, 1984).

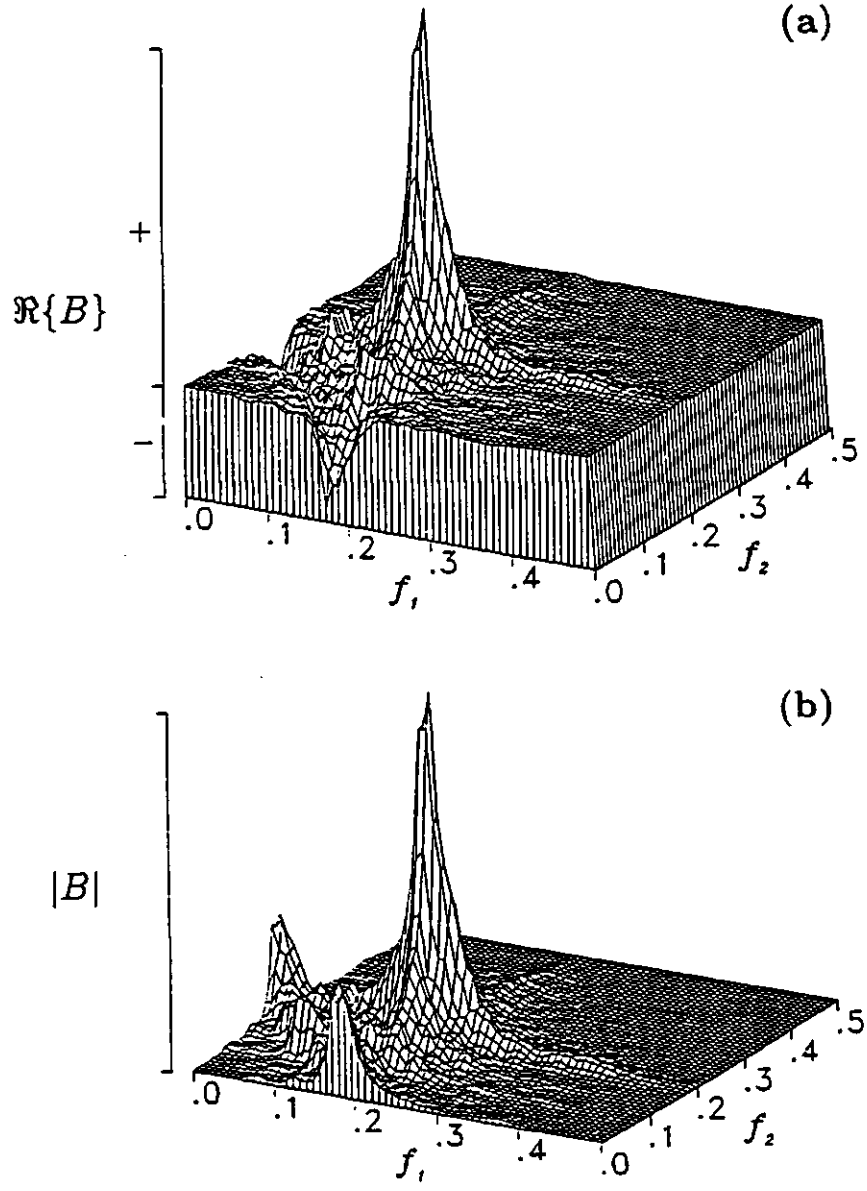

FIGURE 2.24 Real part of the bi-spectrum (a) and bi-amplitude (b) for one run of current velocity data, collected at Stanhope Lane Beach as part of the C^2S^2. The skewness arising from coupling between wind wave and infragravity wave frequencies is of opposite sign to the skewness that arises from coupling between wind wave frequencies, where f_1 and f_2 are frequencies in the velocity data(from Doering, 1988).

frequencies within the records. Doering recognised that, whilst total skewness estimates are of interest to sediment transport investigations, they do not provide any indication of the various wave-wave interactions that contribute to skewness (Figure 2.24). Doering (1988) used bi-spectral techniques, on the other hand, to examine current velocity measurements, and found that the variation of wind-wave velocity skewness and asymmetry associated with wave shoaling were quantitatively well predicted by the Ursell number, but were not dependent upon bottom slope or breaking wave type. Incident band motions tended to transport sediment onshore, promoted by the associated onshore-skewed flow, whilst interaction between the infragravity band-induced flow and sediment suspended by the incident band motions, tended to create offshore transport (where the flow linked to the infragravity band motions was skewed in the offshore direction).

Furthermore, Doering and Bowen (1988) related the pattern of flow velocity skewness to the mobilisation, suspension and transport of sediment in the nearshore environment. Where the flow is skewed onshore through the shoaling region, reaches a maximum seaward of wave breaking, becoming skewed offshore in the surf zone due to a dominance of infragravity wave skewness, it could indicate the convergence of sediment, and possibly the development, or migration, of a breakpoint-bar. Figure 2.25 illustrates the patterns of fluid flow, erosion, deposition and morphological response, inferred from the field measurements of Greenwood and Sherman (1984) on a barred beach. The convergences (deposition) and divergences (erosion) of sediment transport can be seen across the beach profile, occurring through spatial decreases and increases, respectively, in the orbital asymmetries (see also Jaffe *et al*, 1984). Findings from several recent field, laboratory and theoretical investigations into the processes which drive cross-shore sediment transport on beaches have illustrated how the examination of the nature of velocity moments can provide an effective approach towards understanding and quantifying the relevant nearshore hydrodynamic parameters.

2.4.3 SEDIMENT TRANSPORT PREDICTIONS vs. OBSERVATIONS

The energetics-based moment predictors of cross-shore sediment transport are not, in

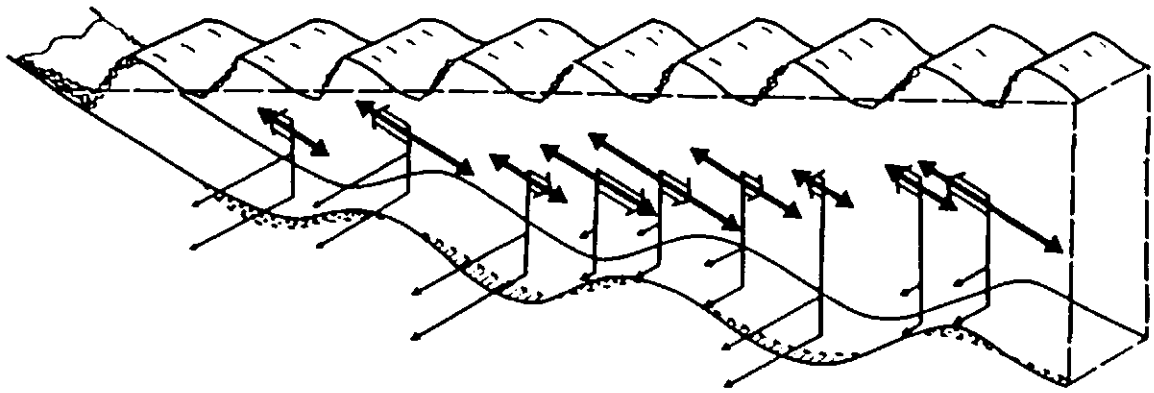

FIGURE 2.25 Fluid flows, sediment flux and morphological response over nearshore bars. The relative magnitude of near-bed, cross-shore oscillatory flow is shown by the solid double arrow and the direction and magnitude of the net flows (resulting from mean flows and flow asymmetries) by the broad open arrow. Longshore flow magnitude is denoted by a thin arrow, cross-hatching represents areas of erosion and dots areas of deposition. The post-storm profile is shown as a solid line (from Greenwood and Sherman, 1984).

themselves, measures of sediment transport. What moment predictors can do is to reveal the relative importance, the magnitude and direction, of the various hydrodynamic processes which promote cross-shore transport of sand on beaches. So, in order to substantiate the transport picture conjured up by velocity moment pointers, it is also necessary to obtain some information of what the sediment concentrations in the water column, and on the seabed, are doing. Here lies a further problem. Observing and measuring bedload transport is intrinsically more difficult than for suspended load transport because the density of the bottom flow impedes the use of conventional acoustic and optical backscatter sensor techniques. King *et al.* (1984) employed sediment traps in an oscillatory tunnel to investigate bedload transport under oscillatory flow conditions. Accelerations were found to play an important role, having considerable effect on the magnitude of the sediment velocity with a fixed fluid velocity amplitude, and the phase of the response and the initiation of the sediment motion. Gallagher and Seymour (1992) used the same facility to generate vigorous bedload transport, and the time-varying sediment transport was measured by video imaging of dyed natural sand. Results from this tracer imaging study showed similar trends to the findings of King *et al.* (1984). Observations of bedload transport in the natural beach environment are understandably not plentiful and instrumentation capable of measuring bedload transport are currently being developed including, for example, the use of a hydrophone to measure self-generated noise resulting from colliding grains on the seabed (*e.g.* Hardisty, 1987; 1989).

Observations of suspended load transport have proved more accessible. Water sampling techniques have generally proved inadequate, but the development of the optical backscatter sensor (OBS) and the acoustic concentration meter (ACM) or acoustic backscatter (ABS) sensor has enabled the collection of high-resolution time series of suspended sediment concentration (Downing *et al.*, 1981; Sternberg *et al.*, 1984) and remote acoustic measurements of the concentration profile (*e.g.* Vincent *et al.*, 1991; Thorne *et al.*, 1993), respectively. Optical back-scatter sensors, usually deployed in a vertical array, provide point measurements of suspended sediment concentration (SSC) which when deployed with co-located electro-magnetic current

meters, allow an investigation of the response of the near-bed SSC to the wave-induced flow (*e.g.* Hanes and Huntley, 1986; Doering and Bowen, 1988).

Jaffe *et al.* (1984) considered the role of suspended sediment in cross-shore beach profile change. Measurements of cross-shore current velocity (EMCM) and suspended sediment concentrations (OBS) were made across the surf zone during a storm. Time-averaged cross-shore suspended sediment fluxes were estimated, for each measurement location, using two methods. Firstly, fluxes were computed using,

$$\overline{cu} = \frac{1}{34.1} \int_{t=0}^{t=34.1\,\mathrm{min}} \int_{z=0}^{z=\eta} c(z,t)\, u(z,t)\, dz dt \tag{2.37}$$

here c is suspended sediment concentration, u is current velocity, z represents elevation above the seabed, and η is the instantaneous sea surface elevation, 1/34.1min is equivalent to 2048s of data, the length of data runs. Secondly, fluxes were calculated, as the products of the time-average quantities, by

$$\bar{c}\,\bar{u} = \int_{z=0}^{z=\eta} \left(\frac{1}{34.1} \int_{t=0}^{t=34.1\,\mathrm{min}} c\,(z,t)\, dt \right) * \left(\frac{1}{34.1} \int_{t=0}^{t=34.1\,\mathrm{min}} u\,(z,t)\, dt \right) dz \tag{2.38}$$

Fluxes calculated using Eqn. (2.38) were directed offshore at all sensor stations (Figure 2.26), but using Eqn. (2.37) were directed onshore at four out of seven instrument stations. Differences between the two calculated flux values are related to the correlation which existed between velocity and sediment concentration fluctuations. Jaffe *et al.* point out that Eqn. (2.37) includes the fluctuation correlations, while Eqn. (2.38) does not. This is illustrated by re-working the former equation thus:

$$c = \bar{c} + c' \tag{2.39}$$

$$\text{and } u = \bar{u} + u' \tag{2.40}$$

where instantaneous suspended sediment concentration (c) and flow velocity (u) comprise both mean ($\bar{}$) and oscillating ($'$) components. The expression Eqn. (2.37) multiplies c and u together before time-averaging, and this can be re-written as:

$$\overline{cu} = \overline{(\bar{c} + c')(\bar{u} + u')} = \bar{c}\bar{u} + \overline{\bar{c}u'} + \overline{c'\bar{u}} + \overline{c'u'} \tag{2.41}$$

$$= \bar{c}\bar{u} + \overline{c'u'} \tag{2.42}$$

Eqn. (2.42) yields an expression for the total cross-shore sediment transport rate, comprising both mean and oscillating components, at any given height above the bed. In this expression, the first term represents the local mean sediment transport rate, $\bar{c}\bar{u}$, and the second term, the *flux coupling*, $\overline{c'u'}$, describes the oscillatory component of

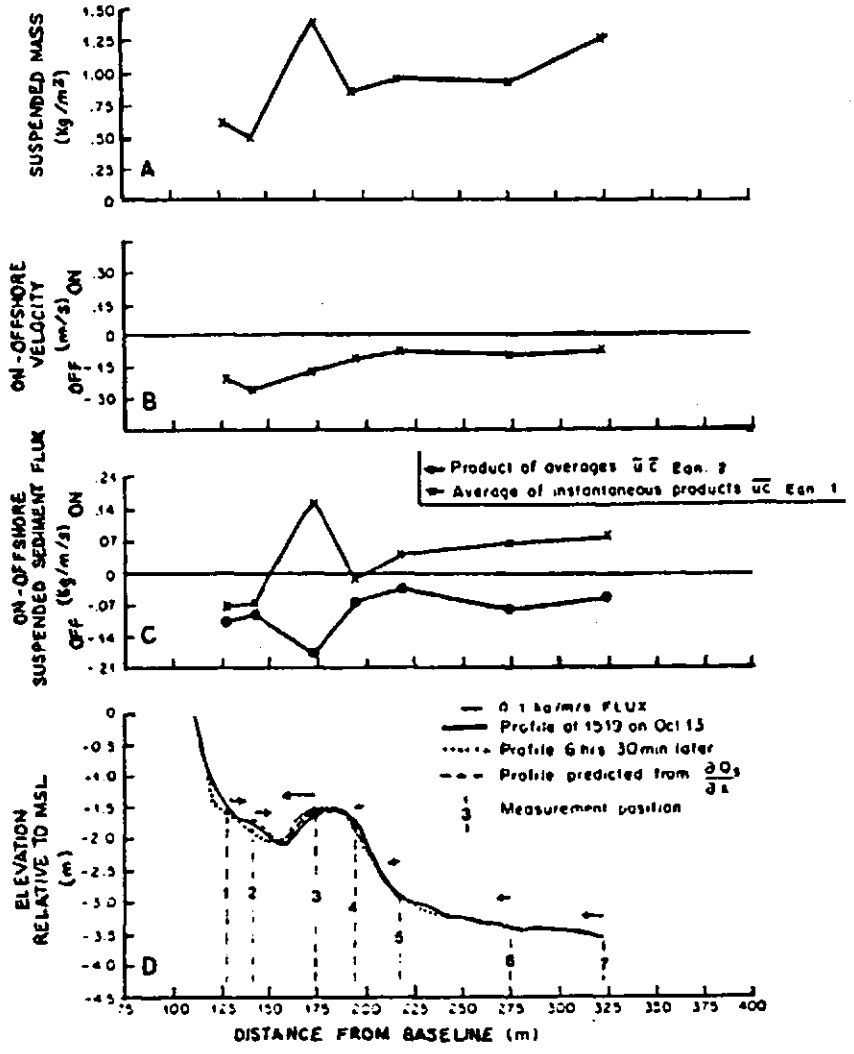

FIGURE 2.26 (a) The cross-shore variation in suspended mass (b) Cross-shore variation of mean cross-shore velocities at 0.5m above the bed (c) Comparison of suspended sediment flux calculated from average and instantaneous quantities (d) Compares the profile measurements with predicted values (from Jaffe *et al.*, 1984).

cross-shore transport. This flux coupling term is typically non-zero in the surf zone, where a low value generally denotes a randomness of fluctuations relative to each other, and a high value indicates a high degree of correlation.

A more detailed analysis of the flux coupling term, by either co-spectral or time domain techniques, can reveal the importance of the mean, incident and long period components to the total cross-shore suspended sand transport (*e.g.* Hanes and Huntley, 1986; Doering, 1988; Beach and Sternberg, 1991; Osborne and Greenwood, 1992a,b; Russell, 1993). Huntley and Hanes (1987) discuss measurements collected as part of the first C^2S^2, where a co-located miniature optical back-scatter sensor (MOBS) and electromagnetic current meter (EMCM) were deployed outside, but near the surf zone. Data were subjected to co-spectral methods where, the co-spectrum between u and c (cross-shore velocity and suspended sediment concentration, respectively) is the measure of the net sediment transport contribution due to motion at any particular frequency (Figure 2.27). The integral of the co-spectrum over all frequencies is, consequently, equal to the total net sediment transport rate. Using these co-spectral techniques, Huntley and Hanes observed a strong onshore transport due to incident waves and a weaker offshore transport due to long period motion, near the sea floor. Mean transport, about 0.05m above the bed, was offshore in direction due to a dominant offshore mean flow, whilst the offshore transport driven by the infragravity wave-induced flow, higher in the water column, contributed less significantly through the increased time lag between flow and sediment response.

Doering and Bowen (1988) carried out co-spectral analysis on their data, also collected at the C^2S^2, in order to compare the behaviour of velocity moments with measurements of sediment transport. Co-spectra revealed onshore transport of sediment, observed at the short wave frequency, where the strong onshore flow, associated with the passage of each skewed wave crest, influenced not only the mobilisation and suspension of the sediment but also the onshore transport of the sediment. The implication was that the bulk of the sediment suspended by the passage of a wave crest settles before the offshore flow associated with the following wave trough can force it seawards. Conversely, the offshore transport by infragravity

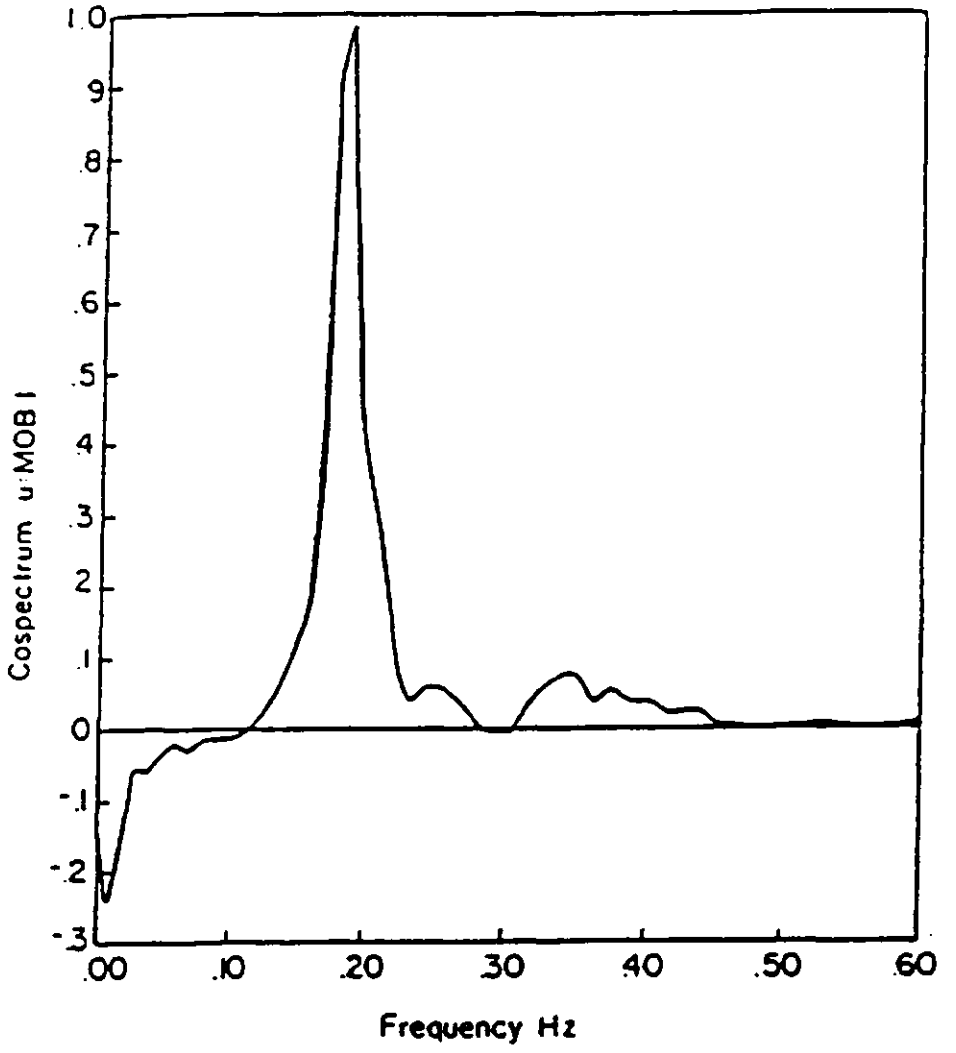

FIGURE 2.27 Co-spectrum of cross-shore velocity and suspended sediment concentration. The largest positive contribution is centred at the incident wave frequency (≈ 0.18Hz) with a smaller positive contribution around 0.35Hz, corresponding to the first harmonic of the incident waves. Here a positive co-spectrum implies an onshore transport of suspended sediment (from Huntley and Hanes, 1987).

frequency motions was linked to the offshore skewed flow corresponding to the bound long wave forced by an incoming wave group. This reverse sediment transport follows the observations made by other workers (*e.g.* Larsen, 1982; Shi and Larsen, 1984) who were interested in the process in deep water, whereby coupling occurs between incoming wave groups and a bound long wave. The passage of a wave group and bound long wave over an erodible bed causes the re-suspension of sediments under high waves, which in conjunction with a long wave trough (reverse flow) will create a net reverse sediment transport (averaged over the time-scale of the wave groups) in a direction opposite to wave propagation. Where high waves occur with a long wave crest, a net forwards transport of sediment should arise.

O'Hare and Huntley (1994) considered the role of the incoming wave group/bound long wave coupling phenomenon, in modelling the formation of nearshore bars. The critical factor determining the direction of net sediment transport, taking into account the possibility of long wave reflection, is the correlation between the bottom velocity due to the short waves (which mobilises the sediment) and the velocity of water motion due to the long waves (which transports sediments). Regions where fixed phase relationships exist between short wave groups and long wave motions occur, and zones of net sediment flux and deposition and/or erosion of sediment may arise. O'Hare and Huntley (1994) found that the coupling between short wave groups and associated long waves can lead to regions of sediment convergence and divergence, and thus potentially to bar formation. Bars formed by this mechanism are likely to have a spacing related to the wavelength of the long waves (*i.e.* the wave group length). Osborne *et al.* (1990) and Osborne and Greenwood (1992a,b) examined field measurements of current velocity and suspended sediment concentration obtained on a meso-tidal beach. Important contributors to cross-shore transport under combined wave and current conditions were found to be 'quasi-steady' mean currents with characteristics typical of a set-up driven undertow, oscillatory currents at wind-wave frequencies and, oscillatory currents at long wave frequencies and forced by the incoming wave group-bound long waves. These contributions were found to be common to both barred and non-barred environments. Sediment transport attributable

to mean currents was frequently balanced by the transport driven by net oscillatory currents. The total oscillatory transport was generally dominated by the *incident band* contribution (at least outside the surf zone) and generally directed *onshore*. The mean sediment transport rates were predominantly directed *offshore* , driven by the undertow (Greenwood and Osborne, 1990).

Russell (1993) discusses results collected on a high energy dissipative macro-tidal beach. During calm conditions, wave and current variances were gravity band dominated, with maximum values occurring at the breakpoint, decreasing steadily shorewards. During the storm events, wave and current variances show a general trend of increasing energy shorewards (maximum values occurring in the inner surf zone) dominated by the infragravity wave component. Davidson *et al.* (1993) examined measurements collected on an intermediate macro-tidal beach, over a range of wave and current conditions; sediment transport was found to occur at three specific frequencies, namely, gravity, infragravity and incident-harmonic frequencies. Examination of the relative importance of the mean and fluctuating components of cross-shore suspended sand transport rate led to the following results. Outside the breakpoint, sediment transport processes were dominated by the *incident band* contribution, with a strong onshore directed transport occurring at the short wave frequencies and a weaker offshore directed transport at the long wave frequencies. Inside the inner surf zone, for the selected data runs, the sediment flux was dominated by the *long wave* component, in the offshore direction. These observations agree with other recent findings, where long periods of high suspended sediment concentration occur, corresponding to long period wave-induced flows in the inner surf zone during high energy conditions (*e.g.* Brenninkmeyer, 1976; Beach and Sternberg, 1988; 1991; Russell, 1990). Such studies illustrate the relative contributions of the various hydrodynamic processes which drive the transport of suspended sediment concentrations in the nearshore zone. Investigations of cross-shore sediment transport rates on beaches should include a qualitative and quantitative examination of the coupling relationships which exist between the mean flow components, the incident wave flows and the long wave induced flow components.

2.5 OVERALL AIMS AND OBJECTIVES OF THE PROJECT

The preceding sections in this chapter have reviewed and discussed some important aspects of beach process studies. Additionally, a few of the problems which prevail in this area of research have been highlighted . It is inevitable that only a small fragment of the nearshore sediment transport problem can be examined in the work discussed below.

Incident waves travelling towards the shoreline are known to have a groupy structure, with an alternating sequence of high waves and low waves. Although, the groupiness of ocean waves is considered an important characteristic of the climatology of waves both within, and beyond, the surf zone, few studies have examined the variations in wave groupiness across the surf zone. Wave groupiness is also regarded as a driving mechanism in models of long wave generation and has a role in promoting nearshore sediment transport. Whilst some studies suggest there to be no group structure in the inner surf zone, on the basis that the wave field is more or less fully saturated so that no forcing at the group frequency occurs, other field evidence indicates that wave groupiness can persist inside the breaking region and through the surf zone. Clearly, the behaviour of wave groupiness across the nearshore requires further investigation.

Net sediment transport in a wave-dominated environment arises from the differences in the rate at which sediment is transported back and forth with the oscillatory wave motion. Such differences occur with the second order effects such as wave asymmetry, wave-induced mass transport currents and superimposed tidal or wind-induced currents and the bottom slope. Several cross-shore sediment transport theories exist which allow prediction of the instantaneous rate of sediment transport, from which the net rate of sediment transport can be calculated. These models, which adopt an energetics-type approach, comprise a number of velocity moments. Several recent field, laboratory and theoretical investigations into the processes which drive cross-shore sediment transport on beaches have illustrated how the examination of the nature of velocity moments can provide an effective approach towards understanding and quantifying the relevant nearshore hydrodynamic parameters. If examination of

the velocity moments helps to reveal the relative importance, the magnitude and direction of the various hydrodynamic processes which promote cross-shore transport of sand on beaches, analysis of corresponding suspended sediment concentration data can validate (or otherwise) the predictions of cross-shore sand fluxes. Investigation of the suspended sediment concentrations in the water column are, therefore, also required.

Field measurements of sea surface elevation, cross-shore current velocity and suspended sediment concentration, collected on a macro-tidal intermediate beach during a range of wave and current conditions, will form the basis of the present investigation into some of the phenomena which affect sediment transport, and of course, beach profile change. The primary aims and objectives of this work can be described as:

- Examination of pressure transducer, electro-magnetic current meter and optical back-scatter sensor measurements in order to obtain time-series of sea surface elevation, cross-shore current velocity and suspended sediment concentration, for a range of wave and current conditions.
- Investigation of wave groupiness variations and cross-correlation between the incident wave envelope and long wave motion across the nearshore zone using sea surface elevation data.
- Study the relative importance of the main processes which operate on a macro-tidal beach and assess the role played by the mean flow, incident wave and long wave related parameters.
- Evaluate the suitability of energetics-based sand transport predictors using current velocity derived moments and comparing these moment predictors with the transport rates observed at the field site using suspended sediment concentration measurements.
- Attempt to understand the spatial and temporal variability of some of the hydrodynamic properties which shape and characterise the nearshore zone of a macro-tidal beach environment.

CHAPTER 3
EXPERIMENTAL PROCEDURES AND TECHNIQUES

3.1 INTRODUCTION

Identifying and quantifying the processes which drive sediment transport on a macro-tidal beaches is a relatively poorly studied area of coastal research. In order to obtain a reliable and informative data-set for this purpose, the location for a field experiment on which to measure the wave, current and transport parameters, must first be specified.

A field experiment was carried out at Spurn Head, Humberside on the north-east coast of England during April 1991 by the B-BAND (British Beach And Nearshore Dynamics) collaborative group (Russell *et al.*, 1991). B-BAND is a large-scale field based research project, comprising the Universities of Hull, Cardiff and Plymouth, funded by the Natural Environment Research Council (NERC). The research presented here examines data collected during field deployment on the macro-tidal intermediate beach, at Spurn Head.

3.2 THE HOLDERNESS COASTLINE AND SPURN HEAD

The Humber Estuary (north-east coast of England) is partially closed on the north side by a spit of sandy dune land, known as Spurn Head. This sand and shingle spit, situated at the southern end of the Holderness coastline, is a hook-shaped peninsula extending approximately 5.6km in length and is 0.25km wide (Figure 3.1). To the north of the spit, steep cliffs formed entirely of Pleistocene glacial till or boulder clay,

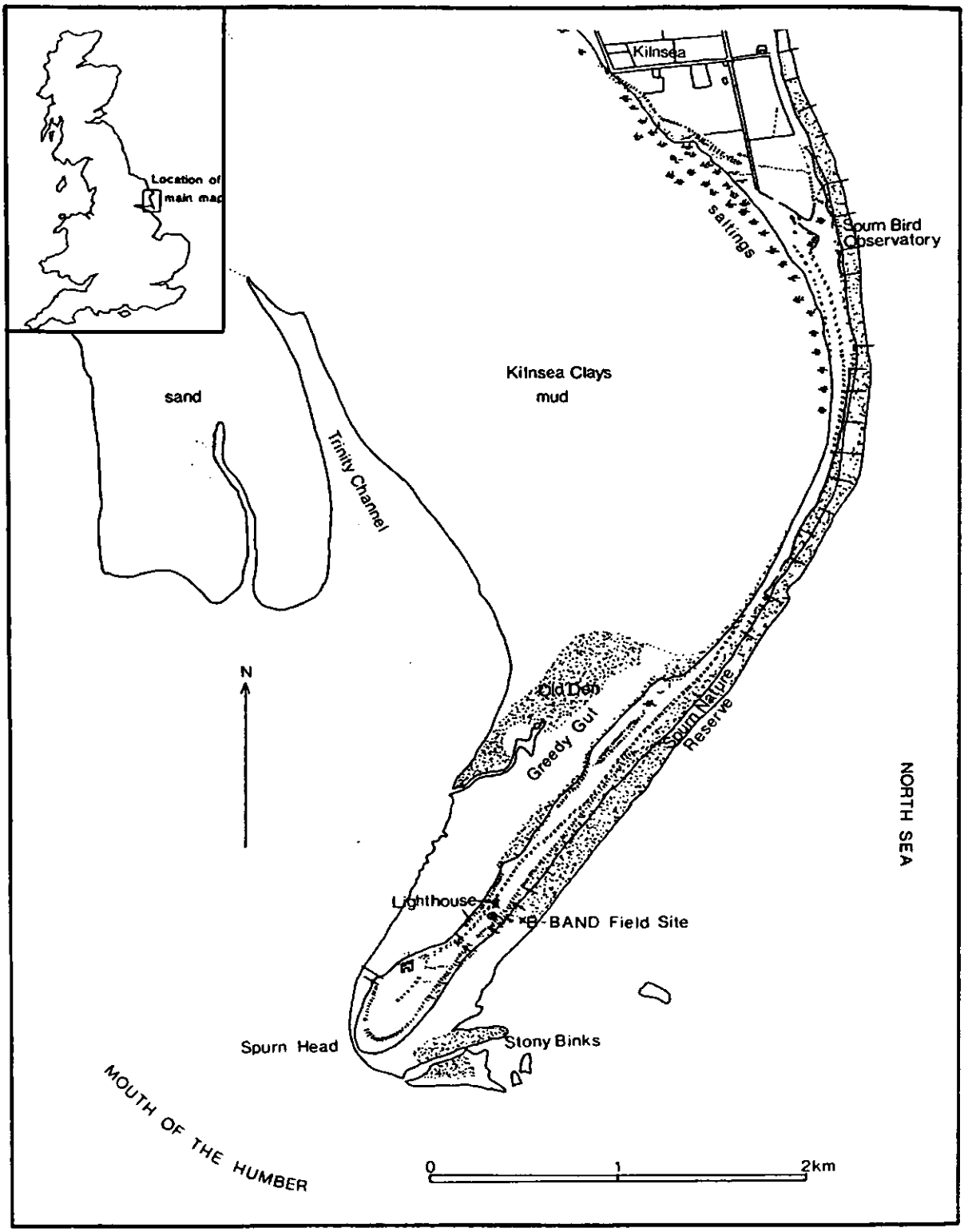

FIGURE 3.1 Spurn Head - field experiment location.

known as the Holderness cliffs, extending northwards from Spurn Head for some 61km to the resistant Chalk outcrop forming Flamborough Head.

The Holderness coast comprises a relatively thin sand and shingle beach overlying a glacial till platform, backed by a rapidly eroding glacial till cliff. These cliffs are typically 3-10m in height, but reach a maximum of 30m in some locations. The till/boulder clay disappears at a point 500m south of Kilnsea where the sandy spit of Spurn Head has developed. The narrow sandy beaches, on the seaward side of the spit, are fringed by the extensive sand dunes along the length of the spit, whilst on the estuarine side of Spurn Head are expanses of muddy tidal flats. The coast on the southern side of the Humber Estuary comprises post-glacial deposits overlying glacial boulder clay; the beach on the southern coast is wider than that of the northern coastline.

Overall the area comprises a region of rapid erosion in the Holderness cliffs, which is balanced by deposition inside and on Spurn Head, the Humber Estuary and along the southern coastline. Whilst the severe erosion of the Holderness coastline is undoubtedly the most important contributor to the deposition around Spurn Head, the southern coast and in the estuary; the land drainage system and the floor of the North Sea might also be considered as a potential source of sediments (Al-Bakri, 1986). The Holderness coastline is known to provide sand and coarser sediment to the beach at Spurn Head, whilst silts and clays are carried offshore by waves and currents and further wave and current activity are considered to be primarily responsible for the re-working and re-distribution of these materials (Winkelmolen, 1978; Pringle, 1985). Phillips (1963) examined the movement of sediment and currents around the spit, using tracer pebble techniques. She found that tidal currents played a very important role in shaping the form of the beach and offshore banks and illustrated the asymmetries which exist between the flood and ebb tidal currents at various locations around the sand spit and estuary.

The glacial till (boulder clay) cliffs of Holderness have been well documented owing to the rapid rates of erosion (*e.g.* Mason and Hansom, 1989). The University of Hull has established a permanent field station on the seaward face of the sand spit, for

the purpose of collecting wave data and monitoring the response of the intertidal beach profile to tidal and wave forcing (Hoad, 1991). Mason and Hansom (1988) examined cliff erosion and its contribution to the sediment budget of the Holderness coast. They observed distinct upper and lower beaches along much of the coastline: the upper beach was steeper (sloping at 4-7°) and coarser (mean particle size = 2.6mm) than the lower beach which sloped at 0-2° and had a mean particle size of 0.26mm. They also described how, when the beach veneer was thin, then storm waves would expose parts of the underlying till plug (which locally are termed 'ords').

Pringle (1985) examined the role of ords (Figure 3.2) in the erosion of the Holderness coastline. Where an ord occurred, the massive injection of beach sediment went to form the ord's most prominent constructional feature, the lower beach ridge which extends southwards from the centre of the ord. Pringle examined twelve months of observer wave data collected at Withernsea in 1969/1970, and found that a net southward movement of $1.44 \times 10^5 m^3$ sand occurred. Pringle's findings disagree considerably with those of Winkelmolen (1978), who analysed size, shape and sediment density data. Winkelmolen proposed the southwards drift of beach material to play a subordinate role in the sand transport mechanisms along Holderness and considered the main movements occurred in the deeper offshore waters.

The erosion and destruction that is characteristic of the Holderness coastline and Spurn Head, has been well documented. Valentin (1954) calculated that the average annual coastal retreat for the period 1852-1952 was approximately 1.20m, which suggests a supply of approximately $1 \times 10^6 m^3$ of material per annum to the coastal processes. Mason and Hansom (1988) observed coastal erosion along Holderness to vary both spatially and temporally. Examining map data for the last 100 years or so, a mean retreat of $1.34 myr^{-1}$ was calculated, which would contribute over $5.5 \times 10^7 m^3$ of sand to the beach. The equivalent value calculated from aerial photographs between 1968 and 1984 was $2.5 myr^{-1}$. Similarly, the stretch of coastline between Skipsea and Atwick has cliffs which are thought to be retreating at an average rate of $1.5\text{-}2.0 myr^{-1}$ (Mason, 1985). Pethick (1992) on the other hand, discussed the breaching of Spurn Head, stating that the Holderness coastline "the fastest disappearing

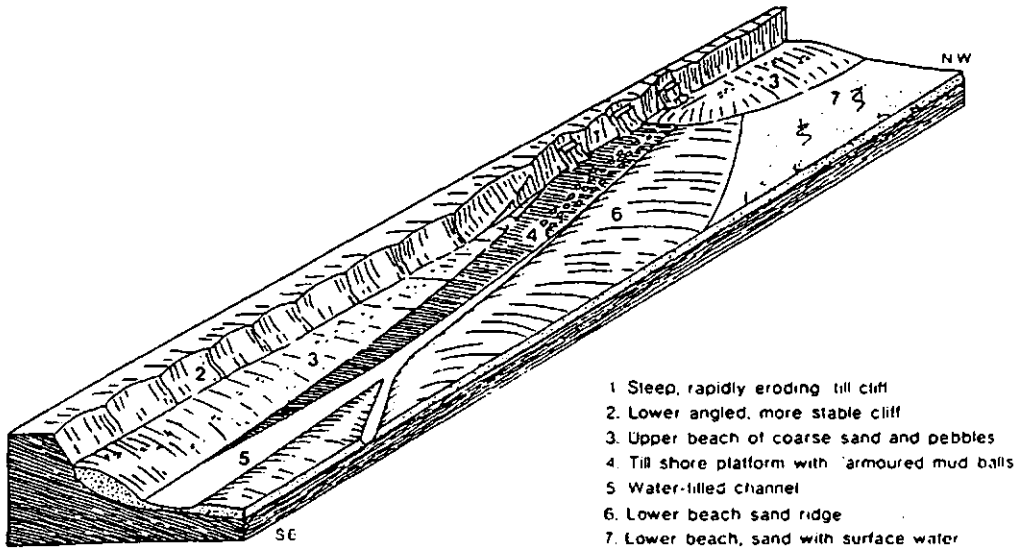

FIGURE 3.2 Characteristic features of a Holderness Ord (from Pringle, 1985).

coastline in Europe" to be eroding at a rate of $1.8myr^{-1}$. These figures, although estimates from various methods and locations along the Holderness coastline, illustrate the rapid erosion rates and subsequent coastal retreat of the surrounding land and potential sediment transport.

Investigations into the forces which drive the transfer of sediment at Holderness and Spurn Head are undoubtedly important. Extensive studies describing the origin of Spurn Head have been carried out by De Boer (1963, 1964, 1973) who has attempted to piece together its history. The modern day Spurn Head was considered to be a contemporary representative of a succession of spits that have formed at the mouth of the Humber Estuary, developed for a period of time, and then swept away. This indicated a cycle of change that appeared to take 250 years for its completion. De Boer (1967) estimated that approximately five such cycles of change have occurred between the earliest known reference (about 670 AD) and the present day.

However, Pethick (1992) believes that the head of the spit (formed from sand and shingle and overlying glacial till) has remained fairly static, whilst the neck has crept westwards - built up from the sand and shingle washed along the coast and deposited in the mouth of the Humber Estuary. The development of coastal defence works began in the 1840s, with the placing of groynes which have not only interrupted the natural pattern of sediment transport on the peninsula, but also caused the deformation of the peninsula. Such changes in orientation to wave approach angles could, therefore, have exacerbated the vulnerability of the neck of the sand spit. This hypothesis might well be valid; For instance, during the 4 week British Beach And Nearshore Dynamics (B-BAND) field experiment (from which the data for this research was collected), the neck of the sand spit was once more breached (Plate 3.1). Thus, it is becoming increasingly important to understand the processes which on a small-scale are creating erosion and deposition of the beach profile and, on the large-scale are causing the re-shaping of the sand spit as a whole.

PLATE 3.1 Breaching of the neck of Spurn Head during the B-BAND field experiment (April, 1991).

3.2.1 THE B-BAND FIELD SITE

The B-BAND field experiment was located on the seaward side of the sand spit, just below the disused lighthouse tower. The mobile laboratory (caravan) was situated close to the tower behind the dunes which backed the beach. The profile of the beach at the instrument deployment site was characterised by a narrow sandy terrace which was exposed at low tide and a steep upper beach face and berm (Plate 3.2). Gradients varied from 0.0975 over the high tide beach face to 0.023 at the low tide terrace (Figure 3.3). The morphodynamic regime at the field experiment location fluctuated between dissipative at low water, and reflective at mid- to high-water. The tidal range of this macro-tidal beach was approximately 3-7 metres (Table 3.1).

The beach at the experiment location was covered by a veneer of sand and shingle overlying a glacial till plug. This glacial deposit at the field site is periodically exposed over a large area of the upper beach profile (particularly in winter or during storms). Across the beach profile there was a variation in sediment size and type. At the instrument rig locations, on the lower beach, the median grain size (D_{50}) was approximately 0.35mm - a well-sorted medium sand. Over the upper beach face the sediment comprised coarser sand, pebbles and occasionally cobbles.

The wave climate along the Holderness coastline is generally limited by the relatively short fetches of the North Sea, but wave conditions during the field deployment period covered a wide range, from calm to the two-year return period storm with breaking wave heights in excess of three metres. The incoming waves varied from irregular and short-period local waves to a regular swell with strong groupiness characteristics. Longshore transport processes running south-west along the shoreline tend to dominate at Spurn Head, where incoming waves are observed to approach the shoreline at highly oblique angles. Environmental conditions during the field study (*e.g.* wind direction and force) were recorded at the time of the experiment. In addition, the Coast Guard also supplied some information on the local conditions. These data are displayed in Table 3.2.

PLATE 3.2 The beach at Spurn Head, showing the narrow, sand and shingle intertidal terrace, steep upper beach face, backed by berm and sand dunes. Photograph was taken looking approximately northwards (Courtesy of D.A. Huntley).

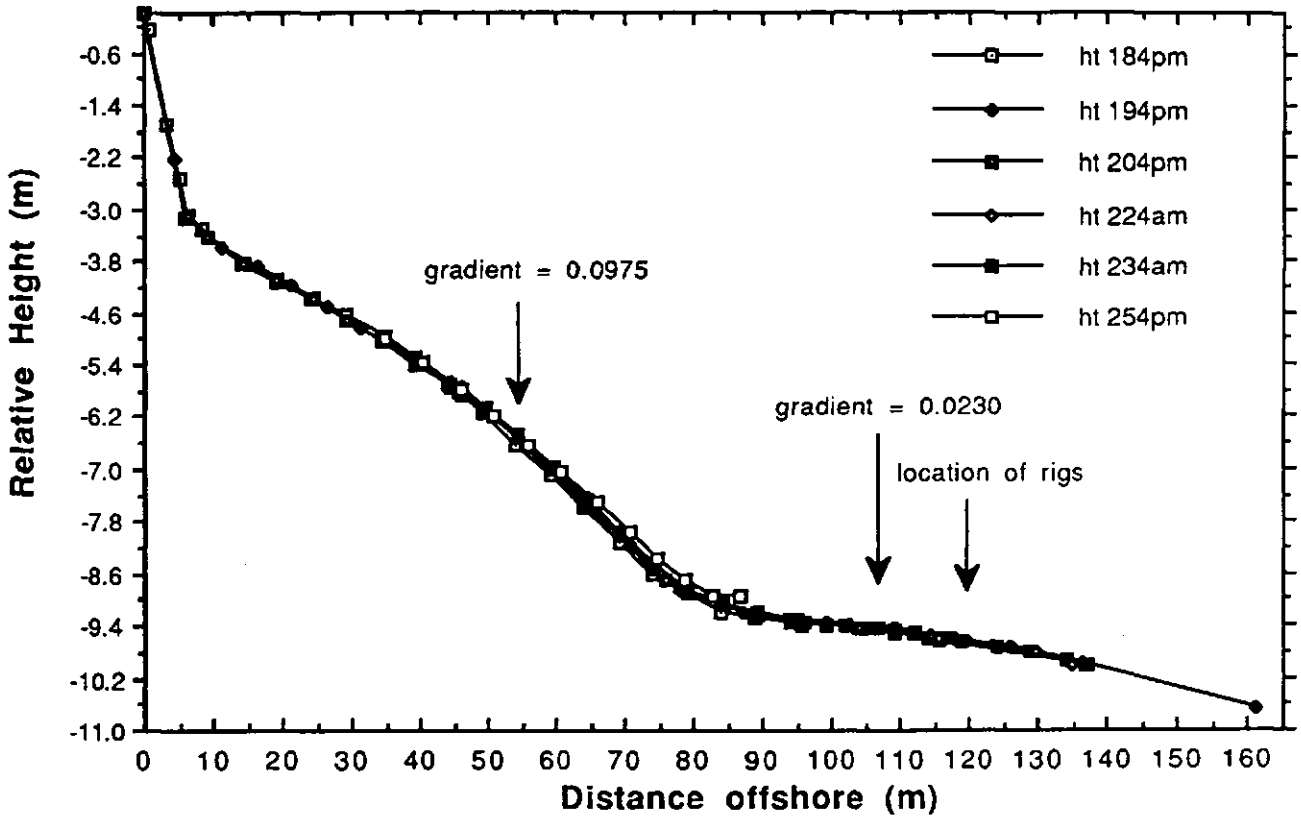

FIGURE 3.3 Beach profile at Spurn Head field site during 18-25 April, 1991. The symbol legend refers to the date of the survey, for example, 184 = 18 April 1991, am or pm indicates the part of the day during which sampling occurred and ht is relative height.

DATE	DETAILS	TIDAL RANGE (m)	LOW WATER TIME (BST) IMMINGHAM (≈24mins after Spurn Head)		LOW WATER HEIGHT (Chart Datum) (C.D. = -3.9m; O.D. Newlyn)	
14/04/91		6.0	1242	___	1.2	___
15/04/91	Deploy	6.4	0108	1322	0.8	1.0
16/04/91	Sensors	6.5	0146	1402*	0.8	0.9
17/04/91	SPRING	6.4	0224	1441*	0.8	0.9
18/04/91		6.1	0301	1520*	1.0	1.0
19/04/91		5.5	0340	1604*	1.3	1.2
20/04/91		4.8	0422	1655*	1.7	1.5
21/04/91		4.2	0514*	1802	2.2	1.8
22/04/91		4.1	0627	1929*	2.5	1.9
23/04/91	NEAP	3.4	0756*	2055*	2.6	1.8
24/04/91		3.9	0918	2205	2.4	1.5
25/04/91		4.4	1022	2303*	2.1	1.3
26/04/91	Recover	4.9	1116	2349	1.8	1.1
27/04/91	Sensors	5.3	1201	0030	1.6	1.1
28/04/91		5.6	1240	___	1.4	___
29/04/91	SPRING	5.7	0105	1317	1.1	1.3

*Tides logged

TABLE 3.1 Tide range and heights during April 1991 at Spurn Head.

DATE	TIME	WIND	FORCE	VISIBILITY
16/04/91	0001	NNW	3	GOOD
	0401	N	3	GOOD
	0800	N'LY	4	GOOD
	1200	N'LY	7	GOOD
	1600	N'LY	7	GOOD
	2001	N	6-7	GOOD
17/04/91	0000	N	6-7	GOOD
	0400	N	7-8	GOOD
	0800	N	6	GOOD
	1200	N	6	GOOD
	1600	N	6-7	GOOD
	2000	N'LY	7	MODERATE
18/04/91	0001	NW	4-5	GOOD
	0400	W'LY	3-4	GOOD
	0800	W	5	GOOD
	1200	NNW	4-5	GOOD
	1600	NNW	6	GOOD
	2000	NNW	4-5	GOOD
19/04/91	0001	NW	5-6	GOOD/RAIN
	0400	NNE	5-6	GOOD
	0800	NE	7	GOOD
	1200	N	5-6	GOOD
	1600	N	8	GOOD
	2000	N	6	GOOD
20/04/91	0001	N	5	GOOD
	0400	NW	5	GOOD
	0800	N	4-5	GOOD
	1200	NE	3	GOOD
	1600	E	2	GOOD
	2000	___	___	GOOD/CALM
21/04/91	0001	SSW	3	GOOD
	0400	SW	3	GOOD
	0800	SW	3	GOOD
	1200	SW	5	GOOD
	1600	SW	5	GOOD
	2000	NNW	3	GOOD
22/04/91	0001	N	6	GOOD
	0400	NW	4-5	GOOD
	0800	NW	5	GOOD
	1200	NW	6	GOOD
	1600	N'LY	6	GOOD
	2000	NNW	4	GOOD
23/04/91	0001	W	3	GOOD
	0400	W	3	GOOD
	0800	W'LY	3-4	GOOD
	1200	NE	2-3	GOOD
	1600	SE	3	GOOD
	2000	S'LY	3	GOOD

TABLE 3.2 Weather conditions at Spurn Head (Supplied by Humber Pilotage, 1992).

3.3 FIELD DEPLOYMENT OF INSTRUMENTS

The primary objective of the B-BAND project is to quantify the processes dominating the beach environment and also to understand the response of the beach profile to waves and currents. Consequently, the instrumentation necessary for such an experiment must be capable of monitoring the waves, currents and sediment transport throughout a range of conditions. Russell *et al.* (1991) provides a description of the configuration of the instrumentation deployed in the B-BAND field experiments.

Instrumentation for measuring the various properties of the nearshore hydrodynamics at Spurn Head comprised pressure transducers (PT's) to investigate sea surface elevations and also a range of electromagnetic current meters (EMCM's) to examine the horizontal component of the nearshore velocity field. A square sensor array (Plate 3.3 and Figure 3.4) was selected to enable the monitoring of waves, currents and sediment fluxes through a box, with dimensions of 20m by 20m. The offshore limit of the sensor rigs is controlled by the length of cable between the sensors and the mobile laboratory (situated behind the dunes). In the case of Spurn Head the seaward extent of the deployment was an approximate distance of 120m offshore of the high water level.

The field experiment at Spurn Head comprised the deployment of the central B-BAND square array of four instrument rigs (Rigs A1, A2, A3 and A4) adjacent to a shore-normal array of four sensor stations (deployed by the University of Hull), shown in Figure 3.4. The sensor rigs at the corners of the central 'square' comprised three EMCM's spaced at heights of 0.10, 0.25 and 0.63m above the bed, three OBS's placed at heights of 0.04, 0.10 and 0.25m above the bed, plus one PT.

Measurement of long-term, net (over a tidal cycle) morphological changes was achieved through regular beach levelling surveys at each low tide. Whilst smaller-scale and shorter-term topographical fluctuations were recorded through the positioning of a grid of depth-of-disturbance rods (Osborne, 1990) within the central A-Rig square. In addition, the regular photographing of the survey area at low tide provided visual evidence for any small-scale or large-scale morphological changes which occurred through the field study period. Environmental checks involving the recording of all

PLATE 3.3 Location of the square array of instrument rigs in the surf zone at low tide.

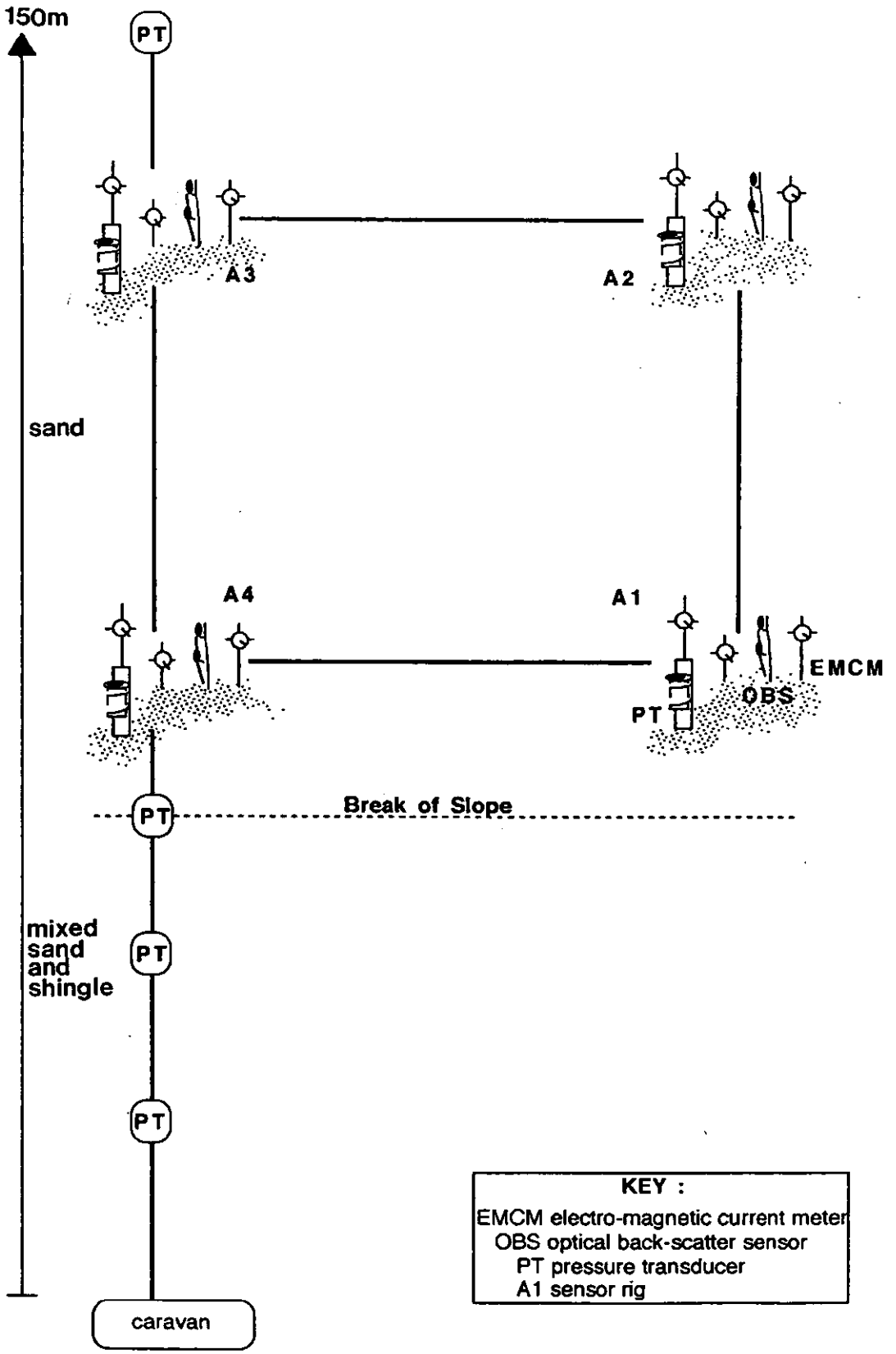

FIGURE 3.4 Field set-up of the instruments deployed at Spurn Head, including pressure transducers (PT's), electromagnetic current meters (EMCM's) and optical backscatter sensors (OBS's).

weather and sea states throughout the period of the field deployment are also available to complement all other field results.

3.3.1 SEA SURFACE ELEVATION

Basinski (1989) classified the numerous techniques for wave measurement, illustrating several possibilities for application to the nearshore zone. Whilst many indirect and direct methods exist, the pressure-type wave meters which operate according to the principle of a varying hydrostatic pressure under the sea surface, have proved reliable in previous B-BAND field studies (*e.g.* Russell *et al*, 1991). Although these pressure sensors do not measure the sea surface directly, a less noisy signal is produced than might result from, for example, a surface-piercing wave staff (Osborne, 1990) and the sensors have a reputation for being relatively reliable and rugged (*e.g.* Davidson, 1990; Russell, 1990).

The four central pressure sensors (see Plate 3.4) deployed at Spurn Head, were manufactured by Sensor Technics (see Appendix I). These pressure transducers (BT/PT2000 series) were selected for their accuracy and long-term reliability; the transmitters are fully temperature compensated and signal conditioned to provide a 1-6V output. In addition to their reliability, the design comprised a rugged stainless steel transmitter which was constructed for the hostile conditions of the nearshore environment. The BT/PT2000 series feature a unique diaphragm/oil-fill (fluid fill is dimethysiloxane) isolation technique which is designed to minimise the amount of oil required for optimal performance over a temperature range. Hydrostatic changes are registered by the diaphragm of the stationary pressure gauge (which is secured to the seabed), and the fluctuations are translated to the sensor by the incompressible oil-fill contained in the sensor housing. In turn, the mechanical transducer conveys the measurements as electric signals. The transducer is fully temperature-compensated, being temperature tested from 0-70°C relative to 25°C, showing low susceptibility to drift (see Davidson, 1990). Such pressure transmitters are designed to cope with extreme burst pressures (typically exceeds normal operating pressure by 10 times). The PT2015G1A has an operating pressure of 0-15psi, with proof pressure (the

PLATE 3.4 Pressure transducer and housing secured to mounting in the beach face.

maximum pressure which may be applied without causing damage to the sensing element) of 30psi, and burst pressure of 1000psi (where the medium is contained until this extreme burst pressure limit is exceeded).

3.3.2. CURRENT VELOCITY

Cross-shore and longshore components of nearshore horizontal flow were measured simultaneously through use of bi-directional electromagnetic current meters. Electromagnetic current meters operate on the principle of Faraday's Law of electromagnetic induction. A magnetic field is set up in the water by means of a coil carrying an electric current, and the water passing through this field creates a potential gradient perpendicular to the direction of flow, by means of electromagnetic induction. It is the resultant potential difference which is detected by two electrodes, housed in the head of the current meter. A D.C. square wave is generated in the coil with a constant current, this is switched to reverse the square wave about zero. When water passes through this magnetic field a small e.m.f. is generated across the pair of electrodes directly proportional to the velocity. The voltage is then amplified, sampled and the resulting voltage stored on a capacitor. Subsequently, the magnetic field is reversed, and the amplified voltage stored on a second capacitor so that the difference in the voltages on the two capacitors is proportional to the change in e.m.f. This process takes place across the two pairs of electrodes set at right angles to each other, to measure the vector velocity in the plane perpendicular to the magnetic field axis.

Four spherical (5.5cm diameter) and two open annular or ring-shaped (17cm diameter) current meters, manufactured by Valeport Marine Scientific Ltd (see Appendix I) were deployed at Spurn Head. In addition, three discus-shaped current meters (11cm diameter) were also deployed. These sensors were originally manufactured by Colnbrook Instrument Development Ltd (but have since been taken over by Valeport Ltd). Plate 3.5 illustrates a typical instrument rig, deployed at Spurn Head, comprising two annular electromagnetic current meters, one pressure transducer and three optical backscatter sensors.

According to the manufacturers specifications, typical noise levels for the

Series 800 range electromagnetic current meters include, discus < 5mms^{-1} rms., annular < 10mms^{-1} rms. and spherical < 20mms^{-1} rms.; the linearity of these sensors can be described by typical errors from best-fit data as, discus < 5mms^{-1}, annular < 10mms^{-1} and spherical < 20mms^{-1}; the gain accuracy of the sensors is better than 1% of reading, when calibrated in the manufacturers tow tank. Background noise levels should be better than ± 1mV (based on the 11cm discus Colnbrook sensor).

Aubrey and Trowbridge (1985, 1988) and Guza (1988) tested the response of Marsh-McBirney spherical current meters (similar to the Valeport spherical sensors) to a variety of dynamic (pure steady, pure oscillatory and combined steady/oscillatory) conditions. Aubrey and Trowbridge (1985) questioned the suitability of using spherical electromagnetic current meters for surf zone experiments and the accuracy of estimating higher order velocity moments. Doering and Bowen (1987) examined co-located pressure and velocity measurements, in order to provide a calibration check in the field for the performance of the sensors. Their cross-spectral analysis has shown that co-located current meter data were nearly identical, and this was true for data from both inside and outside the surf zone. Doering and Bowen (1987) concluded that these current meters were suitable instruments for the estimation of non-dimensional velocity moments, even under breaking wave conditions.

3.3.3 SUSPENDED SEDIMENT CONCENTRATION (SSC)

Instrumentation capable of measuring suspended sediment concentrations (SSC's) in the nearshore environment, or more specifically inside the surf zone lags far behind the development of sensors for measuring flow dynamics. The most promising techniques for measuring suspended sediment concentrations across the nearshore include indirect methods such as, optical- or acoustic-related devices which measure instantaneous concentrations (*e.g.* Hanes and Huntley, 1986), as opposed to the direct methods, such as suspended sediment samplers or traps (*e.g.* Thornton, 1977).

Sediment concentrations in suspension above the seabed were measured at the Spurn Head field experiment through deployment of arrays of Optical Backscatter Sensors (OBS's). The Optical Backscatter Sensors developed by Downing *et al* (1981)

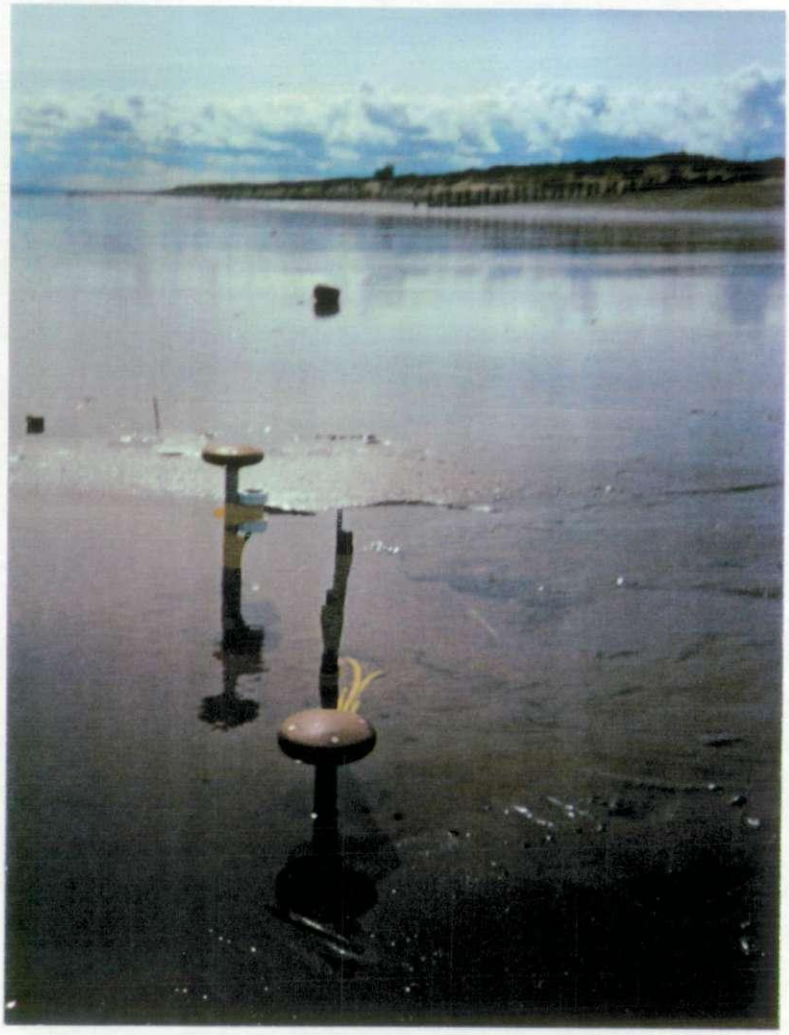

PLATE 3.5 Typical instrument rig at the Spurn Head field site, showing two Colnbrook (discus-shaped) electromagnetic current meters, one pressure transducer attached to the stem of an EMCM and three optical backscatter sensors, on their own mounting.

provide high-temporal resolution (10Hz) and recent studies of SSC's in the nearshore environment have produced some interesting findings (*e.g.* Hanes and Huntley, 1986; Huntley and Hanes, 1987; Russell, 1990; Sternberg *et al.*, 1990). Fast-response measurements of suspended sediment concentrations can be obtained at fixed elevations above the sea bed when the sensors are deployed in vertical arrays in the beach face. The OBS (see Appendix I) is a type of nephelometer for measuring turbidity and solids concentrations by detecting scattered radiation from suspended particulate matter. Whilst most nephelometers detect both forward and backscattered radiation, the OBS sensor detects only radiation scattered at angles >140°. The OBS (Plate 3.6) is designed to be rugged and robust, and capable of surviving the high energy conditions of the coastal zone. Their main disadvantages include: the intrusive nature of the OBS's to the surrounding aqueous solution and their inability to monitor the total concentration profiles, unlike sensors such as, the Acoustic Concentration Meter (ACM) described by Hanes *et al.* (1988).

The OBS has a sensitivity to high-angle backscatterance which is maximised through the use of a large area detector. The OBS (Figure 3.5) consists of a detector, comprising four silicon photo-diodes, a linear solid state temperature transducer, and an infra-red emitting diode (IRED). Sensor components are housed in a glass-filled polycarbonate shell with optical-grade epoxy resin. The compact arrangement of the instrument's components allows minimal internal scatterance and absorption losses since the distance between the emitter and detector is short. The operation of the OBS system is more fully described in the manual provided by D & A Instruments (1988).

The response of the OBS is dependent upon the size distribution, composition, and shape of the particles suspended in the water column. Since the size and refractive indices of the suspended solids encountered by the OBS influence the light scattering properties of the sediment in suspension, the calibration of OBS's must, therefore, be conducted using a homogeneous suspension of sediment from the experimental site (Downing *et al.*, 1981). However, this suggested calibration procedure poses a range of problems, in particular the calibration of OBS's in a homogeneous sediment suspension mixture. In the real beach environment, the situation is naturally made

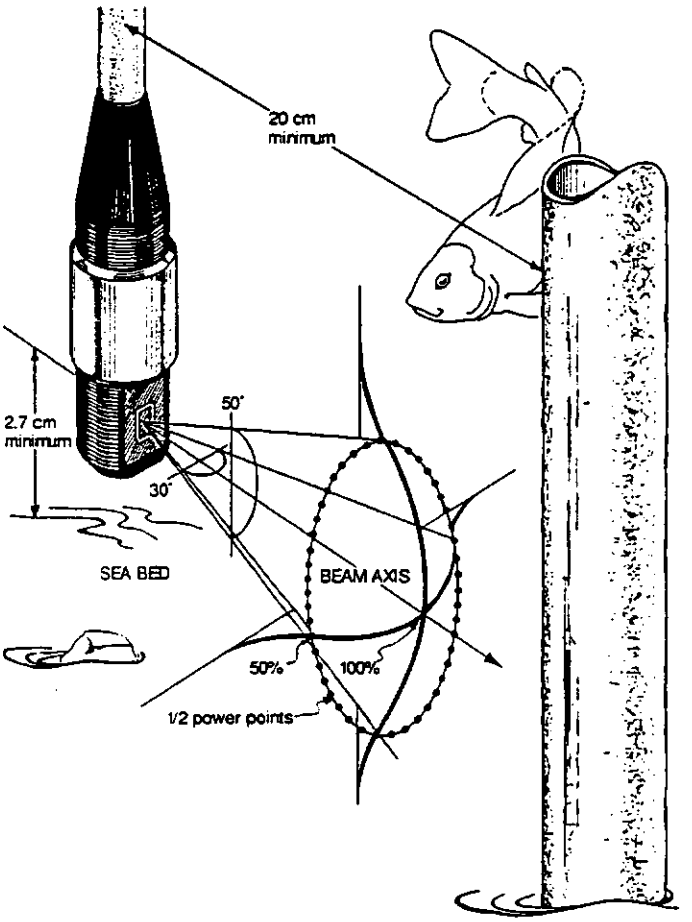

FIGURE 3.5 The OBS beam pattern (from D & A Instruments, 1988).

PLATE 3.6 Close-up of three optical backscatter sensors fixed by tape to the mounting structure, secured in the seabed.

complicated by suspension of a range of sediment particle sizes, and the suspended sediment concentration measurements examined in this study were calibrated using a non-homogeneous mixture of sediment sampled at the field site. It should be noted that calibration of OBS data in the laboratory relied upon the assumption that particle size distribution was independent of height above the seabed. Whilst it is generally considered that there is a natural fining of sediment grain size upwards through the water column. Because the actual distribution of grain size above the sea floor is not known, it is therefore assumed reasonable to calibrate the optical backscatter sensors in a relatively constant distribution of suspended sediment.

Recently, Green and Boon (1993) have proposed a method for estimating the concentrations of non-homogeneous (*i.e.* sand and silt mixtures) sediment suspensions using optical backscatter sensors. Their technique appears to remove the need to calibrate against an arbitrary range of mixtures. Instead, sensor calibration need only be performed against 'end-member' sediments (>63μ sand and <63μ silt samples) to create a single set of calibrations which are then applied to backscatter data from any non-homogeneous suspension, made up from the end-members. This method is, however, based upon the assumption that constituent interaction (*e.g.* grain shielding and multiple scattering) does not significantly affect the sensor response. It will be interesting to see how well this method applies to the natural beach environment, where more than two end-members tend to occur.

3.3.4 DATA LOGGING TECHNIQUES

In total, 32 channels of data were collected. Sampling was continuous throughout the 10 tides measured, digitising at a frequency of 2Hz. With approximately 9 hours per tide, the total yield was 90 hours of data or 20 million data points (the equivalent of 130 megabytes of data). A description of the B-BAND data set is provided in Table 3.3.

The extensive and high-quality data set which resulted from the Spurn Head field experiment was achieved through the development of an efficient electronic system for the data collection procedure. Figure 3.6 shows the B-BAND data

TABLE 3.3 Summary of the B-BAND Spurn Head field experiment data-set.

ORDER OF TIDES LOGGED	SPURN '91 DATE	Tide time SPURN (HW Grimsby -14 mins) (LW Immingham -24 mins)		LW CHECKS: Beach Profile	LW CHECKS: No of DOD rods measured	LW CHECKS: Instrument heights	(!) Tide Height	Data Recorded	No of 17 min files	WORKING PT'S A1	PT'S A2	PT'S A3	PT'S A4	WORKING EMCM'S A1	EMCM'S A2	EMCM'S A3	EMCM'S A4	WORKING OBS'S A1	OBS'S A2	OBS'S A3	OBS'S A4	Wind and wave conditions	Equipment Notes
		0122	LW	X	X	X	0.8															Small waves 1'-2' choppy N.E. wind	Blew one channel on bottom annular EMCM on A4
	Tue 16th	0721	HW				6.9	X	O														A1 OBS didn't work when deployed
164pm	April	1338	LW	X	X	X	0.9															Strong N. wind 0.6m CHOPPY	A3 OBS didn't work when deployed
1		1931	HW				7.1	JH √	5	√	√	√	√	√	2	3	2½	X	3 √	X	?	Strong N. wind 3m CLEAN SWELL	
		0200	LW	X	X	X	0.8																
	Wed 17th	0759	HW				6.9	X	O													Strong N. wind 2m swell	A3 rig is now skewed round and lying at 13°
174pm	April	1417	LW	X	X	X	0.9																Top Valeport sphere on A4 was badly bent, it broke off later
2		2013	HW				7.0	JH √	23	√	√	√	√	√	2	3	1½	X	3 √	X	X	Fresh N. wind 2m cleanish swell	A4 OBS were cut off to prevent damage
		0237	LW	X	X	X	1.0																
	Thur 18th	0840	HW				6.8	X	O														
184pm	April	1456	LW	√	9 √	√	1.0															Mod to fresh N.N.E. wind 0.6-1.0m swell with sidechop	Bottom EMCM on A3 may be buried occasionally
3		2101	HW				6.8	HP √	27	√	√	√	√	√	2	3	1½	X	3 √	X	X	Mod to fresh N.N.E. wind 2m Swell&sidechop	
		0316	LW	X	X	X	1.3															Mod to fresh N.N.E. wind swell&sidechop	
	Fri 19th	0921	HW				6.6	X	O														
194pm	April	1540	LW	√	9 √	√	1.2															Fresh N.E. wind 0.6m peaky swell	A3 OBS fixed and re-deployed
4		2152	HW				6.5	JH √	27	√	√	√	√	√	2	3	1½	X	3 √	3 √	X	Fresh N.N.E. wind 1.35m swell&sidechop	
		0358	LW	X	X	X	1.7															Mod N/N.W. wind 0.8-1m choppy swell	
	Sat 20th	1009	HW				6.3	X	O														Problems with middle OBS on A2?
204pm	April	1631	LW	√	9 √	√	1.5															NO WIND 0.4m peaky swell	Powered up OBS's but top sensor(s/n 70) didn't work
5		2256	HW				6.1	PR √	30	√	√	√	√	√	2	3	1½	X	2 √	3 √	2 √	NO WIND (SW swell) 0.4m very clean	
		0450	LW	√	9 √*	√*	2.2															No wind (light S.W.) 0.4m clean swell	
214am	Sun 21st April	1110	HW				6.0	HP √	31	√	√	√	√	√	2	3	1½	X	2 √	3 √	2 √	Mod to fresh S.W. wind 0.3m slight chop	PT's Didn't work for the first 5, 17min runs
6		1738	LW	√	25 √	√	1.8															mod to fresh S.W wind 0.2m choppy	
		0016	HW				5.7	X	0														
	Mon 22nd	0603	LW	√*	X	X	2.5															Mod N.W. wind 0.3m clean swell	
224pm	April	1232	HW				5.8	PR √	39	√	√	√	√	√	2	3	1½	X	2 √	3 √	2 √	Fresh N.N.E. wind 0.9m swell&chop	
7		1905	LW	√	25 √	√	1.9															Fresh N.E. wind 0.6m choppy swell	

* Incomplete Measurements (Tide covering instruments)
(!) Tide Ht. chart datum (chD=-3.9m O.D Newlyn) for LW Immingham.

TABLE 3.3 (continued from previous page).

ORDER OF TIDES LOGGED	SPURN '91 DATE	Tide time SPURN (HW Grimsby -14 mins) (LW Immingham -24 mins)		Beach Profile	No of DOD rods measured	Instrument heights	(1) Tide Height	Data Recorded	No of 17 min files	WORKING PT'S A1	PT'S A2	PT'S A3	PT'S A4	WORKING EMCM'S A1	EMCM'S A2	EMCM'S A3	EMCM'S A4	WORKING OBS'S A1	OBS'S A2	OBS'S A3	OBS'S A4	Wind and wave conditions	Equipment Notes
234am		0146	HW				5.7	ET √	40	1 √	1 √	1 √	1 √	1 √	2 √	3 √	1 √	X	2 √	2 √	2 √		
8	Tue 23rd April	0732	LW	√	X	X	2.6															Light W. wind 0.8m clean swell	
9		1402	HW				5.8	PR √	34	1 √	1 √	1 √	1 √	1 √	2 √	3 √	1 √	X	2 √	2 √	2 √	Light sea breeze 1.5m clean swell	
234pm		2031	LW	√	25 √	√	1.8															Mod S. wind 0.4m choppy	
		0307	HW				5.8	X	0														
	Wed 24rd April	0854	LW	X	X	X	2.4															Mod S.E. wind 0.6m choppy swell	
		1516	HW				6.0	X	0													Mod S.E. wind 0.3m choppy swell	
		2141	LW	X	X	X	1.5															Mod S.E. wind 0.5m choppy swell	
		0408	HW				6.1	X	0														
	Thur 25th April	0958	LW	√	25 √	√	2.1																
254pm		1641	HW				6.3	√	36	1 √	1 √	1 √	1 √	1 √	2 √	3 √	1 √	X	2 √	2 √	2 √	Mod to fresh E. wind 0.3m wind waves	
10		2239	LW				1.3																

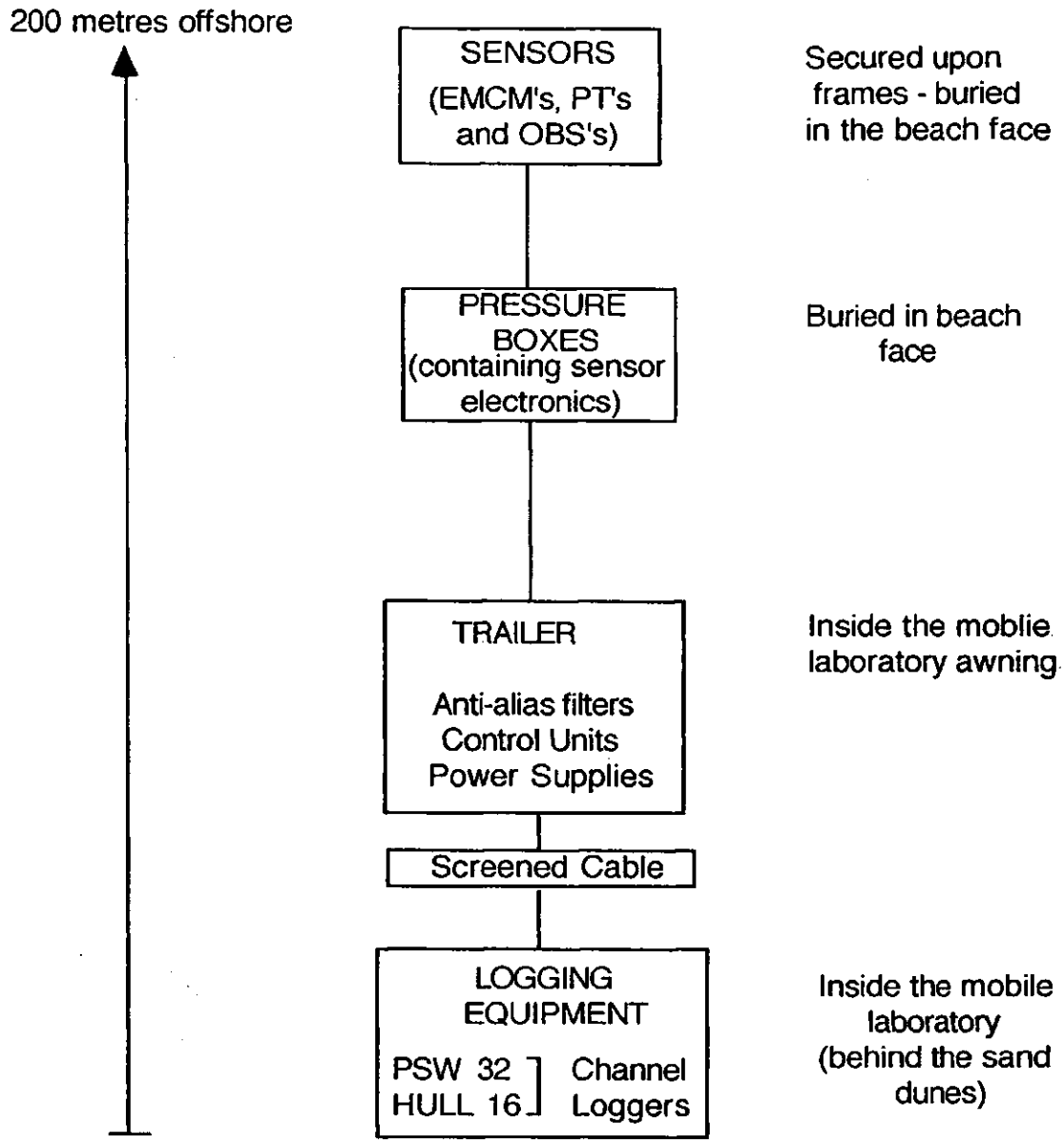

FIGURE 3.6 Data collection procedure for the Spurn Head field deployment.

collection set-up, comprising various sensors for monitoring the nearshore processes (*i.e.* EMCM's, PT's and OBS's), the sensors were secured by rigid stainless steel mounting structures buried in the beach face. Prior to the field deployment of the sensors, laboratory checks were run to examine the noise levels and frequencies of each probe (Table 3.4). The output noise for each sensor, measured during input to the ADC (analogue-to-digital converter), was generally taken to be <3mV, which was equivalent to <6.0mm for the sea surface elevation, $<1.8 cms^{-1}$ peak-to-peak for the current velocity and $<0.2 gl^{-1}$ for the suspended sediment concentration.

The electronic components of each sensor are protected and enclosed in robust pressure cases which were covered with netting and lead weights and positioned securely below the beach face. The pressure cases were connected by cable to the units held in a small trailer under an awning alongside the caravan. The trailer, containing control units, power supplies and anti-alias filters (using a cut-off of 1Hz) for signal conditioning and to prevent aliasing when digitising, was connected to the logging equipment inside the caravan by screened cable which allowed the filtered signals some additional protection against noise. Inside the caravan, a Microlink™ data acquisition system included an ADC, further signal conditioning to remove any noise or glitches and a multiplexer which sampled each channel of data in sequence. Finally, the data is stored. The data was transferred from the Microlink system to the hard disk of a micro-computer (IBM™ Opus) via an IEEE (Institute of Electrical and Electronic Engineers)-parallel link. Post-deployment, the data were backed up onto 3.5" floppy disks before conversion into ASCII (American Standard Code for Information Interchange) form and transfer via Kermit onto the VAX mainframe computer system at the University of Wales, Cardiff. The B-BAND data were converted into physical units using the results of the sensor calibrations and distributed to both the Universities of Hull and Plymouth. The Spurn Head data are stored in Plymouth upon the PRIME mainframe computer system, a Macintosh SE hard disk, 3.5" floppy disks and a 9-track magnetic tape.

Date	Instrument Probe/electronics No.		Pre-filter Noise Frequency	Pre-filter Noise Peak to peak mV	Pre-filter Offset mV	Post-filter Noise Frequency	Post-filter Noise Peak to peak mV	Post-filter Offset mV	Translation of noise levels to equivilent units (rms values)
21/3/91	A3 SPHERICAL. TOP	X	SF. 1MHz	12	4	0.5 MHz	2-3	4	
		Y	SF. 1MHz	12	-5	0.5 MHz	2-3	-5	
21/3/91	A3 SPHERICAL. MID	X	SF. 1MHz	12	0	0.5 MHz	2-3	0	
		Y	SF. 1MHz	12	6	0.5 MHz	2-3	6	
21/3/91	A3 SPHERICAL. BOT	X	SF. 1MHz	12	4	0.5 MHz	2-3	4	
		Y	SF. 1MHz	12	5	0.5 MHz	2-3	5	0.92-1.28
22/3/91	A4 ANNULAR. BOT	X	SF. 1MHz	20	7	0.5 MHz	3-4	14	cm/s
		Y	SF. 1MHz	20	68	0.5 MHz	3-4	68	
22/3/91	A4 ANNULAR . MID	X	SF. 1MHz	20	75	0.5 MHz	3-4	75	
		Y	SF. 1MHz	20	-27	0.5 MHz	3-4	-27	
22/3/91	A4 SPHERICAL. TOP	X	SF. 1MHz	20	14	0.5 MHz	3-4	14	
		Y	SF. 1MHz	20	-8	0.5 MHz	3-4	-8	
22/3/91	A1 PT		2.86 KHz	1000	1600	20 KHz	3	1600	
	A2 PT		2.86 KHz	1000	1320	20 KHz	3	1320	0.28-0.45
22/3/91	A3 PT		2.86 KHz	1000	2070	20 KHz	3	2070	cm
	A4 PT		2.86 KHz	1000	1390	20 KHz	3	1390	
26/3/91	Second box down.	x	SF. 1MHz	5mV	-22	0.5 MHz	3	-22	
	probe (490)	y	SF. 1MHz	5mV	-27	0.5 MHz	3	-27	
26/3/91	Third box down.	x	SF. 1MHz	5mV	-27	0.5 MHz	3	-27	
	probe (487)	y	SF. 1MHz	5mV	-31	0.5 MHz	3	-31	
8/4/91	Top box .	x	SF. 1MHz	5mV	-83	0.5 MHz	3	-83	
	Probe 489	y	SF. 1MHz	5mV	-13	0.5 MHz	3	-13	0.28-0.45
8/4/91	Bottom box.	x	SF. 1MHz	5mV	-18	0.5 MHz	3	-18	cm/s
	Probe 486	y	SF. 1MHz	5mV	-13	0.5 MHz	3	-13	
10/4/91	OBS A4	70	227 Hz	1500	-15	0.5 MHz	3	-15	
		66	(SF)	(SF)	-6	0.5 MHz	3	-6	
		65			-143			-143	
10/4/91	OBS A2	213	227 Hz	100	-2	0.5 MHz	3	-2	
		141	(SF)		3	0.5 MHz	3	3	
		139			5			6	0.07-0.14
10/4/91	OBS A3	138	227 Hz	100	70	0.5 MHz	3	70	g/l
		140	(SF)		60	0.5 MHz	3	60	
		137			0			0	
10/4/91	OBS A1	sensor 212 board 69	227 Hz (SF)	100	40	0.5 MHz	3	40	
0.5 MHz	3								
	SF = Switching Frequency . 0.5 MHz = PSU noise.								

TABLE 3.4 Noise levels and frequencies for the sensors deployed at Spurn Head.

3.4 SUMMARY

This chapter has discussed the second B-BAND field experiment which was carried out on Spurn Head, Humberside. Spurn Head, a mature sand and shingle spit, is located on the fastest eroding coastline in Europe, recently undergoing a number of breaches which have further weakened the fragile peninsula's coastal defences. The instrumentation used to measure the wave and current conditions and suspended sediment concentrations over a four week period, have been examined. The next chapter investigates the methods used to handle the data collected at this field experiment - from the calibration of the raw data to the analysis routines used to help understand some of the processes which brought about sediment transport in this macro-tidal environment.

CHAPTER 4
DATA MANIPULATION AND ANALYSIS

4.1 INTRODUCTION

Data analysis, in this study, comprised a range of data manipulation techniques including; data calibration, selection, treatment and storage, time-series analysis, spectral analysis, determination of a groupiness factor, cross-correlation analysis, velocity moment and flux coupling analysis. The methods and techniques developed for examining pressure transducer, electromagnetic current meter and optical back-scatter sensor measurements will be discussed.

4.2 DATA MANIPULATION

Data collection at the Spurn Head field site generated an extensive data-set which, in turn, has generated numerous opportunities for research. Prior to carrying out the analysis, the field sensors had to undergo post-deployment calibration (in order to compare with pre-deployment measurements). Subsequently, the data were examined and treated for spikes or glitches and a representative sub-set of the data was selected.

4.2.1 DATA CALIBRATION AND CORRECTION PROCEDURES

Calibration of the instruments was carried out before and after the field deployment. The calibration procedures were carried out at the Royal Naval Engineering College (R.N.E.C.) Manadon, Plymouth and in the Institute of Marine Studies, University of

Plymouth. Calibrated measurements from the Spurn Head data were obtained by inputting the various sensor calibration parameters into the Fortran programme 'Filecal.For', written by Dr. Mark Davidson (University of Plymouth).

Electromagnetic current meters (EMCM's) were calibrated in the laboratory by towing each sensor over a range of speeds (from 0 to $\pm$ 2.0ms^{-1}) in the 50m long testing tank at R.N.E.C. Manadon. A group of three sensors were calibrated at the same time, and runs were carried out for both *x* and *y* channels of each instrument in both positive and negative directions. Interference between the two sensors was not found to be a problem if the sensors were fixed greater than four sensor diameters apart. Calibration was carried out, as far as possible, with the sensors in their field configuration, so that any interference which may have occurred would be representative of the natural field conditions. In the laboratory, mean voltage was recorded for each tow and plotted against tow speed (Figure 4.1). Instrument offsets and gains were calculated from a first-order least squares regression fit of towing tank data, where:

$$\text{Actual velocity}(ms^{-1}) = \text{Gain}(ms^{-1}V^{-1}) * \text{Output}(V) + \text{Offset}(ms^{-1}) \qquad (4.1)$$

and

$$\text{Gain} = \text{Sensitivity}^{-1}(\text{inV}(ms^{-1})^{-1}, \text{ the gradient of the regression line}) \qquad (4.2)$$

Zero offset values of the sensors were required for computation of the actual current velocity measurements. Pre- and post-deployment zero offsets were calculated in the laboratory for still water conditions, using an average of pre- and post-field experiment offset values in the following relationship,

$$\text{Offset}\ (ms^{-1}) = \text{Offset}\ (V) * \text{Gain}\ (ms^{-1}V^{-1}) \qquad (4.3)$$

In the field, zero offsets were recorded by holding the sensors still in a container filled with seawater and the output voltage recorded over the span of a data run.

The pressure transducers (PT's) were also calibrated in the towing tank at Manadon. The sensors were lowered to specified depths in the water column, at $\approx$ 0.25m depth intervals through 0 to 3m, whilst the voltage output was recorded. The first-order least squares regression fit was plotted for the pressure transducer calibration data using voltage output and corresponding depth values (Figure 4.2). The gradient of the regression line was used to estimate the sensitivity and gain of the instruments.

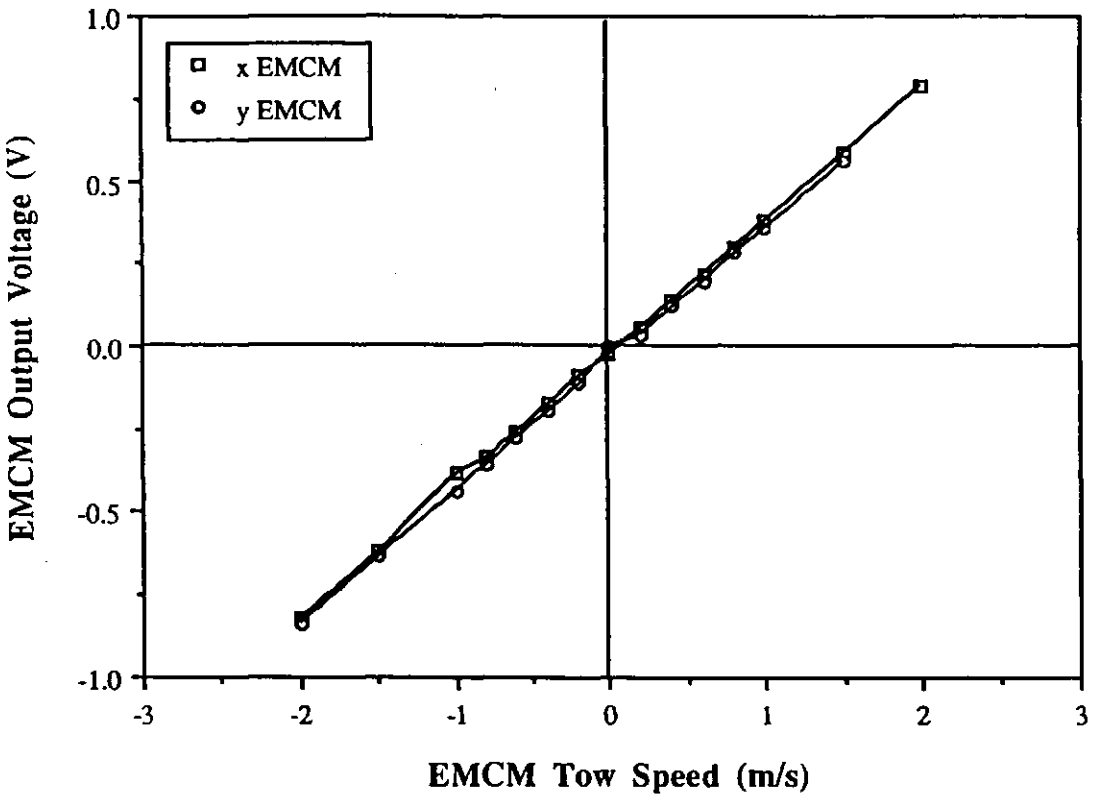

FIGURE 4.1 Post-deployment calibration of the bottom current meter on Rig A2 for the cross-shore and longshore channels.

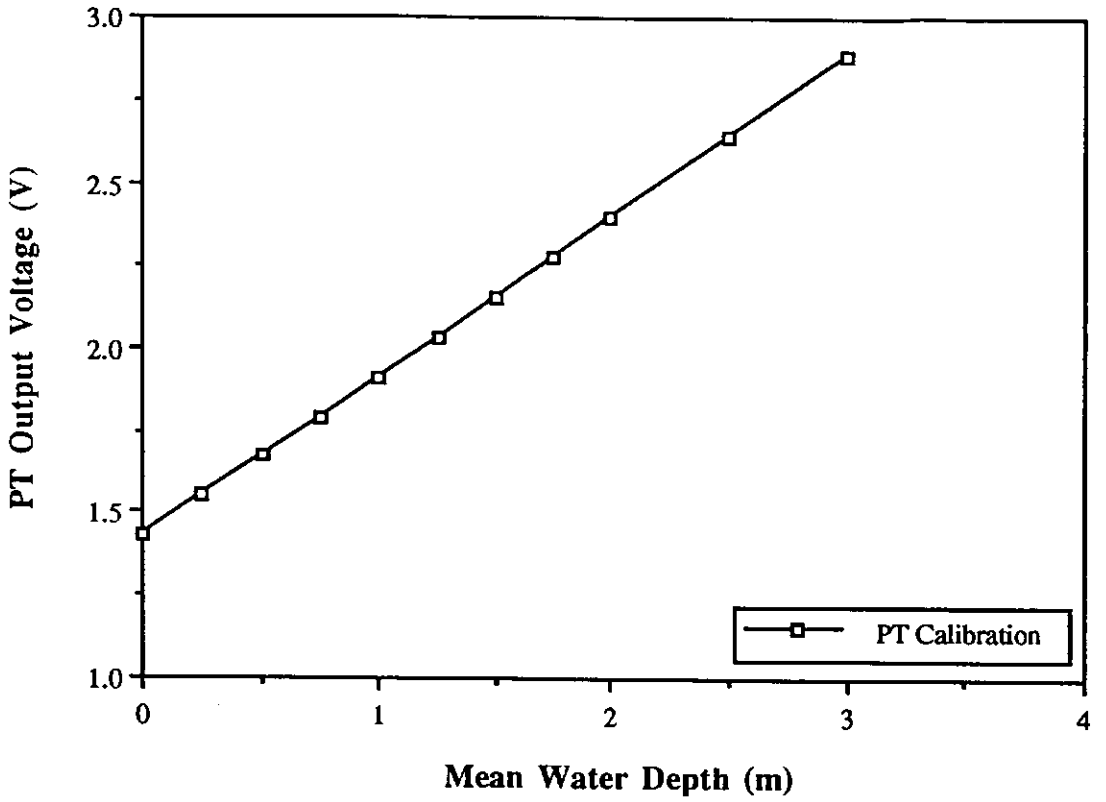

FIGURE 4.2 Post-deployment calibration of the pressure transducer on Rig A2.

Actual sea surface elevation was derived from the pressure transducer measurements using the following expression,

$$\text{Actual surface elevation(m)} = \text{Gain } (mV^{-1}) * (V_{raw} - V_0) \qquad (4.4)$$

where the zero offset (V_0) was recorded during the Spurn Head field experiment whilst the pressure transducers were dry.

Optical back-scatter sensors (OBS's) were calibrated in the re-circulating facility at R.N.E.C. Manadon which is shown in Plate 4.1. The re-circulating tank had a capacity of ≈ 50litres and was designed and constructed by Mr. Tony Saunders at the Naval College. Inside the tank, the optical backscatter sensors were subjected to a non-homogeneous suspension of the field sediment sampled near each instrument rig location during the Spurn Head experiment. A range of particle sizes existed at the instrument rig location, so the sediment sample used in the calibration procedure needed to be representative of the sediment being transported back and forth over the sensors at Spurn Head.

Basically, the OBS calibration tank operated by sediment being introduced into the top of the system (into the white funnel). Water travelling from the top of the system moved the sediment through the system of tubes, over the 'lemon squeezer-sediment distributors', and down into the lower chamber. The purpose of the distributors was to introduce a homogeneous 'curtain' of sediment into the tank. In the lower chamber, three optical back-scatter sensors and siphon tube-sediment samplers were placed, attached to supporting stainless steel rods, and held in place by a retort stand and clamps. Once in the lower chamber, the sediment became suspended in the water. The fluid and sediment were then constantly pumped from the bottom cylindrical container up to the top again, and so on. Suspended sediment concentrations were measured by the optical back-scatter sensors whilst the siphoning tubes, positioned adjacent to the OBS's, were operated over the duration of the calibration data run to collect water/sediment mixtures being seen by the OBS's.

The concentrations in the water samples were measured by filtering, drying and weighing the collected sand. The sand collected at the field site comprised a range of sand particle sizes which, as discussed in Section 3.3.3 earlier, was more representative

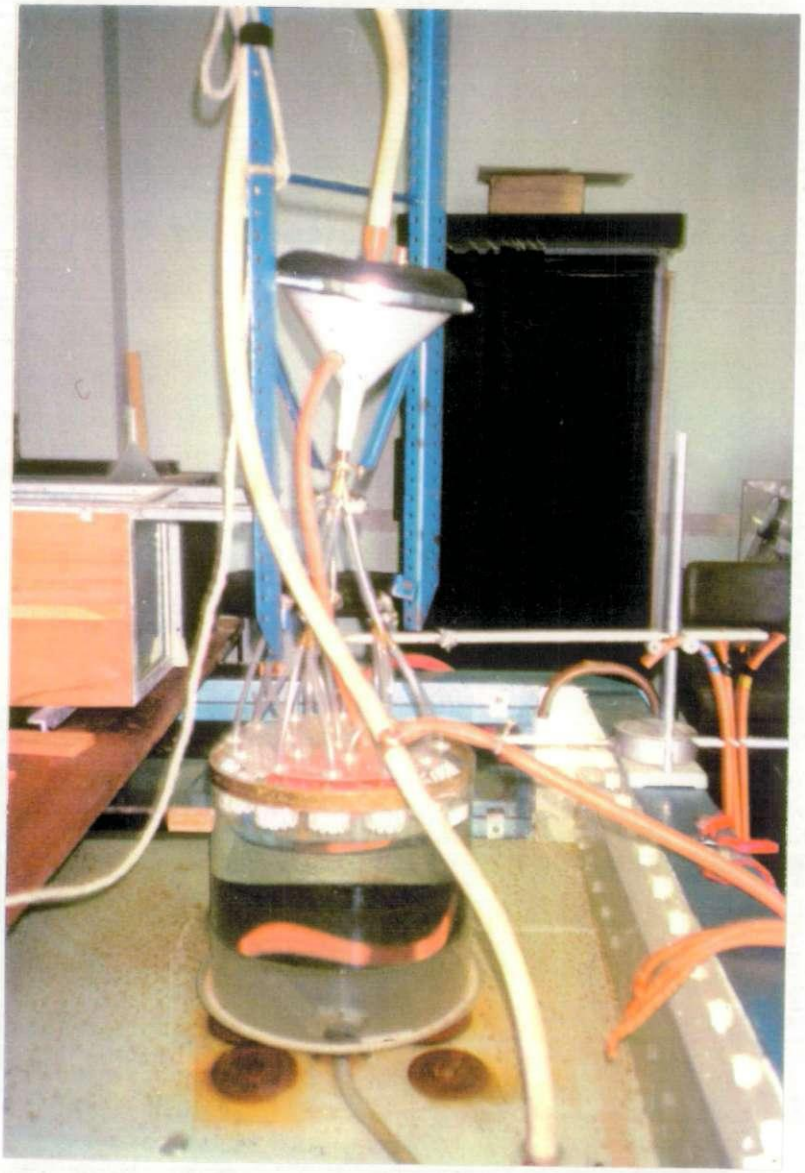

PLATE 4.1 The re-circulating facility for calibrating the OBS sensors.

of the natural beach environment in which the OBS's were operating, than using specific grain sizes. Increasing concentrations of sand were introduced into the re-circulating unit, *i.e.* at nominal concentrations of 0, 2, 4, 6, 10, 20, 35gl^{-1}, and the mean voltage recorded at each sequential increase in concentration. The mean voltage of each OBS output was plotted against the concentrations of the siphon samples and a regression line calculated (Figure 4.3). Unfortunately, the background concentration in the re-circulating system tended to increase throughout each calibration experiment and thus, with increasing concentration of sediment in the tank the background concentration, also increased. This increased background concentration may have resulted either from collisions of the sediment grains circulating in the tank, thus causing grains to flake or break up, or a more probable explanation may be abrasion of the sediment grains as they passed through the water pump. Whatever the cause, a slowly increasing suspension of very fine particles occurred as the calibration proceeded. In carrying out the optical backscatter sensor calibration calculations, therefore, the increased background concentration needed to be accounted for. Correcting the actual OBS readings required the assumption that back-ground turbidity was proportional to the sand concentration so that,

$$\frac{\text{Background reading post - calibration experiment (V)} - \text{Background reading at } 0gl^{-1}}{\text{Actual end concentration of dry sand } \left(gl^{-1}\right)}$$

$$= \text{Overall background turbidity per unit concentration of dry sand (BT1)} \qquad (4.5)$$

$$\text{Background turbidity (BT1)} * \text{Concentration of dry sand (i.e. with each serial addition)}$$

$$= \text{Background turbidity for one concentration (BT2)} \qquad (4.6)$$

and

$$\text{OBS mean reading (V)} - \text{(BT2)} = \text{Corrected OBS reading} \qquad (4.7)$$

The corrected suspended sediment concentration values are plotted on the same graph as the original readings and a best-fit line drawn through the data (Figure 4.3). Figure 4.3 shows the calibration results for the mid-OBS (this was used because the electronic board in the bottom-OBS stopped working due to water leakage into the pressure case).

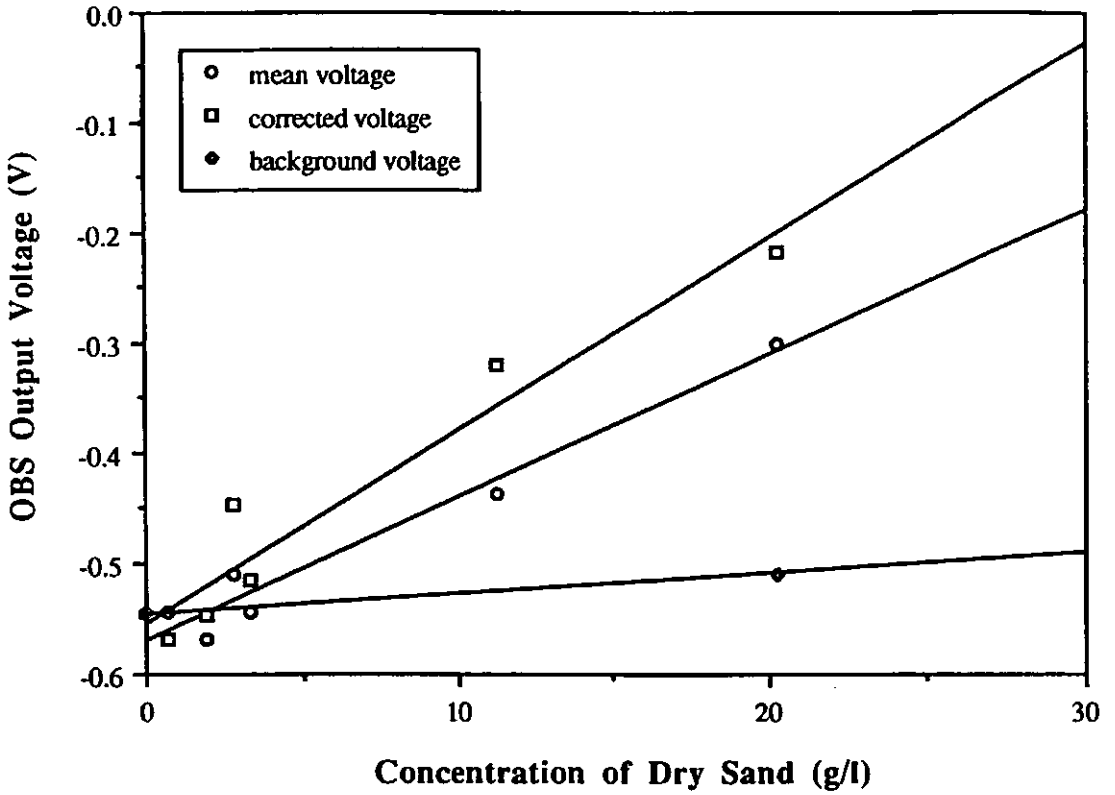

FIGURE 4.3 Post-deployment calibration of the mid-optical backscatter sensor on Rig A2.

Consequently, the previous B-BAND calibration results from the Llangenith field experiment were used to calibrate the OBS sensor examined here. The example, shown in Figure 4.3, displays the regression line which represents the calibration equation for the conversion of the suspended sediment concentration measurements from the middle sensor on Rig A2. Similar calculations were carried out for the remaining OBS measurements.

4.2.2 DATA SELECTION

Owing to the consistent reliability and good quality of the data, Rig A2 (see Figure 3.4) was selected as the point source of measurements for analysis in this study. Of the ten tides logged at the Spurn Head field experiment, three tides, with varying characteristics were selected for data analysis. Table 3.3 (in the previous chapter) displayed the characteristics and primary information concerning the three tides examined including the state of the instruments through the field experiment, the number of files logged, and the wind and wave conditions. Tide 164PM, comprised four data runs, with 17 minutes of data in each run. Tide 164PM was logged on April 16th, 1991 during a violent storm event with a very strong wind, a maximum offshore significant wave height (H_S) value of 1.6m and swell waves of up to 3m breaking wave height. Tide 184PM (April 18th, 1991) covered moderate swell and choppy conditions and a maximum H_S value of 1.1m and a moderate wind. Tide 234PM (April 23rd, 1991) displayed calmer conditions with smaller swell and choppy waves and a maximum H_S value of $\approx$ 0.8m. Selecting these three tidal cycles has enabled the examination of a diverse range of nearshore hydrodynamic conditions at Spurn Head.

4.2.3 PRE-ANALYSIS PROCESSING, QUALITY CONTROL AND STORAGE

The calibrated data were distributed to the Universities of Hull and Plymouth from the Spurn Head data-base which was maintained at the University of Cardiff. The selected tidal cycles of data were forwarded to the two Institutes via a portable Apple Macintosh hard disk (40MB), magnetic tape or 3.5" floppy discs. The chosen data format was ASCII a type of binary code.

Examination of the data points in each data run was the initial step in processing the sensor measurements. Within the data-set, the data runs were divided amongst files which, in turn, were divided into sub-directories and directories. Each main directory was labelled according to tidal cycle (*e.g.* Tide 164PM, Tide 184PM), the files were further divided into sub-directories, according to sensor type (*i.e.* PT, longshore EMCM, cross-shore EMCM and OBS) and sensor position (A2T, A2M, A2B, A3B, A3T, A3M, A4M and A4B, where T=top, M=middle and B=bottom) and files, labelled according to run number, for Rigs A2, A3 and A4, respectively.

Examination of the calibrated data files was carried out using the PRIME mainframe computer system, based at the University of Plymouth. Time series of the measurements were created from the original ASCII files of calibrated data for each instrument. The procedure involved the extraction of a selected column of data, representing one sensor data run, and creating a column of values for time (*e.g.* 0.5s interval between each data point) to form a time series. The original selected tides data were stored on the PRIME mainframe system, Macintosh hard disk, magnetic tape and 3.5" floppy disks.

If the original data runs contained any anomalous points, they were removed using the editing facilities on the PRIME taking care not to significantly alter the information in the run. A visual examination of all time series enabled the location of any glitches, spikes or discontinuities. Generally the glitches were single spikes caused by seaweed passing over the sensor. Larger and longer period erroneous events were most likely to be caused by the instruments being either momentarily out of the water (*i.e.* the passing of a large wave trough), or as the water level decreased through the tidal cycle. Single point glitches (*i.e.* spikes) were removed and the space filled by a mean value of the time series after removal of the anomalous points; where major discontinuities (*i.e.* of duration >20 consecutive data points $\approx$ 10 seconds of data) occurred the file was excluded from any further data analysis.

Data manipulation of the time series, spectral analysis and plotting of the larger quantity data-sets were carried out on the PRIME mainframe system at the University of Plymouth, using an IBM Opus PC as the remote terminal. The final statistical

procedures and presentation of results was achieved using spreadsheet and/or statistical packages held on an Apple Macintosh SE.

4.3 ANALYTICAL PROCEDURES AND DATA HANDLING TECHNIQUES

Subsequent to the initial processing routines described in Section 4.2, the resulting current velocity, sea surface elevation and suspended sediment concentration data-sets were presented in a standard format, as digital data-points varying in time. Interpretation of these instantaneous fluctuations of pressure, current and suspended sediment concentration was achieved through the following techniques.

4.3.1 TIME SERIES ANALYSIS

A time series, a finite number of values of a process x, represented as a function of an independent variable t (where t is usually time), can be either 'deterministic' if future values can be predicted exactly or 'random' (stochastic), if future values can only be partly determined on the basis of past values (Chatfield, 1984). The vast majority of time series are stochastic, where precise predictions cannot be obtained and only statistical probabilities for future values can be produced.

Each time series is only a segment of a single realisation and as Priestley (1981) concluded, "it is from these data that we must infer as much as is possible about the properties of the entire process". The most important assumptions made about time series are that the corresponding stochastic process is stationary (containing no general trend) and that, as Jenkins and Watts (1968) stated, 'such a stationary stochastic process should be suitably described by the lower moments of its probability distributions'. The mean, variance, covariance function and the Fourier transform of the covariance function or power spectrum, comprise some of the lower moments of the probability distributions. The point here is that spectral analysis (in its usual form) says nothing about skewness, kurtosis *etc*. In fact, it could be argued that the assumptions in spectral analysis break down if these higher moments are large, although, in our case here, it is still a useful method of analysis.

The first phase of time series analysis was a continuation of the quality control

methods described previously in Section 4.2.2. This involved plotting the measurements against time so that any anomalous or dominant features of the time series (*e.g.* trend, discontinuities or spikes) can be identified and where necessary treated. Failure to pin-point faults or trends in the time series can influence any subsequent analysis and, therefore, the interpretation of results.

The choice of time series analysis methods is dependent upon whether the ultimate objective is to examine the trend of the observations or to examine the local fluctuations. In the case of the Spurn Head data-set, a dominant trend was seen in the pressure data owing to the superimposition of the tidal elevation, from flood to ebb tides, on the pressure records. Since it is the local fluctuations rather than the very long period motions which are important to this study, the trend was removed using a standard Fortran '77 routine, in order to obtain a quasi-stationary time series.

In order to examine the relative importance of the low- and high-frequency nearshore wave motions it was necessary to separate the time series into these constituent parts, and this was achieved through application of a Kaiser-Reed (1977) filter. It should be noted that prior to digital filtering of the time series, the records had to be de-meaned using another standard Fortran '77 routine (in addition to the original de-trending procedure) owing to possible distorting effects that the mean might have in any subsequent spectral analysis. The method of filtering, based upon the window function approach, utilised an adjustable weighting (window) function as part of the Nearly Equal Ripple Approximation (NER) method (Kaiser and Reed, 1977). The NER smoothing filter design is characterised by approximately equal pass-band and stop-band magnitude errors. The designs are very nearly the most efficient possible consistent with the filter performance specifications. The digital filter was written as a Fortran '77 programme (Appendix II) and incorporated the NER subroutine provided by Kaiser and Reed (1977). The filter specifications included $\lambda = 34, \beta_e = 0.05$ and $\partial_w = 0.01$ and where λ was the stopband loss (in dB), β_e the relative location of the ideal edge of the passband relative to the Nyquist frequency (Hz), and ∂_w the relative width of the transition band (Hz). The 0.05 Hz cut-off frequency was established through location of the main spectral trough between the incident and infra-gravity band peaks

(Kim, 1985). The spectral analysis techniques are described in more detail in Section 4.3.2. Figures 4.4(b) and (c) show examples of low- and high-passed components of a pressure transducer time series, whilst Figure 4.4(a) provides a comparison of these filtered time series with the original de-meaned and de-trended record.

4.3.2 SPECTRAL ANALYSIS

Spectral analysis provides a method of estimating the spectral density function (s.d.f.) of a particular time series and the application of techniques examining the s.d.f., are described as 'frequency domain' analyses as opposed to those routines which utilise 'time domain' analyses through the investigation of the sample auto-correlation function. Spectral analysis is essentially a modification of 'Fourier' analysis whereby any bounded function which repeats itself every T seconds can be represented exactly by a sum of sine and cosine terms called the Fourier series representation.

Spectral analysis was performed on the time series using a modified version of the I.E.E.E. cross-spectral analysis package described by Carter and Ferrie (1979). In this routine, two digital waveforms were fed into the programme where they underwent four basic steps in the estimation routine. Each time series was first segmented into N segments with each segment containing P data points. Secondly, each segment was multiplied by a smooth weighting function. The smooth weighting function was necessary in order to reduce errors which might be induced by side lobe leakage (Carter and Ferrie, 1979). Thirdly, the discrete Fourier coefficients were calculated using a Fast Fourier Transform (FFT) technique. Fourthly, these coefficients were then used to calculate the components of the power spectral density 'matrix' by squaring and adding the coefficients and averaging of these raw power spectral estimates over all the N segments.

Statistical error is the uncertainty in power spectral density measurements owing firstly to the quantity of data collected, secondly to the underlying probability nature of the data and thirdly, to the method adopted for deriving the desired parameter (Otnes and Enochson, 1972). The Spurn Head time series of 2048 data points was divided into 8 sequential segments of 256 data points (sampling frequency, Δt = 2Hz)

(a)

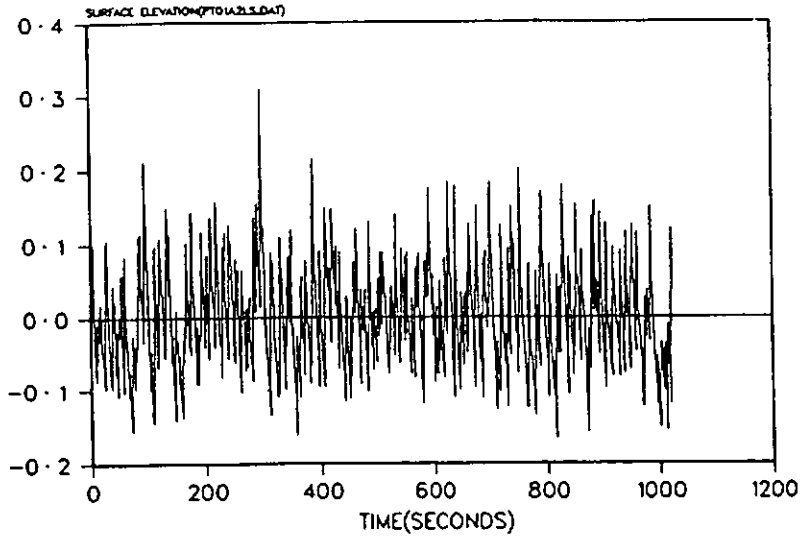

(b)

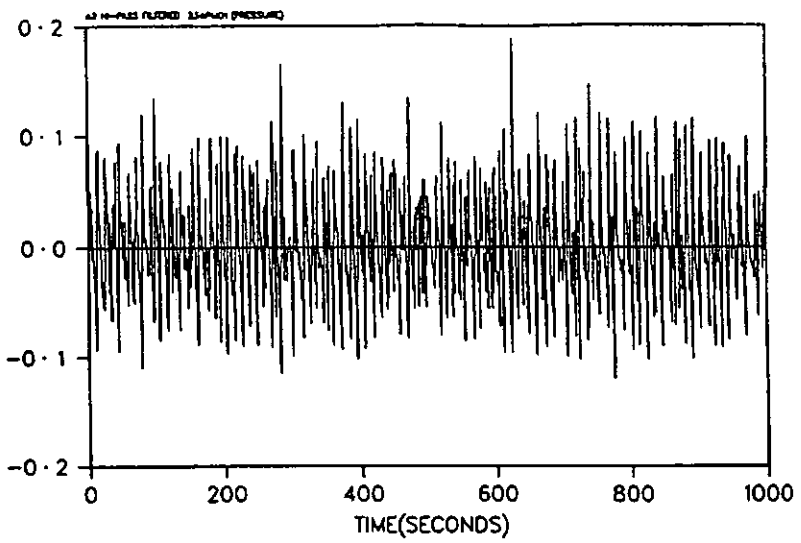

(c)

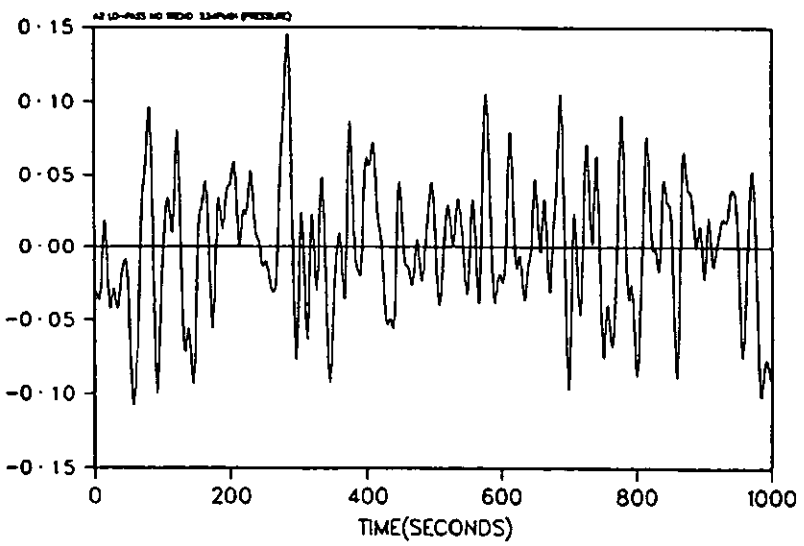

FIGURE 4.4 Examples of (a) Original pressure time series (b) High-pass component of pressure time series (c) Low-pass component of pressure time series

which formed 15 segments with a 50% overlap and consequently a spectral resolution of 0.0078 Hz was attained. The number of degrees of freedom was approximately, ν =27, according to Nuttal (1971) since, for 50% overlapping segments,

$$\nu = 3.82 * Nd - 3.24 \tag{4.8}$$

where Nd is the number of disjoint (non-overlapping) segments. The 95% confidence bounds, for a χ^2-squared (chi-squared) distribution, were described by multipliers which are best represented graphically (Jenkins and Watts, 1968). Hence, at the 95% confidence level the confidence limits for the spectral variance estimates were established using a Jenkins and Watts (1968) nomogram shown in Figure 4.5. The upper and lower confidence limits, with ν degrees of freedom at the 100 (1-α) percent confidence limit, are determined thus:

$$\frac{\nu}{x_\nu(\alpha/2)} \, , \, \frac{\nu}{x_\nu(1-\alpha/2)} \tag{4.9}$$

Typical spectra for the Spurn Head data-set are shown in Figure 4.6(a) and (b). These spectra are characterised by 27 degrees of freedom (d.o.f.) and lower and upper confidence limits of 0.62 and 1.80 respectively. Figures 4.6 (a) and (b) illustrate examples of spectra for a high tide and low tide pressure transducer data run from Tide 234PM (April 23, 1991).

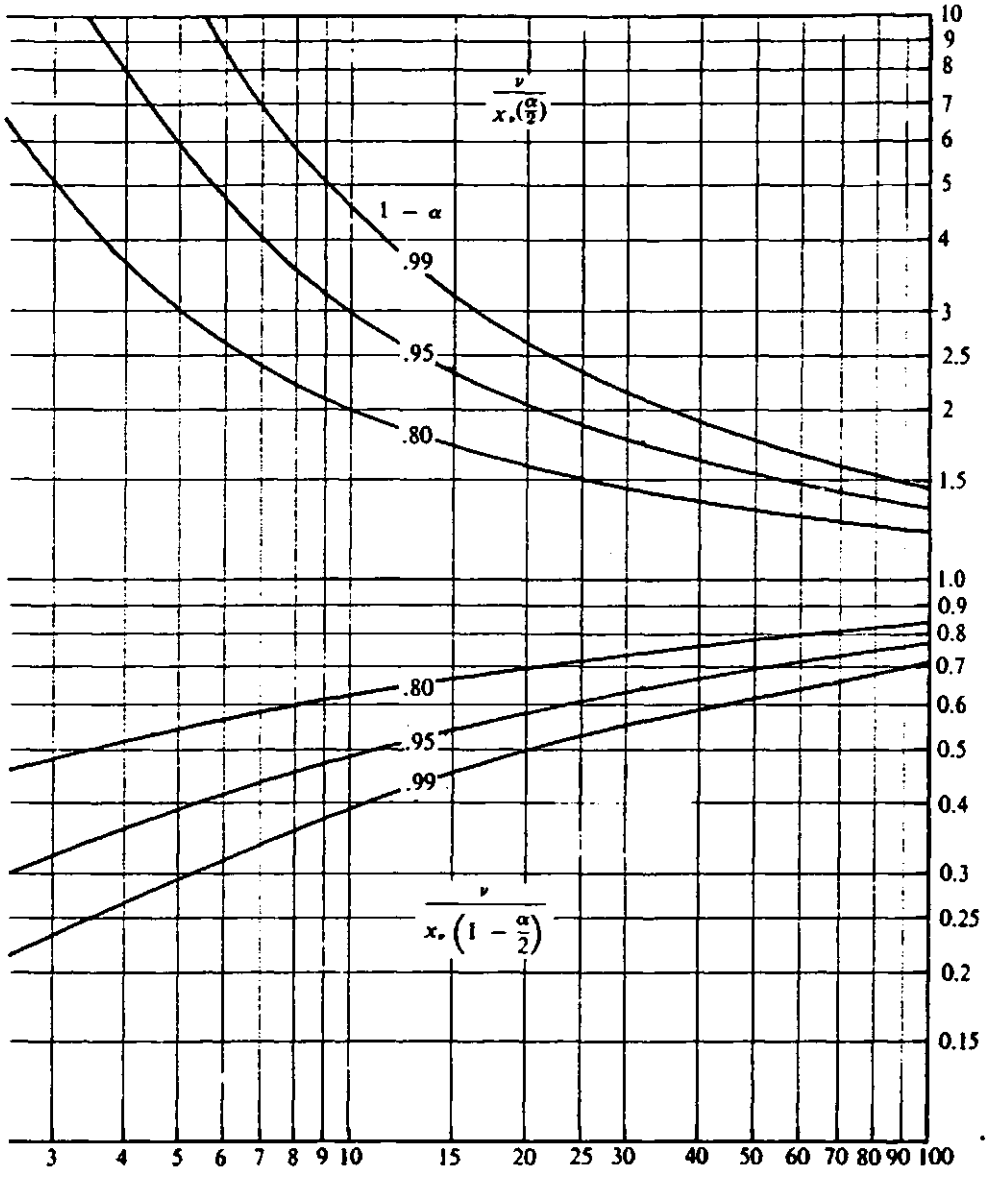

FIGURE 4.5 Plot of $\frac{\nu}{x_\nu(\alpha/2)}$, $\frac{\nu}{x_\nu(1-\alpha/2)}$ vs. ν for (1-α) = 0.80, 0.95 and 0.99 (from Jenkins and Watts, 1968).

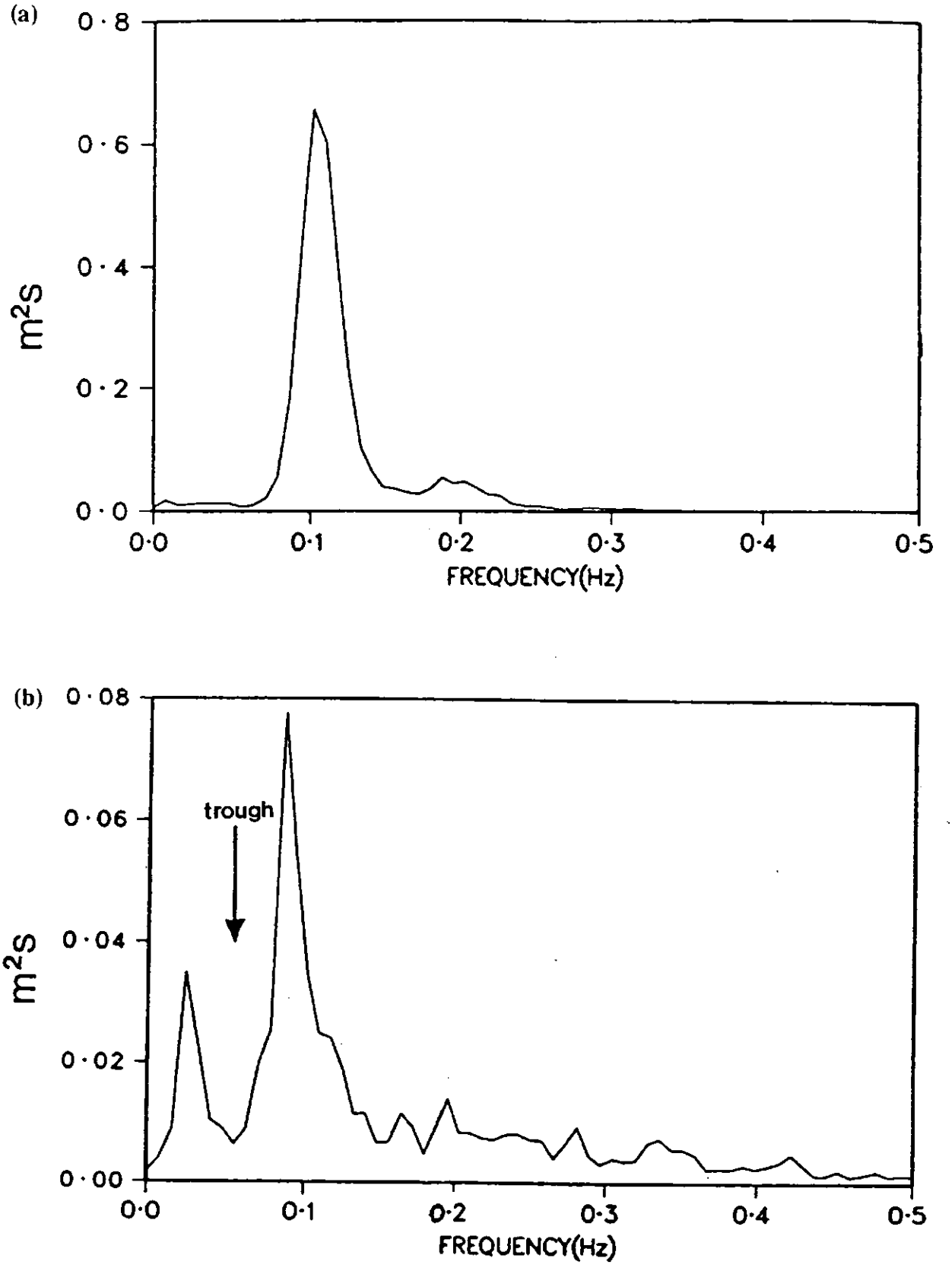

FIGURE 4.6 Examples of pressure spectra (a) at high tide and (b) at low tide. Only truncated spectra are shown here, the original pressure spectra normally extend to 1Hz.

4.3.3 DETERMINATION OF THE BREAKPOINT POSITION

It is essential that the location of the breaker point is determined in order to make an accurate interpretation of the findings when examining data from a point source. First the near-bed cross-shore and longshore current velocities and incident wave variance (Figure 4.7) were plotted for each tidal cycle, using electromagnetic current meter data from the bottom sensor on Rig A2 (0.1m height above the bed). Figure 4.7 illustrates the mean cross-shore and longshore current velocities for Tide 234PM. The steady cross-shore current reaches a maximum value, outside the surf zone, of $0.15ms^{-1}$ on both flood and ebb tides, and $<0.1ms^{-1}$ inside the surf zone. The steady longshore current reached a maximum value $0.45ms^{-1}$ inside the surf zone, and $0.35ms^{-1}$ outside the surf zone. Inside the surf zone, the mean longshore current is negative (directed southwards), whilst, outside the surf zone, the values are positive (directed northwards). On the other hand, the mean cross-shore current values are negative inside the surf zone (undertow directed offshore) and positive outside the surf zone, being directed onshore. From a first glance at Figure 4.7, the breakpoint would most likely have passed over the sensors where the mean cross-shore currents are near-zero.

The cross-shore and longshore variance data for Tide 234PM is shown in Figures 4.8(a) and (b). The incident band gravity wave is expected to increase seawards from the shoreline, to the breakpoint, and then decrease seawards beyond the breakpoint (Davidson *et al.*, 1993). The cross-shore current incident band variance (Figure 4.8a) and the longshore current incident band variance (Figure 4.8b) indicate the same trend. Using these variations in cross-shore mean current and variance, the breakpoint is estimated to have occurred during Runs 9-10 (flood tide) and Runs 28-30 (ebb tide) and for longshore mean current and variance, the breakpoint occurred during Runs 8-10 (flood tide) and Runs 29-30 (ebb tide). Using this technique, the breakpoints were estimated for the three selected tidal cycles. Unfortunately, Tide 164PM only comprised four data runs which all occurred well outside the surf zone, so that the breakpoint could not be calculated here. The breakpoints on Tides 184PM and 234PM were estimated to occur in mean water depths of $\approx$ 1.667m (averaged over Runs 22/23) for 184PM and $\approx$1.366m (averaged for Runs 10 (Flood) and 29 (Ebb)) for

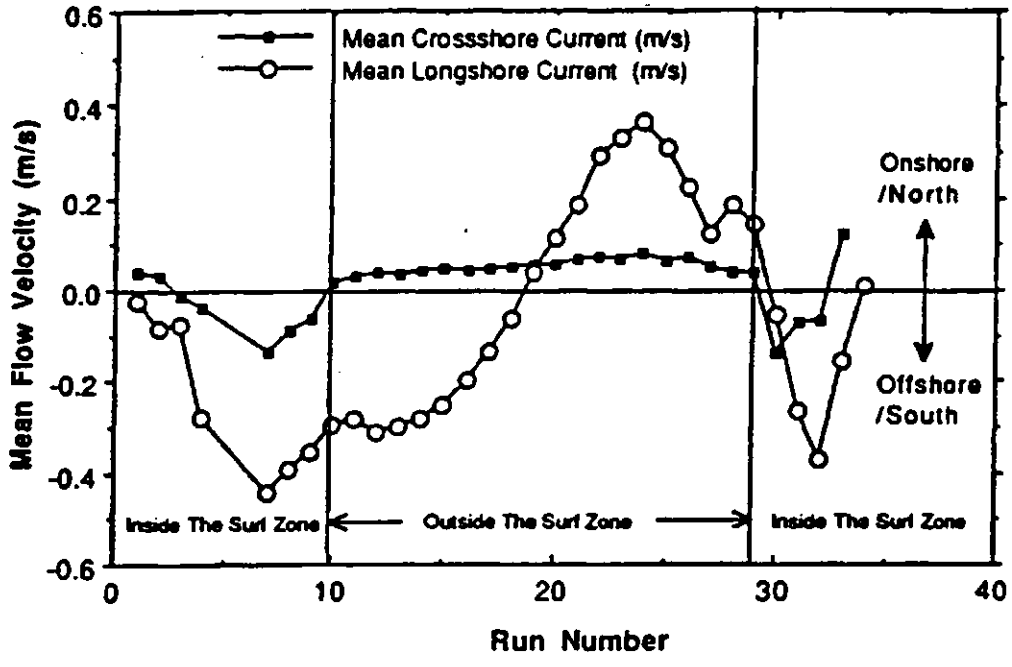

FIGURE 4.7 Tide 234PM mean cross-shore and longshore currents at Spurn Head (from Davidson *et al.*, 1993).

(a)

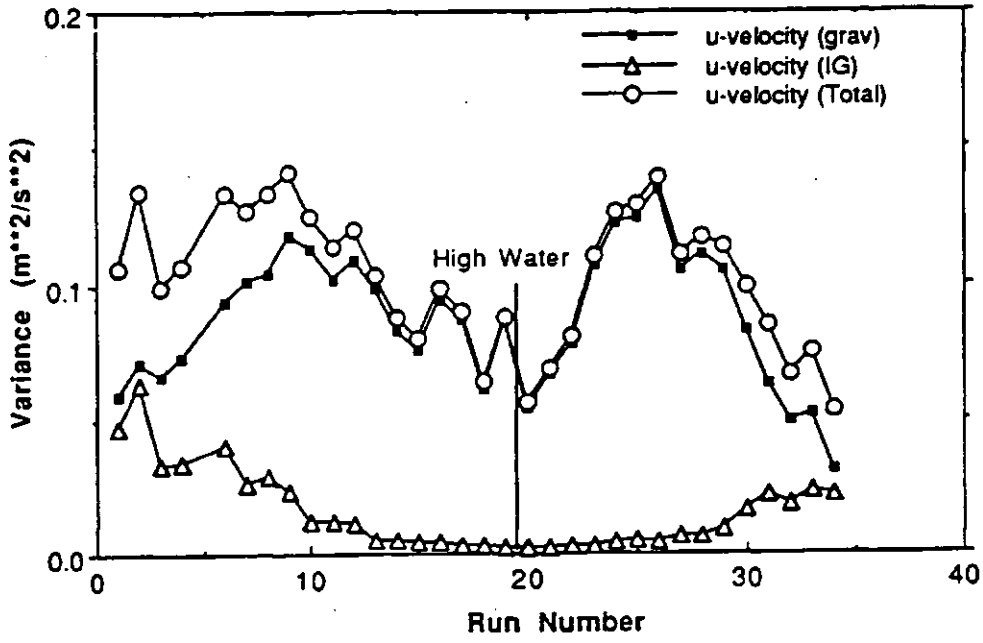

(b)

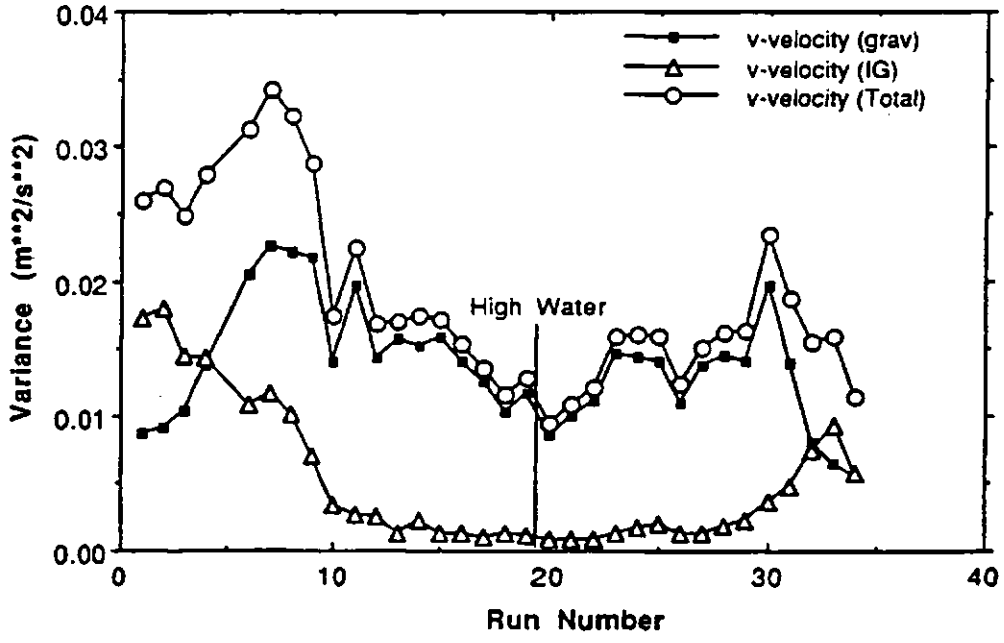

FIGURE 4.8 Cross-shore (a) and Longshore (b) current variance for Tide 234PM, including total, gravity and infragravity components (from Davidson *et al*, 1993).

234PM.

4.3.4 DERIVATION OF SIGNIFICANT WAVE HEIGHT (H_S)

In shallow water the significant wave height, H_S (height of the highest 1/3 of waves) can be calculated as four times the equivalent standard deviation of the sea surface elevation :

$$H_S = 4\sqrt{\sigma^2} \tag{4.10}$$

where σ^2 is the total variance of the oscillatory velocity (Guza and Thornton, 1980; 1982) assuming that the processes are Gaussian and narrow banded. The significant wave height was calculated, using spectral techniques, for the gravity wave band energy by eliminating the long period contributions. The infragravity wave energy can cause errors when calculating significant incident wave heights (Davidson, 1990) and was, therefore, excluded from the calculation of the significant wave heights.

The use of seabed mounted pressure transducers allowed the collection of measurements of pressure fluctuations associated with the nearshore wave motions. A pressure transducer mounted on the seabed registers a pressure, exerted by a wave at the sea surface, which is then attenuated with increasing depth through the water column. Thus, pressure-type gauges are probably best restricted to use in depths of less than a few metres (Komar, 1976; Horikawa, 1978) because of the wave pressure attenuation problem, unless the appropriate corrections are applied.

Davidson (1992) investigated the use of linear wave theory in the frequency domain for the conversion of seabed pressure to surface elevation. Linear wave theory was found to provide a very good estimate of the actual sea surface elevation, even in regions where it might be expected to be inappropriate. Assuming linear wave theory here, correction of the pressure measurements for the effect of wave pressure attenuation with depth can be achieved by predicting what the wave pressure should be at the surface. Where the pressure fluctuations are associated with the wave motions, the rate of decrease of pressure fluctuations with depth will be greater for shorter period waves. The variability of underwater pressures due to progressive waves according to Airy wave theory is given by the formula,

$$\Delta p = \rho g \eta \frac{\cosh k(z+h)}{\cosh kh} \tag{4.11}$$

where Δp is the amplitude of pressure oscillations in water caused by progressive surface waves of amplitude η, ρ is the density of water, k is the wave number, h is the water depth, z is the vertical axis (with z increasing upwards where the origin is at the sea surface), and g is the acceleration due to gravity.

The use of tables and formulae for sinusoidal and Cnoidal gravity waves (*e.g.* Skovgaard *et al.*, 1974) provided a useful method for calculating the correction factor necessary to convert the Spurn Head pressure data for the three selected tides. In agreement with Airy wave theory, the pressure correction was established by assuming sinusoidal wave theory and through a series of calculations of the sinusoidal wave functions the following correction was calculated,

$$p^{+}_{max} = \rho g \frac{H}{2} \frac{\cosh k(z+h)}{\cosh kh} \tag{4.12}$$

where p^{+}_{max} is excess pressure, ρ is density of water, g is the acceleration due to gravity, H is wave height, k is wavenumber ($=2\pi/L$), z is vertical axis and h is mean water depth. The peak period, T, is first estimated from the spectrum of the data. From this, the deep water wavelength, L_o is next calculated where:

$$L_o = \frac{g}{2\pi} T^2 \tag{4.13}$$

The ratio of mean water depth to deep water wavelength must then be calculated, *i.e.* h/L_o. Having arrived at the value of this ratio, the nearest value in the sinusoidal wave function table (Table 4.1) is found and the corresponding value for *cosh kh* is then used as the correction factor. Table 4.2 illustrates the values of the corrected and un-corrected wave height for the three tides, and the correction factor applied. It is promising to see that the greatest correction applied to these data was a factor of 1.10, used for certain runs in Tide 184PM when the PT was in depths greater than 4m. Davidson (1990) estimated that the total gravity band variance was altered by less than 1% even in the greater depths examined, using a correction factor based upon linear wave theory. In this study, the value of the correction factor applied to the A2 PT gravity band variances ranged from 1.00 to 1.10 and thus did not make an important difference to the data. It is probably advisable, however, that pressure transducer

$\frac{h}{L_o}$	tanh kh	$\frac{h}{L}$	kh	sinh kh	cosh kh	G	$\frac{H}{H_o}$
0.000	0.000	0.0000	0.000	0.000	1.00	1.000	∞
002	112	0179	112	113	01	0.992	2.12
004	158	0253	159	160	01	983	1.79
006	193	0311	195	197	02	975	62
008	222	0360	226	228	03	967	51
0.010	0.248	0.0403	0.253	0.256	1.03	0.958	1.43
015	302	0496	312	317	05	938	31
020	347	0576	362	370	07	918	23
025	386	0648	407	418	08	896	17
0.030	0.420	0.0713	0.448	0.463	1.10	0.878	1.13
035	452	0775	487	506	12	858	09
040	480	0833	523	548	14	838	06
045	507	0888	558	588	16	819	04
0.050	0.531	0.0942	0.592	0.627	1.18	0.800	1.02
055	554	0993	624	665	20	781	1.01
060	575	104	655	703	22	762	0.993
065	595	109	686	741	24	744	981
070	614	114	716	779	27	725	971
0.075	0.632	0.119	0.745	0.816	1.29	0.707	0.962
080	649	123	774	854	31	690	955
085	665	128	803	892	34	672	948
090	681	132	831	929	37	655	942
095	695	137	858	0.968	39	637	937
0.10	0.709	0.141	0.886	1.01	1.42	0.620	0.933
11	735	150	940	08	48	587	926
12	759	158	0.994	17	54	555	920
13	780	167	1.05	25	60	524	917
14	800	175	10	33	67	494	915
0.15	0.818	0.183	1.15	1.42	1.74	0.465	0.913
16	835	192	20	52	82	437	913
17	850	200	26	61	90	410	913
18	864	208	31	72	1.99	384	914
19	877	217	36	82	2.08	359	916
0.20	0.888	0.225	1.41	1.94	2.18	0.335	0.918

$\frac{h}{L_o}$	tanh kh	$\frac{h}{L}$	kh	sinh kh	cosh kh	G	$\frac{H}{H_o}$
0.20	0.888	0.225	1.41	1.94	2.18	0.335	0.918
21	899	234	47	2.05	28	313	920
22	909	242	52	18	40	291	923
23	918	251	57	31	52	271	926
24	926	259	63	45	65	251	929
0.25	0.933	0.268	1.68	2.60	2.78	0.233	0.932
26	940	277	74	75	2.93	215	936
27	946	285	79	2.92	3.09	199	939
28	952	294	85	3.10	25	183	942
29	957	303	90	28	43	169	946
0.30	0.961	0.312	1.96	3.48	3.62	0.155	0.949
31	965	321	2.02	69	3.83	143	952
32	969	330	08	3.92	4.05	131	955
33	972	339	13	4.16	28	120	958
34	975	349	19	41	53	110	961
0.35	0.978	0.358	2.25	4.68	4.79	0.100	0.964
36	980	367	31	4.97	5.07	091	967
37	983	377	37	5.28	37	083	969
38	984	386	43	61	5.70	076	972
39	986	395	48	5.96	6.04	069	974
0.40	0.988	0.405	2.54	6.33	6.41	0.063	0.976
41	989	415	60	6.72	6.80	057	978
42	990	424	66	7.15	7.22	052	980
43	991	434	73	7.60	7.66	047	982
44	992	443	79	8.07	8.14	042	983
0.45	0.993	0.453	2.85	8.59	8.64	0.038	0.985
46	994	463	91	9.13	9.18	035	986
47	995	472	2.97	9.71	9.76	031	987
48	995	482	3.03	10.3	10.4	028	988
49	996	492	09	11.0	11.0	026	990
0.50	0.996	0.502	3.15	11.7	11.7	0.023	0.990
∞	1.000	∞	∞	∞	∞	0.000	1.000

TABLE 4.1 Sinusoidal wave functions (from Skovgaard *et al.*, 1974).

	TIDE 164PM		TIDE 184PM		TIDE 234PM	
RUN No.	GRAVITY BAND H_S	GRAVITY BAND H_S corrected	GRAVITY BAND H_S	GRAVITY BAND H_S corrected	GRAVITY BAND H_S	GRAVITY BAND H_S corrected
1	1.2580	1.3586			0.2272	0.2272
2	1.3120	1.4039			0.2810	0.2810
3	1.3888	1.5000	0.6945	0.7293	0.2884	0.2913
4	1.5149	1.6210	0.7041	0.7252	0.3820	0.3858
5			0.7386	0.7977		
6			0.7703	0.8319	0.5196	0.5248
7			0.8760	0.9461	0.5812	0.5928
8			0.7240	0.7819	0.6404	0.6561
9			0.8389	0.8808	0.6655	0.6855
10			0.7307	0.8038	0.6762	0.6965
11			0.7717	0.8103	0.6829	0.7034
12					0.7069	0.7422
13			0.7043	0.7747	0.7279	0.7643
14			0.9049	0.9954	0.6875	0.7219
15			0.8603	0.9291	0.6435	0.6628
16			0.9630	1.0304	0.7129	0.7628
17			1.0022	1.0724	0.6252	0.6690
18			0.9443	1.0104	0.7418	0.7789
19			0.8898	0.9521	0.7066	0.7561
20			0.9709	1.0389	0.5791	0.6196
21			0.9554	0.9841	0.7359	0.7874
22			0.9116	0.9389	0.6703	0.7038
23			0.7651	0.7804	0.7336	0.7703
24			0.6392	0.6520	0.7734	0.8121
25			0.4768	0.4816	0.7262	0.7625
26			0.3314	0.3347	0.7146	0.7360
27					0.7071	0.7283
28					0.6749	0.6951
29					0.6548	0.6679
30					0.5855	0.5972
31					0.3330	0.3363
32					0.3822	0.3860
33					0.0839	0.0839

TABLE 4.2 Correcting gravity band significant wave heights (H_S) for the depth attenuation effect on the pressure transducer.

measurements for estimation of the sea surface elevation and significant wave height, be restricted to depths of only a few metres, since the data may be inaccurate as the necessary correction factor increases (*e.g.* Horikawa, 1978). It should be noted that for better accuracy, each frequency component in the spectrum should be individually corrected with an appropriate correction factor for its frequency, to produce a surface elevation spectrum. In the present work, only the peak frequency correction factor has been used for all parts of the spectrum.

4.3.5 GROUPINESS FACTOR

A groupiness factor based upon the envelope of the incident wave time series is examined in this work. The derived groupiness factor is used to examine the variability of incident wave groupiness across the nearshore zone, over the three selected tidal cycles from Spurn Head. The groupiness factor is examined as a function of mean water depth and significant wave height for each data run of the three tides, including storm and calm conditions.

List (1991) developed a groupiness factor (GF) similar to the one used in this work, by first high-pass filtering the surface elevation time series $(\eta(t))$, to remove the infragravity band motions, then forming $|\eta(t)|$ to introduce envelope-related variance to the series. The resulting time series is then low-pass filtered to remove the incident waves, resulting in a low frequency signal with variance related only to amplitude modulations. Then the final step is to multiply the low-pass filtered $|\eta(t)|$ by $\pi/2$ which results in an envelope function termed, A(t), providing the basis for List's groupiness factor.

This incident wave envelope function was used here as the basis for estimating groupiness. Figure 4.9 illustrates a step-by-step account of this procedure. The corrected (for depth-attenuation effect), de-meaned and de-trended pressure data were separated into long wave and incident wave components using the digital filter described in Section 4.3.1. Calculation of the wave envelope time series was obtained by de-meaning and squaring the high-frequency measurements. This was followed by further digital filtering to produce the low-pass of the high-pass squared values of the

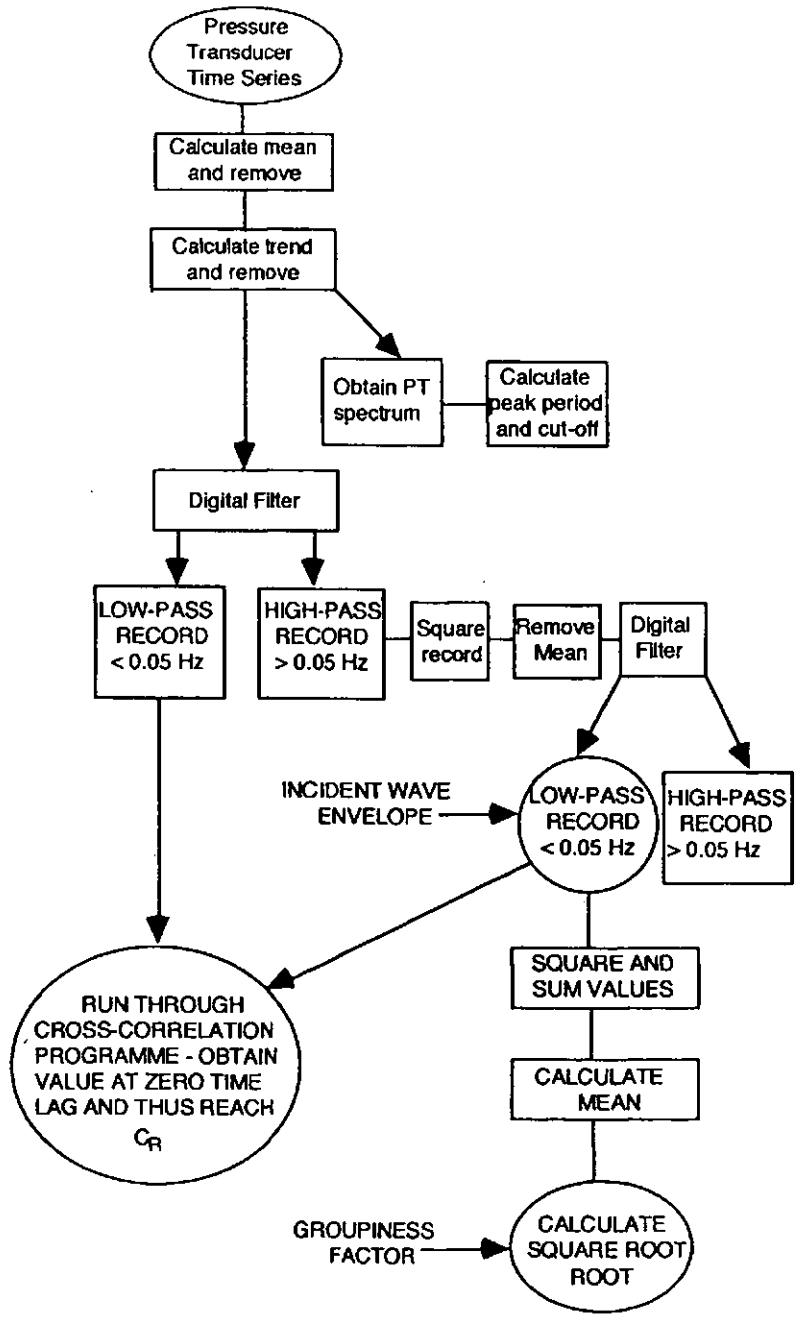

FIGURE 4.9 Calculation of the incident wave envelope time series and groupiness factor.

surface elevation data. From this point, the groupiness factor (GF) was taken to be the root-root-mean-square (rms.) of the incident wave envelope time series:

$$GF = \left\{ \overline{\left[\left(\eta_S(t)^2 \right)_{LP} \right]^2} \right\}^{1/4} \tag{4.14}$$

where $\eta_S(t)$ is the high frequency part of the surface elevation time series and the sub-script *LP* denotes low-pass filtering. The GF was calculated for all data runs of the three selected tides. The characteristics of the wave groupiness factor across the nearshore zone and a comparison with existing groupiness factor work, will be discussed in Chapter 5.

4.3.6 CROSS-CORRELATION ANALYSIS

The incident wave envelope time series were cross-correlated with the long period motion time series. This was in order to investigate the hypothesis that the long wave motion is forced outside the surf zone and that the amplitude of the breaking short waves are modulated by long wave elevations inside the surf zone (Abdelrahman and Thornton, 1987).

Pressure data were used to estimate correlation functions between the incident wave envelope and the corresponding low-frequency motion through implementation of an I.E.E.E. algorithm described by Carter and Ferrie (1979). Cross-correlations between two channels of data (*i.e.* the incident wave envelope and the low-frequency motion time series) were calculated for time lags of up to ± 80 seconds, which as Kim (1985) suggested, may determine any non-dispersive time lag between the two channels. The following expression defines the cross-correlation function, C_R, which describes the degree of linear agreement between two data sets in the time domain, thus:

$$C_R = \frac{\Sigma(x_i - \bar{x})(y_i - \bar{y})}{\sqrt{\Sigma(x_i - \bar{x})^2}\sqrt{\Sigma(y_i - \bar{y})^2}} \tag{4.15}$$

where $\bar{\theta}$ and θ_n are the mean and nth value of the θ time series respectively, and θ represents x or y. Cross-correlation functions were calculated for each of three tides, in addition to the relative 'correlograms' depicting the shape of the correlation coefficient.

4.3.7 VELOCITY MOMENT ANALYSIS

The two most important velocity moments in the cross-shore sediment transport equation (Eqn. 2.34) described by Guza and Thornton (1985a) relate velocity to the sediment transport where the dominant terms were found to be,

Bedload Transport $$\frac{\overline{u^3}}{\left(\overline{u^2}\right)^{3/2}} \tag{4.16}$$

Suspended Load Transport $$\frac{\overline{|u|^3 u}}{\left(\overline{u^2}\right)^2} \tag{4.17}$$

(a) BEDLOAD TERM

In order to identify the separate contributions to these moment terms, the cross-shore current velocity is assumed to comprise mean flow ($\bar{u}$), high-frequency (u_S) and low-frequency (u_L) components:

$$u = \bar{u} + u_S + u_L \tag{4.18}$$

When expanded in terms of these three components, the bedload term Eqn. (4.16) can be expressed as ten terms:

$$\begin{aligned} = \; & \overline{\left(u^3\right)} + \overline{\left(u_S{}^3\right)} + \overline{\left(u_L{}^3\right)} + \overline{\left(3\bar{u}u_S{}^2\right)} + \overline{\left(3\bar{u}u_L{}^2\right)} + \overline{\left(6\bar{u}u_S u_L\right)} \\ & + \overline{\left(3u_L{}^2 u_S\right)} + \overline{\left(3u_S{}^2 u_L\right)} + \overline{\left(3\bar{u}^2 u_S\right)} + \overline{\left(3\bar{u}^2 u_L\right)} \end{aligned} \tag{4.19}$$

(each of the above ten terms were normalised by dividing through by $(u^2)^{3/2}$). These ten bedload terms describe various mechanisms which operate within the nearshore system as follows,

TERM 1 $\overline{u^3}$ → Mean flow cubed.

TERM 2 $\overline{u_S{}^3}$ → Skewness of the incident waves.

TERM 3 $\overline{u_L{}^3}$ → Skewness of the long period waves.

TERM 4 $\overline{3\bar{u}u_S{}^2}$ → Incident waves mobilise sand, which is then moved by the mean flow.

TERM 5 $\overline{3\bar{u}u_L^2}$ → Long waves mobilise sand,
which is then moved by the mean flow.

TERM 6 $\overline{6\bar{u}u_S u_L}$ → Correlation between all three components,
expected to be zero.

TERM 7 $\overline{3u_L^2 u_S}$ → Correlation between long period variance
and incident wave velocity.

TERM 8 $\overline{3u_S^2 u_L}$ → Correlation between incident wave variance
and long period velocity.

TERM 9 $\overline{3\bar{u}^2 u_S}$ → Correlation between mean flow
and incident wave velocity, will be zero.

TERM 10 $\overline{3\bar{u}^2 u_L}$ → Correlation between mean flow
and long wave velocity, will be zero.

Each of these ten terms were calculated using data from the bottom electromagnetic current meter on Rig A2 at the Spurn Head field experiment, for the three selected tidal cycles. These results will be discussed in Chapter 6.

(b) SUSPENDED LOAD TERM

The term describing the suspended load transport is more complicated than the expression representing the bedload term. One major difference between the two terms is the inclusion of the total velocity, as its modulus, in the suspended load transport moment (Eqn. 4.17). In order to separate the component influences, the assumption is made that the short wave velocity (u_S) is much greater than the mean flow ($\bar{u}$) or the long period motion (u_L). This assumption is generally valid except near the shoreline, where the long period motions become more important compared to the incident band motions. Expanding the suspended load transport moment (Eqn. 4.17) to incorporate the mean, incident and long period motion contributions, generates three further terms:

TERM 1 $\overline{\left(u_S^2\right)^{3/2} u_S}$ → Incident wave term.

TERM 2 $\overline{4\left(u_S^2\right)^{3/2} u_L}$ → Long wave term.

TERM 3 $\overline{3\left(u_S^2\right)^{3/2} \bar{u}}$ → Mean flow term.

Each of the three terms was normalised by dividing by $<u^2>^2$ and calculated for all cross-shore current velocity records (bottom current meter on Rig A2) of the three selected tidal cycles. Their characteristics will be discussed in Chapter 6.

4.3.8 SEDIMENT FLUX ANALYSIS

Measurements of co-located current velocity and suspended sediment concentration fluctuations at fixed heights above the seabed may be used to derive net sand transport rates. Net cross-shore sediment transport rate, as discussed in Chapter 2, comprises mean and oscillatory components. The contribution made by the various mean flow, long period and short wave motions to net cross-shore transport rate (Jaffe *et al.*, 1984), can be examined by expanding (Eqn. 2.42) where:

$$\begin{aligned} \overline{cu} &= \overline{(\bar{c} + c_L + c_S)(\bar{u} + u_L + u_S)} \\ &= \overline{u_L c_L} + \overline{u_S c_S} + \bar{u}\,\bar{c} + \overline{u_S c_L} + \overline{u_L c_S} + \overline{\bar{u} c_L} + \overline{\bar{u} c_S} + \overline{u_L \bar{c}} + \overline{u_S \bar{c}} \end{aligned} \tag{4.20}$$

Of these un-normalised cross-shore sediment flux terms there will be three non-zero terms:

TERM 1 $\overline{u_L c_L}$ → Long wave motion drives suspended sediment transport.

TERM 2 $\overline{u_S c_S}$ → Short wave motion drives suspended sediment transport.

TERM 3 $\bar{u}\,\bar{c}$ → Mean flow driving suspended sediment transport.

The variation of these flux-related terms through the nearshore zone is examined over the three tidal cycles, in Chapter 7, using suspended sediment concentration time series from the bottom OBS and cross-shore current velocity data from the bottom EMCM on Rig A2.

4.4 SUMMARY

Within this chapter, the analytical techniques and procedures have been discussed. Time series analysis and spectral analysis were the two main techniques applied to the Spurn Head data. Pressure data were examined to calculate significant wave height, the wave breakpoint position and to estimate wave groupiness, and to investigate the long wave/wave envelope relationship. Electromagnetic current meter data were used to calculate velocity moments, whilst optical backscatter sensor measurements were examined to compute cross-shore sediment flux terms. The next chapter examines the groupiness factor and the correlation between the incident wave envelope and the bound long wave motion across the nearshore zone.

CHAPTER 5
INCIDENT WAVE GROUPS AND LONG WAVE MOTION

5.1 INTRODUCTION

The passage of a wave group and bound long wave over an erodible bed generates sediment suspension under high waves which, in conjunction with a negative (offshore) long wave flow, may result in net offshore sediment transport. Formation of bars on beaches may also be driven by the incident wave groups/bound long wave relationship as the waves approach the shoreline. Whilst it is generally accepted that groupiness of ocean waves is an important parameter of the wave climatology, both within and beyond the surf zone, few studies have examined the variations in wave groupiness across the surf zone where waves are considerably affected by the breaking process. This chapter examines observations of incident wave groups and long waves, in order to estimate the variation of wave groupiness across the nearshore zone over a range of wave and tidal conditions. It investigates the hypothesis that long wave motion is forced outside the surf zone and that the short period incoming waves are modulated by long wave elevations inside the surf zone.

5.2 WAVE GROUPINESS

Incident waves travelling towards the shoreline are known to have a groupy structure with an alternating sequence of high wave and low wave groups. Associated with the wave groups are gradients in the radiation stress, generating a forced long wave (of

infragravity frequency) whereby a depression in mean sea-level is correlated with groups of high waves and a rise in mean sea-level corresponds to groups of low waves (see Section 2.3.3(c)).

The Spurn Head data revealed some well-defined groupy wave characteristics. Figures 5.1-5.3 provide some examples of (a) the surface elevation time series, (b) the corresponding wave envelope time series and (c) the associated pressure power spectrum, for runs measured outside the surf zone from Tide 164PM, 184PM and 234PM. The spectra in Figure 5.1(c) to 5.3(c) illustrate the progression from storm waves at Spurn Head, April 16, 1991 to the low-energy swell for April 23, 1991.

Figure 5.1, for example, describes deep water (mean water depth ≈ 4.6m) measurements from Tide 164PM, the stormy tidal cycle of data. Figure 5.1(a) represents the surface elevation time series for Run 1 (well outside the surf zone) in Tide 164PM, where the beating of the incoming waves produces the pronounced regular groupy nature seen here. Figure 5.1(b) shows the corresponding wave envelope time series for this run. The long period fluctuations represent alternating sequences of high wave and low wave groups associated with the amplitude of the bound long wave. Figure 5.1(c) illustrates the equivalent power spectrum for the pressure measurements. A dominant peak is seen at the wind wave frequency (≈0.10Hz) with a smaller secondary peak occurring at the low frequency end of the spectrum (≈0.025Hz). The overall groupiness factor (GF) varies from 0.263 for the storm tide (164PM), 0.156 for Tide 184PM to 0.118 for Tide 234PM. It should be noted that the time axes in Figures 5.1-5.4(a) and (b) are actually synchronous. However, after each filtering of the original time series to create, for example, low- and high-pass components and the wave envelope time series, a number of data points was lost as part of the filtering procedure either end of the time series (see Section 4.3.1). Consequently the pressure time series shown in (a) of Figures 5.1-5.4 is the corresponding run of data for the resultant wave envelope time series in (b) of Figures 5.1-5.4. The original pressure time series contained 2048 data points, the wave envelope time series after two filtering routines contained 1454 data points, however, the data in (a) and (b) are actually compatible.

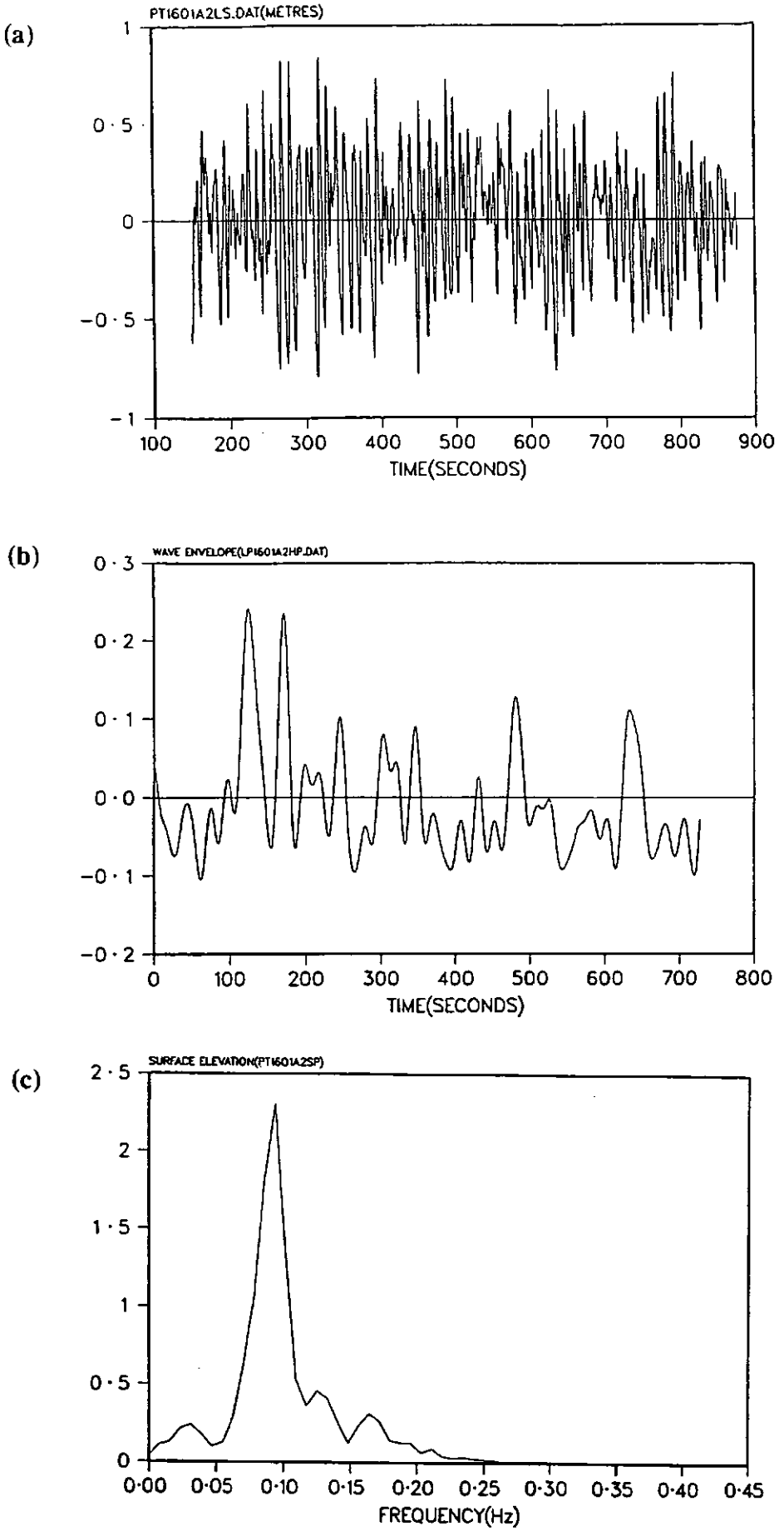

FIGURE 5.1 (a) Pressure time series (b) Wave envelope time series and (c) Pressure spectrum for Run 1, Tide 164PM (mean water depth is 4.60m; GF is 0.263).

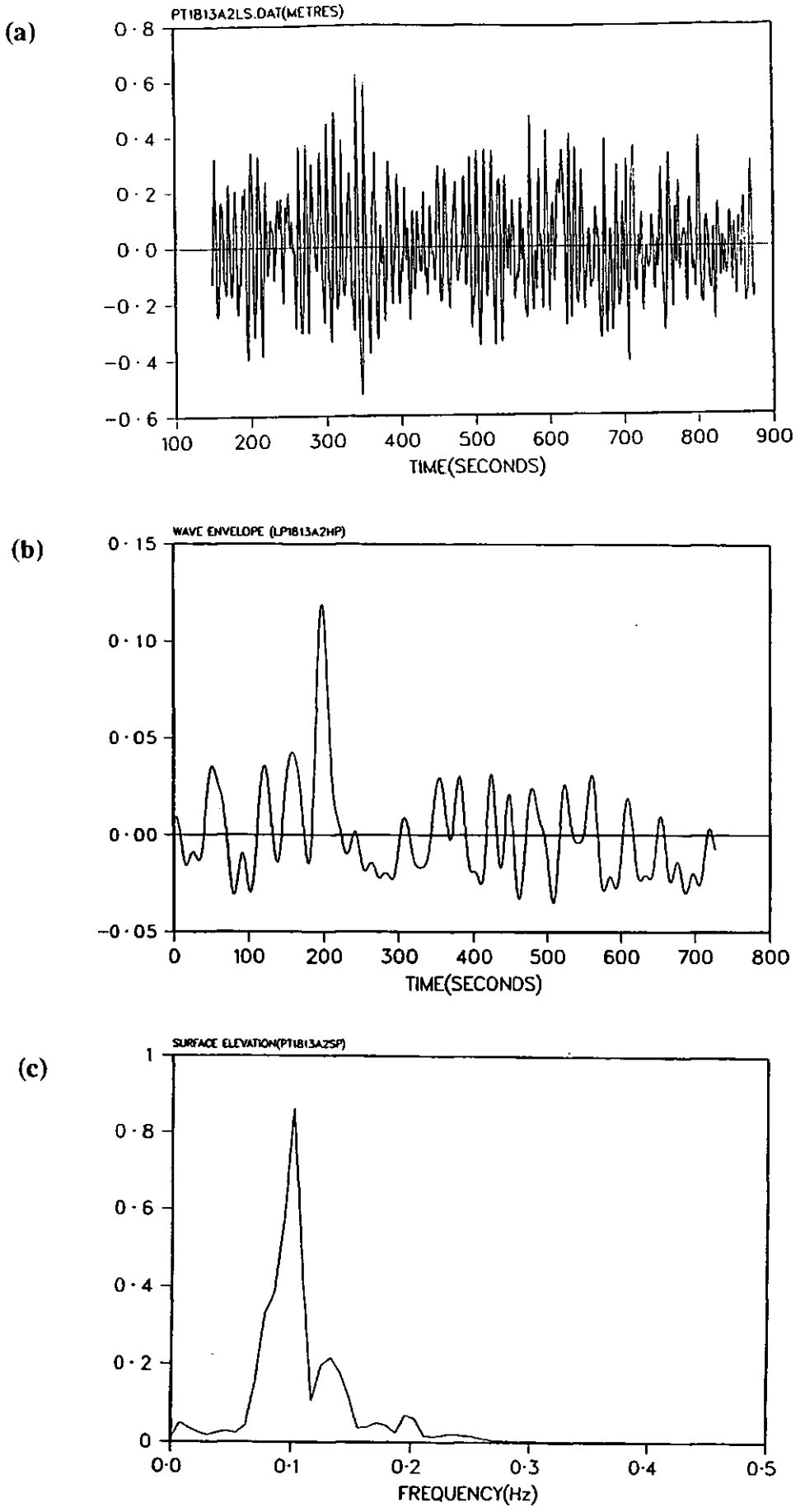

FIGURE 5.2 (a) Pressure time series (b) Wave envelope time series and (c) Pressure spectrum for Run 13, Tide 184PM (mean water depth is 4.22m; GF is 0.156).

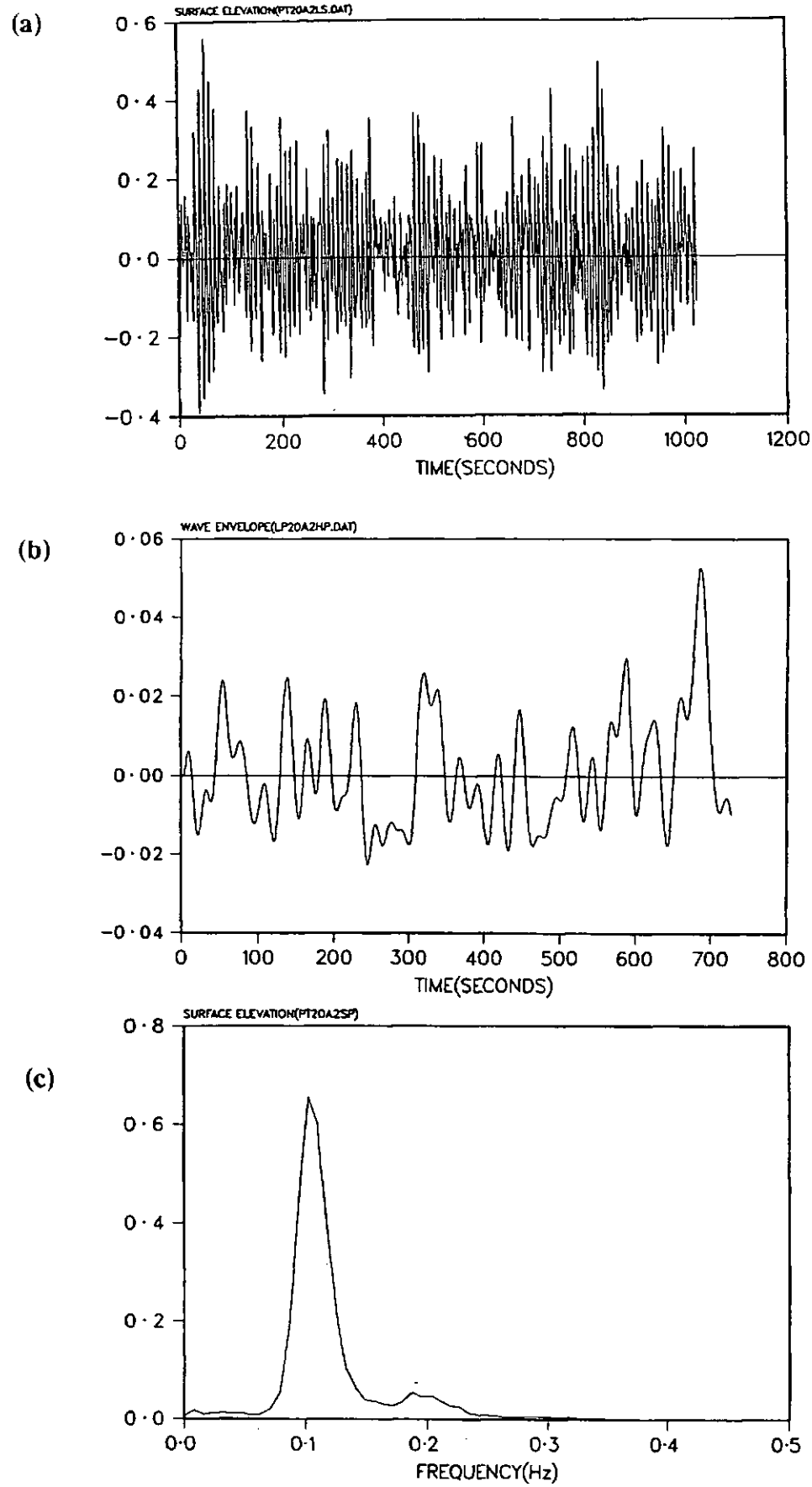

FIGURE 5.3 (a) Pressure time series (b) Wave envelope time series and (c) Pressure spectrum for Run 20, Tide 234PM (mean water depth is 2.99m; GF is 0.118).

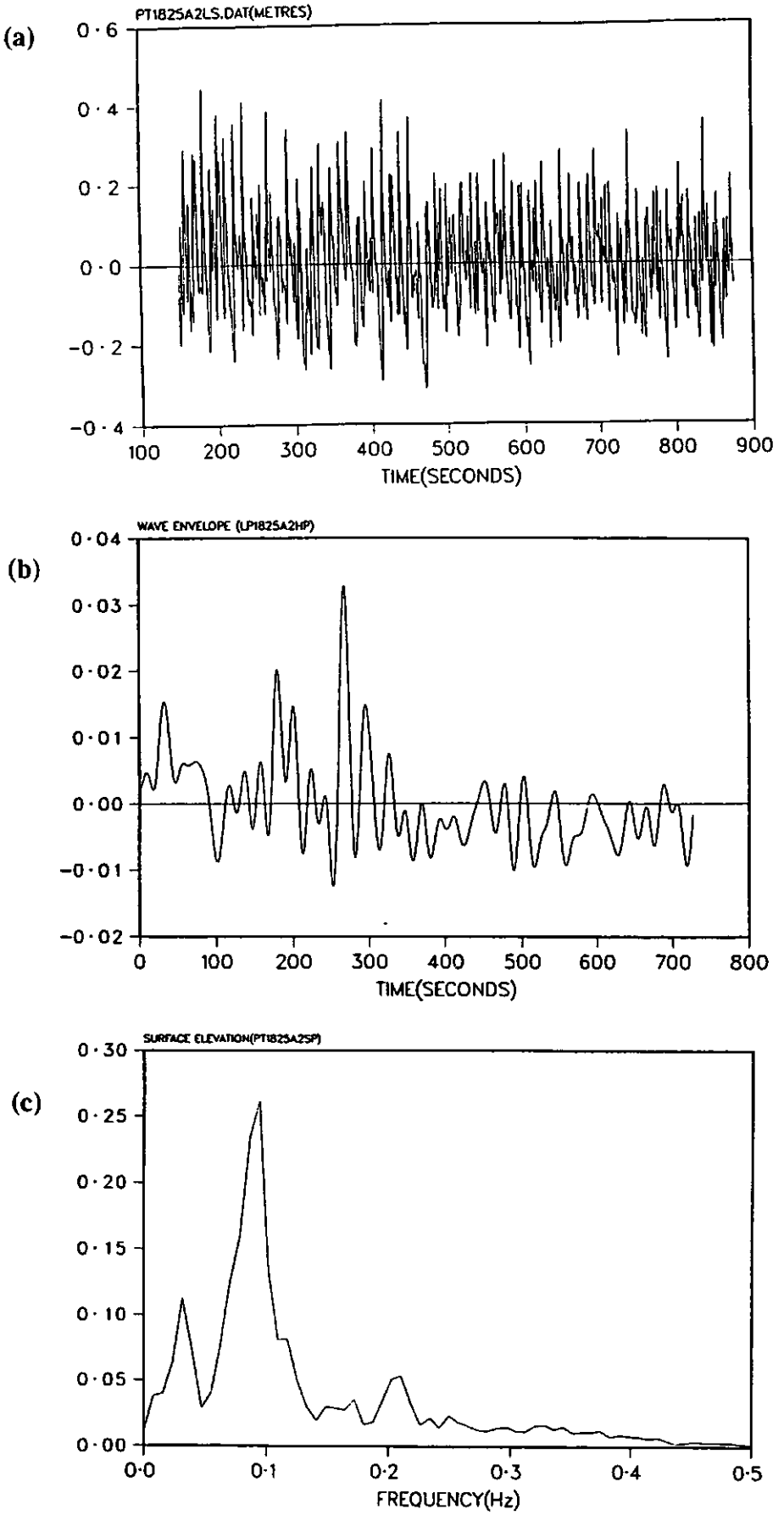

FIGURE 5.4 (a) Pressure time series (b) Wave envelope time series and (c) Pressure spectrum for Run 25, Tide 184PM (mean water depth is 0.6m; GF is 0.08).

Figure 5.4 illustrates the sea surface elevation time series (a), wave envelope time series (b) and power spectrum (c) for Run 25 of Tide 184PM, which was measured inside the surf zone, near the shoreline at low tide (mean water depth ≈ 0.643m). This provides an interesting comparison between the previous deeper water examples obtained outside the surf zone. There is a noticeable decrease in incident wave energy and an accompanying increase in the low frequency band energy. A corresponding change is evident in the groupiness factor which similarly decreases from 0.156 (high tide, measurements outside the surf zone) to 0.0823 (low tide, measurements inside the surf zone).

The groupiness factors for all runs are shown in Tables 5.1-5.3. Figures 5.5 (a), (b) and (c) display the variation of groupiness factor with mean water depth, GF values are shown for each of the data runs in the three tidal cycles. Groupiness appears to increase with increasing water depth in both Tides 184PM and 234PM. In order to establish whether or not there is a relationship between these data, Figure 5.5(d), combines the groupiness measurements in one plot. Despite the examination of three very different tidal cycles, the data exhibit a definite relationship whereby outside the breakpoint groupiness does not vary significantly (Figure 5.5), whilst onshore of the breakpoint, groupiness decreases to near zero only at the shoreline. The observations suggest that groupiness does not decay immediately at the breakpoint but actually continues through the surf zone.

Figure 5.6 depicts the variation of groupiness factor with significant wave height (H_S) for Tides 164PM(a), 184PM(b) and 234PM(c). The observations suggest that wave groupiness increases linearly with increasing wave height. When the measurements are displayed together (Figure 5.6(d)) there appears to be a remarkable degree of correlation between the different data examined. Placing a 'best-fit' line through the data (Figure 5.6(e)) yields a correlation value, $R^2 = 0.937$. Thus, the groupiness factor does not appear to respond significantly to varying offshore wave conditions, instead yielding a similar trend of gradual decrease with decreasing wave height and water depth, for the storm tide (164PM) and the calmer conditions of the later tides (*i.e.* 184PM and 234PM).

RUN No.	WATER DEPTH (m)	WAVE HEIGHT H_S (m)	TIDE 164PM GF (m)
1	4.602	1.3586	0.263
2	4.534	1.4039	0.267
3	4.399	1.5000	0.283
4	4.179	1.6210	0.291

TABLE 5.1 Tide 164PM wave groupiness factor (GF) against mean water depth, and significant wave height.

RUN No.	WATER DEPTH (m)	WAVE HEIGHT H_S (m)	TIDE 184PM GF (m)
3	1.624	0.7292	0.136
4	2.049	0.7252	0.145
5	2.468	0.7977	0.149
6	2.862	0.8319	0.153
7	3.229	0.9461	0.199
8	3.565	0.7819	0.174
9	3.830	0.8808	0.204
10	4.040	0.8038	0.150
11	4.161	0.8103	0.170
13	4.217	0.7747	0.156
14	4.134	0.9954	0.195
15	3.962	0.9261	0.192
16	3.757	1.0304	0.204
17	3.533	1.0724	0.205
18	3.277	1.0104	0.194
19	2.967	0.9521	0.212
20	2.660	1.0389	0.209
21	2.294	0.9841	0.194
22	1.876	0.9389	0.164
23	1.458	0.7804	0.140
24	1.053	0.6520	0.120
25	0.643	0.4816	0.082
26	0.296	0.3347	0.057

TABLE 5.2 Tide 184PM wave groupiness factor (GF) against mean water depth, and significant wave height.

RUN No.	WATER DEPTH (m)	WAVE HEIGHT H_S (m)	TIDE 234PM GF (m)
1	0.167	0.2272	0.039
2	0.223	0.2810	0.045
3	0.295	0.2913	0.046
4	0.458	0.3858	0.061
6	0.737	0.5248	0.084
7	0.904	0.5928	0.098
8	1.094	0.6596	0.106
9	1.308	0.6855	0.115
10	1.555	0.6965	0.125
11	1.785	0.7034	0.124
12	2.010	0.7422	0.149
13	2.228	0.7643	0.146
14	2.418	0.7219	0.140
15	2.597	0.6628	0.135
16	2.742	0.7628	0.155
17	2.856	0.6690	0.186
18	2.943	0.7789	0.138
19	2.987	0.7561	0.146
20	2.993	0.6196	0.118
21	2.955	0.7874	0.150
22	2.865	0.7038	0.139
23	2.706	0.7703	0.144
24	2.497	0.8121	0.156
25	2.265	0.7325	0.144
26	2.012	0.7360	0.127
27	1.756	0.7283	0.137
28	1.470	0.6951	0.115
29	1.177	0.6679	0.108
30	0.858	0.5972	0.092
31	0.574	0.3363	0.064
32	0.290	0.3860	0.044
33	0.085	0.0839	0.033

TABLE 5.3 Tide 234PM wave groupiness factor (GF) against mean water depth, and significant wave height.

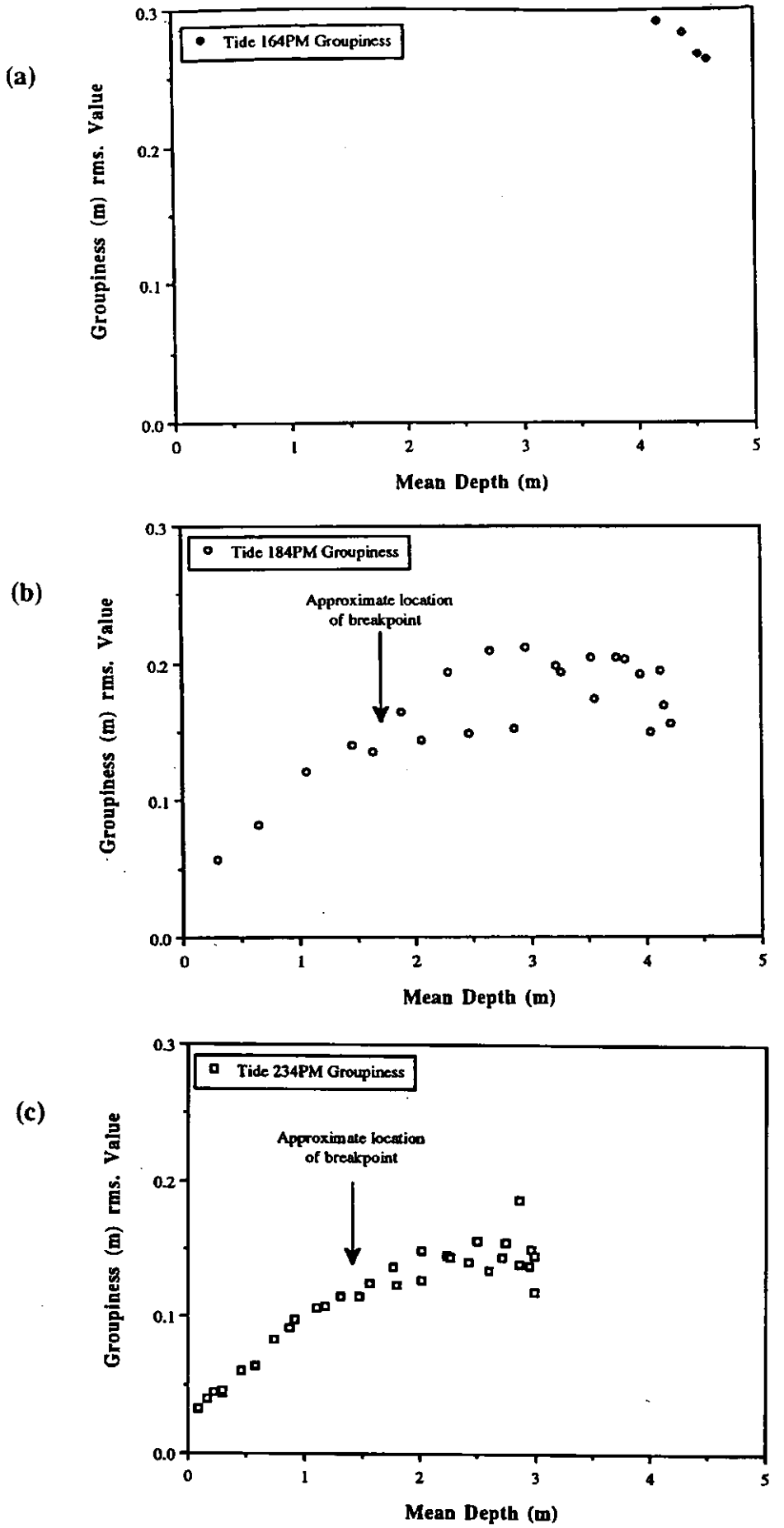

FIGURE 5.5 Variations in groupiness factor with depth across the nearshore at Spurn Head during (a) Tide 164PM (b) Tide 184PM and (c) Tide 234PM.

(d)

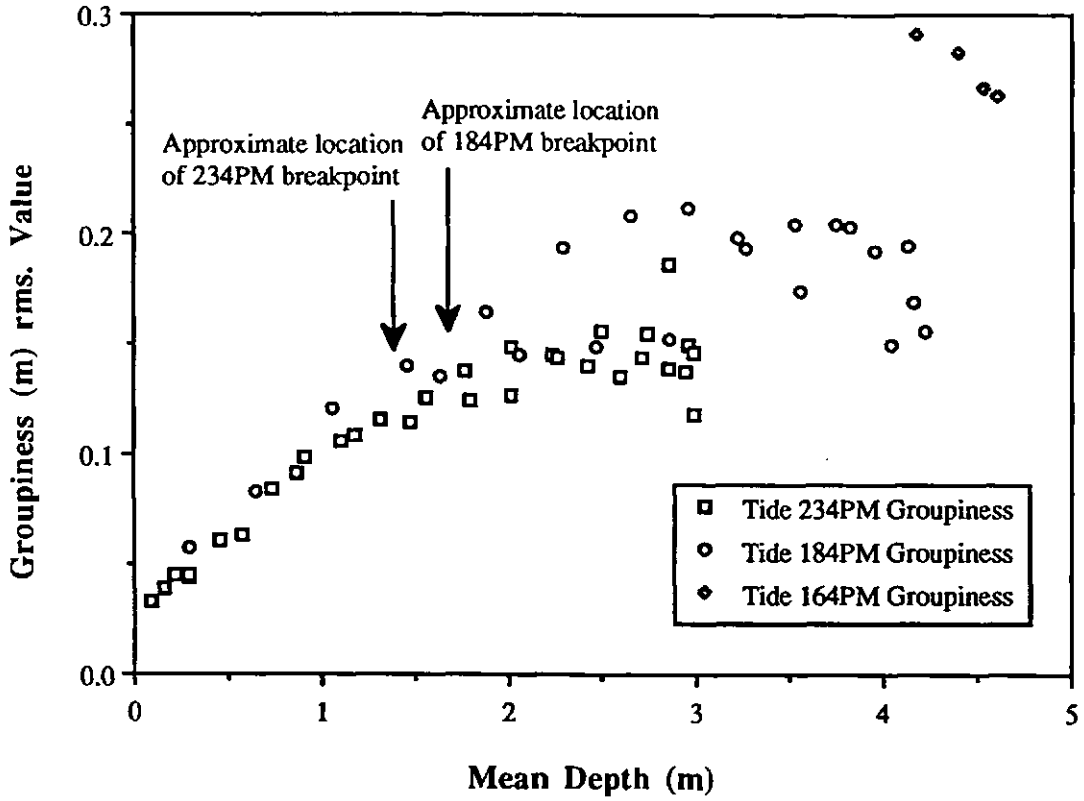

FIGURE 5.5 (d) Combined plot to show linear relationship between groupiness factor and depth across the nearshore at Spurn Head for all three tides.

(a)

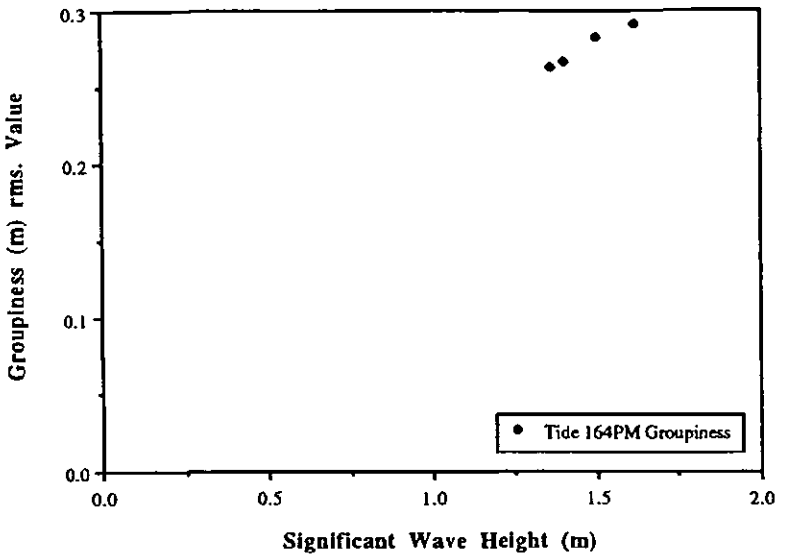

(b)

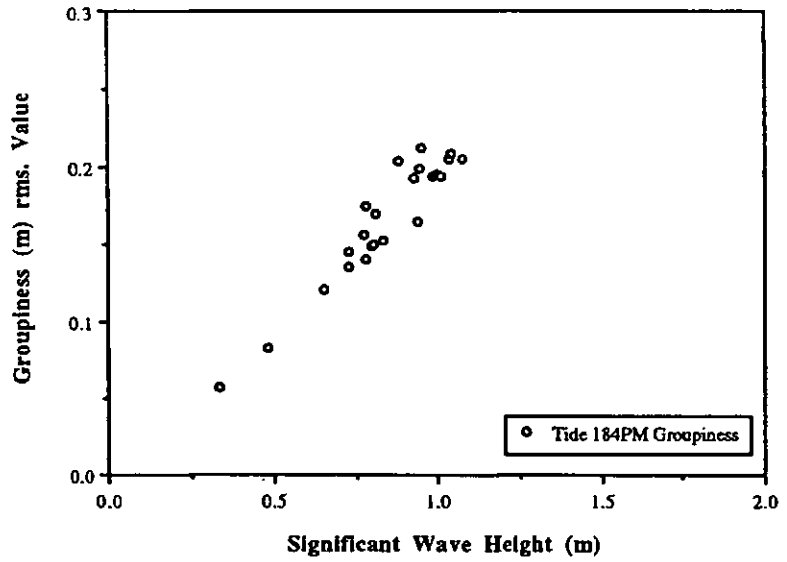

(c)

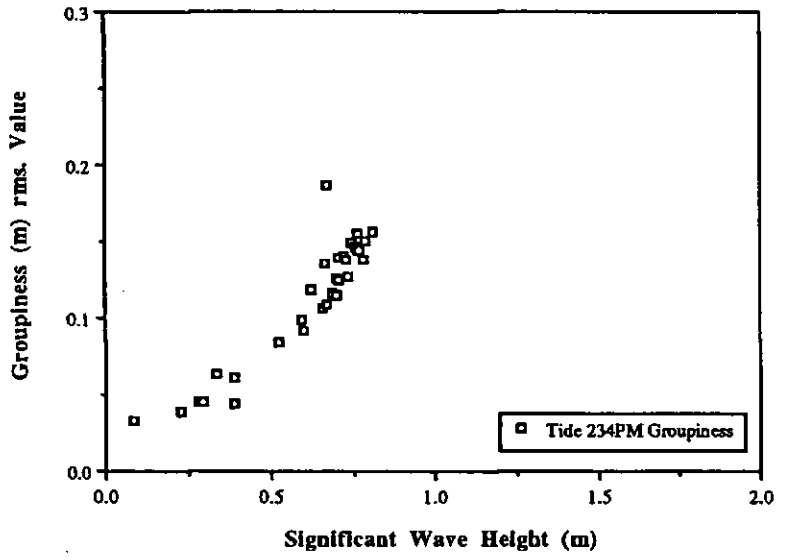

FIGURE 5.6 Variations in groupiness factor with wave height across the nearshore at Spurn Head for (a) Tide 164PM (b) Tide 184PM and (c) Tide 234PM.

(d)

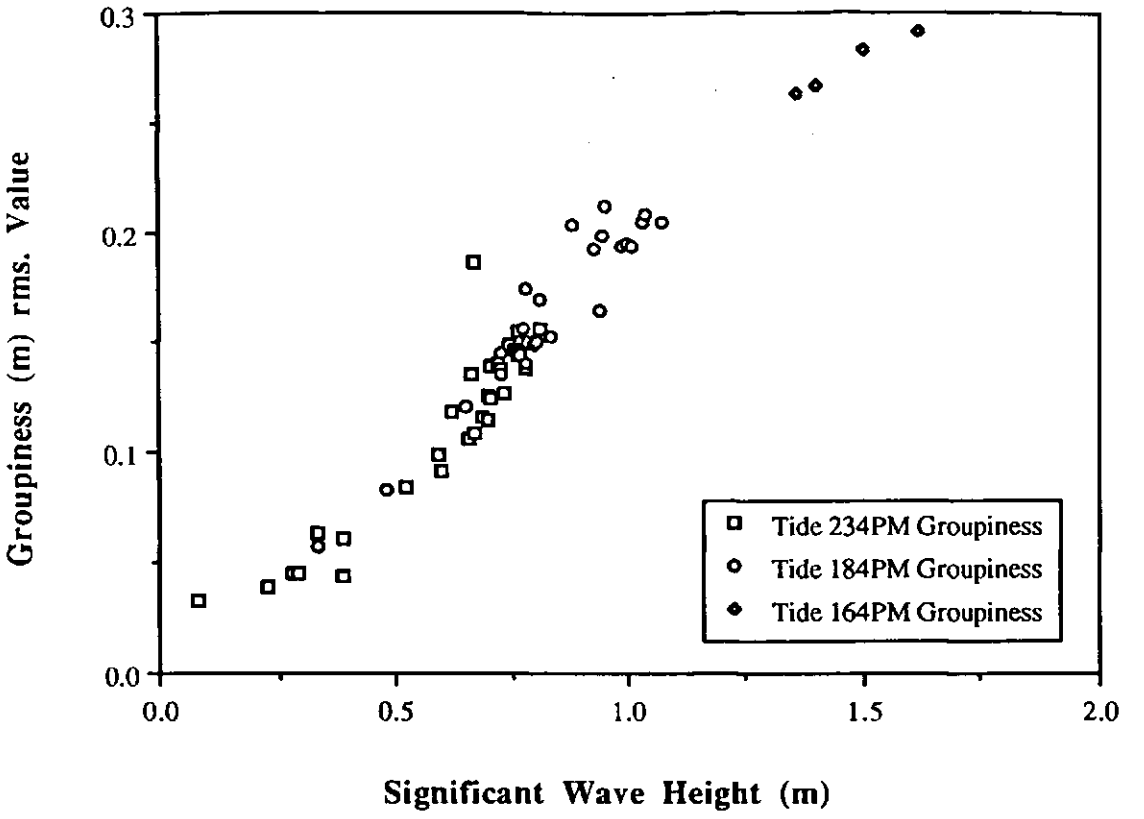

(e)

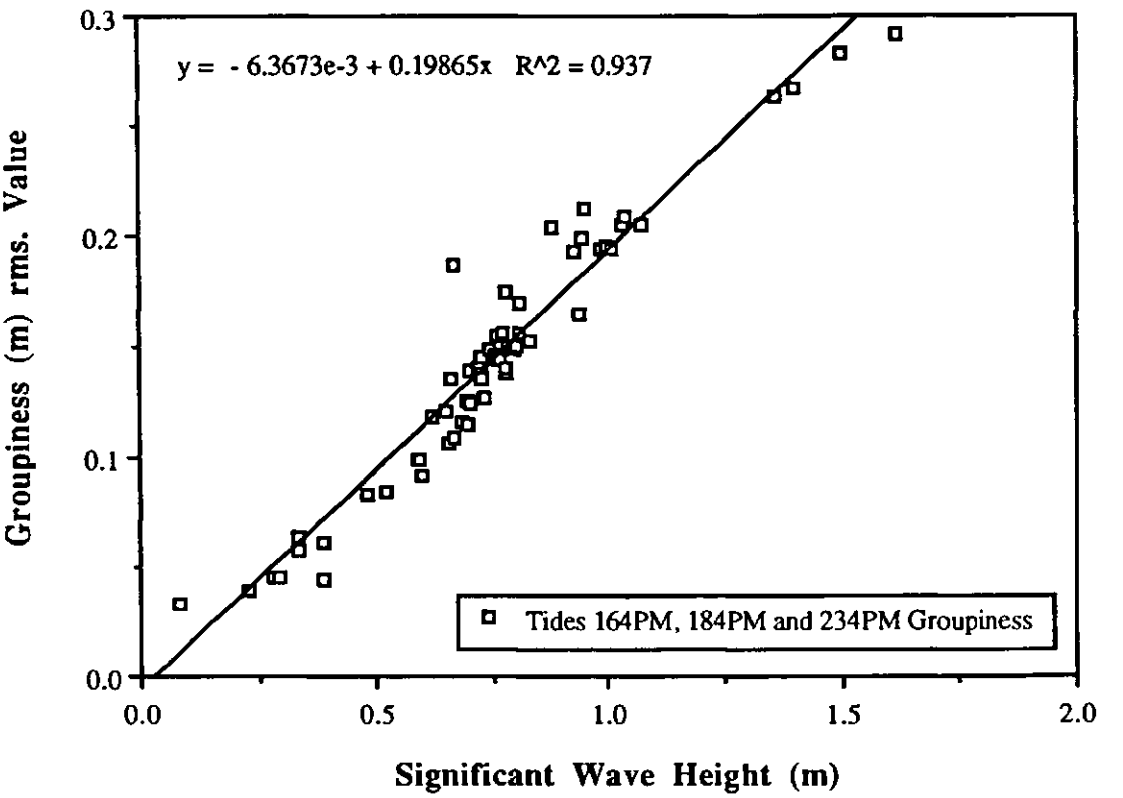

FIGURE 5.6 (d) and (e) Combined plots to show linear relationship between groupiness factor and wave height across the nearshore at Spurn Head for all three tides.

5.3 CORRELATION BETWEEN WAVE ENVELOPES AND LONG WAVES

Investigating whether or not long waves are directly forced by incident wave groups can be achieved by calculating correlations between long waves and incident wave envelopes (Huntley and Kim, 1984; Abdelrahman and Thornton, 1987) (see Section 4.3.6). Correlations between the incident wave envelope and long period motions were calculated for all runs of the three selected tidal cycles. Figures 5.7(a)(b) and (c) show the cross-correlation between the incident wave envelope and the cross-shore component of long waves for selected runs from each tide. Correlation functions during Run 01, Tide 164PM, (Figure 5.7(a)) show similar features to those during Run 13, Tide 184PM (Figure 5.7(b)), and Run 20, Tide 234PM (Figure 5.7(c)). The maximum correlation coefficients between the long period motion and the incident wave envelope during these runs of the three different tidal cycles occur at, or very near, zero time lag. Correlations between the low frequency motion and envelope at zero time lag, are given in Tables 5.4-5.6.

Figure 5.8 (a), (b) and (c) show the correlation values at zero time lag for each data run of the three selected tidal cycles. The correlations are high and negative for the runs made outside the surf zone, indicating that well defined wave groups, with associated forced waves propagate across the nearshore zone, until shoaling and/or wave breaking radically alters the group structure. As the waves propagate into shallow water, however, the correlation coefficient at time lag zero changes sign from negative to positive in the inner surf zone.

(a)

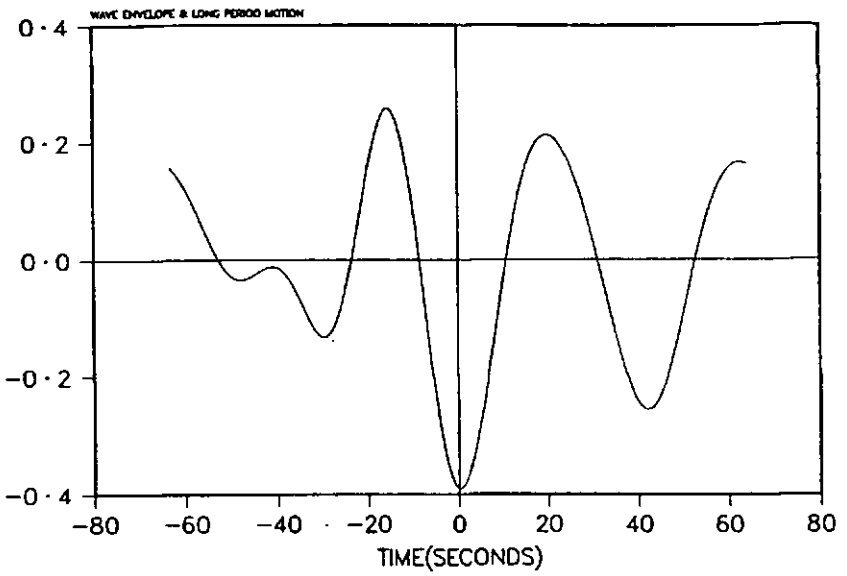

(b)

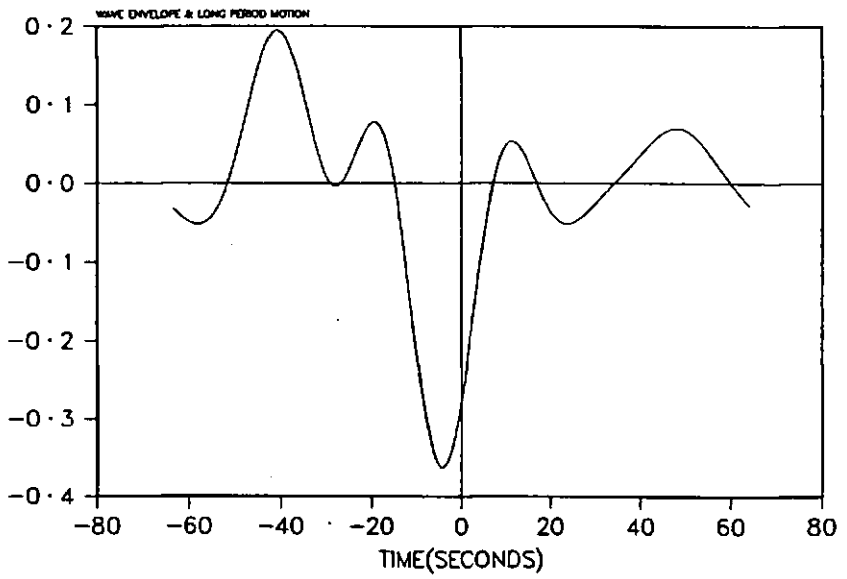

(c)

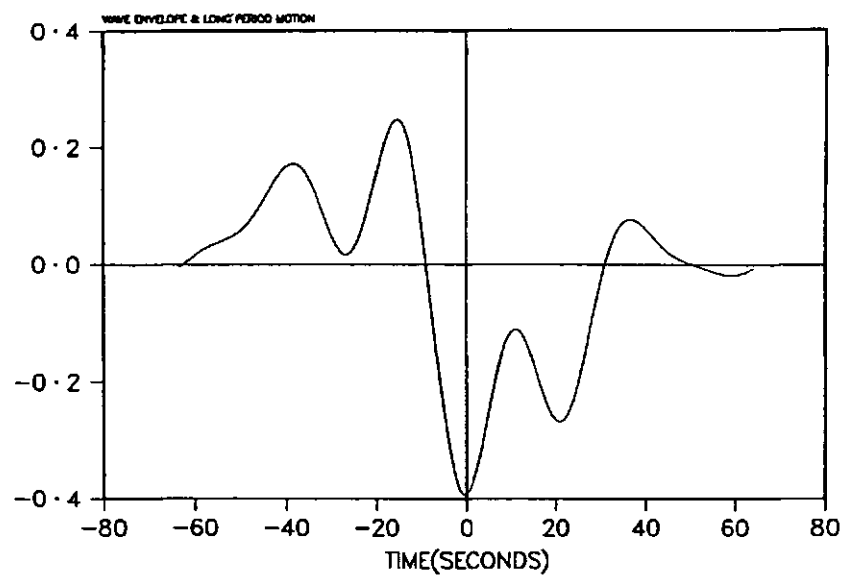

FIGURE 5.7 Correlation function between the long wave and wave envelope for (a) Run 1(Tide 164PM) (b) Run 13 (Tide 184PM) and (c) Run 20 (Tide 234PM).

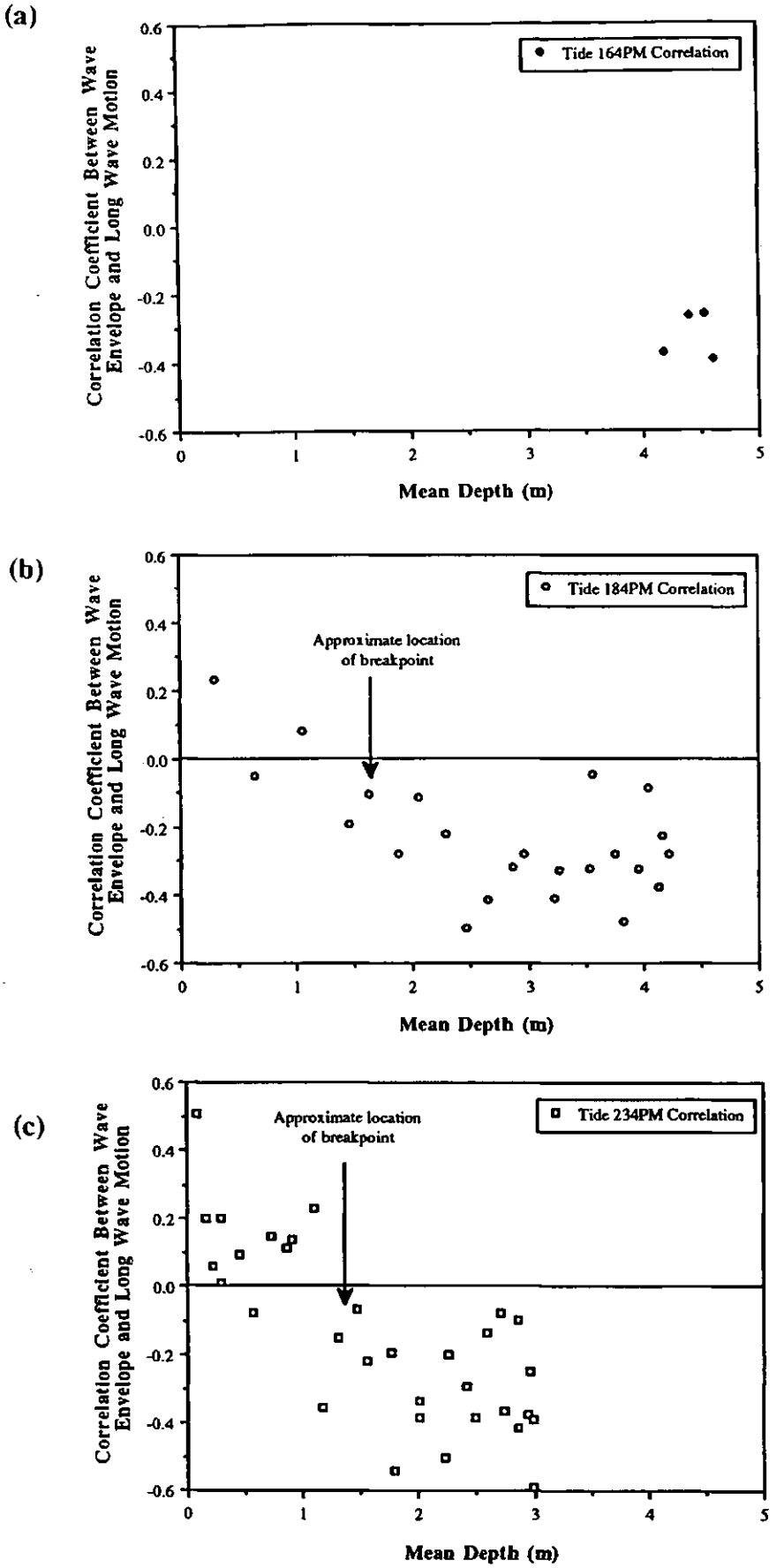

FIGURE 5.8 Variation of cross-correlation coefficient (at zero time lag) with depth for (a) Tide 164PM (b) Tide 184PM and (c) Tide 234PM.

(d)

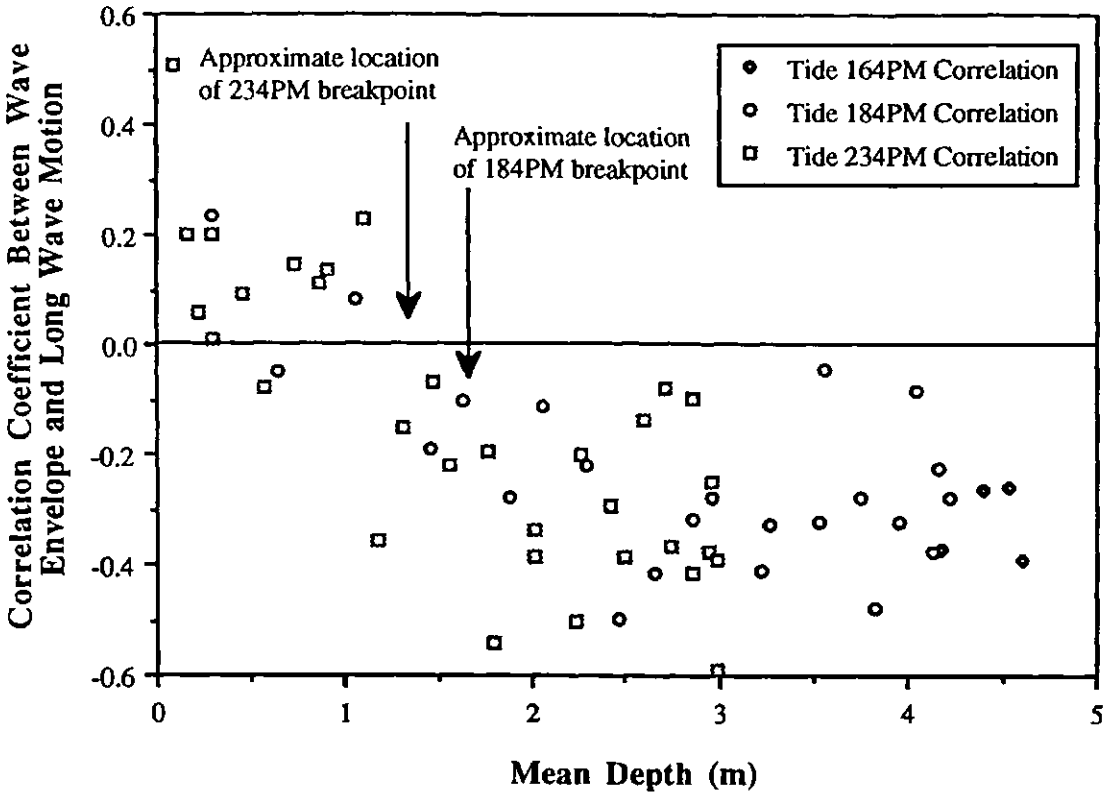

FIGURE 5.8 (d) Combined plot of cross-correlation coefficient (at zero time lag) for all three tides.

RUN No.	WATER DEPTH (m)	WAVE HEIGHT H_S (m)	TIDE 164PM C_R (at zero time lag)
1	4.602	1.3586	-0.390
2	4.534	1.4039	-0.256
3	4.399	1.5000	-0.265
4	4.179	1.6210	-0.370

TABLE 5.4 Correlation, at zero time lag, between incident wave envelope and long period motion for Tide 164PM.

RUN No.	WATER DEPTH (m)	WAVE HEIGHT H_S (m)	TIDE 184PM C_R (at zero time lag)
3	1.624	0.7292	-0.104
4	2.049	0.7252	-0.110
5	2.468	0.7977	-0.497
6	2.862	0.8319	-0.319
7	3.229	0.9461	-0.410
8	3.565	0.7819	-0.044
9	3.830	0.8808	-0.480
10	4.040	0.8038	-0.085
11	4.161	0.8103	-0.224
13	4.217	0.7747	-0.278
14	4.134	0.9954	-0.376
15	3.962	0.9261	-0.323
16	3.757	1.0304	-0.278
17	3.533	1.0724	-0.321
18	3.277	1.0104	-0.328
19	2.967	0.9521	-0.276
20	2.660	1.0389	-0.417
21	2.294	0.9841	-0.221
22	1.876	0.9389	-0.277
23	1.458	0.7804	-0.189
24	1.053	0.6520	0.081
25	0.643	0.4816	-0.049
26	0.296	0.3347	0.235

TABLE 5.5 Correlation, at zero time lag, between incident wave envelope and long period motion for Tide 184PM.

RUN No.	WATER DEPTH (m)	WAVE HEIGHT H_S (m)	TIDE 234PM C_R (at zero time lag)
1	0.167	0.2272	0.202
2	0.223	0.2810	0.059
3	0.295	0.2913	0.200
4	0.458	0.3858	0.095
6	0.737	0.5248	0.144
7	0.904	0.5928	0.137
8	1.094	0.6596	0.231
9	1.308	0.6855	-0.152
10	1.555	0.6965	-0.220
11	1.785	0.7034	-0.541
12	2.010	0.7422	-0.386
13	2.228	0.7643	-0.500
14	2.418	0.7219	-0.295
15	2.597	0.6628	-0.138
16	2.742	0.7628	-0.365
17	2.856	0.6690	-0.415
18	2.943	0.7789	-0.374
19	2.987	0.7561	-0.589
20	2.993	0.6196	-0.392
21	2.955	0.7874	-0.251
22	2.865	0.7038	-0.099
23	2.706	0.7703	-0.079
24	2.497	0.8121	-0.387
25	2.265	0.7325	-0.202
26	2.012	0.7360	-0.339
27	1.756	0.7283	-0.195
28	1.470	0.6951	-0.066
29	1.177	0.6679	-0.355
30	0.858	0.5972	0.111
31	0.574	0.3363	-0.080
32	0.290	0.3860	0.008
33	0.085	0.0839	0.507

TABLE 5.6 Correlation, at zero time lag, between incident wave envelope and long period motion for Tide 234PM.

5.4 DISCUSSION

5.4.1 GROUPINESS FACTOR

The variations in incident wave groupiness were examined through calculation of a groupiness factor. The groupiness factor did not appear to decrease with broadening of the wave band. This was shown by the consistency of the data examined from three tidal cycles with a range of offshore wave conditions. The present data suggest that the groupiness factor maintains a linear relationship with wave height, whether the prevailing nearshore conditions are storm sea or fair-weather swell. Similar results for deep water groupiness were found by List (1991). His values of wave groupiness were not strong functions of the incident wave band width and did not vary greatly from low energy swell to a locally generated storm sea. As he suggested, these observations contradict the hypothesis that wave groups are the product of superimposition of random linear waves, since a broad band of energetic waves should possess less groupy tendencies.

Outside the breaking region the groupiness factor appeared fairly constant. Through the surf zone the groupiness factor was seen to change. Outside the breakpoint, the incoming wave groups induce gradients in the radiation stress which force a phase-locked or bound long wave, with the wave envelope and long wave elevation 180° out of phase. When breaking occurs, a gradual decay of the wave group structure is observed and there is a general decrease in groupiness in the shallower water as the larger waves break. Groupiness factor, however, did <u>not</u> decay immediately at the breakpoint, as is often assumed. Instead there was a persistence of groupiness across the surf zone.

List (1991) was also surprised to observe the presence of a high level of groupiness in a fully saturated surf zone. The simplest explanation offered was that the smaller, unbroken waves acted as a source of the groupiness. On the other hand, he also provided the more comprehensive notion relating incident wave interaction with long wave-induced depth and current modulations. List concluded that the total groupiness within a saturated surf zone is most likely to be a complicated function of the entire time history of the short wave/long wave interaction through the breaking

region.

It would have been useful in this Spurn Head study to have separated the long wave motions into incoming and outgoing components, in order to understand the nature of the long period response in the surf zone. Without this investigation it is difficult to suggest what happened to the bound long wave subsequent to the waves breaking. Theories do exist which offer a number of possible scenarios. For example, List (1986) found the out-going long waves to have a component correlated to the incident wave groups, with a sign and lag suggesting release and reflection of the bound long wave. Guza *et al.* (1984) carried out a similar investigation. Both the seawards and shorewards propagating components were found to be correlated with the incident wave envelope, and the outgoing long wave appeared to result from reflection of the incoming long wave.

5.4.2 CROSS-CORRELATION ANALYSIS

The nature of the short wave/long wave interaction across the nearshore has been examined using cross-correlation analysis. At zero time lag, at the greater depths the correlations were all negative, as would be expected with the bound long wave solutions of Longuet-Higgins and Stewart (1962, 1964). At the smaller depths, the correlation value at zero time lag tended towards zero, or even positive nearer the shoreline. The cross-correlation values near zero which occurred just inside the breakpoint may be explained by the occurrence of a standing long wave nodal position or by the competing effects of forced and free long wave energies (Abdelrahman and Thornton, 1987).

The positive correlations which were observed inside the surf zone may be explained by the modulation of short wave breaker heights. Modulation of the height of breaking incident waves may have been brought about by depth variations induced by the bound long waves. The depth-modulation may in turn be considered to be induced either by the forced or the free long waves (Roelvink and Stive, 1989). List (1986) divided the long waves in the surf zone into onshore and offshore components. His work indicated that through the surf zone whilst the incident waves decrease in

height, with short wave amplitude variability with position in the surf zone, the bound long wave energy increased towards the shoreline.

Besides this qualitative description, a quantitative comparison is also needed between the data examined in the present work and other recent field measurements. Figures 5.9(a)-(d) show the comparison between the Spurn Head data, examined in the present work, and the data discussed in the cross-correlation paper by Abdelrahman and Thornton (1987). The correlation values (at zero time lag) are shown for Tides 164PM and Tide 184PM, and Tide 234PM in Figures 5.9(a) and (b), respectively as a function of mean depth. Figures 5.9(c) and (d) represent correlation results as a function of depth using field data presented by Abdelrahman and Thornton (1987) for 6 February, 1980 (Santa Barbara Beach) and 10 November, 1978 (Torrey Pines Beach). Abdelrahman and Thornton (1987; hereafter AT87) provide values for each instrument location on two Californian beaches which were examined as part of the NSTS experiment. Although the tables have been wrongly labelled (the labels are juxtaposed) in their paper, the data have been compared with the Spurn Head results presented earlier in this study. The general trends of the Spurn Head correlation coefficient (at zero time lag) values (Figures 5.9(a) and (b)) are similar to those of the AT87 field measurements (Figures 5.9(c) and (d)). A consistent pattern of correlation coefficients is seen where negative correlation coefficient values occur outside the surf zone and positive correlation coefficient values are present closer to the shoreline. In Figures 5.9(c) and (d) a zero correlation was taken to represent the approximate location of the breaker line, in line with the work by AT87.

The two data-sets do differ to some extent. The greater degree of scatter which is evident in the Spurn Head data (Figures 5.9(a) and (b)) is caused by the back-and-forth sweep of the tides over the instrument locations. However, the greater number of data runs examined in the Spurn Head correlation analysis allows a more detailed examination of the variability of the wave envelope/long wave motion correlation relationship across the nearshore zone, than the smaller number of data points presented by AT87. An overall comparison between the two data-sets is shown in Figure 5.10. Figure 5.10 incorporates the three tidal cycles (Tides 164PM, 184PM and

(a)

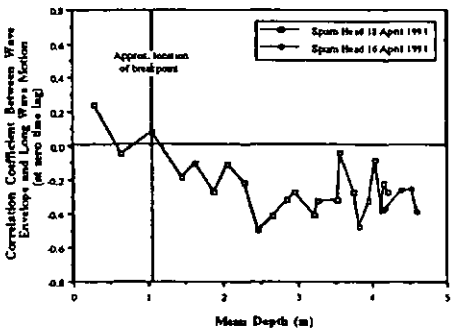

(b)

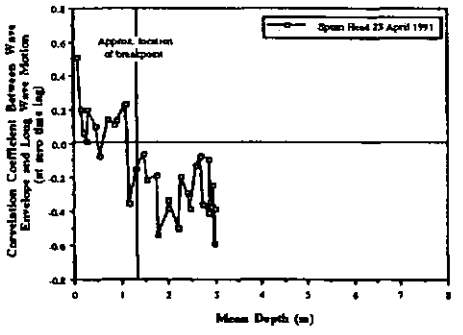

(c)

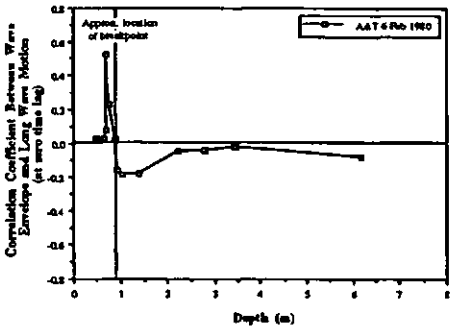

(d)

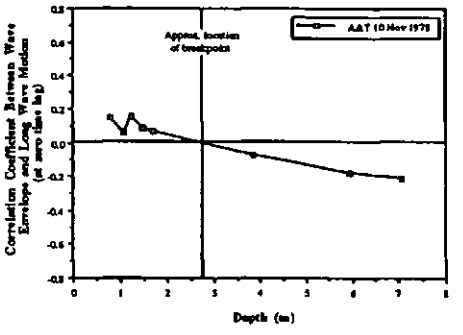

FIGURE 5.9 Correlation (at zero time lag) between wave envelope and long wave motion as a function of depth for (a) Spurn Head 16 &18 April, 1991 (b) Spurn Head 23 April, 1991 (c) NSTS Santa Barbara 6 February, 1980 (AT87) and (d) NSTS Torrey Pines 10 November, 1978 (AT87).

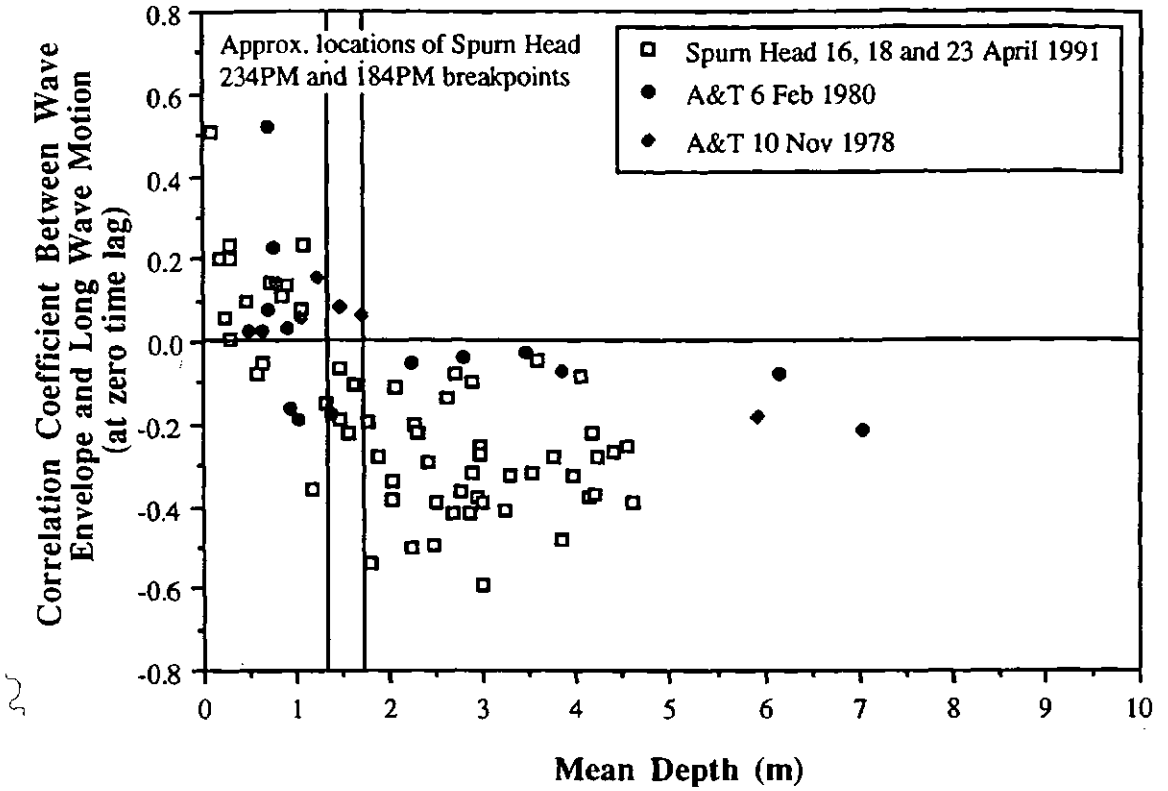

FIGURE 5.10 Combined plot of correlation coefficient values (at zero time lag) as a function of mean depth for B-BAND Spurn Head data from 16, 18 and 23 April, 1991; NSTS Santa Barbara data from 6 February, 1980 and NSTS Torrey Pines data from 10 November, 1978 (From Abdelrahman and Thornton, 1987).

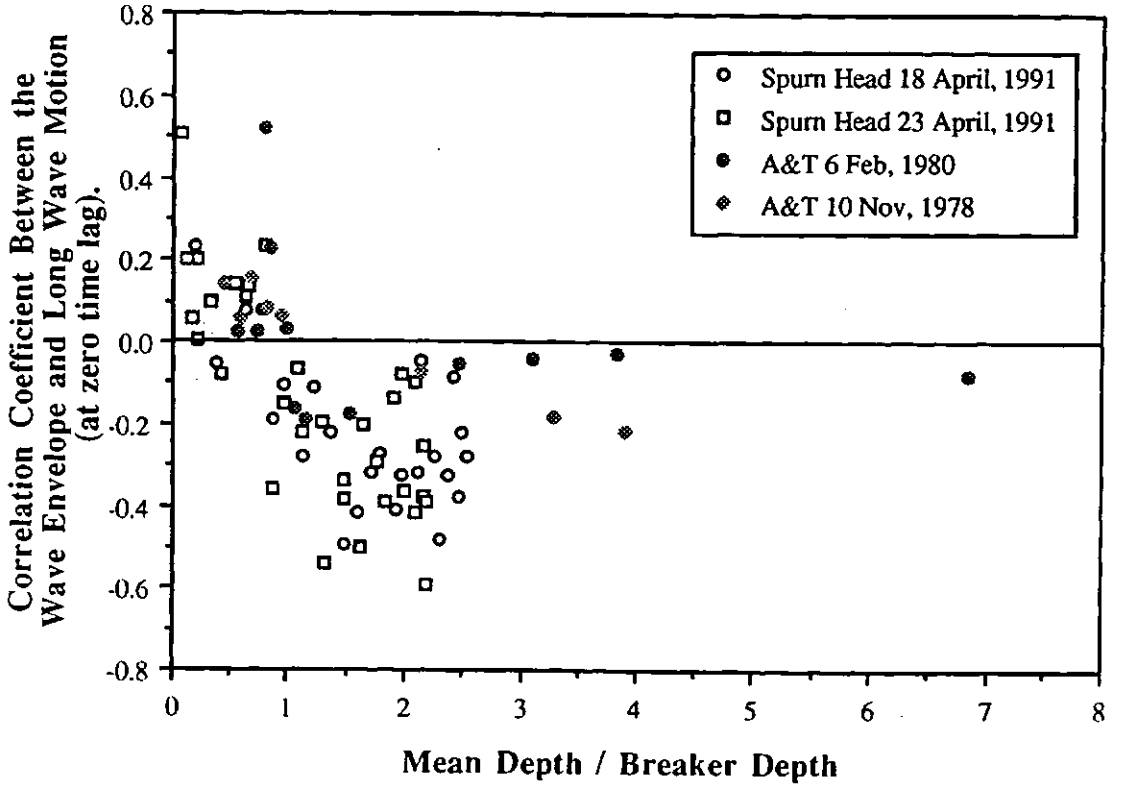

FIGURE 5.11 Combined plot of correlation coefficient values (at zero time lag) as a function of h / h_b for the Spurn Head and NSTS field data.

234PM) from the Spurn Head cross-correlation analysis and the correlation values from the two days of NSTS data calculated by AT87. We see in Figure 5.10, as in Figures 5.9(a)-(d), that the Spurn Head data can be plotted quite comfortably alongside existing field data, to produce reasonable agreement between the trends of two very different data-sets, although the Spurn Head offshore values are of much greater magnitude.

In Figure 5.11 the correlation coefficient values (at zero time lag) have been plotted against the dimensionless h/h_b, here we see a similar distribution of negative values outside the breakpoint and positive values inside the surf zone. However, the pattern of the NSTS data show a slight displacement in relation to the general pattern of the Spurn Head data. Roelvink and Stive (1989) suggested that the smaller negative correlation values found offshore by Abdelrahman and Thornton (1987) may well have been caused by long wave fields from other sources which in turn would decrease the coherence. In their laboratory experiments, Roelvink and Stive (1989) found higher negative correlations offshore which would agree more closely with the findings from the Spurn Head field experiment.

In the present study, the positive correlation values found in the inner surf zone may well reflect the changing bound long wave/incident wave group relationship which occurs towards the shoreline. As the waves break, the short wave amplitude variability decreases, limiting the groupiness effect of the incident waves. The bound long wave travelling towards to the shoreline may then generate fluctuations in the sea surface which help to maintain an element of groupiness inside the surf zone and generate, in turn, the observed positive correlations. This idea agrees well with the model proposed by Abdelrahman and Thornton (1987), which also showed the short waves to be modulated in amplitude, wavenumber and direction due to the slowly varying depth caused by long period standing waves.

Whilst many numerical and laboratory models assume that groupiness decreases to zero at the breakpoint, the data analysed in this study, based upon field results, reveal a persistence of groupiness through the surf zone. Also, the fact that data from three very different tidal cycles show similar trends, in both the groupiness and the cross-correlation work, suggests that both factors are independent of offshore

wave climate. This might have important implications for the modelling of nearshore sediment response.

5.5 SUMMARY

This chapter examined the observations of incident wave groups and long waves in order to assess the variation of wave groupiness across the nearshore zone over a wide range of wave and tidal conditions on the macro-tidal beach environment at Spurn Head, Humberside. The theory that the long wave motion is forced outside the surf zone and that the short incident waves are modulated inside the surf zone, was investigated.

Wave groupiness did not decay immediately at the breakpoint. Instead there was a persistence of the groupiness through the surf zone. The most suitable model for groupiness within a saturated surf zone relates incident wave interaction with long wave-induced depth and current variations.

Outside the surf zone, the cross-correlation between the long wave motion and the wave envelope has a constant negative value and is relatively insensitive to depth. At the breakpoint the correlation decreased to zero, whilst within the inner surf zone positive correlation values occurred. The interaction between long waves and short waves varied systematically through the surf zone. The next chapter will examine the relative importance of these and related hydrodynamic processes which drive cross-shore sediment transport.

CHAPTER 6
SPATIAL SHAPE FUNCTIONS :
Parameterising the processes which drive cross-shore sediment transport

6.1 INTRODUCTION

Recent studies of the processes which operate in the nearshore zone and the mechanisms which drive sediment transport have suggested the important role of velocity moments (Section 2.4.1). Calculation of velocity moments may enable a more detailed understanding of the wave motion climatology and help establish the most important parameters for wave-driven coastal change. This chapter examines **velocity moments** in order to assess the applicability of energetics-based sediment transport predictors.

6.2 CROSS-SHORE SEDIMENT TRANSPORT MODELLING AND VELOCITY MOMENTS

The moments most often applied to sediment transport modelling are the mean, variance (a measure of wave energy) and skewness (a measure of the vertical asymmetry of the waves). Theories such as those by Bowen (1980a) and Bailard (1981, 1987), on the other hand, generate a number of other current velocity moments. The relative magnitudes and distributions of these moments are not well known. Following the work by Bailard, Guza and Thornton (1985a) found that two velocity

moments dominated the bedload and suspended load transport, respectively. In the research at Spurn Head, these terms were decomposed into mean flow, long wave and short wave contributions in order to estimate the relative importance of these flow properties across the nearshore zone.

6.2.1 BEDLOAD TERM

Figures 6.1 to 6.3 show the variation of the total cross-shore bedload moment, with mean depth. As shown in Section 4.3.7(a) this bedload term, when decomposed according to mean flow, long wave and short wave components, comprised ten sub-terms which describe various mechanisms within the nearshore system, as follows,

TERM 1 $\overline{u^3}$ → Mean flow cubed.

TERM 2 $\overline{u_S^3}$ → Skewness of the incident waves.

TERM 3 $\overline{u_L^3}$ → Skewness of the long period waves.

TERM 4 $\overline{3\bar{u}u_S^2}$ → Incident waves mobilise sand, which is then moved by the mean flow.

TERM 5 $\overline{3\bar{u}u_L^2}$ → Long waves mobilise sand, which is then moved by the mean flow.

TERM 6 $\overline{6\bar{u}u_S u_L}$ → Correlation between all three components, expected to be zero.

TERM 7 $\overline{3u_L^2 u_S}$ → Correlation between long period variance and incident wave velocity.

TERM 8 $\overline{3u_S^2 u_L}$ → Correlation between incident wave variance and long period velocity.

TERM 9 $\overline{3\bar{u}^2 u_S}$ → Correlation between mean flow and incident wave velocity, will be zero.

TERM 10 $\overline{3\bar{u}^2 u_L}$ → Correlation between mean flow and long wave velocity, will be zero.

Each of the above ten terms were normalised by dividing through by $(u^2)^{3/2}$, and

FIGURE 6.1 Variation in net cross-shore bedload term with depth for Tide 164PM.

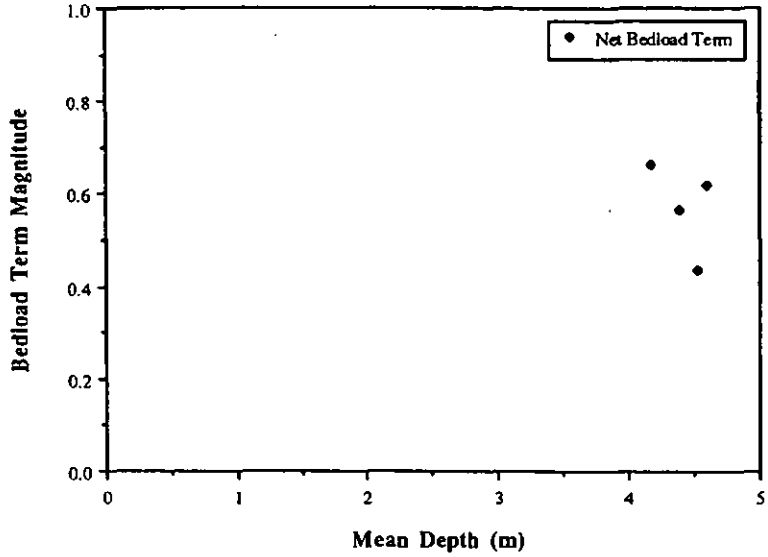

FIGURE 6.2 Variation in net cross-shore bedload term with depth for Tide 184PM.

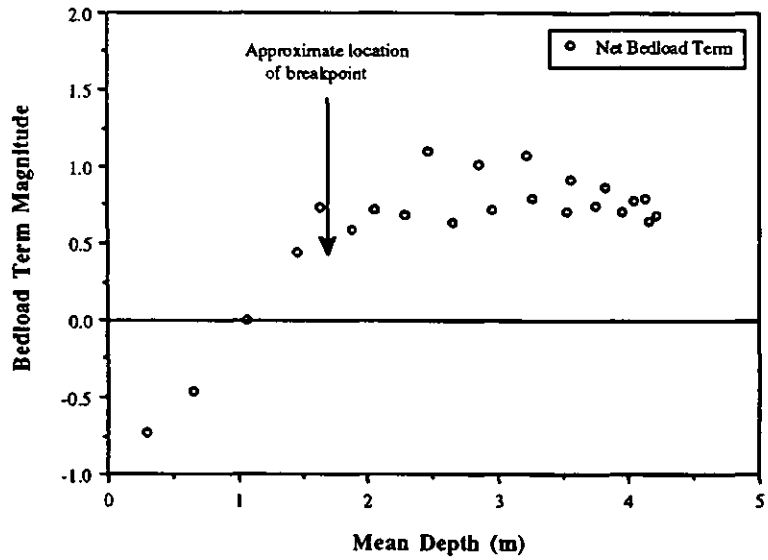

FIGURE 6.3 Variation in net cross-shore bedload term with depth for Tide 234PM.

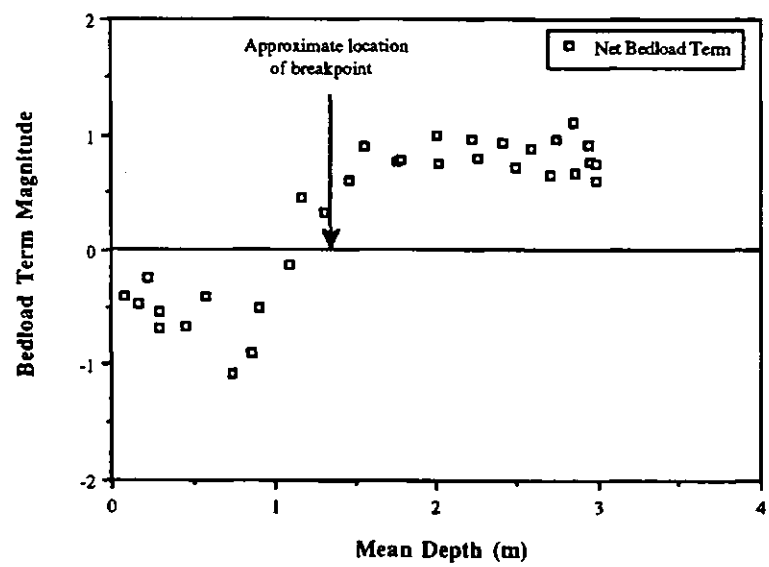

calculated for the three tidal selected cycles using cross-shore current measurements from the bottom sensor on Rig A2 (≈0.10m above the bed).

(a) OBSERVATIONS

In order to investigate the variation of these moments with offshore position, the normalised values of each moment have been plotted against depth. Figures 6.4 to 6.13 illustrate the variation of the ten skewness (bedload) terms shown previously, plotted as functions of mean depth. In Figures 6.4-6.13 these spatial moment 'shape functions' are shown for each of the three tides. Each plotted point represents the value of a moment averaged over an individual data run, for the bottom EMCM on Rig A2. Within velocity moment computations the different signs which arise imply sediment transport in opposite directions; with positive moments indicating onshore and negative moments indicating offshore transport.

A plot of the normalised Bedload Moment Number 1 versus depth for the three tidal cycles is shown in Figure 6.4. Term 1, which is equivalent to the skewness of the mean flow cubed is dominated by a negative offshore peak which occurs inside the surf zone.

Figure 6.5 contains a plot of Bedload Moment Number 2 (the short wave skewness parameter) against mean depth. This term increases linearly from the shoreline to a maximum (+0.92 for Tide 234PM) just beyond the breaker line and then decreases slowly offshore. Term 2 is positive throughout the nearshore, indicating that Term 2 is always in the onshore direction.

Bedload Term 3, which is essentially the skewness of the long wave velocity shown in Figure 6.6, is greatest (positive) at the shoreline decreasing to zero around the breaker position. Figures 6.7 and 6.8 involving Bedload Term 4, representing an Inman/Bagnold-type term where short waves mobilise sediment which is moved by the mean flow, and Bedload Term 5, representing an Inman/Bagnold term where the long waves mobilise the sediment to be then transported by the mean flow, show a similar pattern. In Figures 6.7 and 6.8 there is general trend similar to that of Bedload Term 1 (Fig. 6.4), of increasing negative values with increasing depth from the shoreline

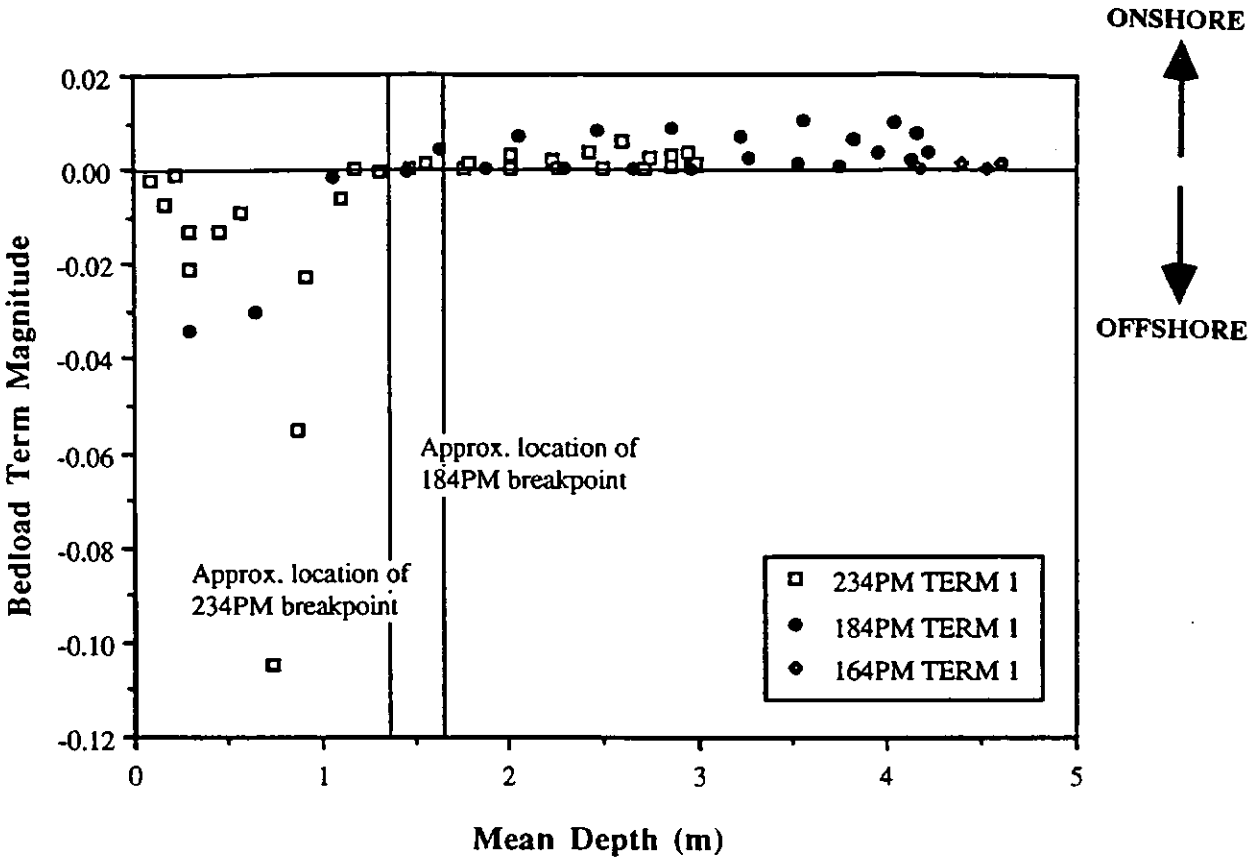

FIGURE 6.4 Variation of Bedload Term 1 with mean depth for Tides 164PM, 184PM and 234PM.

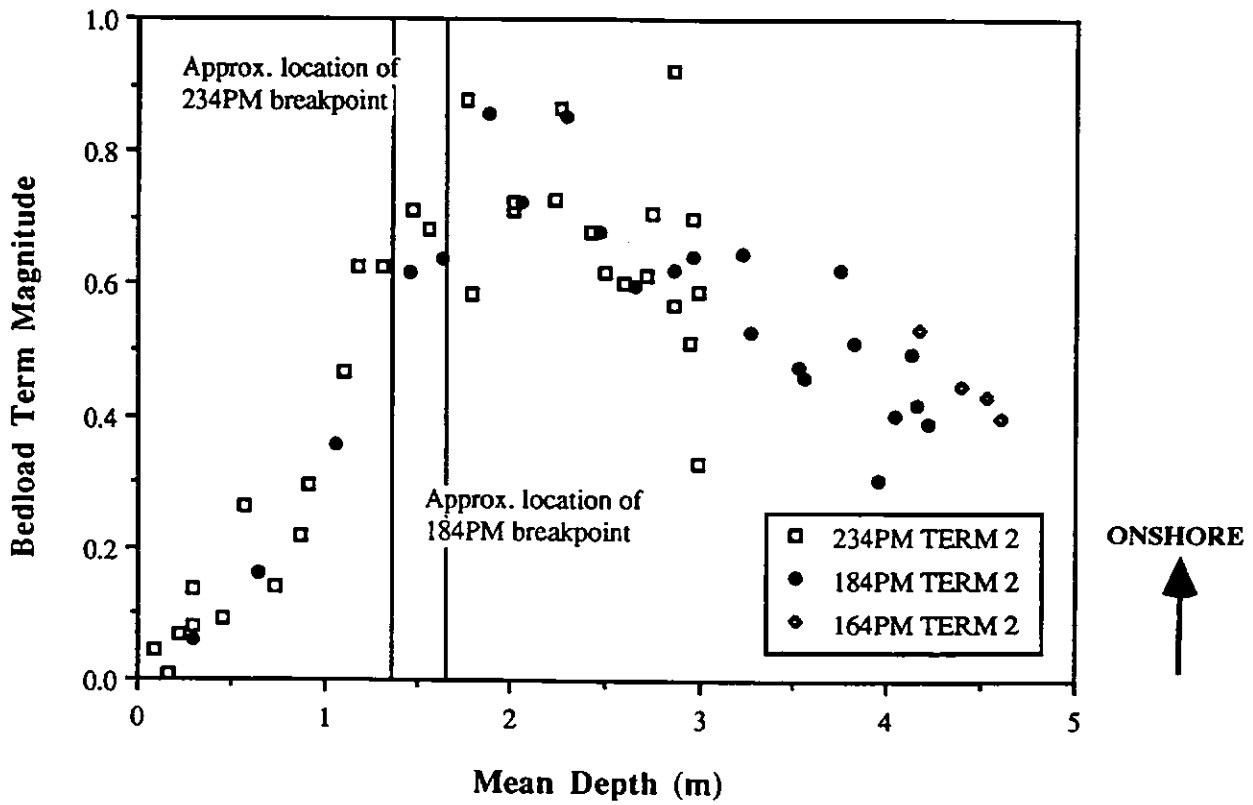

FIGURE 6.5 Variation of Bedload Term 2 with mean depth for Tides 164PM, 184PM and 234PM.

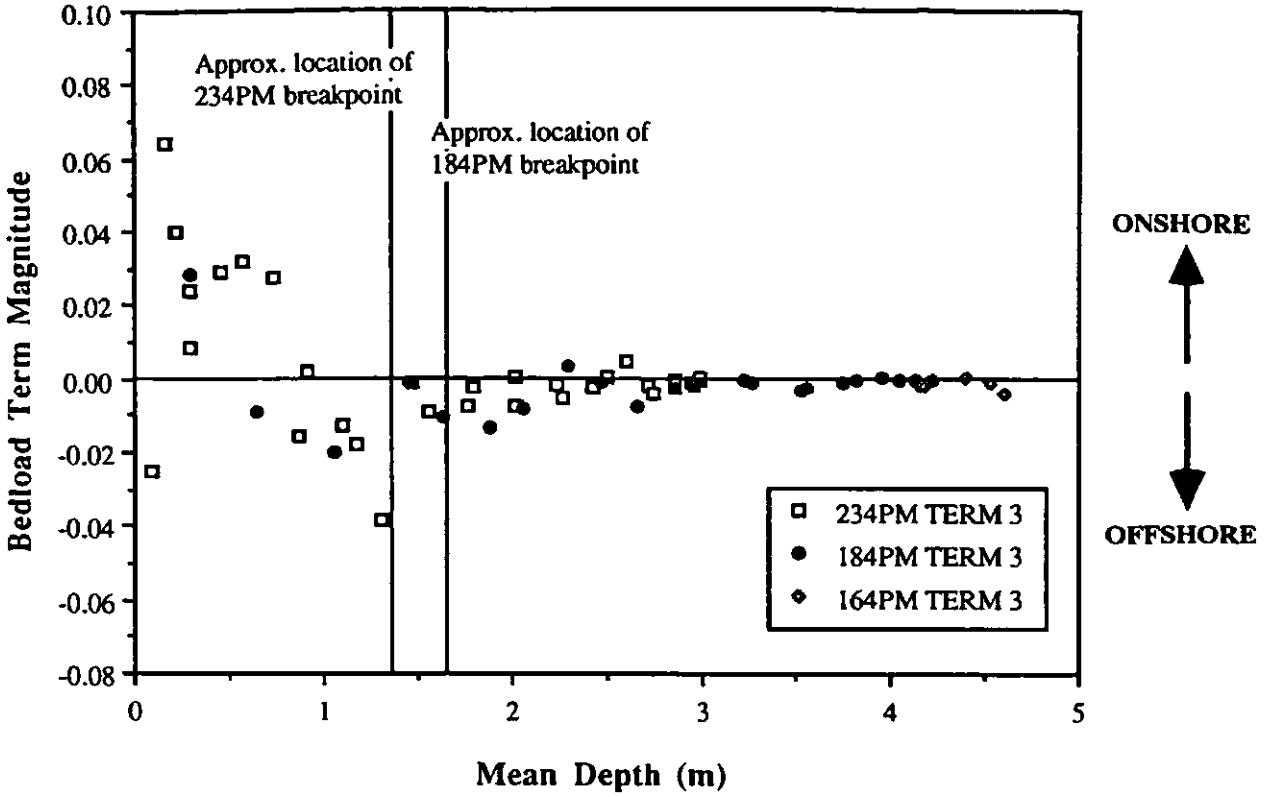

FIGURE 6.6 Variation of Bedload Term 3 with mean depth for Tides 164PM, 184PM and 234PM.

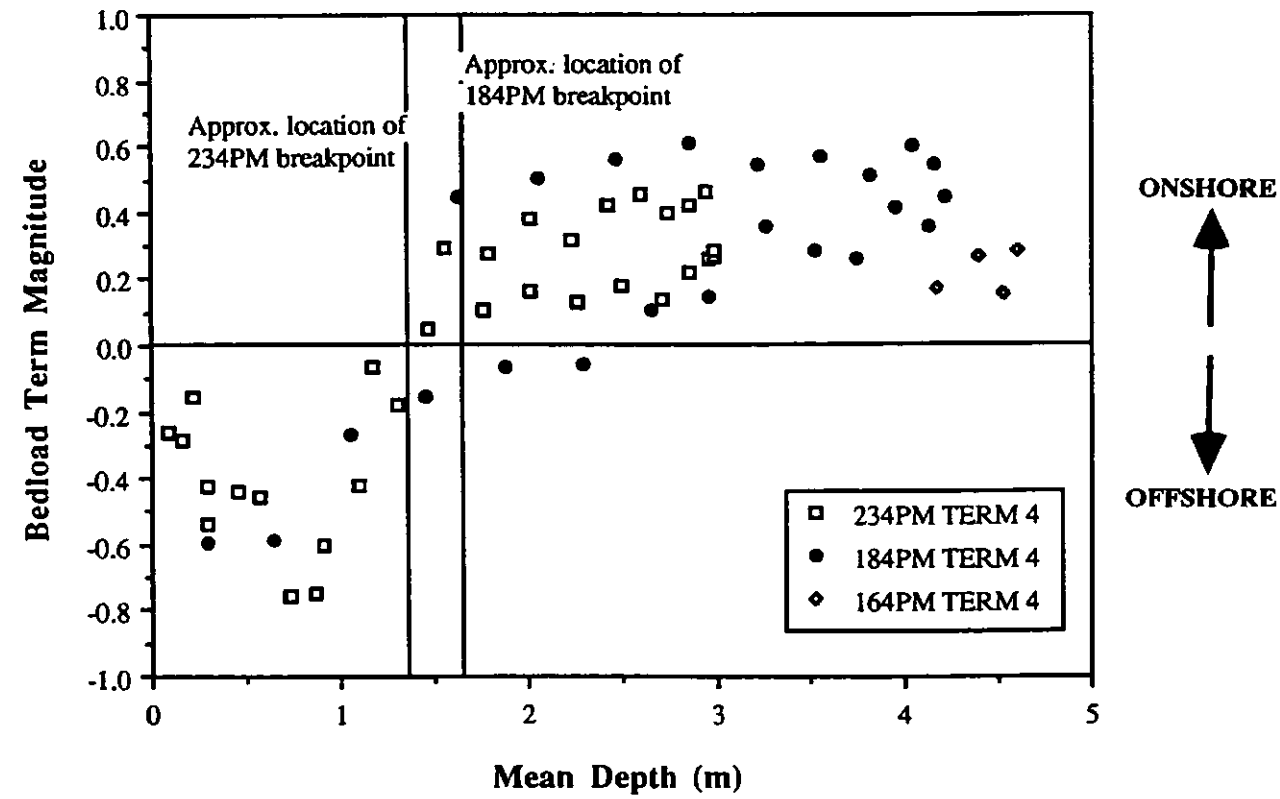

FIGURE 6.7 Variation of Bedload Term 4 with mean depth for Tides 164PM, 184PM and 234PM.

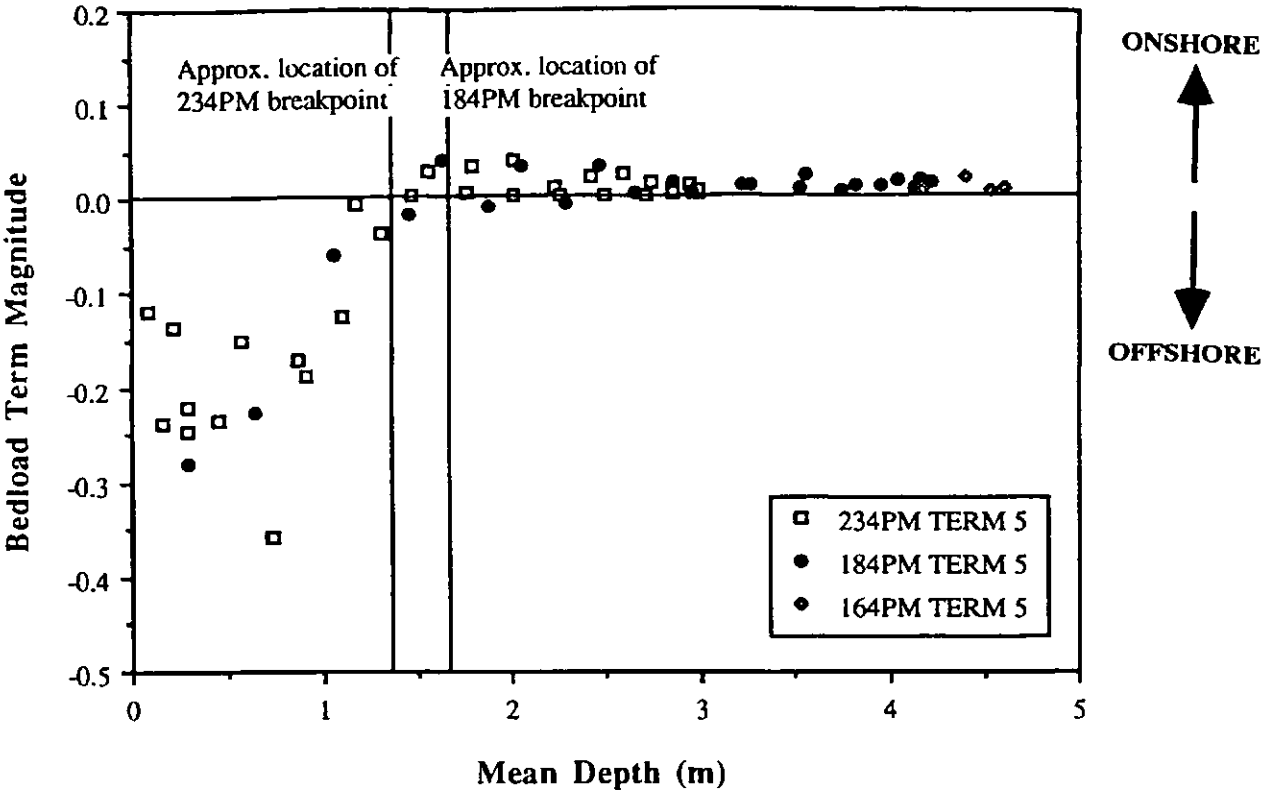

FIGURE 6.8 Variation of Bedload Term 5 with mean depth for Tides 164PM, 184PM and 234PM.

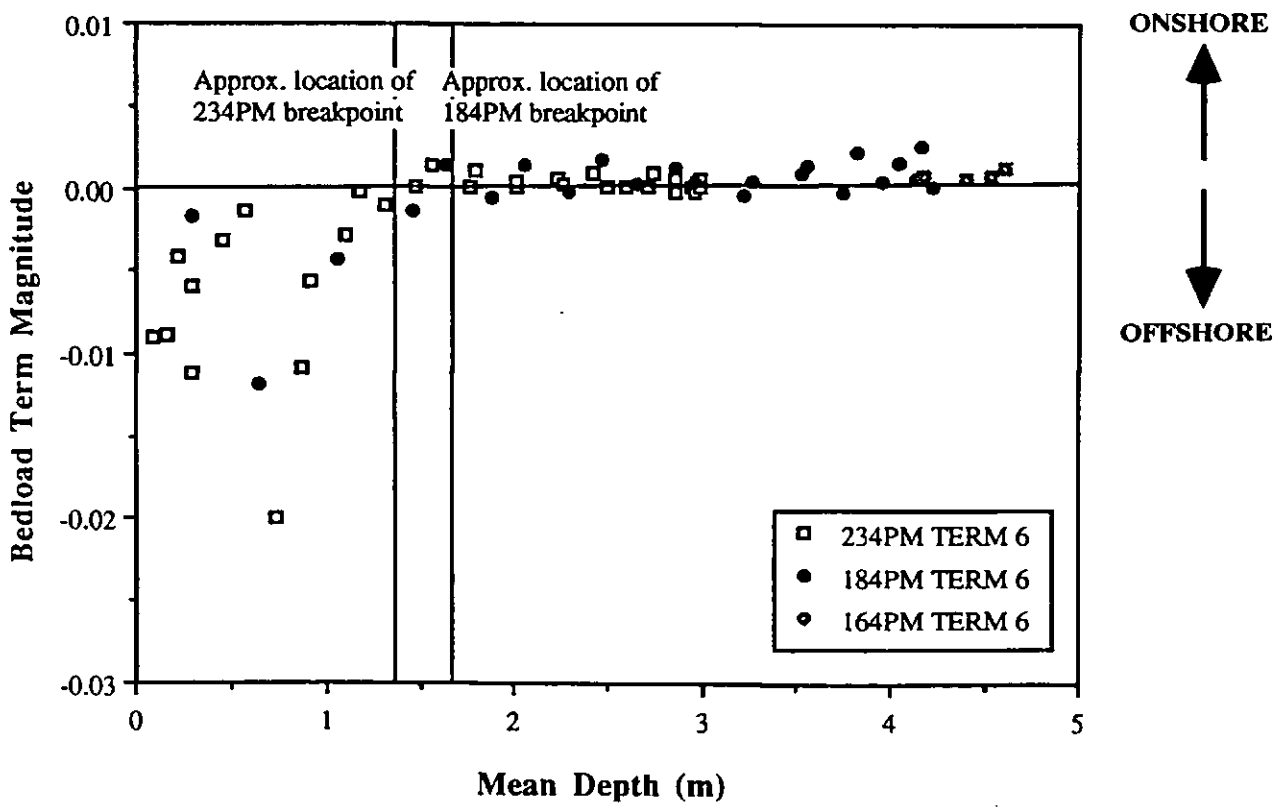

FIGURE 6.9 Variation of Bedload Term 6 with mean depth for Tides 164PM, 184PM and 234PM.

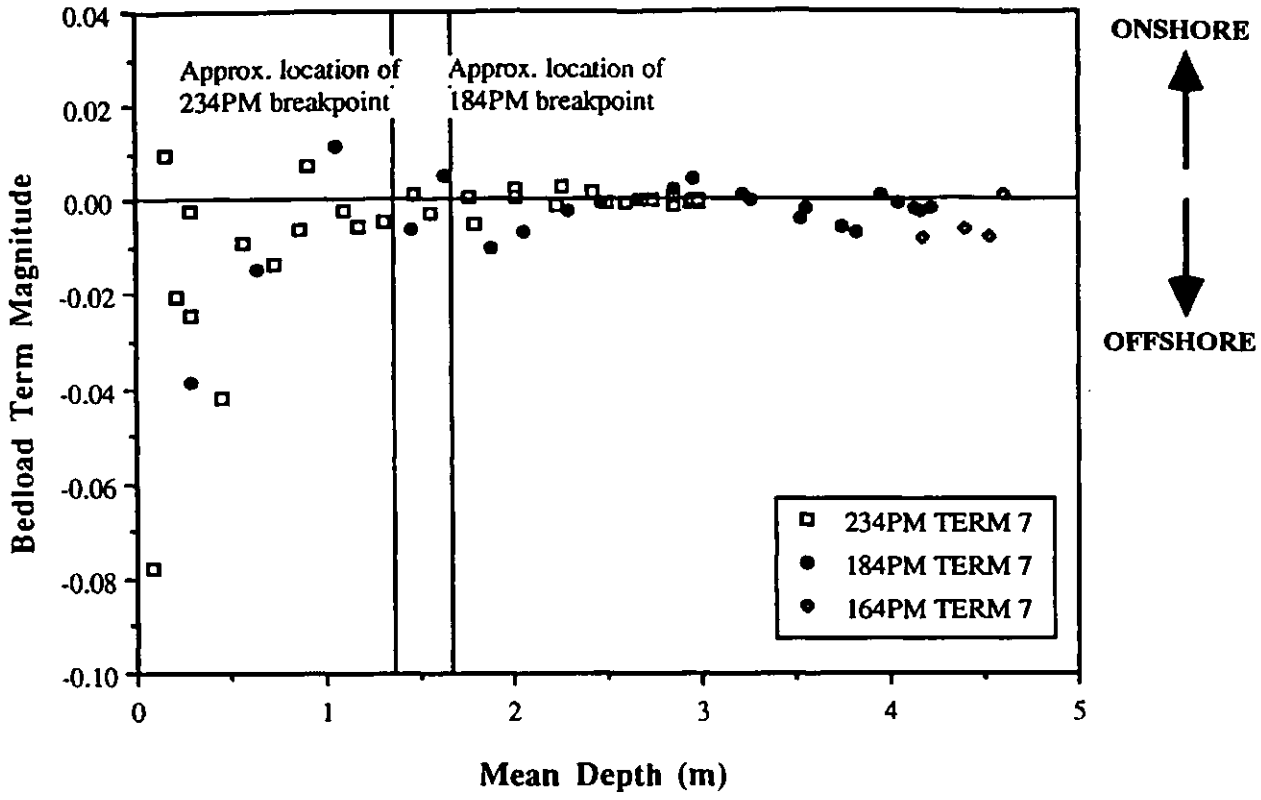

FIGURE 6.10 Variation of Bedload Term 7 with mean depth for Tides 164PM, 184PM and 234PM.

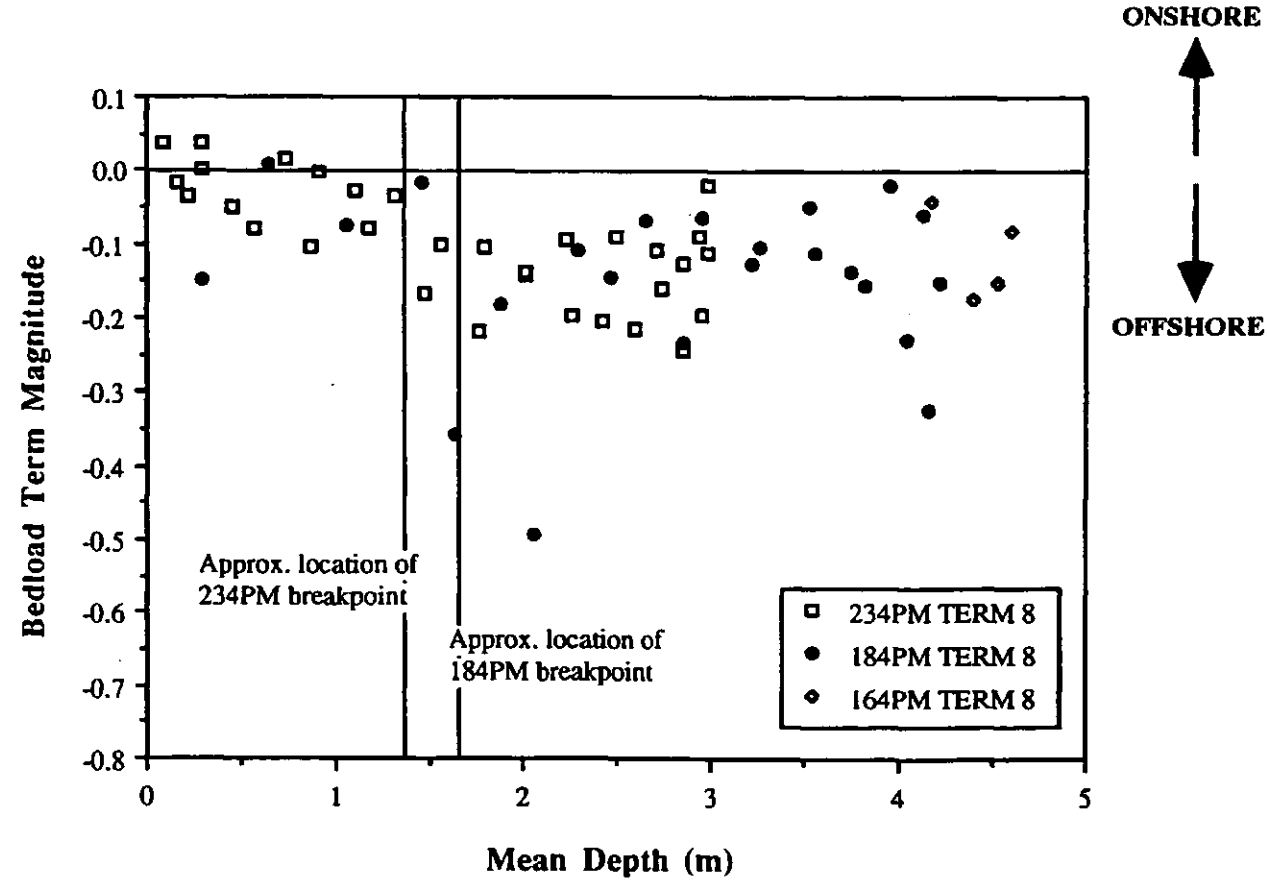

FIGURE 6.11 Variation of Bedload Term 8 with mean depth for Tides 164PM, 184PM and 234PM.

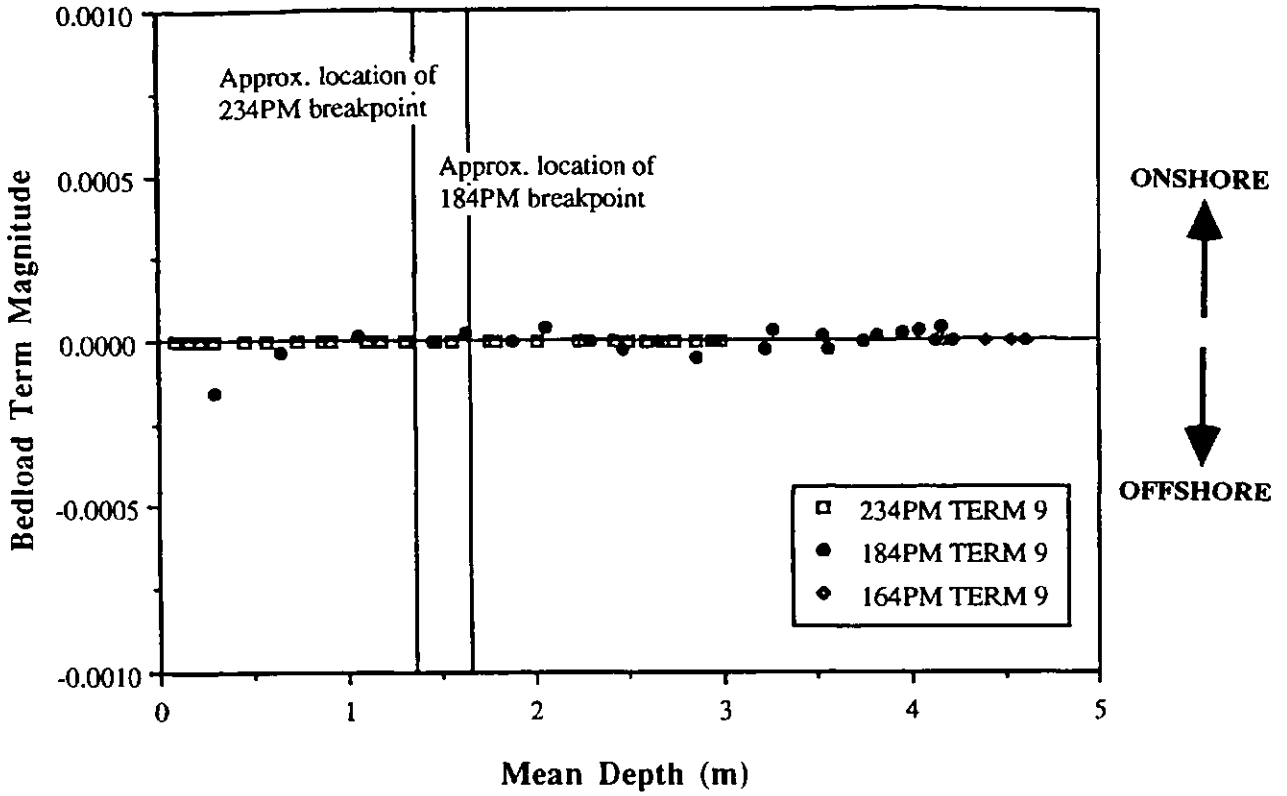

FIGURE 6.12 Variation of Bedload Term 9 with mean depth for Tides 164PM, 184PM and 234PM.

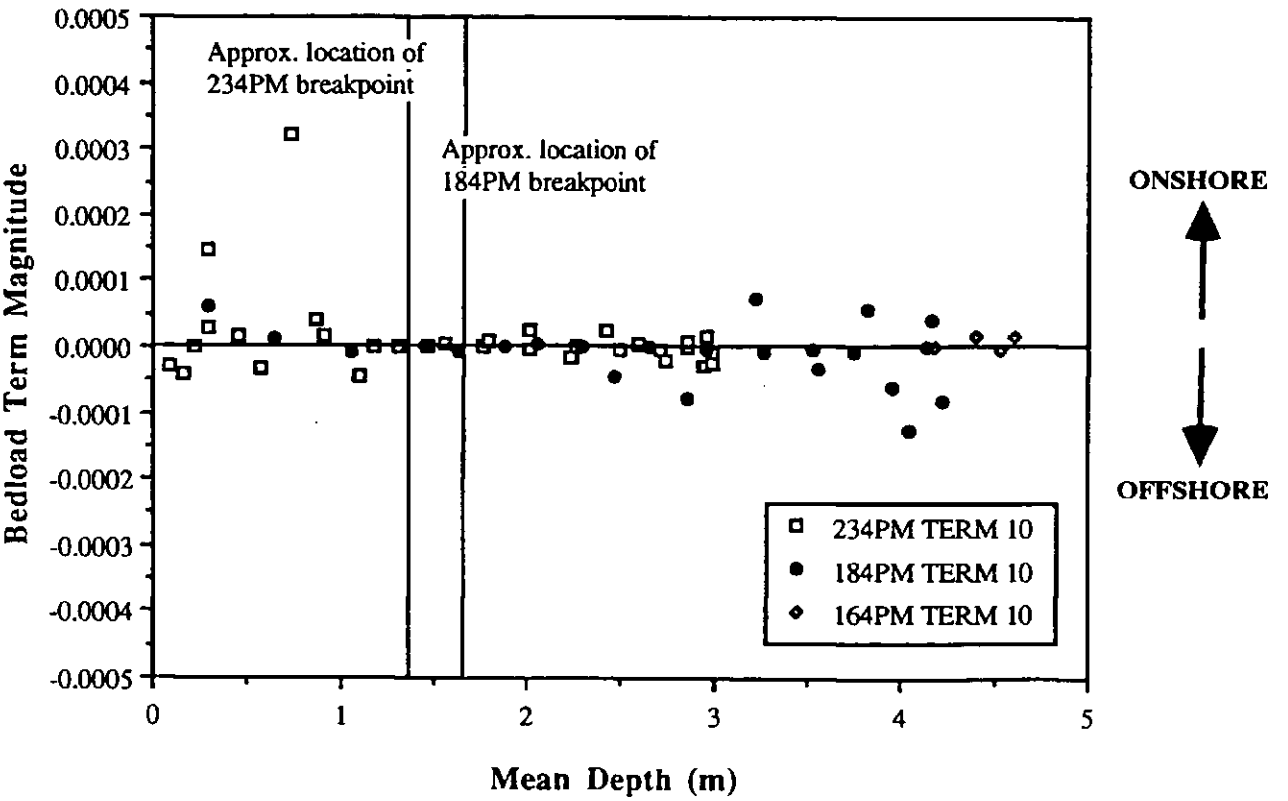

FIGURE 6.13 Variation of Bedload Term 10 with mean depth for Tides 164PM, 184PM and 234PM.

attaining a maximum value just inside the breakpoint. Maximum negative values of -0.75 (Tide 234PM) for Term 4 and -0.36 (Tide 234PM) for Term 5 occur just shorewards of the breakpoint, followed by an increase in the magnitude of the moment to zero at the breakpoint. In the case of Bedload Term 4, the greatest magnitude in the onshore direction occurs at +0.61 (Tide 184PM) offshore of the breakpoint, whilst Bedload Term 5 has near-zero values seaward of the breaking region.

Bedload Term 6 (which encompasses all three mean, incident and infragravity components in one velocity moment) and Term 7 (which describes coupling between the long wave envelope and the short wave velocity) should effectively be zero, and are indeed very small. The magnitudes of Term 6 (Figure 6.9) and Term 7 (Figure 6.10) are generally negligible, being mostly near-zero throughout the nearshore with the exception of a small offshore peak inside the breaker zone.

The velocity moment which represents the correlation between the short wave envelope and the long wave motion in the nearshore, Bedload Term 8, is one of the four most significant of the ten skewness moments. In the scatter diagram in Figure 6.11, the data points tend to be of increasing magnitude with increasing depth across the entire surf zone. At the shoreline the initial observations are slightly positive (a maximum of +0.039 for Tide 234PM) progressing to considerable negative values (-0.23 for Tide 184PM) in the deeper water offshore of the breaker line.

The remaining bedload velocity moments are not significant parameters, Terms 9 and 10 describe coupling between a mean flow and the short wave and long wave velocities, respectively. As expected, the data points in Figures 6.12 and 6.13 are scattered around zero across the nearshore zone and throughout each of the three tidal cycles.

Tables 6.1-6.3 provide a summary of the average values of each data run for the four dominant bedload velocity moments (*i.e.* Terms 2, 4, 5 and 8) for each of the three tidal cycles. The un-normalised and normalised terms are tabulated against run number, run start time, mean depth, significant wave height, mean current and $(u^2)^{3/2}$.

TABLE 6.1 Tide 164PM Un-normalised and Normalised Values of the Most Important Bedload Terms.

Run Number	Start Time	h (m)	H_S (m)	Mean Current (ms^{-1})	Time Av. $(u^2)^{3/2}$	Term 2 unnorm -alised	Term 2 normal -ised	Term 4 unnorm -alised	Term 4 normal -ised	Term 5 unnorm -alised	Term 5 normal -ised	Term 8 unnorm -alised	Term 8 normal -ised
1	19-08-	4.602	1.359	0.0369	0.0502	0.0199	0.3967	0.0144	0.2862	0.0006	0.0125	-0.0042	-0.0846
2	19-28-30	4.534	1.404	0.0212	0.0656	0.0283	0.4317	0.0099	0.1512	0.0005	0.0084	-0.0100	-0.1524
3	19-49-	4.399	1.500	0.0462	0.0882	0.0393	0.4455	0.0234	0.2656	0.0020	0.0232	-0.0154	-0.1745
4	20-10-	4.179	1.621	0.0277	0.1001	0.0534	0.5339	0.0169	0.1687	0.0009	0.0091	-0.0042	-0.0420

Where the dominant normalised bedload moments are :

$$\text{Term 2} = \frac{\overline{u_s^3}}{\left(u^2\right)^{3/2}}$$

$$\text{Term 4} = \frac{\overline{3\bar{u}u_s^2}}{\left(u^2\right)^{3/2}}$$

$$\text{Term 5} = \frac{\overline{3\bar{u}u_L^2}}{\left(u^2\right)^{3/2}}$$

$$\text{Term 8} = \frac{\overline{3u_s^2 u_L}}{\left(u^2\right)^{3/2}}$$

TABLE 6.2 Tide 184PM Un-normalised and Normalised Values of the Most Important Bedload Terms.

Run Number	Start Time	h (m)	H_s (m)	Mean Current (ms^{-1})	Time Av. $(u^2)^{3/2}$	Term 2 unnorm -alised	Term 2 normal -ised	Term 4 unnorm -alised	Term 4 normal -ised	Term 5 unnorm -alised	Term 5 normal -ised	Term 8 unnorm -alised	Term 8 normal -ised
3	17-11-28	1.624	0.730	0.0580	0.0457	0.0291	0.6368	0.0204	0.4456	0.0018	0.0398	-0.0163	-0.3556
4	17-29-06	2.049	0.725	0.0657	0.0416	0.0301	0.7218	0.0209	0.5027	0.0015	0.0352	-0.0205	-0.4934
5	17-46-55	2.468	0.798	0.0660	0.0356	0.0241	0.6776	0.0198	0.5572	0.0013	0.0351	-0.0052	-0.1468
6	18-04-43	2.862	0.832	0.0615	0.0270	0.0168	0.6200	0.0166	0.6124	0.0005	0.0174	-0.0063	-0.2338
7	18-22-34	3.229	0.946	0.0613	0.0334	0.0216	0.6453	0.0182	0.5450	0.0005	0.0142	-0.0042	-0.1265
8	18-40-42	3.565	0.782	0.0586	0.0191	0.0087	0.4576	0.0108	0.5658	0.0005	0.0258	-0.0021	-0.1124
9	18-59-06	3.830	0.881	0.0530	0.0234	0.0120	0.5165	0.0120	0.5123	0.0003	0.0142	-0.0036	-0.1549
10	19-16-55	4.040	0.804	0.0513	0.0138	0.0055	0.4012	0.0082	0.5979	0.0003	0.0198	-0.0032	-0.2299
13	20-45-54	4.217	0.775	0.0348	0.0116	0.0045	0.3902	0.0052	0.4477	0.0002	0.0172	-0.0018	-0.1535
14	21-04-22	4.134	0.995	0.0392	0.0294	0.0145	0.4955	0.0105	0.3580	0.0003	0.0119	-0.0018	-0.0599
15	21-21-24	3.962	0.929	0.0461	0.0286	0.0087	0.3057	0.0119	0.4182	0.0005	0.0164	-0.0006	-0.0207
16	21-39-39	3.757	1.030	0.0312	0.0394	0.0245	0.6232	0.0103	0.2625	0.0004	0.0102	-0.0054	-0.1368
17	21-58-37	3.533	1.072	0.0399	0.0535	0.0255	0.4758	0.0153	0.2850	0.0007	0.0126	-0.0026	-0.0492
18	22-17-33	3.277	1.010	0.0466	0.0440	0.0233	0.5297	0.0159	0.3614	0.0006	0.0144	-0.0046	-0.1046
19	22-35-47	2.966	0.952	0.0189	0.0489	0.0314	0.6417	0.0070	0.1435	0.0003	0.0059	-0.0031	-0.0641
20	22-53-41	2.660	1.039	0.0166	0.0708	0.0423	0.5973	0.0076	0.1079	0.0005	0.0075	-0.0048	-0.0671
21	23-11-48	2.294	0.984	-0.0081	0.0685	0.0585	0.8536	-0.0039	-0.0569	-0.0003	-0.0041	-0.0075	-0.1100
22	23-30-15	1.876	0.939	-0.0099	0.0773	0.0661	0.8562	-0.0050	-0.0648	-0.0006	-0.0073	-0.0142	-0.1835
23	23-48-05	1.458	0.780	-0.0240	0.0660	0.0405	0.6171	-0.0100	-0.1518	-0.0011	-0.0167	-0.0011	-0.0169
24	00-05-53	1.053	0.652	-0.0464	0.0593	0.0213	0.3587	-0.0161	-0.2718	-0.0036	-0.0600	-0.0045	-0.0759
25	00-24-21	0.643	0.482	-0.1222	0.0604	0.0097	0.1607	-0.0352	-0.5832	-0.0138	-0.2280	0.0005	0.0085
26	00-42-17	0.296	0.335	-0.1161	0.0462	0.0028	0.0616	-0.0276	-0.5970	-0.0130	-0.2817	-0.0068	-0.1482

Table 5.4.1 Un-normalised and Normalised Values of the Most Important Bedload Terms.

Run Number	Start Time	h (m)	H_s (m)	Mean Current (ms^{-1})	Time Av. $(u^2)^{3/2}$	Term 2 unnorm -alised	Term 2 normal -ised	Term 4 unnorm -alised	Term 4 normal -ised	Term 5 unnorm -alised	Term 5 normal -ised	Term 8 unnorm -alised	Term 8 normal -ised
1	07-47-37	0.167	0.227	-0.0675	0.0421	0.0003	0.0074	-0.0122	-0.2884	-0.0100	-0.2385	-0.0006	-0.0154
2	08-05-53	0.223	0.281	-0.0375	0.0527	0.0037	0.0700	-0.0082	-0.1553	-0.0071	-0.1357	-0.0019	-0.0364
3	08-23-49	0.295	0.291	-0.0805	0.0409	0.0033	0.0812	-0.0172	-0.4212	-0.0090	-0.2211	0.0015	0.0362
4	08-50-20	0.458	0.386	-0.0848	0.0471	0.0044	0.0943	-0.0206	-0.4383	-0.0111	-0.2355	-0.0024	-0.0512
6	09-27-12	0.737	0.525	-0.2061	0.0836	0.0119	0.1427	-0.0631	-0.7549	-0.0300	-0.3585	0.0012	0.0142
7	09-45-26	0.904	0.593	-0.1100	0.0588	0.0174	0.2957	-0.0352	-0.5991	-0.0110	-0.1866	-0.0002	-0.0031
8	10-03-53	1.094	0.660	-0.0723	0.0613	0.0286	0.4656	-0.0261	-0.4263	-0.0076	-0.1244	-0.0017	-0.0281
9	10-22-10	1.308	0.686	-0.0285	0.0582	0.0365	0.6275	-0.0106	-0.1817	-0.0020	-0.0351	-0.0020	-0.0345
10	10-41-33	1.555	0.697	0.0379	0.0469	0.0320	0.6823	0.0136	0.2897	0.0013	0.0282	-0.0048	-0.1029
11	10-59-44	1.785	0.703	0.0396	0.0466	0.0274	0.5874	0.0128	0.2739	0.0016	0.0349	-0.0048	-0.1035
12	11-17-59	2.010	0.742	0.0500	0.0422	0.0300	0.7122	0.0160	0.3786	0.0017	0.0398	-0.0059	-0.1402
13	11-36-14	2.228	0.764	0.0403	0.0361	0.0264	0.7295	0.0115	0.3186	0.0004	0.0116	-0.0034	-0.0931
14	11-54-34	2.418	0.722	0.0475	0.0287	0.0195	0.6794	0.0121	0.4215	0.0007	0.0241	-0.0059	-0.2042
15	12-13-09	2.597	0.663	0.0487	0.0209	0.0125	0.6013	0.0095	0.4568	0.0006	0.0268	-0.0045	-0.2137
16	12-31-40	2.742	0.763	0.0410	0.0293	0.0206	0.7055	0.0116	0.3961	0.0005	0.0179	-0.0047	-0.1610
17	12-49-51	2.856	0.669	0.0409	0.0258	0.0238	0.9247	0.0109	0.4221	0.0003	0.0121	-0.0063	-0.2445
18	13-08-04	2.943	0.779	0.0396	0.0167	0.0086	0.5141	0.0078	0.4656	0.0003	0.0163	-0.0015	-0.0888
19	13-26-19	2.987	0.756	0.0279	0.0279	0.0165	0.5906	0.0075	0.2704	0.0002	0.0065	-0.0032	-0.1131
20	13-45-05	2.993	0.620	0.0263	0.0131	0.0043	0.3308	0.0038	0.2879	0.0001	0.0084	-0.0003	-0.0196
21	14-04-09	2.955	0.787	0.0240	0.0184	0.0128	0.6978	0.0048	0.2617	0.0001	0.0078	-0.0036	-0.1977
22	14-23-34	2.865	0.704	0.0210	0.0229	0.0131	0.5701	0.0050	0.2182	0.0002	0.0068	-0.0029	-0.1264
23	14-45-15	2.706	0.770	0.0155	0.0376	0.0231	0.6136	0.0053	0.1414	0.0001	0.0034	-0.0041	-0.1084
24	15-08-41	2.497	0.812	0.0230	0.0459	0.0284	0.6196	0.0083	0.1805	0.0001	0.0030	-0.0041	-0.0885
25	15-28-25	2.265	0.763	0.0145	0.0443	0.0383	0.8654	0.0057	0.1288	0.0002	0.0049	-0.0086	-0.1950
26	15-47-05	2.012	0.736	0.0214	0.0509	0.0369	0.7242	0.0081	0.1598	0.0002	0.0044	-0.0071	-0.1393
27	16-05-31	1.756	0.728	0.0128	0.0407	0.0357	0.8786	0.0043	0.1065	0.0002	0.0059	-0.0089	-0.2186
28	16-23-46	1.470	0.695	0.0060	0.0438	0.0312	0.7129	0.0020	0.0458	0.0001	0.0029	-0.0074	-0.1681
29	16-42-18	1.177	0.668	-0.0080	0.0442	0.0277	0.6272	-0.0028	-0.0628	-0.0002	-0.0051	-0.0035	-0.0797
30	17-01-30	0.858	0.597	-0.1386	0.0485	0.0106	0.2187	-0.0364	-0.7509	-0.0082	-0.1685	-0.0051	-0.1048
31	17-19-58	0.574	0.336	-0.0647	0.0299	0.0080	0.2662	-0.0137	-0.4590	-0.0045	-0.1509	-0.0024	-0.0797
32	17-38-50	0.290	0.386	-0.0807	0.0249	0.0034	0.1386	-0.0134	-0.5385	-0.0061	-0.2460	0.0001	0.0026
33	17-57-43	0.085	0.084	-0.0390	0.0257	0.0012	0.0452	-0.0067	-0.2603	-0.0031	-0.1200	0.0010	0.0391

(b) CROSS-SHORE VARIATIONS

The ten normalised bedload terms, calculated for each data run of the three tides, have been averaged into measurements made seaward of the surf zone and those measurements obtained within the surf zone (Table 6.4). Figures 6.14-6.16 show the averaged bedload moments outside the surf zone, whilst Figure 6.17 and 6.18 show the corresponding values within the surf zone. For the three days, which had a range of characteristics, the following velocity moments are dominant :

Tide 164PM (Fig. 6.14)	Seaward of the Surf Zone	Terms 2, 4 and 8
Tide 184PM (Fig. 6.15)	Seaward of the Surf Zone	Terms 2, 4 and 8
Tide 234PM (Fig. 6.16)	Seaward of the Surf Zone	Terms 2, 4 and 8
Tide 164PM*	Within the Surf Zone	No data collected
Tide 184PM (Fig. 6.17)	Within the Surf Zone	Terms 2, 4 and 5
Tide 234PM (Fig. 6.18)	Within the Surf Zone	Terms 2, 4 and 5

* Storm too violent, so data logging stopped.

Seawards of the surf zone, the bedload terms which dominate are, therefore, Term 2 (the skewness of the short wave velocity), Term 4 (the term where short waves mobilise the sediment, which is then moved by a mean flow) and Term 8 (the term describing the correlation between the short (or incident) wave groups and the long wave motion). Inside the breakpoint, the moments which dominate are Terms 2 and 4 (described previously) and Term 5 (the term which represents the stirring of sediment by long waves and the subsequent transport by a mean flow).

Figures 6.19 and 6.20 show bar chart plots of the most important bedload velocity moments both beyond and within the breaking wave region. The similarity of these terms through each of the tides, independent of incident wave conditions, not only in direction, but also in percentage contribution to the total skewness, indicates a good degree of consistency between the data. It is also interesting to note the variation of Term 8 through the nearshore system since this reflects the earlier wave groupiness analysis (see Chapter 5). Term 8 describes the correlation between the incident wave

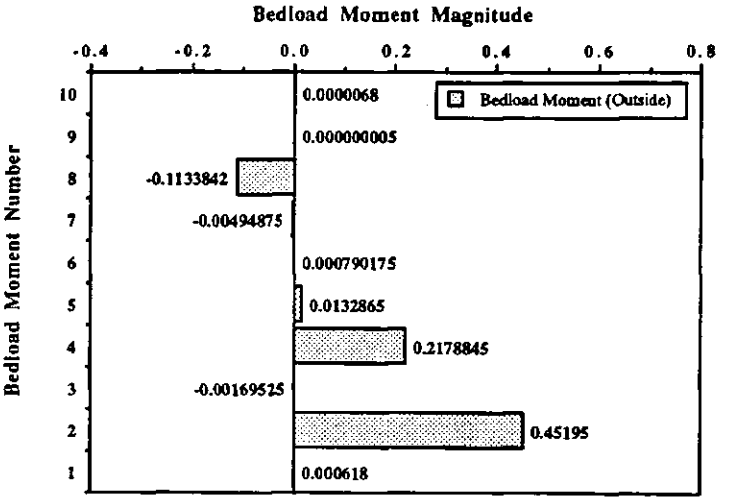

FIGURE 6.14 Tide-averaged Bedload Terms 1-10 for measurements made **outside** the surf zone during Tide 164PM.

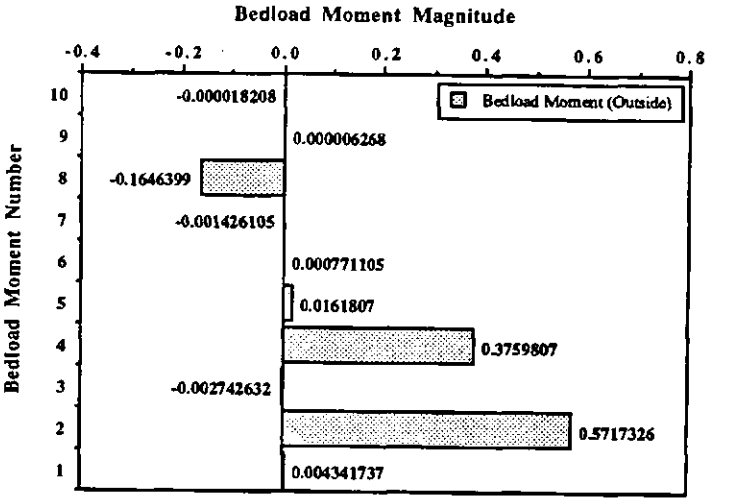

FIGURE 6.15 Tide-averaged Bedload Terms 1-10 for measurements made **outside** the surf zone during Tide 184PM.

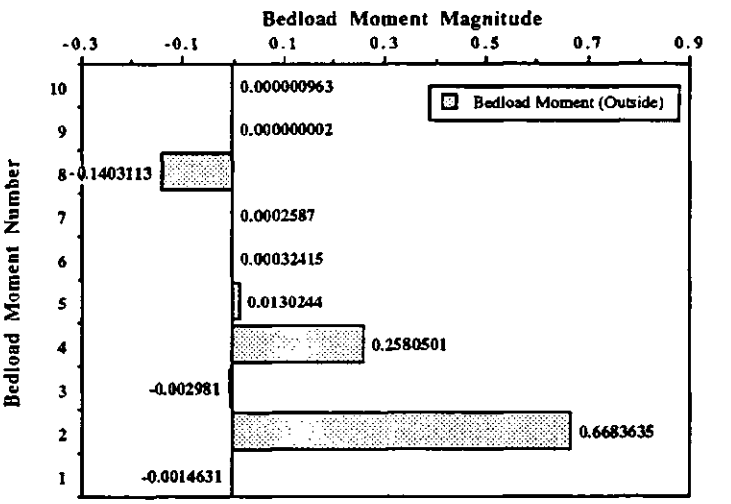

FIGURE 6.16 Tide-averaged Bedload Terms 1-10 for measurements made **outside** the surf zone during Tide 234PM.

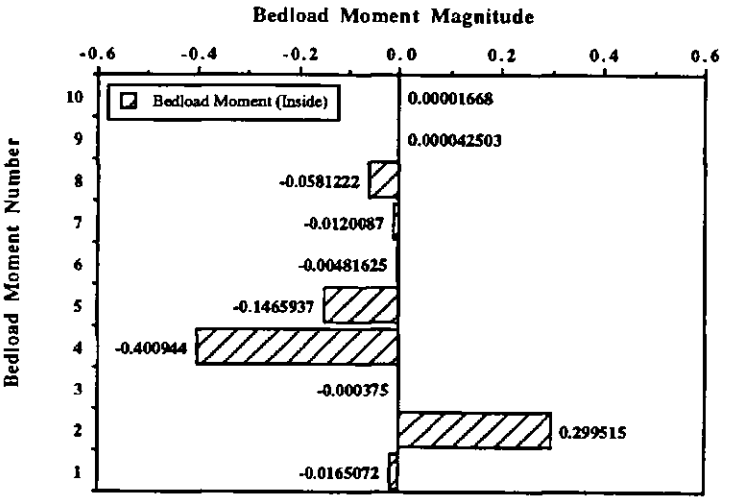

FIGURE 6.17 Tide-averaged Bedload Terms 1-10 for measurements made **inside** the surf zone during Tide 184PM.

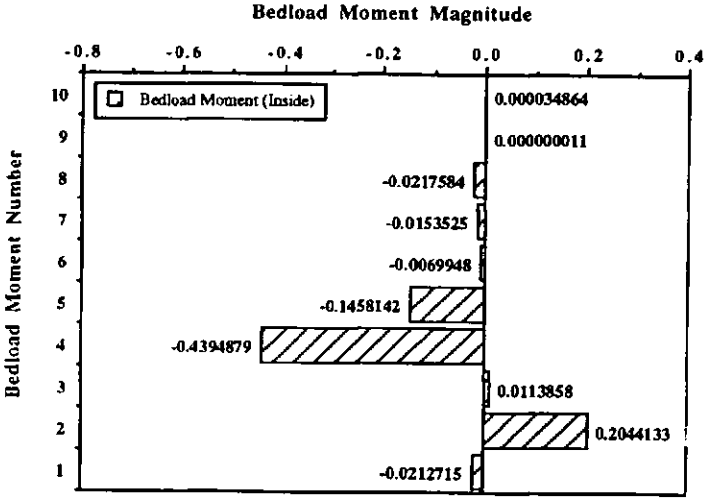

FIGURE 6.18 Tide-averaged Bedload Terms 1-10 for measurements made **inside** the surf zone during Tide 234PM.

TABLE 6.4 Average Values of Bedload Term Observations for Tides 164PM, 184PM and 234PM.

Bedload Term Number	TIDE 164PM Average of Runs Offshore of the Breakpoint.	TIDE 184PM Average of Runs Offshore of the Breakpoint.	TIDE 184PM Average of Runs Onshore of the Breakpoint.	TIDE 234PM Average of Runs Offshore of the Breakpoint.	TIDE 234PM Average of Runs Onshore of the Breakpoint.
1	0.0006	0.0043	-0.0165	-0.0015	-0.0213
2	0.4520	0.5717	0.2995	0.6684	0.2044
3	-0.0017	-0.0027	-3.75×10^{-4}	-0.0030	0.0114
4	0.2179	0.3760	-0.4009	0.2581	-0.4395
5	0.0133	0.0162	-0.1466	0.0130	-0.1458
6	0.0008	7.71×10^{-4}	-0.0048	3.24×10^{-4}	-0.0070
7	-0.0049	-0.0014	-0.0012	2.59×10^{-4}	-0.0154
8	-0.1134	-0.1646	-0.0581	-0.1403	-0.0218
9	4.85×10^{-9}	6.27×10^{-6}	4.25×10^{-5}	1.75×10^{-9}	1.08×10^{-8}
10	6.80×10^{-6}	1.82×10^{-5}	1.67×10^{-5}	9.63×10^{-7}	3.49×10^{-5}

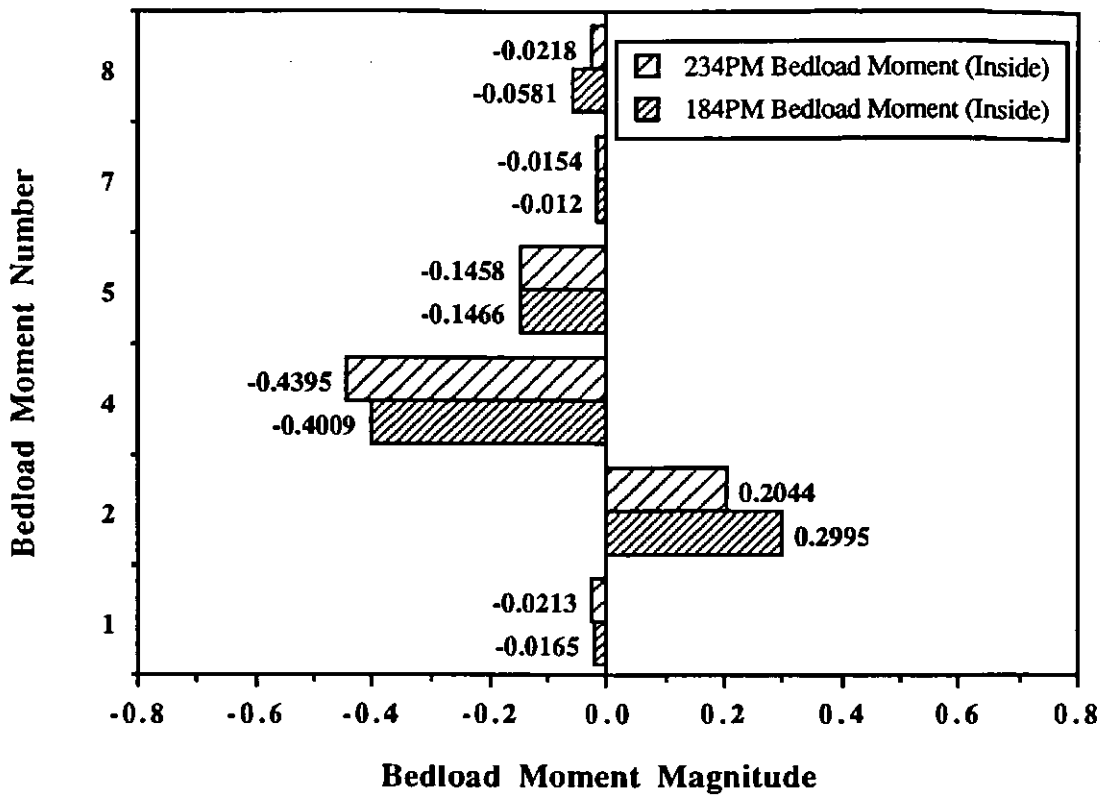

FIGURE 6.19 Dominant Bedload Terms averaged **inside** the surf zone and per tide for Tides 184PM and 234PM.

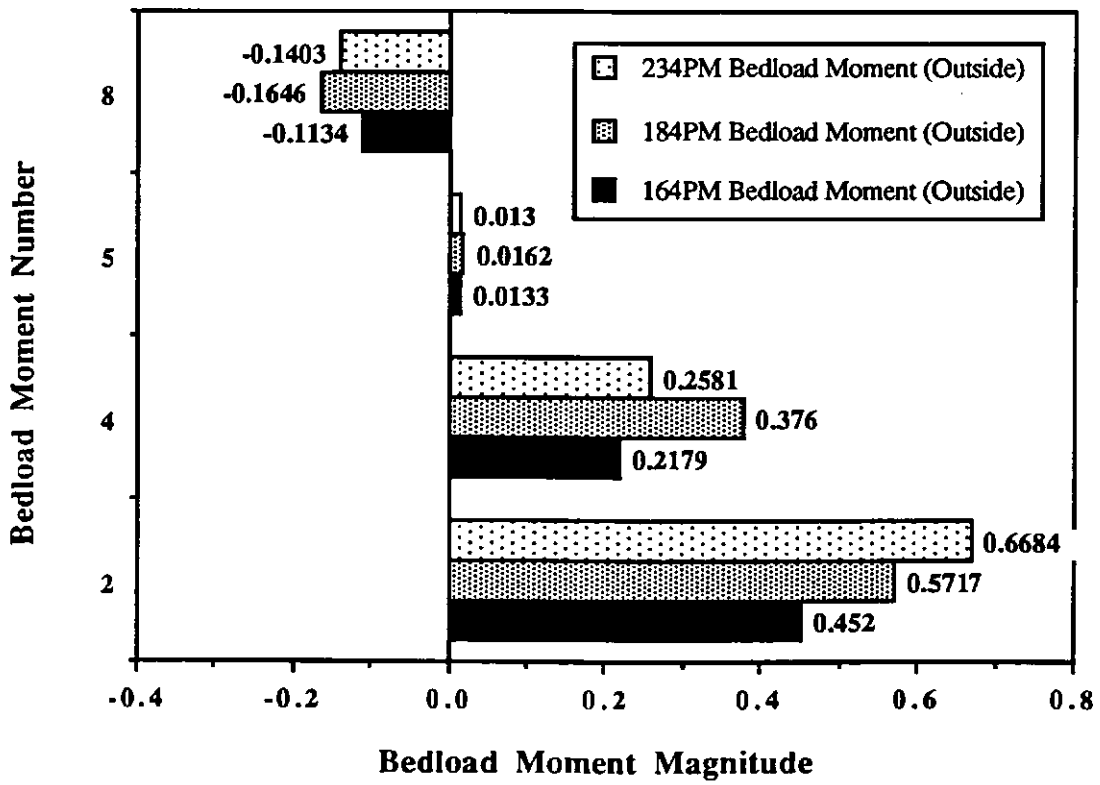

FIGURE 6.20 Dominant Bedload Terms averaged **outside** the surf zone and per tide for Tides 164PM, 184PM and 234PM.

envelope and the long wave motion and its behaviour supports the cross-correlation work which shows a large negative value occurring outside the breakpoint in the deeper water, a trend towards zero as wave breaking occurs and then positive values as the shoreline is approached (Figure 5.8(d)).

6.2.2 SUSPENDED LOAD TERM

The previous section examined the spatial distributions of nearshore velocity moments relating to cross-shore bedload sediment transport processes. Figures 6.21 to 6.23 show the variation of the total cross-shore suspended load moment with depth. This suspended load term may also be expressed in terms of short wave, long wave and mean flow contributions as before, to generate three velocity sub-terms (see 4.3.7(b)):

TERM 1 $\overline{\left(u_S^2\right)^{3/2} u_S}$ → Incident wave term.

TERM 2 $\overline{4\left(u_S^2\right)^{3/2} u_L}$ → Long wave term.

TERM 3 $\overline{3\left(u_S^2\right)^{3/2} \bar{u}}$ → Mean flow term.

Each of the three terms was, normalised by dividing by $\langle u^2 \rangle^2$, and calculated for all cross-shore current velocity records (bottom current meter on Rig A2) of the three selected tidal cycles.

(a) OBSERVATIONS

The three suspended load moments are treated in a similar fashion to the bedload terms described in the previous section (Section 6.2.1), so that Figures 6.24 to 6.26 display the spatial distribution (variation with mean depth) of Terms 1, 2 and 3. Each scatter diagram in Figures 6.24-6.26 shows the 'shape function' for the average values of each suspended load term for one run for all three tidal cycles, where one run is equivalent to one data point on the scatter graph. It should be noted that the breaker lines are approximately located at 1.88m depth for Tide 184PM and at 1.18m and 1.56m for Tide 234PM. Unfortunately owing to data logger problems during the recording of the storm, Tide 164PM contains only four runs and the breakpoint is not known for that day, though all runs were from outside the breakpoint.

FIGURE 6.21 Variation in net cross-shore suspended load term with depth for Tide 164PM.

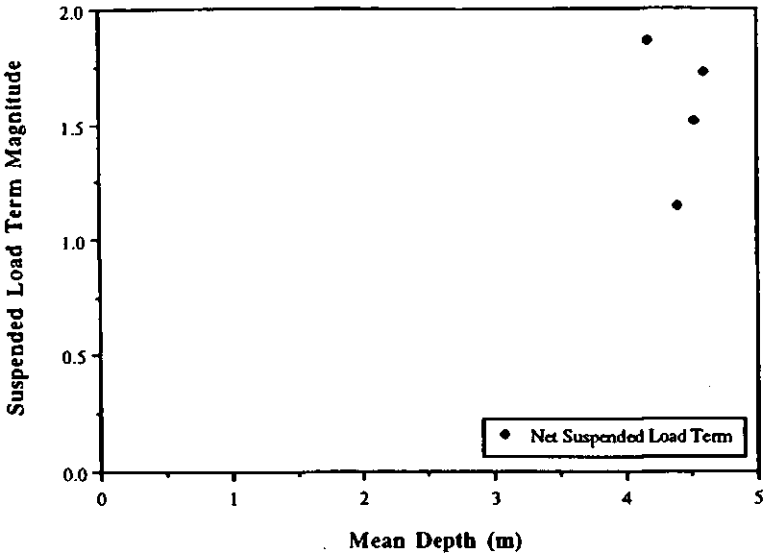

FIGURE 6.22 Variation in net cross-shore suspended load term with depth for Tide 184PM.

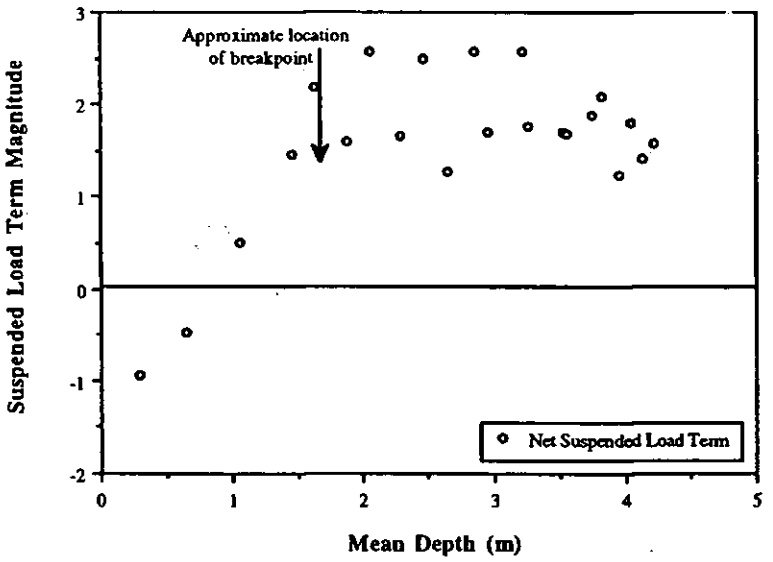

FIGURE 6.23 Variation in net cross-shore suspended load term with depth for Tide 234PM.

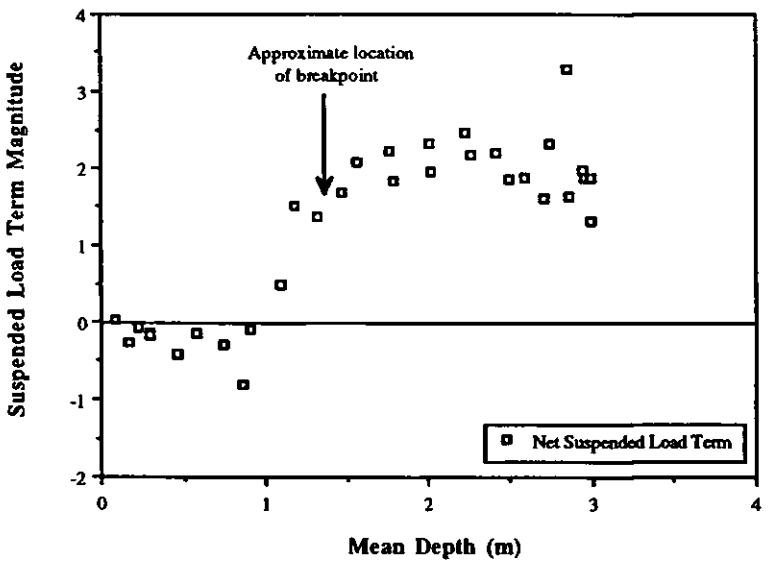

FIGURE 6.24 Variation in Suspended Load Term 1 with depth for Tides 164PM, 184PM and 234PM.

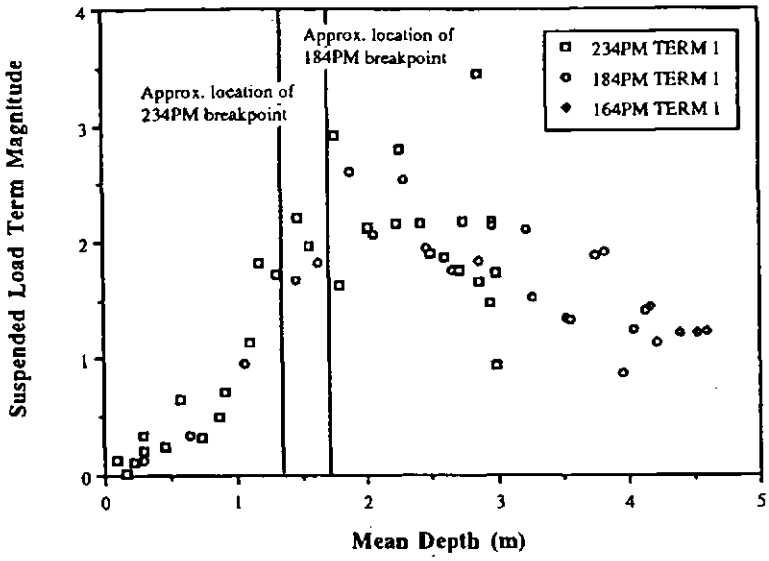

FIGURE 6.25 Variation in Suspended Load Term 2 with depth for Tides 164PM, 184PM and 234PM.

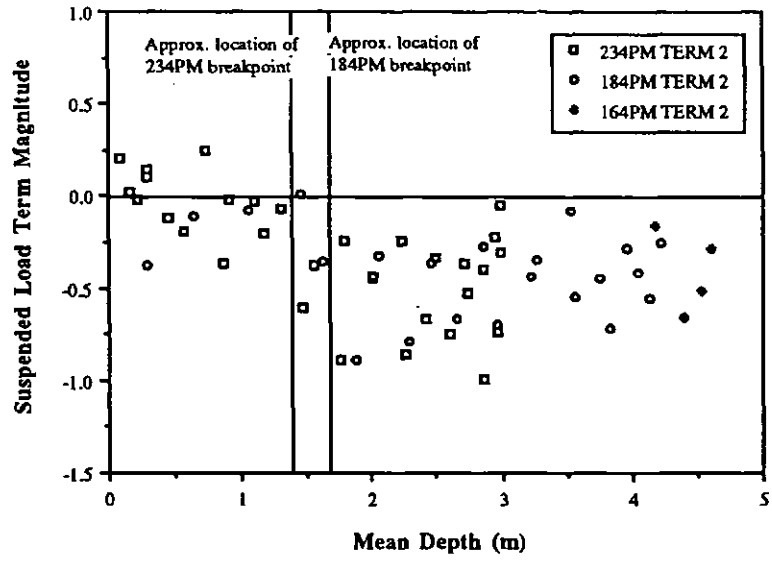

FIGURE 6.26 Variation in Suspended Load Term 3 with depth for Tides 164PM, 184PM and 234PM.

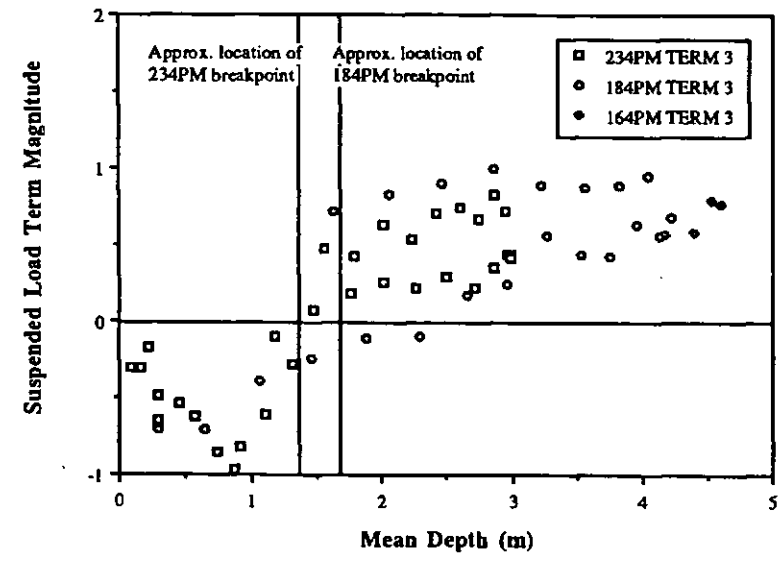

In Figure 6.24, Term 1 represents the short wave skewness (a sediment stirring parameter) multiplied by the short wave velocity, which mobilises and transports the suspended sediment. Suspended load Term 1 increases linearly from the shoreline to a maximum (+3.45 for Tide 234PM) just beyond the breaker line and then decreases slowly offshore. Suspended Load Term 1 displays very similar characteristics to Bedload Term 2, described in Section 6.2.1 with positive (or onshore) values throughout the scatter diagram.

Suspended Load Term 2, the short wave skewness which mobilises the sediment, is correlated with the long wave velocity which transports the sediment, is shown in Figure 6.25 for each of the three tidal cycles. The distribution of data in Figure 6.25 agrees closely with Bedload Term 8 which similarly relates the correlation between the short wave envelope and the long period motion in the nearshore zone. The magnitude of Term 2 increases linearly from the shoreline with increasing depth across the surf zone and values range from +0.243 (Tide 234PM) to -0.988 (Tide 234PM). The characteristics of both Suspended Load Term 2, shown here, and Bedload Term 8 (Section 6.2.1) parallel the earlier observations of wave groupiness in the nearshore. In Section 5.3 the variations which occur in the cross-correlation coefficient between the incident wave envelope and the long wave motion, measured using pressure transducer data, were discussed and the time-averaged data yields a comparable pattern.

The third suspended load velocity moment, Term 3, encompasses the interaction of the short wave skewness with a mean flow contribution. Hence, the sediment is transported by the mean flow as a result of the action of the short wave skewness stirring mechanism. Close agreement exists between this suspended load term (Figure 6.20) and the bedload velocity moment Term 4 (Figure 6.7). This is not surprising since both velocity moments relate short wave velocity and mean flow. In Figure 6.26, there is a rapid decrease in the values with increasing depth from the shoreline up to the maximum negative value at -0.960 (Tide 234PM) from here the general trend of Term 3 is to increase positively with increasing depth offshore, passing through zero at the breakpoint.

Tables 6.5-6.7 illustrate the range of values for the suspended load velocity moments (both un-normalised and normalised) for Tides 164PM, 184PM and 234PM, Terms 1-3 are contrasted with run number, run start time, mean depth, significant wave height, mean current and $\langle u^2 \rangle^2$ which is the normalising parameter for the suspended load velocity moments.

(b) CROSS-SHORE VARIATIONS

Treating the suspended load terms in a similar manner to the previous bedload velocity moments, measurements of the three terms have been averaged according to whether the measurement occurred offshore or onshore of the breakpoint. Table 6.8 records these average values against suspended load term number. In Figures 6.27-6.29 the averaged values of Terms 1-3 for measurements outside the breakpoint are shown and in Figures 6.30-6.31 measurements inside of the breakpoint are presented.

Examination of Figures 6.27-6.31, reveals a strong similarity between the different tidal conditions. The information contained within the bar charts for each of the three different tidal cycles provides some indication of the direction and relative magnitude of the various velocity moments and hence of the various processes interacting within the nearshore. Outside of the breakpoint, the largest term, Term 1, is directed onshore as is Term 3, whilst Term 2 is negative and directed offshore. Inside of the breakpoint, Term 1 continues to be directed onshore and is of similar magnitude to Term 3, while Term 3 and the less significant Term 2 are negative and directed offshore. Figures 6.32 and 6.33 provide an easier visual comparison of the averaged terms. The most noticeable feature in Figure 6.32 is the large positive (onshore) transport by wind-waves (Term 1), associated with onshore skewed flow. The interaction between the sediment mobilised by the short waves and the long wave-induced flow (Term 2) leads to an offshore transport throughout the nearshore since the flow generated by the long waves is skewed offshore. The mean flow/short wave skewness term (Term 3) comprises an offshore-directed flux within the surf zone and onshore-directed flux on the seaward side of the breakpoint, and is thus related to the position of the measurement relative to the breakpoint.

TABLE 6.5 Tide 164PM Un-normalised and Normalised Values of the Suspended Load Terms.

Run Number	Start Time	h (m)	H_s (m)	Mean Current (ms^{-1})	Time Av. $\langle u^2 \rangle^2$	**Term 1** unnorm -alised	**Term 1** normal -ised	**Term 2** unnorm -alised	**Term 2** normal -ised	**Term 3** unnorm -alised	**Term 3** normal -ised
1	19-08-	4.602	1.359	0.0369	0.0713	0.0229	1.2387	-0.0051	-0.2773	0.0142	0.7649
2	19-28-30	4.534	1.404	0.0212	0.1023	0.0324	1.2265	-0.0135	-0.5122	0.0211	0.7975
3	19-49-	4.399	1.500	0.0462	0.1267	0.0478	1.2179	-0.0257	-0.6539	0.0229	0.5837
4	20-10-	4.179	1.621	0.0277	0.1381	0.0671	1.4444	-0.0073	-0.1581	0.0266	0.5723

Where the normalised suspended load moments are : $\text{Term 1} = \dfrac{\left(u_s^2\right)^{3/2} u_s}{\left\langle u^2 \right\rangle^2}$

$$\text{Term 2} = \frac{4\left(u_s^2\right)^{3/2} u_L}{\left\langle u^2 \right\rangle^2}$$

$$\text{Term 3} = \frac{3\left(u_s^2\right)^{3/2} \bar{u}}{\left\langle u^2 \right\rangle^2}$$

TABLE 6.6 Tide 184PM Un-normalised and Normalised Values of the Suspended Load Terms.

Run Number	Start Time	h (m)	H_s (m)	Mean Current (ms^{-1})	Time Av. $\langle u^2 \rangle^2$	Term 1 unnorm -alised	Term 1 normal -ised	Term 2 unnorm -alised	Term 2 normal -ised	Term 3 unnorm -alised	Term 3 normal -ised
3	17-11-28	1.624	0.730	0.0580	0.0163	0.0298	1.8233	-0.0057	-0.3493	0.0117	0.7187
4	17-29-06	2.049	0.725	0.0657	0.0144	0.0298	2.0656	-0.0046	-0.3198	0.0119	0.8276
5	17-46-55	2.468	0.798	0.0660	0.0117	0.0229	1.9556	-0.0042	-0.3601	0.0105	0.8965
6	18-04-43	2.862	0.832	0.0615	0.0081	0.0149	1.8398	-0.0022	-0.2701	0.0081	1.0015
7	18-22-34	3.229	0.946	0.0613	0.0108	0.0227	2.1075	-0.0047	-0.4357	0.0096	0.8946
8	18-40-42	3.565	0.782	0.0586	0.0051	0.0068	1.3356	-0.0028	-0.5402	0.0045	0.8815
9	18-59-06	3.830	0.881	0.0530	0.0067	0.0129	1.9260	-0.0048	-0.7203	0.0059	0.8891
10	19-16-55	4.040	0.804	0.0513	0.0033	0.0041	1.2509	-0.0014	-0.4130	0.0031	0.9537
13	20-45-54	4.217	0.775	0.0348	0.0026	0.0030	1.1409	-0.0007	-0.2477	0.0018	0.6849
14	21-04-22	4.134	0.995	0.0392	0.0091	0.0128	1.4134	-0.0050	-0.5523	0.0051	0.5610
15	21-21-24	3.962	0.929	0.0461	0.0087	0.0076	0.8717	-0.0024	-0.2755	0.0055	0.6328
16	21-39-39	3.757	1.030	0.0312	0.0134	0.0253	1.8868	-0.0059	-0.4406	0.0058	0.4304
17	21-58-37	3.533	1.072	0.0399	0.0202	0.0271	1.3420	-0.0016	-0.0785	0.0088	0.4340
18	22-17-33	3.277	1.010	0.0466	0.0156	0.0238	1.5329	-0.0053	-0.3437	0.0088	0.5645
19	22-35-47	2.966	0.952	0.0189	0.0179	0.0382	2.1398	-0.0125	-0.6971	0.0044	0.2482
20	22-53-41	2.660	1.039	0.0166	0.0293	0.0516	1.7617	-0.0196	-0.6696	0.0051	0.1737
21	23-11-48	2.294	0.984	-0.0081	0.0281	0.0712	2.5394	-0.0220	-0.7844	-0.0028	-0.0999
22	23-30-15	1.876	0.939	-0.0099	0.0329	0.0858	2.6082	-0.0293	-0.8917	-0.0037	-0.1119
23	23-48-05	1.458	0.780	-0.0240	0.0265	0.0444	1.6745	0.0004	0.0157	-0.0064	-0.2407
24	00-05-53	1.053	0.652	-0.0464	0.0231	0.0223	0.9643	-0.0017	-0.0737	-0.0091	-0.3956
25	00-24-21	0.643	0.482	-0.1222	0.0237	0.0080	0.3367	-0.0026	-0.1109	-0.0166	-0.7018
26	00-42-17	0.296	0.335	-0.1161	0.0166	0.0022	0.1321	-0.0062	-0.3753	-0.0118	-0.7100

TABLE 6.7 Tide 234PM Un-normalised and Normalised Values of the Suspended Load Terms.

Run Number	Start Time	h (m)	H_s (m)	Mean Current (ms^{-1})	Time Av. $\langle u^2 \rangle^2$	Term 1 unnorm -alised	Term 1 normal -ised	Term 2 unnorm -alised	Term 2 normal -ised	Term 3 unnorm -alised	Term 3 normal -ised
1	07-47-37	0.167	0.227	-0.0675	0.0147	0.0002	0.0136	0.0003	0.0231	-0.0044	-0.3002
2	08-05-53	0.223	0.281	-0.0375	0.0197	0.0024	0.1216	-0.0004	-0.0211	-0.0033	-0.1672
3	08-23-49	0.295	0.291	-0.0805	0.0141	0.0030	0.2132	0.0015	0.1054	-0.0069	-0.4904
4	08-50-20	0.458	0.386	-0.0848	0.0170	0.0041	0.2413	-0.0020	-0.1185	-0.0091	-0.5355
6	09-27-12	0.737	0.525	-0.2061	0.0228	0.0118	0.3228	0.0089	0.2429	-0.0314	-0.8589
7	09-45-26	0.904	0.593	-0.1100	0.0242	0.0165	0.7223	-0.0003	-0.0123	-0.0186	-0.8142
8	10-03-53	1.094	0.660	-0.0723	0.0394	0.0274	1.1329	-0.0007	-0.0291	-0.0147	-0.6078
9	10-22-10	1.308	0.686	-0.0285	0.0225	0.0387	1.7164	-0.0015	-0.0648	-0.0064	-0.2839
10	10-41-33	1.555	0.697	0.0379	0.0169	0.0334	1.9726	-0.0063	-0.3726	0.0081	0.4784
11	10-59-44	1.785	0.703	0.0396	0.0168	0.0273	1.6292	-0.0040	-0.2397	0.0072	0.4297
12	11-17-59	2.010	0.742	0.0500	0.0147	0.0311	2.1186	-0.0066	-0.4464	0.0093	0.6335
13	11-36-14	2.228	0.764	0.0403	0.0119	0.0259	2.1683	-0.0028	-0.2373	0.0064	0.5358
14	11-54-34	2.418	0.722	0.0475	0.0088	0.0190	2.1637	-0.0059	-0.6669	0.0062	0.7061
15	12-13-09	2.597	0.663	0.0487	0.0057	0.0107	1.8648	-0.0043	-0.7452	0.0043	0.7494
16	12-31-40	2.742	0.763	0.0410	0.0090	0.0196	2.1733	-0.0047	-0.5227	0.0060	0.6653
17	12-49-51	2.856	0.669	0.0409	0.0076	0.0263	3.4522	-0.0075	-0.9876	0.0063	0.8270
18	13-08-04	2.943	0.779	0.0396	0.0043	0.0063	1.4734	-0.0010	-0.2226	0.0031	0.7250
19	13-26-19	2.987	0.756	0.0279	0.0085	0.0147	1.7378	-0.0025	-0.2977	0.0037	0.4374
20	13-45-05	2.993	0.620	0.0263	0.0031	0.0029	0.9357	-0.0001	-0.0432	0.0013	0.4195
21	14-04-09	2.955	0.787	0.0240	0.0048	0.0106	2.1867	-0.0036	-0.7406	0.0021	0.4332
22	14-23-34	2.865	0.704	0.0210	0.0065	0.0108	1.6612	-0.0025	-0.3912	0.0023	0.3538
23	14-45-15	2.706	0.770	0.0155	0.0126	0.0221	1.7562	-0.0046	-0.3662	0.0028	0.2225
24	15-08-41	2.497	0.812	0.0230	0.0164	0.0312	1.8993	-0.0055	-0.3355	0.0048	0.2922
25	15-28-25	2.265	0.763	0.0145	0.0157	0.0439	2.8028	-0.0135	-0.8635	0.0035	0.2235
26	15-47-05	2.012	0.736	0.0214	0.0189	0.0401	2.1249	-0.0081	-0.4301	0.0049	0.2596
27	16-05-31	1.756	0.728	0.0128	0.0140	0.0408	2.9178	-0.0125	-0.8922	0.0026	0.1859
28	16-23-46	1.470	0.695	0.0060	0.0154	0.0340	2.2041	-0.0093	-0.6056	0.0012	0.0778
29	16-42-18	1.177	0.668	-0.0080	0.0156	0.0285	1.8257	-0.0031	-0.2006	-0.0016	-0.1025
30	17-01-30	0.858	0.597	-0.1386	0.0177	0.0090	0.5084	-0.0064	-0.3610	-0.0170	-0.9603
31	17-19-58	0.574	0.336	-0.0647	0.0093	0.0061	0.6575	-0.0017	-0.1846	-0.0058	-0.6252
32	17-38-50	0.290	0.386	-0.0807	0.0073	0.0025	0.3442	0.0011	0.1494	-0.0047	-0.6471
33	17-57-43	0.085	0.084	-0.0390	0.0076	0.0010	0.1322	0.0016	0.2081	-0.0023	-0.3040

TABLE 6.8 Average Values of Suspended Load Term Observations for Tides 164PM, 184PM and 234PM.

Suspended Load Term Number	TIDE 164PM Average of Runs Offshore of the Breakpoint.	TIDE 184PM Average of Runs Offshore of the Breakpoint.	TIDE 184PM Average of Runs Onshore of the Breakpoint.	TIDE 234PM Average of Runs Offshore of the Breakpoint.	TIDE 234PM Average of Runs Onshore of the Breakpoint.
1	1.2819	1.7523	0.7769	2.0534	0.5105
2	-0.4004	-0.4661	-0.1361	-0.4804	-0.0052
3	0.6796	0.5878	-0.5121	0.4277	-0.5496

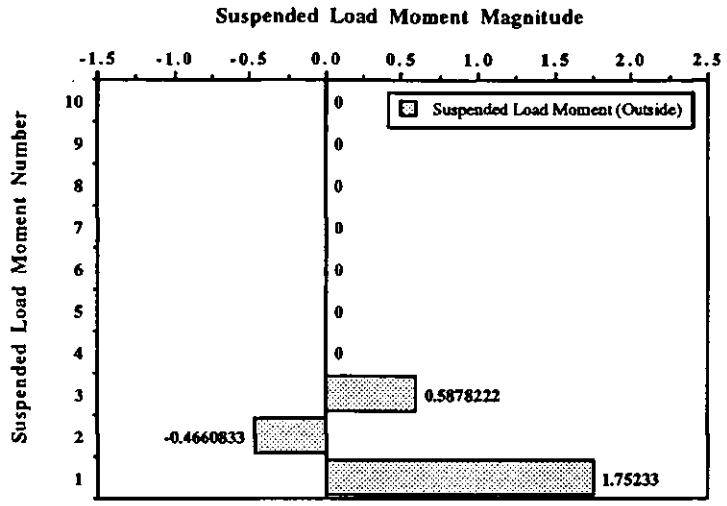

FIGURE 6.27 Tide-averaged Suspended Load Terms 1-3 for measurements made **outside** the surf zone during Tide 164PM.

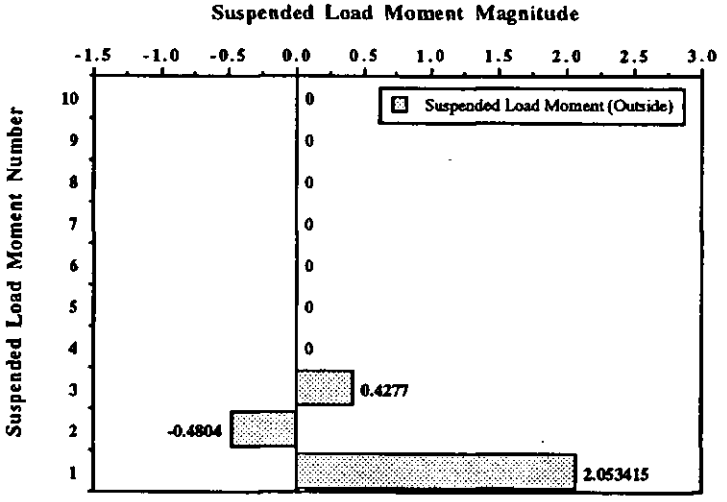

FIGURE 6.28 Tide-averaged Suspended Load Terms 1-3 for measurements made **outside** the surf zone during Tide 184PM.

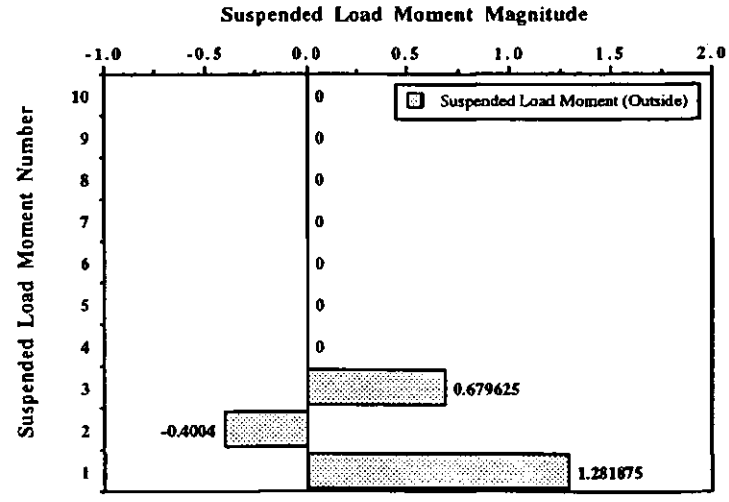

FIGURE 6.29 Tide-averaged Suspended Load Terms 1-3 for measurements made **outside** the surf zone during Tide 234PM.

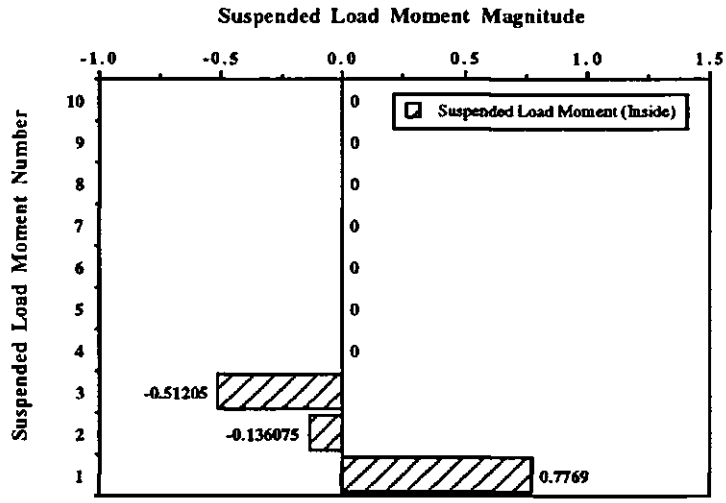

FIGURE 6.30 Tide-averaged Suspended Load Terms 1-3 for measurements made **inside** the surf zone during Tide 184PM.

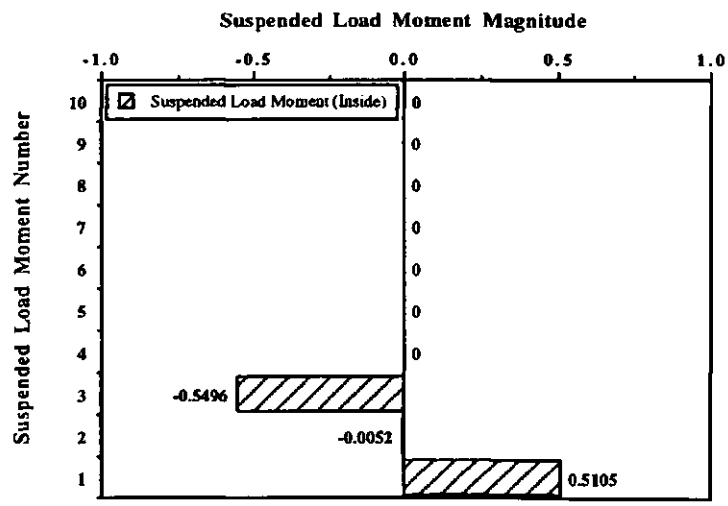

FIGURE 6.31 Tide-averaged Suspended Load Terms 1-3 for measurements made **inside** the surf zone during Tide 234PM.

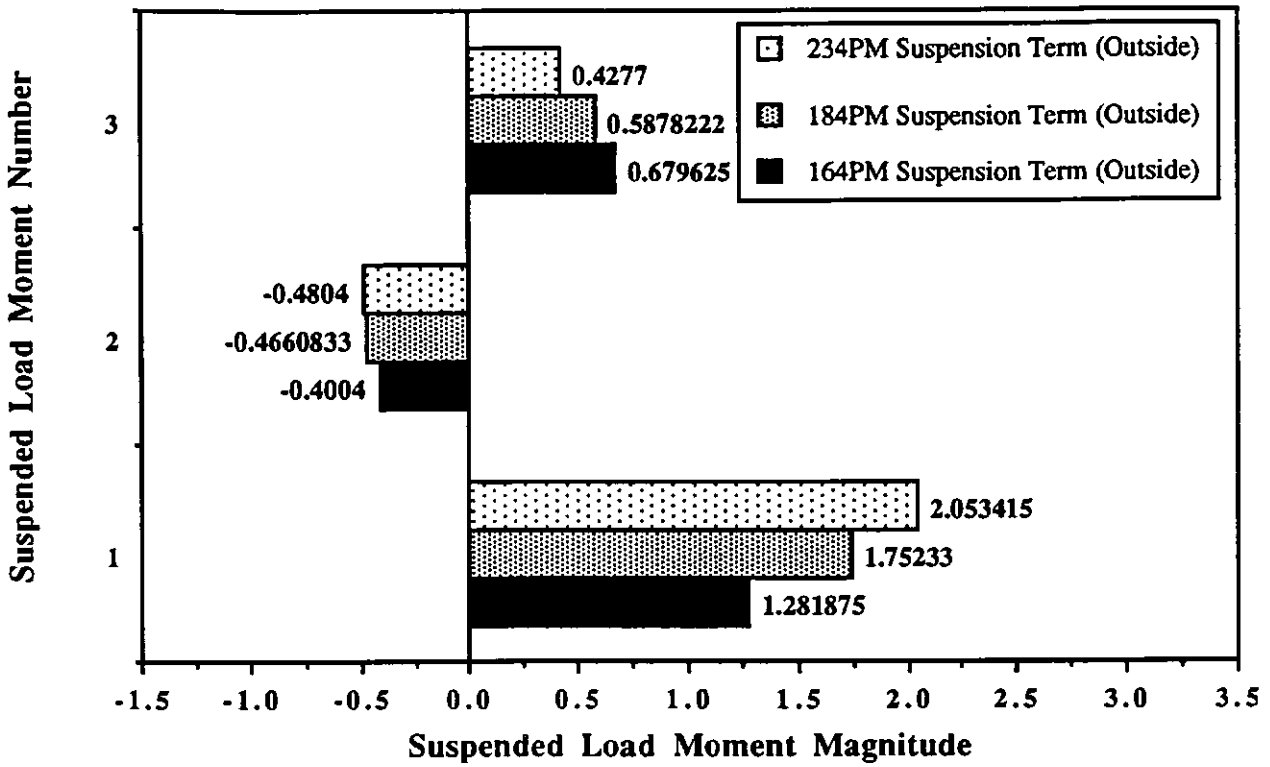

FIGURE 6.32 Suspended Load Terms averaged **outside** the surf zone and per tide for Tides 164PM, 184PM and 234PM.

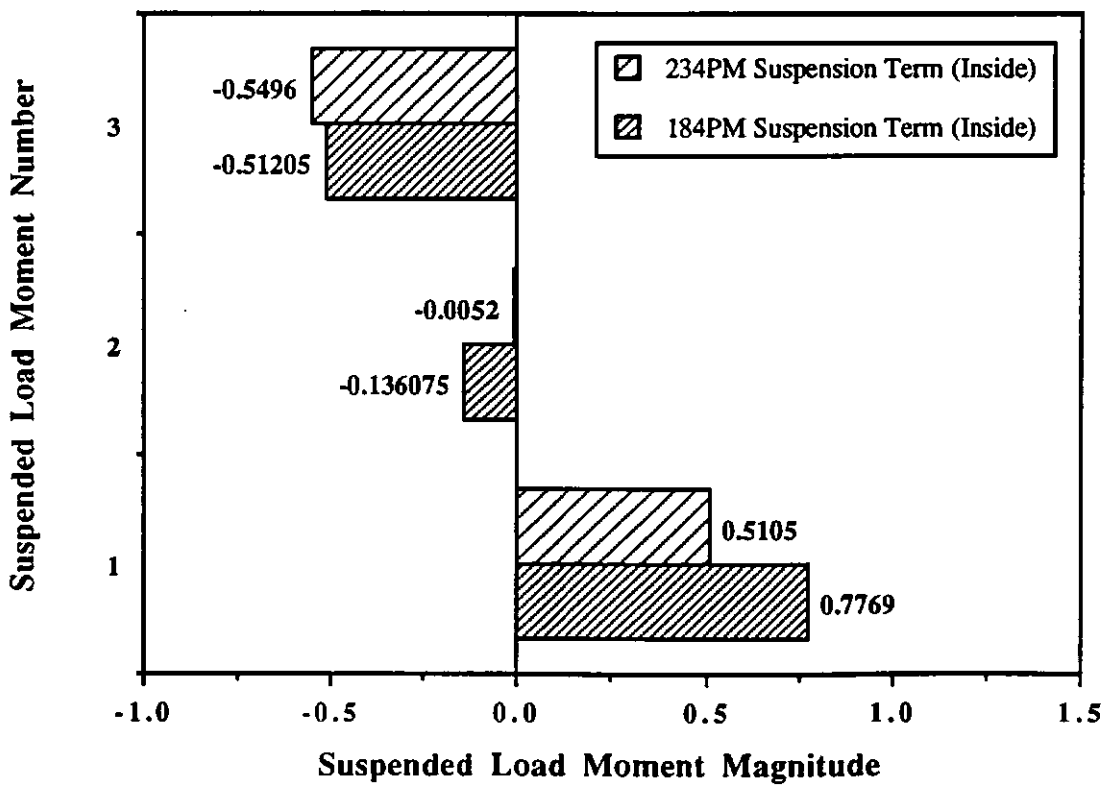

FIGURE 6.33 Suspended Load Terms averaged **inside** the surf zone and per tide for Tides 164PM, 184PM and 234PM.

6.3 DISCUSSION

Near-bed sediment transport is assumed to respond to the near-bed water velocity in an instantaneous manner. Examination of the magnitudes and distributions of moments of the velocity field across the nearshore should, therefore, be a reasonable indication of relative importance of the various velocity-driven sediment transport processes.

Guza and Thornton (1985a) established that the bedload and suspended load transports are each dominated by certain velocity moments. The field observations examined in this study show that both the bedload and suspended load moments are characterised by consistent patterns. As functions of mean water depth they are surprisingly insensitive to the different wave conditions for the three tidal cycles examined. The similarity of the normalised values of the moments suggest that the normalisation results in values which are relatively insensitive to wave height variations. There is also some evidence that the scaling with mean water depth is more appropriate than the more intuitive scaling with the ratio of depth to breaking wave depth (*e.g.* Roelvink and Stive, 1989). For example, examine the breakpoint depth for Tide 184PM, and the somewhat different breakpoint depths on flood and ebb tides for Tide 234PM, despite the obvious difference between tidal cycles there is no clear evidence that the respective moment values are displaced relative to each other by these differences. The constant similarity, or pattern, which is evident in the various velocity moments for the different tidal cycles on this beach suggest that some quasi-universal 'shape functions' exist for sand transport predictors.

The velocity moments examined here have been decomposed, in order to demonstrate the relative contributions made by the mean flow and high and low frequency wave components. The schematic diagram in Figure 6.34 illustrates the most important of the terms which constitute the 'bedload' or skewness-type moment. The 'suspended load' terms are similarly depicted as run-averaged, tide-averaged and spatially-averaged (depending upon position either side of the wave breaking region) quantities and summarised in Figure 6.35. The moment which dominates the suspended load transport part of the cross-shore transport equation comprises the three sub-moments, Terms 1, 2 and 3, which are equivalent to the previous bedload terms

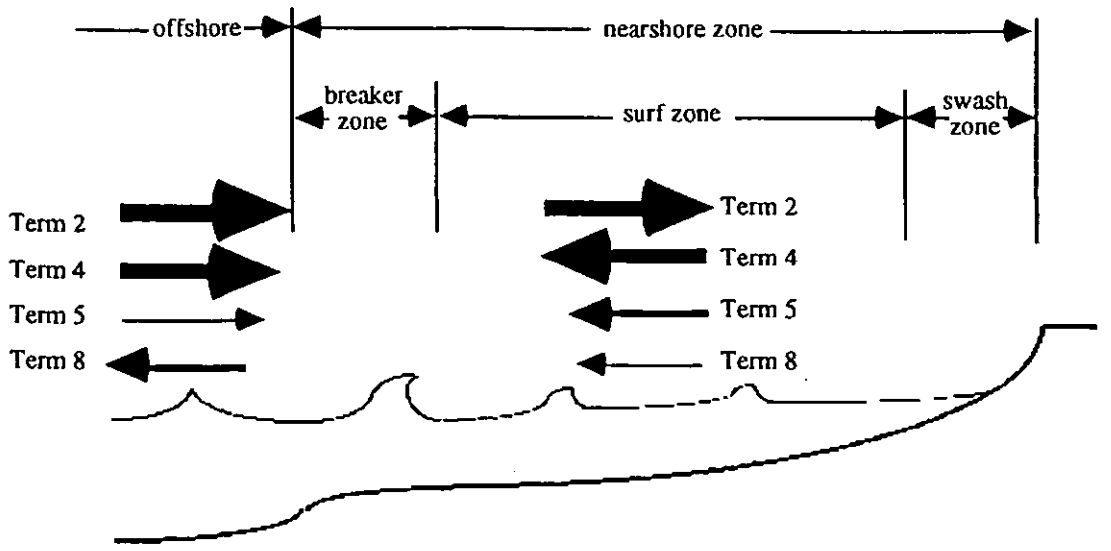

Where the dominant normalised bedload moments are :

$$\text{Term 2} = \frac{\overline{u_s^3}}{(u^2)^{3/2}}$$

$$\text{Term 4} = \frac{\overline{3\bar{u}u_s^2}}{(u^2)^{3/2}}$$

$$\text{Term 5} = \frac{\overline{3\bar{u}u_L^2}}{(u^2)^{3/2}}$$

$$\text{Term 8} = \frac{\overline{3u_s^2 u_L}}{(u^2)^{3/2}}$$

Figure 6.34 Schematic diagram showing magnitude and direction of the bedload moments across the nearshore region.

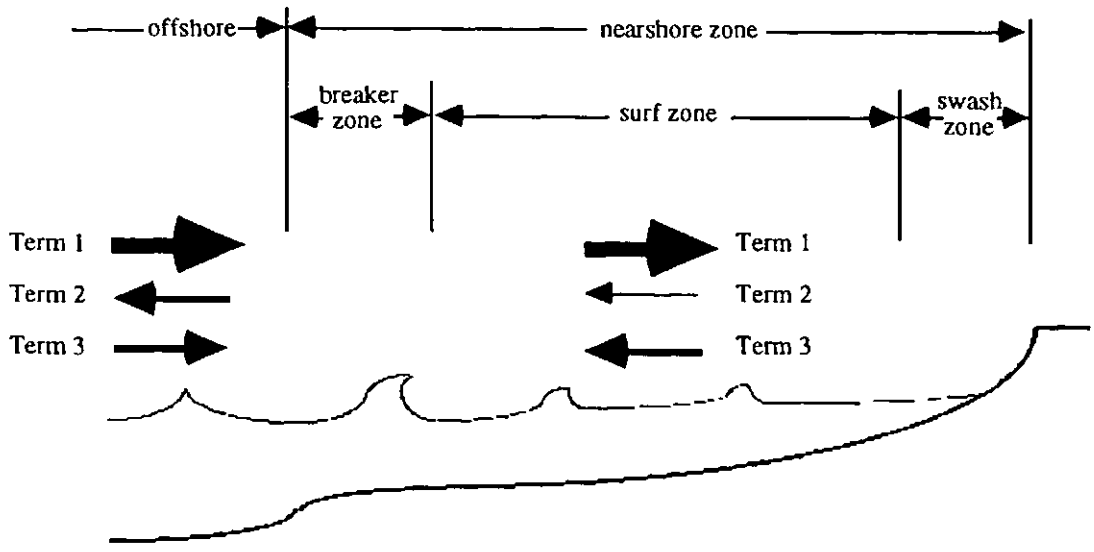

Where the normalised suspended load moments are :

$$\text{Term 1} = \frac{\left(u_s^2\right)^{3/2} u_s}{\left\langle u^2 \right\rangle^2}$$

$$\text{Term 2} = \frac{4\left(u_s^2\right)^{3/2} u_L}{\left\langle u^2 \right\rangle^2}$$

$$\text{Term 3} = \frac{3\left(u_s^2\right)^{3/2} \bar{u}}{\left\langle u^2 \right\rangle^2}$$

Figure 6.35 Schematic diagram showing magnitude and direction of the suspended load moments across the nearshore region.

thus : Suspended Load Term 1 ≈ Bedload Term 2

Suspended Load Term 2 ≈ Bedload Term 8

Suspended Load Term 3 ≈ Bedload Terms 4 and 5

The short wave term matches the skewness term, the long wave term reflects the same characteristics as the correlation term, and the mean flow term shows the same patterns. Although the suspended load-related parameters are a power higher than the previous bedload terms, the results show remarkably similar patterns. Only the bedload-related velocity moments are named in the following discussion, but according to the relationship between the bedload and suspended load-related terms described above, the discussion is intended to encompass the characteristics of both.

The largest bedload moment, Term 2, describes the skewness of the short incident waves. This reaches a maximum just seaward of wave breaking as the waves are shoaling. Osborne (1990) examined both barred and non-barred beach morphodynamics. In the non-barred example, the greatest potential for onshore transport was considered to be where the oscillatory transport component is largest as a result of skewness in the shoaling waves, just seaward of the breakpoint. Osborne *et al.* (1990) also suggested that the total oscillatory transport to be dominated by the gravity wave band and is usually in the direction of wave propagation. The present velocity moment study provides quantitative confirmation of Osborne's suggestions.

Bedload Terms 4 and 5, describing the interaction of the mean flow with the incident waves and long waves, respectively, show the expected variation based on the mean flow in the nearshore. Offshore flow occurs inside the surf zone, and onshore flow occurs outside the surf zone in deeper water. The influence of the long wave as a stirring agent is only significant in the shallower water, where the mean flow is offshore.

The opposing weaker offshore transport of sediment by the infragravity waves, evident in Figure 6.34, is influenced by the skewed flow associated with the bound long wave, forced by incident wave groupiness across the nearshore region (Longuet-Higgins and Stewart, 1962). However, it is interesting to examine Bedload Term 8 more closely. In Figure 6.11, the velocity moment data is displayed for each run and,

whilst it is certainly true to say that Term 8 is predominantly negative and, therefore, offshore; in the shallower water depths near to the shoreline Term 8 is slightly positive. Other work has indicated the possibility that low frequency motions may also induce onshore transport of sediment, in a barred beach environment (*e.g.* Greenwood *et al.*, 1990; Beach and Sternberg, 1991; O'Hare and Huntley, 1994). Term 8 describes the correlation between the incident wave envelope and the long wave motion.

The nature of Bedload Term 8 velocity moment, is consistent with the suggestion of Larsen (1982) and Shi and Larsen (1984) that long waves, forced by groupiness in the incoming short waves, generate a reverse or offshore transport of sediment. This transport arises because the offshore flow, induced by the bound long wave coincides with the largest waves of the group and hence, high suspended sediment concentrations. In breaking, the energy of the wind waves is dissipated and the ability of the incident waves to produce onshore transport becomes less important across the surf zone (Osborne *et al.*, 1990). Meanwhile, at the breakpoint the incident wave group structure breaks down and the short wave amplitude becomes modulated by the depth variations induced by the 'forced' long wave. This low frequency wave may induce a greater oscillatory sediment transport than that caused by either the shoaling or breaking incident waves (Osborne and Greenwood, 1992a).

The behaviour of the mean flow tends to vary according to position relative to the breakpoint and whether the waves are shoaling or breaking. The mean near-bed cross-shore flow velocities at the height of the bottom current meter (0.106m) on Rig A2 are directed offshore within the surf zone and weakly onshore outside the surf zone. Bedload Terms 4 and 5 have similar characteristics. Whilst Term 4 couples the incident wave stirring parameter with a mean flow transporting agent, Term 5 links the infragravity wave mobilising and stirring of sediment with movement by a mean near-bed flow. Convergence of Terms 4 and 5 is noticeable in Figures 6.7 and 6.8 and in Figure 6.34. Within the surf zone Terms 4 and 5 are directed offshore in association with the undertow and conversely, they are directed onshore outside the surf zone. The variations in the mean flow term indicate the convergence of the mean near-bed flows in the breaker zone, and the possible formation of a breakpoint bar (Davidson *et al.*,

1993). Whether or not a bar actually forms, and where it forms, depends upon the spatial variation of the various hydrodynamic processes examined in this study. In turn the interaction of a breakpoint bar may also affect the nature of the flows in the nearshore environment. It would be interesting to consider this 'feedback' process in future work.

The back-and-forth sweep of the surf zone over the Spurn Head beach profile will considerably modify the surf- and swash-zone gradients, the breaking wave climate and the reflectivity properties of the profile. If the various shape functions were similarly swept back-and-forth over the beach profile a number of distinct regions may arise in which, a range of sediment transport conditions will result (Foote *et al.*, 1993).

The suggestion of consistent 'shape functions' for sand transport predictions has lead to the development of a model, as yet schematic, for the development of macro-tidal beach profiles (O'Hare, pers. comm.; Foote *et al.*, 1994). Advection of a simple transport shape function by the tidal excursion has been shown to lead to a beach profile similar to the characteristic macro-tidal beach profile. Of course this simple advection of a constant transport shape function is unlikely to explain all the features which are found macro-tidal beaches. Naturally, a full model will need to include the influence of changing effective beach profile, non-equilibrium bed forms, the interactions between wave-induced and tidal mean flows and perhaps the asymmetry in the behaviour of ground water run-off on the beach.

6.4 SUMMARY

An indication of the dominant hydrodynamic processes and interactions across the nearshore is provided by the examination of the relative distribution and magnitude of the various velocity moments. The results may be summarised as follows:

Outside the surf zone The skewness of the oscillatory incident component, the correlation between incident wave stirring and a mean flow transporting parameter, and the coupling between the infragravity stirring agent and a net current moving agent, are

dominant and are directed onshore. The coupling of the incident wave envelope with infragravity motion is smaller in magnitude and directed offshore.

Inside the surf zone The correlation between incident wave energy and the mean flow, the coupling of infragravity wave energy and the mean flow, and the correlation between the short wave envelope and long wave motion are dominant and directed offshore. The skewness of the incident waves is dominant in the onshore direction. The following chapter compares the suspended sediment concentration measurements and cross-shore flux data with velocity moments and net sand transport rates. The relative contribution of the mean flow, long wave and short wave components will also be examined.

CHAPTER 7
CROSS-SHORE SUSPENDED SEDIMENT TRANSPORT RATES

7.1 INTRODUCTION

Prediction of cross-shore sediment transport rates requires that the quantity of sand suspended under a variety of wave and bottom-current conditions be known. This chapter describes the examination of suspended sediment concentration data, in conjunction with current velocity data measured during three days of the Spurn Head field deployment. The purpose of this research is to investigate the cross-shore fluxes of sediment which arise through a range of wave and current interactions and to compare the relative importance of mean flow, short waves and long waves with the 'energetics' predictions of the previous chapter.

7.2 CROSS-SHORE FLUX ANALYSIS

Following the work by Jaffe *et al.* (1984) the net cross-shore suspended sediment transport rate was examined in this study. The flux terms were calculated using suspended sediment concentration and cross-shore current velocity measurements from the bottom OBS sensor and EMCM on Rig A2 (≈0.10m above the seabed). The net sediment transport rate was decomposed (Section 4.3.8) to incorporate contributions from the mean flow, long wave and short wave components, generating nine flux terms.

These un - normalised flux terms are :

$$\text{TERM 1} = \overline{u_L c_L}$$

$$\text{TERM 2} = \overline{u_S c_S}$$

$$\text{TERM 3} = \overline{u}\,\overline{c}$$

$$\left.\begin{aligned}
\text{TERM 4} &= \overline{u_S c_L} \\
\text{TERM 5} &= \overline{u_L c_S} \\
\text{TERM 6} &= \overline{\bar{u} c_L} \\
\text{TERM 7} &= \overline{\bar{u} c_S} \\
\text{TERM 8} &= \overline{u_L \bar{c}} \\
\text{TERM 9} &= \overline{u_S \bar{c}}
\end{aligned}\right\} \approx 0$$

The values of Terms 6-9 will be zero since, in these four functions, a constant (the mean) is multiplied by zero (the time-average of the fluctuations is, by definition, zero). The values of Terms 4 and 5 will also be zero because the product of two fluctuations at different frequencies will average to zero. Conversely, the remaining cross-shore flux terms or functions (Terms 1-3) should assume non-zero values. (Note that the values of Terms 4-9 have, however, been retained in the following discussion in order to provide some indication of how accurate the time-averaging process is for this data-set.

Tables 7.1-7.3 display the run-averaged values of these nine cross-shore flux terms. In addition, the run number and start time, mean water depth, significant wave height and total cross-shore transport values are included in Tables 7.1-7.3 for Tides 164PM, 184PM and 234PM, respectively.

Table 7.4, on the other hand, provides spatially-averaged values of the previous run-averaged cross-shore flux term measurements according to location inside or outside the surf zone. Three cross-shore flux terms can be seen to dominate the measurements : $c_L u_L$, $c_S u_S$ and $\bar{c}\bar{u}$. As expected, the remainder of these cross-shore flux shape functions (*i.e.* Terms 4-9) generate values which tend towards zero for each of the three selected tidal cycles.

Coupling between the long period motion and the sediment response at the infragravity band frequency is described by Term 1 ($c_L u_L$). Conversely, Term 2 ($c_S u_S$)

TABLE 7.1 Tide 164PM Un-normalised Values of the Cross-Shore Flux Terms.

Run Number	Start Time	h (m)	H_s (m)	Total Transport ($kg/m^2/s$	Term 1	Term 2	Term 3	Term 4	Term 5	Term 6	Term 7	Term 8	Term 9
1	19-08-	4.602	1.359	0.5356	-0.0130	-0.1056	0.6560	0.0014	0.0003	$2x10^{-5}$	$-2x10^{-8}$	0.0054	$-2x10^{-6}$
2	19-28-30	4.534	1.404	-0.2075	-0.0328	-0.3024	0.1410	-0.0017	-0.0016	$-1x10^{-5}$	$4x10^{-8}$	-0.0030	$-2x10^{-6}$
3	19-49-	4.399	1.500	-0.3997	-0.1314	-0.6010	0.3252	-0.0051	-0.0014	$-5x10^{-5}$	$-1x10^{-9}$	-0.0014	$-1x10^{-6}$
4	20-10-	4.179	1.621	-0.5094	-0.0595	-0.6255	0.2047	-0.0218	-0.0029	$-7x10^{-5}$	$-1x10^{-7}$	-0.0010	$2x10^{-6}$

Where the unnormalised flux terms are :

Term 1 = $\overline{u_L c_L}$

Term 2 = $\overline{u_S c_S}$

Term 3 = $\bar{u}\,\bar{c}$

Term 4 = $\overline{u_S c_L}$

Term 5 = $\overline{u_L c_S}$

Term 6 = $\overline{\bar{u} c_L}$

Term 7 = $\overline{\bar{u} c_S}$

Term 8 = $\overline{u_L \bar{c}}$

Term 9 = $\overline{u_S \bar{c}}$

TABLE 7.2 Tide 184PM Un-normalised Values of the Cross-Shore Flux Terms.

Run Number	Start Time	h (m)	H_S (m)	Total Transport ($kg/m^2/s$)	Term 1	Term 2	Term 3	Term 4	Term 5	Term 6	Term 7	Term 8	Term 9
3	17-46-55	1.624	0.845	0.0170	-0.0616	-0.0770	0.1570	0.0022	-0.0011	0.0073	-0.0005	-9×10^{-5}	0.0026
4	18-04-43	2.049	0.878	0.1217	-0.0235	0.0094	0.1444	-0.0021	-5×10^{-5}	-0.0059	5×10^{-5}	3×10^{-5}	-0.0023
5	18-22-34	2.468	0.889	0.1727	-0.0134	0.0220	0.1556	-0.0002	-0.0002	0.0023	-8×10^{-5}	-0.0003	-0.0011
6	18-40-42	2.862	0.876	0.1012	-0.0136	0.0182	0.0909	-0.0022	-0.0003	0.0031	0.0003	-0.0003	-0.0011
7	18-59-06	3.230	0.960	0.1000	-0.0162	-0.0252	0.1171	0.0005	0.0007	0.0029	-8×10^{-5}	0.0004	-0.0005
8	19-16-55	3.565	0.837	0.2084	-0.0070	0.1220	0.0852	-2×10^{-6}	-9×10^{-5}	-0.0013	-2×10^{-5}	-9×10^{-5}	0.0013
9	19-34-55	3.830	0.908	0.2276	-0.0101	0.1430	0.0940	0.0007	0.0004	0.0011	0.0002	0.0003	-3×10^{-5}
10	19-53-06	4.040	0.783	0.0916	-0.0017	0.0232	0.0723	-0.0002	-0.0001	-0.0013	-3×10^{-5}	-0.0003	0.0007
11	20-10-59	4.161	0.811	0.0958	-0.0028	0.0183	0.0753	0.0001	-0.0002	0.0034	-5×10^{-5}	0.0001	-0.0042
13	20-45-54	4.217	0.726	0.1813	0.0005	0.0579	0.1123	0.0010	5×10^{-5}	-0.0036	-0.0002	-0.0008	-0.0042
14	21-04-22	4.134	0.964	0.2098	-0.0095	-0.0134	0.1981	0.0006	0.0001	-0.0191	1×10^{-5}	-3×10^{-5}	0.0023
15	21-21-24	3.962	0.927	0.1302	-0.0217	-0.0862	0.1978	-0.0008	-0.0002	0.0039	-8×10^{-5}	-0.0012	0.0031
16	21-39-39	3.757	1.045	0.0189	-0.0276	-0.0947	0.1257	0.0080	-0.0003	-0.0037	-0.0002	-0.0004	0.0068
17	21-58-37	3.533	1.086	-0.3594	-0.0634	-0.5094	0.1976	0.0050	-0.0013	0.0010	-0.0002	-0.0002	0.0016
18	22-17-33	3.277	1.028	-0.4833	-0.0205	-0.7255	0.1453	-0.0042	0.0005	-0.0033	-0.0004	-0.0003	-0.0021
19	22-35-47	2.966	0.983	-0.4310	-0.1311	-0.4260	0.1425	0.0015	-0.0006	-0.0035	-8×10^{-5}	-0.0014	0.0030
21	22-11-48	2.295	1.067	-1.0395	-0.1781	-0.8318	-0.0712	-0.0058	-0.0061	0.0002	-0.0001	0.0008	-0.0072
22	23-30-15	1.876	1.022	-0.9461	-0.3133	-0.6491	-0.0668	-0.0130	-0.0117	-0.0042	0.0001	0.0012	0.0084
23	23-48-05	1.458	0.915	-0.5290	-0.0715	-0.3236	-0.1254	-0.0062	-0.0055	-0.0019	-0.0002	0.0001	-0.0097
24	00-05-53	1.053	0.828	-0.5881	-0.1175	-0.1880	-0.1929	-0.0011	-0.0021	0.0081	4×10^{-5}	-0.0003	-0.0007
25	00-24-21	0.643	0.666	-0.4524	-0.0160	-0.0527	-0.3968	-0.0006	3×10^{-5}	0.0031	0.0008	6×10^{-5}	-0.0013
26	00-42-17	0.296	0.544	-0.7549	-0.0789	-0.2458	-0.4903	-0.0043	-0.0026	0.0221	-0.0002	0.0003	-0.0011

TABLE 7.3 Tide 234PM Un-normalised Values of the Cross-Shore Flux Terms.

Run Number	Start Time	h (m)	H_s (m)	Total Transport ($kg/m^2/s$)	Term 1	Term 2	Term 3	Term 4	Term 5	Term 6	Term 7	Term 8	Term 9
1	07-47-37	0.167	0.227	-0.0447	-0.0026	0.0494	-0.0936	-0.0017	-0.0010	0.0003	0.0002	0.0082	-0.0004
2	08-05-53	0.223	0.281	-0.0232	0.0211	0.0477	-0.0495	-0.0120	0.0026	-0.0009	$-3x10^{-5}$	0.0034	-0.0017
3	08-23-49	0.295	0.291	-0.0361	0.0074	0.0623	-0.0807	0.0002	0.0006	0.0025	$-4x10^{-5}$	0.0008	-0.0002
4	08-50-20	0.458	0.386	-0.1421	-0.0130	-0.0216	-0.1412	-0.0017	-0.0013	0.0645	-0.0002	-0.0017	0.0006
7	09-45-26	0.904	0.593	-0.1238	-0.0054	0.0450	-0.1882	$8x10^{-5}$	0.0006	0.0044	0.0003	-0.0008	-0.0012
8	10-03-53	1.094	0.660	-0.1036	-0.0217	0.0267	-0.1210	0.0005	-0.0005	-0.0003	$-5x10^{-5}$	0.0028	-0.0001
9	10-22-10	1.308	0.686	-0.0971	-0.0432	0.0198	-0.0417	0.0005	-0.0004	0.0004	$4x10^{-5}$	-0.0089	0.0001
10	10-41-33	1.555	0.697	0.0548	-0.0105	-0.0054	0.0657	$-2x10^{-5}$	$6x10^{-5}$	0.0020	$6x10^{-5}$	-0.0049	-0.0016
11	10-59-44	1.785	0.703	0.0634	-0.0131	0.0008	0.0926	$-1x10^{-5}$	-0.0002	0.0019	$1x10^{-5}$	0.0122	0.0004
12	11-17-59	2.010	0.742	0.1135	0.0007	0.0542	0.0669	-0.0001	-0.0002	-0.0013	$-8x10^{-5}$	0.0023	-0.0014
13	11-36-14	2.228	0.764	0.0775	-0.0038	0.0459	0.0493	-0.0006	0.0002	-0.0022	$6x10^{-6}$	0.0070	-0.0006
14	11-54-34	2.418	0.722	0.0732	-0.0063	0.0318	0.0473	-0.0002	0.0002	0.0006	0.0001	0.0001	0.0007
15	12-13-09	2.597	0.663	0.0773	-0.0020	0.0433	0.0412	0.0003	$-6x10^{-5}$	-0.0014	$8x10^{-5}$	0.0001	0.0008
16	12-31-40	2.742	0.763	0.0591	-0.0066	0.0193	0.0433	0.0001	$8x10^{-5}$	0.0013	$-1x10^{-5}$	-0.0002	-0.0001
17	12-49-51	2.856	0.669	0.0058	-0.0141	-0.0538	0.0568	0.0000	$-8x10^{-5}$	0.0019	$-7x10^{-6}$	-0.0017	-0.0004
18	13-08-04	2.943	0.779	0.0668	-0.0016	0.0210	0.0446	0.0004	$9x10^{-5}$	0.0007	$-2x10^{-5}$	-0.0012	-0.0003
19	13-26-19	2.987	0.756	0.0118	-0.0140	-0.0387	0.0645	0.0009	-0.0002	$9x10^{-5}$	$-4x10^{-5}$	0.0047	0.0008
20	13-45-05	2.993	0.620	0.1008	-0.0016	0.0323	0.0836	0.0003	$9x10^{-5}$	-0.0017	$-4x10^{-5}$	0.0042	-0.0031
21	14-04-09	2.955	0.787	0.0585	-0.0205	-0.0135	0.0908	-0.0003	-0.0001	0.0056	$-2x10^{-5}$	-0.0054	0.0009
22	14-23-34	2.865	0.704	0.0710	-0.0046	0.0143	0.0568	0.0013	-0.0002	0.0034	$-2x10^{-5}$	0.0029	-0.0001
24	15-08-41	2.497	0.812	-0.1738	-0.0150	-0.1430	0.0349	0.0004	0.0002	-0.0022	$1x10^{-5}$	-0.0029	-0.0006
25	15-28-25	2.265	0.763	-0.2602	-0.0581	-0.2843	0.0320	-0.0008	$-9x10^{-5}$	0.0033	$9x10^{-6}$	-0.0055	0.0008
26	15-47-05	2.012	0.736	-0.1605	-0.0278	-0.1426	0.0478	-0.0011	-0.0012	-0.0015	$-2x10^{-6}$	0.0032	$-9x10^{-5}$
27	16-05-31	1.756	0.728	-0.1957	-0.0532	-0.2018	0.0395	-0.0012	-0.0003	0.0009	$2x10^{-6}$	0.0033	-0.0002
28	16-23-46	1.470	0.695	-0.3087	-0.0600	-0.2648	0.0221	0.0011	-0.0009	$-5x10^{-5}$	$-8x10^{-5}$	-0.0074	0.0011
29	16-42-18	1.177	0.668	-0.2355	-0.0545	-0.1625	-0.0164	$-7x10^{-5}$	-0.0003	-0.0005	$2x10^{-5}$	0.0030	$6x10^{-5}$
30	17-01-30	0.858	0.597	-0.3388	-0.0534	-0.0444	-0.2343	-0.0006	-0.0005	0.0004	-0.0001	-0.0249	0.0007
31	17-19-58	0.574	0.336	-0.0005	0.0144	0.0527	-0.0665	$8x10^{-5}$	0.0003	0.0014	0.0001	-0.0009	0.0001
32	17-38-50	0.290	0.386	-0.0317	0.0205	0.0572	-0.1067	0.0004	0.0008	0.0011	$-8x10^{-5}$	0.0017	0.0002
33	17-57-43	0.085	0.084	0.0364	0.0243	0.0791	-0.0612	0.0022	0.0020	$-7x10^{-5}$	$6x10^{-6}$	0.0185	0.0002

TABLE 7.4 Average Values of Cross-Shore Flux Term Observations for Tides 164PM, 184PM and 234PM.

Suspended Load Term Number	TIDE 164PM Average of Runs Offshore of the Breakpoint.	TIDE 184PM Average of Runs Offshore of the Breakpoint.	TIDE 184PM Average of Runs Onshore of the Breakpoint.	TIDE 234PM Average of Runs Offshore of the Breakpoint.	TIDE 234PM Average of Runs Onshore of the Breakpoint.
1	-0.0592	-0.0482	-0.0710	-0.0193	-4.7×10^{-3}
2	-0.40862	-0.1592	-0.2025	-0.0551	0.0340
3	0.3317	0.1091	-0.3014	0.0507	-0.1077
4	-6.8×10^{-3}	-4.7×10^{-4}	-3.0×10^{-3}	3.1×10^{-5}	-1.1×10^{-3}
5	-1.4×10^{-3}	-1.1×10^{-3}	-2.5×10^{-3}	1.5×10^{-4}	2.9×10^{-4}
6	2.8×10^{-5}	-1.5×10^{-3}	7.9×10^{-3}	5.7×10^{-4}	6.7×10^{-3}
7	2.1×10^{-8}	-2.2×10^{-5}	1.3×10^{-4}	1.6×10^{-7}	1.0×10^{-5}
8	0.0000	3.3×10^{-4}	-0.0108	7.3×10^{-4}	-1.7×10^{-4}
9	-7.5×10^{-7}	5.3×10^{-4}	-3.2×10^{-3}	-1.6×10^{-4}	-1.5×10^{-4}

relates the incident wave-induced flow to the sediment suspension which occurs at the high-frequency time scales. Suspended sediment transport due to a mean flow transporting agent or driving force is measured by Term 3 ($\tilde{c}\tilde{u}$). The run-averaged measurements of these three dominant functions (*i.e.* Terms 1, 2 and 3) are illustrated in Figures 7.1-7.3. In the following sections the variations of Terms 1, 2 and 3 with mean depth and run number are investigated, but first we discuss, in the next section, the variation of mean flows and sediment suspension concentrations over the tidal cycles.

7.2.1 VARIATIONS IN SUSPENDED SEDIMENT CONCENTRATION AND CROSS-SHORE FLOW VELOCITIES

This section describes the mean near-bed cross-shore flow and concomitant changes in sediment suspension over Tides 164PM, 184PM and 234PM. Mean cross-shore flow velocity values over the four data runs of Tide 164PM (16th April, 1991) are shown in Figure 7.1(a). The mean cross-shore currents, at the height of the EMCM (0.1m) are weak and directed onshore for the storm data runs, located well outside the surf zone. The mean suspended sediment concentration component (Figure 7.1(b)) shows a high concentration of sediment suspended by this storm event. Unfortunately, the limited number of data runs do not offer a great deal of information.

Steady near-bed cross-shore flow velocities through Tide 184PM (18th April, 1991) are plotted in Figure 7.2(a). The breaker zone occurs at Runs 22/23, and Runs 23-26 can be considered, therefore, to be inside the surf zone (see Section 4.3.3 for definition of breakpoint position). The mean cross-shore flow velocities are directed weakly onshore outside the surf zone, and strongly offshore inside the surf zone (the undertow). At the height of the bottom OBS on Rig A2 (0.06m) a marked asymmetry over Tide 184PM is seen in Figure 7.2(b) over the tidal cycle. Suspended sediment concentrations are significantly greater over the ebb tide, compared to those of the flood tide.

Tide 234PM (23rd April, 1991) reveals a similar pattern (using data from the bottom OBS and EMCM on Rig A2), with sediment suspension asymmetry although

(a)

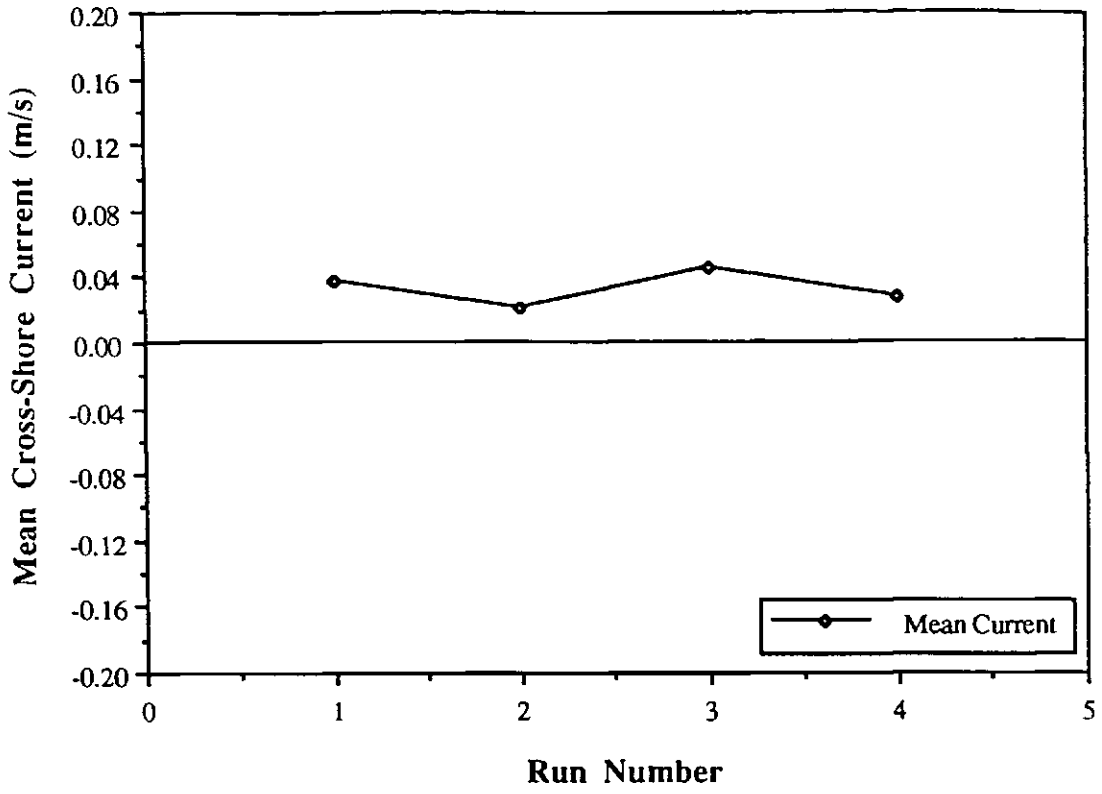

(b)

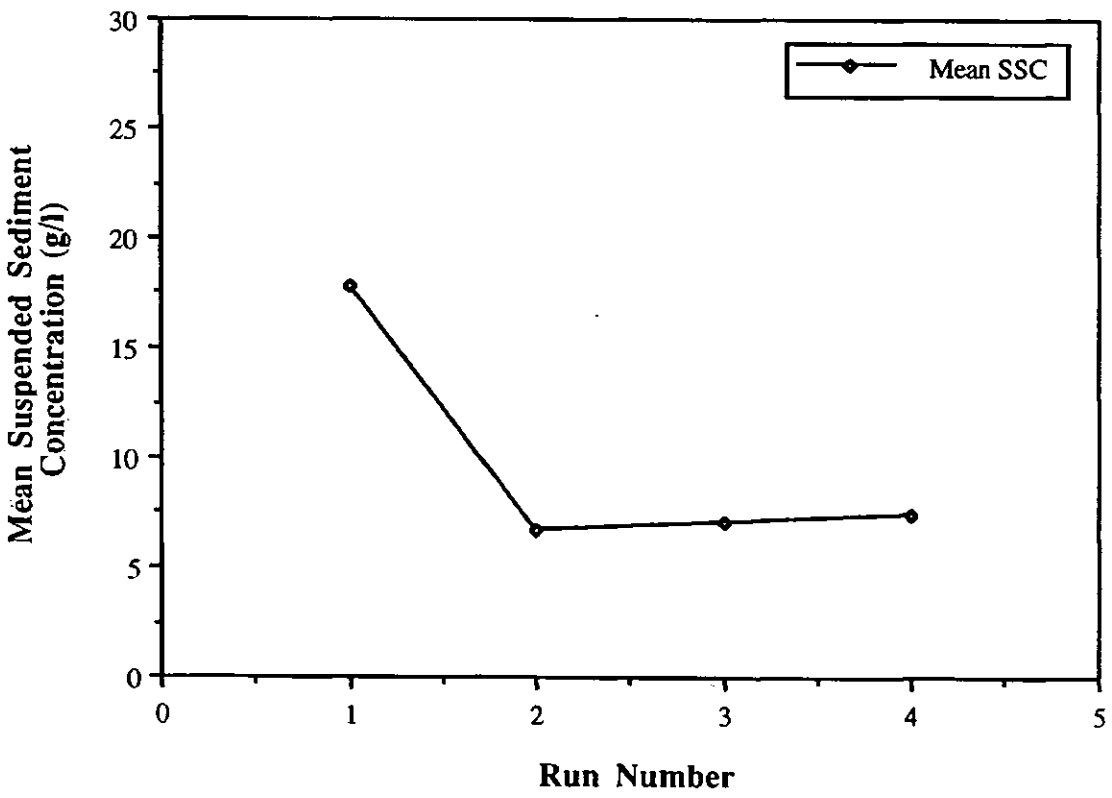

FIGURE 7.1 (a) Variations in mean near-bed cross-shore current with time and (b) variations in mean suspended sediment concentration with time, during April 16, 1991.

(a)

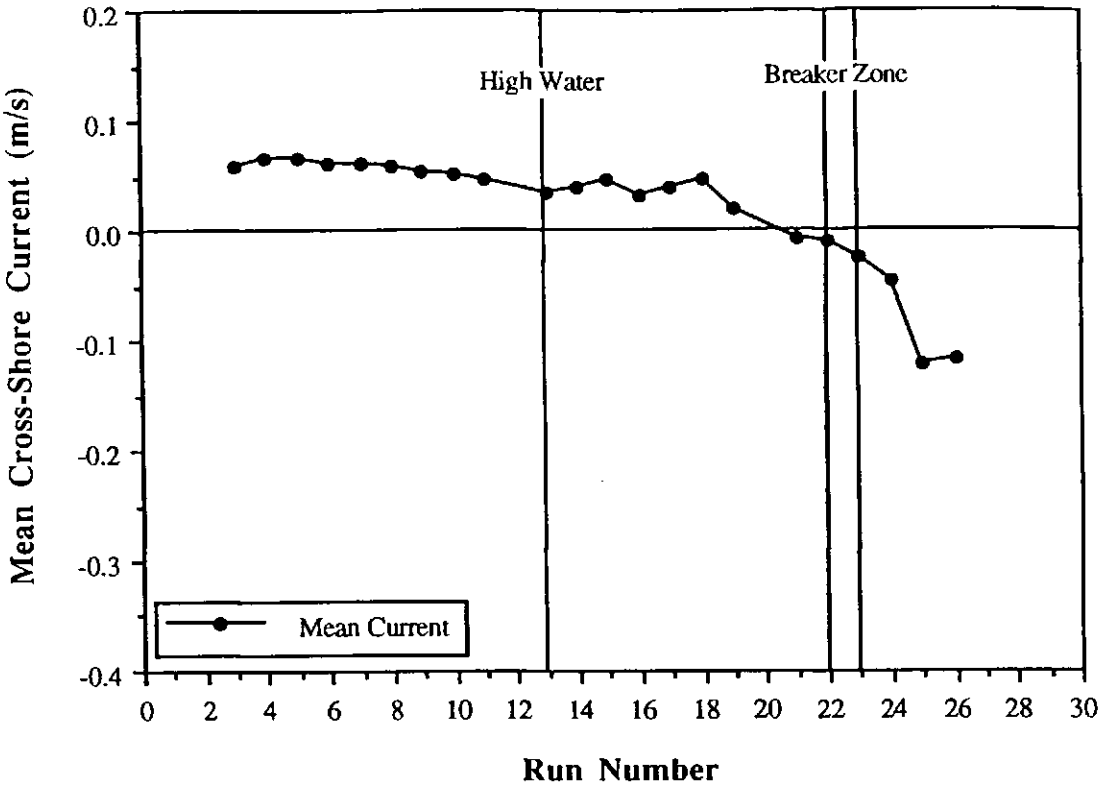

(b)

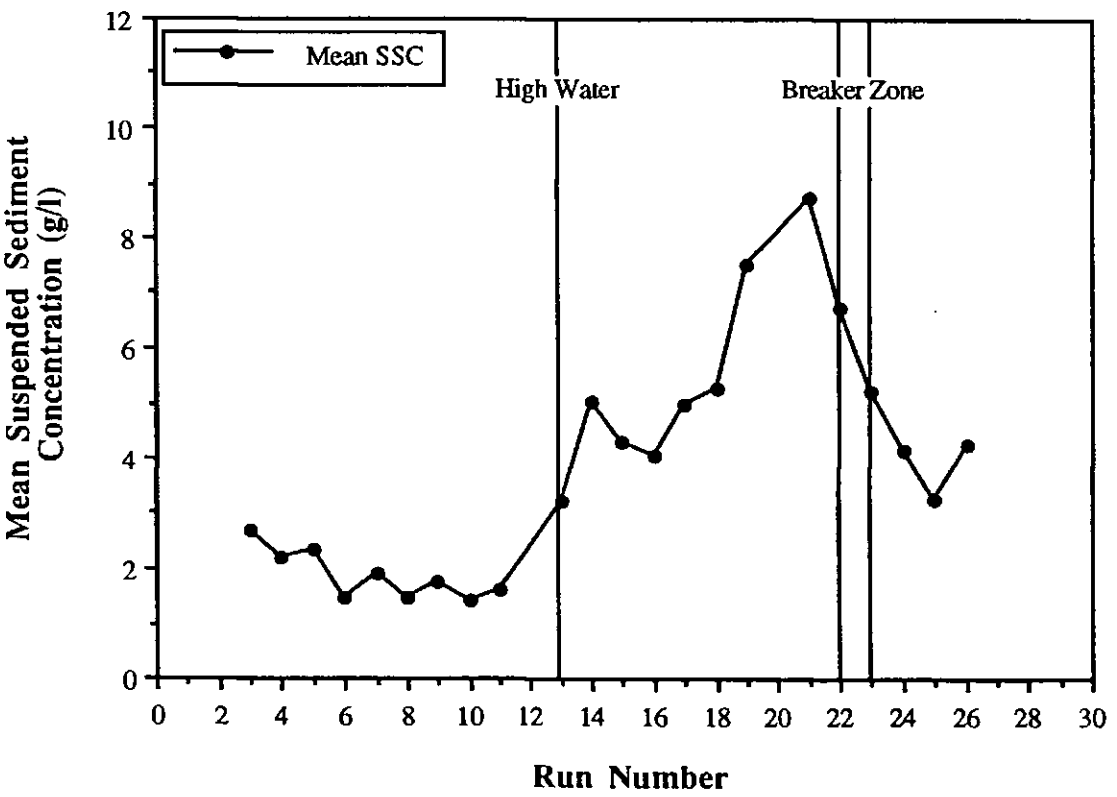

FIGURE 7.2 (a) Variations in mean near-bed cross-shore current with time and (b) variations in mean suspended sediment concentration with time, during April 18, 1991.

(a)

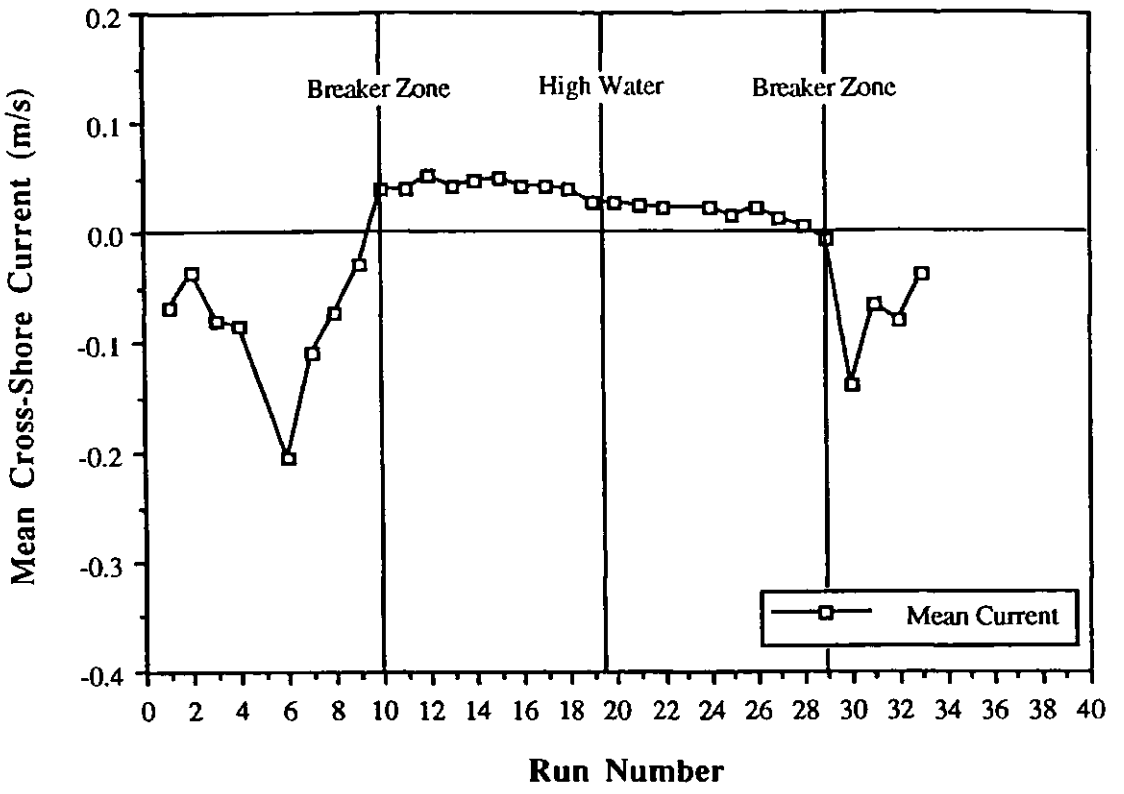

(b)

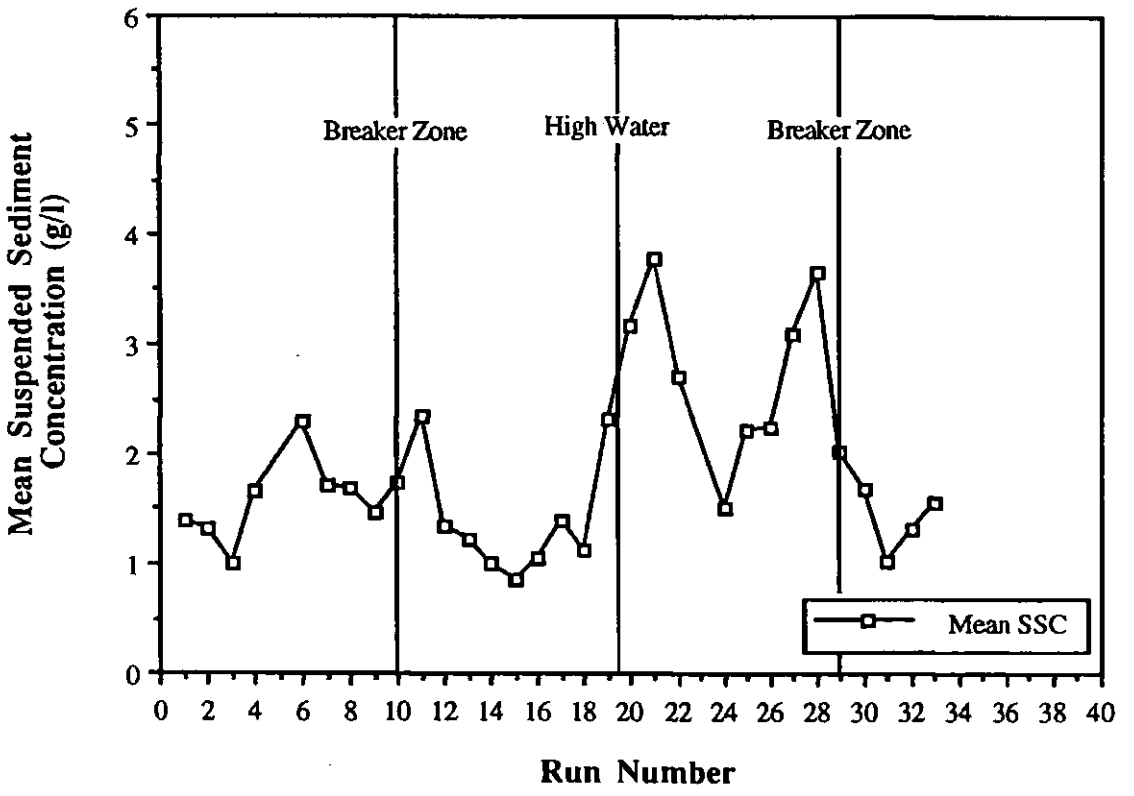

FIGURE 7.3 (a) Variations in mean near-bed cross-shore current with time and (b) variations in mean suspended sediment concentration with time, during April 23, 1991.

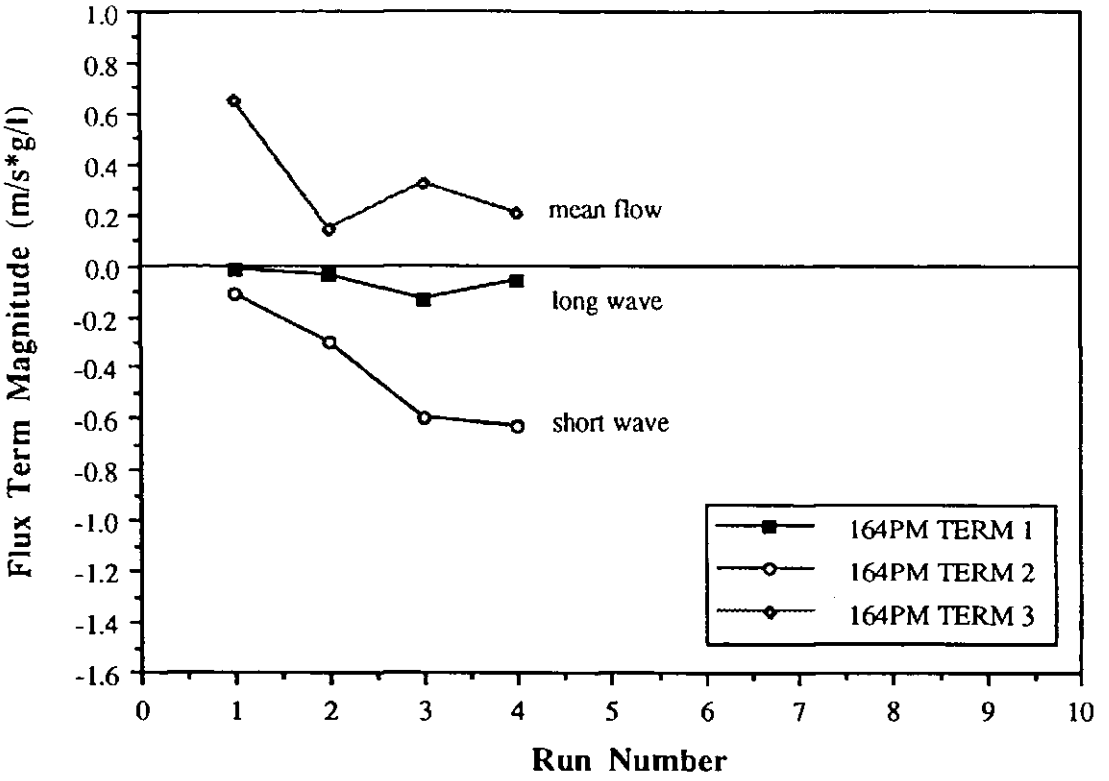

FIGURE 7.4 Variations in Flux Terms 1-3 with time (April 16, 1991).

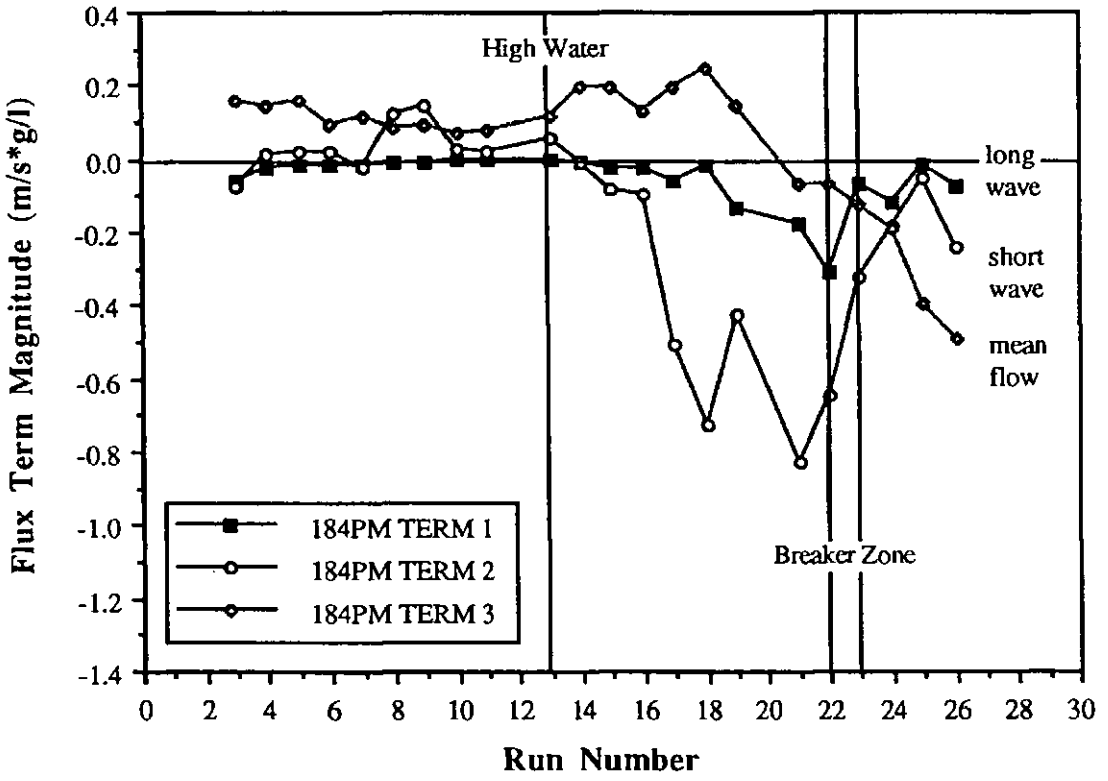

FIGURE 7.5 Variations in Flux Terms 1-3 with time (April 18, 1991).

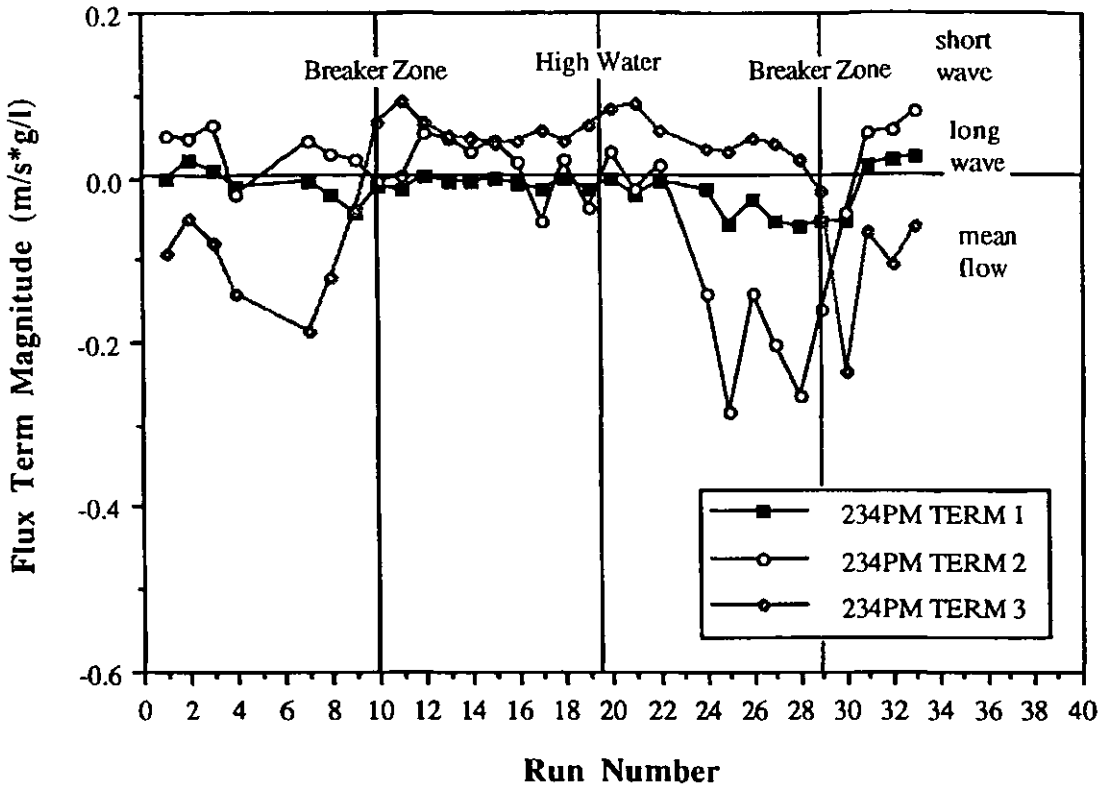

FIGURE 7.6 Variations in Flux Terms 1-3 with time (April 23, 1991).

the suspended sediment concentrations are considerably decreased in magnitude between this tidal cycle and Tides 164PM and 184PM (Figure 7.3(b)). Runs 1-9 inclusive are inside the surf zone over the flood tide; the breakpoint occurs around Run 10. On the ebbing tide, however, the break-point is located near to Run 29 and Runs 30-33 are, therefore, inside the surf zone. The mean near-bed cross-shore flow velocities over Tide 234PM are directed onshore outside the surf zone and strongly offshore within the surf zone (Figure 7.3(a)).

7.2.2 LOW FREQUENCY, HIGH FREQUENCY AND MEAN FLOW CONTRIBUTIONS TO CROSS-SHORE SUSPENDED SEDIMENT FLUX

The wave climate during Tide 164PM (16th April) varied considerably from that of the later tides, for example, Tide 234PM (23rd April). A transition occurred over the duration of the field deployment from a violent storm event, through moderate swell and chop conditions, to ultimately calmer conditions. The relative magnitudes of the cross-shore flux terms reflect this transition, but a similar pattern between the flux terms inside and those flux terms outside the surf zone, is exhibited by each tide.

(a) TEMPORAL VARIATIONS

Figure 7.4 illustrates the velocity and suspended sediment concentration coupling variations, seen in Cross-Shore Flux Terms 1-3, time-averaged for the four runs of Tide 164PM (16th April, 1991) at Spurn Head. Significant wave heights (H_S) during the four runs, shown in Figure 7.4, ranged from 1.36m at 1908h (Run 1) to 1.62m at 2010h (Run 4). Significant-wave-height-to-water-depth ratios (H_S/h) associated with Figure 7.4, range from 0.30 (1908h) to 0.39 (2010h). The four data runs of Tide 164PM relate to the period subsequent to high water with mean water depths of 4.40-4.18m, located well outside the surf zone. Table 7.1 displays the equivalent sampling start time for each data run collected.

The three dominant cross-shore flux functions indicate relatively large rates of offshore transport associated with high frequency wave motions, of increasing magnitude with time (Term 2, $c_S u_S$). This offshore transport may well be associated

with the presence of *ripples*. If we consider the fact that large negative transport values occur in deep water, just after high water, the likelihood is the occurrence of over-steep storm-generated ripples (built up over the slack waters of high tide). The ripple field is subsequently destroyed during the transition from rippled to plane bed conditions with increasing maximum orbital velocities on the ebbing tide. On Tide 184PM (April 18, 1991) this effect was much smaller and on Tide 234PM (April 23, 1991) the effect was smaller still. A relatively large onshore transport rate is generated by the mean flow component ($\overline{c}\overline{u}$) whilst the magnitude of Term 3 tends to decrease with time over the four runs. Term 1 ($c_L u_L$), however, shows the presence of a relatively small offshore transport contribution throughout the four storm tide runs associated with the low frequency wave-induced transport.

In summary then for 164PM, Figure 7.4 illustrates the response of sediment to a range of wave motions occurring in the nearshore velocity field mid-storm event. Onshore-directed mean cross-shore flow velocities throughout Tide 164PM, and a corresponding onshore transport is seen in Figure 7.4 associated with Term 3. Conversely, the near-bed oscillatory transport at Spurn Head is dominated by offshore transport at the incident wave frequencies with a corresponding, but subordinate, offshore transport at low frequencies.

Figure 7.5 illustrates the temporal changes in the cross-shore sediment transport functions (Terms 1, 2 and 3) for Tide 184PM (18th April, 1991) at Spurn Head, two days after the height of the storm which left the sand spit breached. Significant wave heights (H_S) during Tide 184PM ranged from 0.85m at 1746h (Run 3) to 1.09m at 2158h (Run 17). During 18th April, 1991, significant-wave-height-to-water-depth ratios (H_S/h) associated with the three cross-shore flux terms in Figure 7.5, varied from 0.172 (2045h, Run 13) to 0.628 (2348h, Run 23). The break-point which occurred approximately at Runs 22/23 and high water which occurred approximately at Run 13, are depicted in Figure 7.5. Table 7.2 displays the equivalent start times for each data run collected during Tide 184PM.

The three cross-shore sediment functions exhibit characteristics which correspond to the pattern displayed in Figure 7.4. The effects of the storm are still

evident in Tide 184PM (Figure 7.5), and dominant offshore transport peaks occur at or near the break-point in both low and high frequency sediment transport functions. The incident wave component of transport exhibits variability prior to the waves breaking, however, with fluxes directed both onshore and offshore. The importance of the low-frequency energy and high-frequency energy increased substantially towards Runs 22/23, the approximate position of wave breaking. Maximum flux associated with the low-frequency coupling transport term, $c_L u_L$, coincides approximately with the maximum magnitude of the incident band coupling term, $c_S u_S$, located around Runs 20-22. Onshore transport generated by Term 2 ($c_S u_S$) occurs prior to high water and rises to a small peak near Run 9 in Figure 7.5.

During 18th April, mean cross-shore transport (Flux Term 3, $\bar{c}\bar{u}$) measured at 0.06m above the seabed, is directed shorewards up to the region of wave breaking. The mean cross-shore transport rate is largest within the surf zone (Runs 22/23-26) and directed offshore, in conjunction with the undertow. Outside the surf zone, on the contrary, the magnitude of the mean cross-shore transport component is in the onshore direction, with a maximum probably existing through the ebb tide.

Figure 7.6 illustrates the temporal changes in the oscillatory and mean flow transport components across the beach at Spurn Head during 23rd April, 1991 (Tide 234PM). Significant wave heights (H_S) at Rig A2 over the duration of Tide 234PM range from 0.29m at 0823h (Run 3) to 0.81m at 1508h (Run 24). Similarly the significant-wave-height-to-water-depth ratio (H_S/h) for this tidal cycle, span values from 0.265 (1308h, Run 18) to 0.448 (1041h, Run 10). Wave breaking occurs around Runs 9/10 and 28/29, whilst high water is located approximately at Run 19 for Tide 234PM. Table 7.3 displays the equivalent start times for each data run collected during Tide 234PM.

The variation of Term 1 ($c_L u_L$) in Figure 7.6 reveals relatively small rates of offshore transport associated with the low-frequency oscillatory motion with peaks occurring on the flood and ebb tides. Of the two primary offshore-directed peaks in transport, the larger magnitude ebb tide peak occurs just outside the wave breaking region, whilst the secondary offshore transport peak on the flood tide coincides with

the location of the surf zone over the instruments on Rig A2. Negligible onshore transport events, associated with long period fluctuations in the velocity field, are observed in the shallower regions of the surf zone at the later stages of both flood and ebb tides.

The predominant offshore transport rate driven by the incident band-coupling term (Term 2, $c_S u_S$) reaches a peak during the ebb part of the tidal cycle, just prior to breaking, initiated subsequent to high water. This second cross-shore flux term shows a considerable degree of variability over the earlier half of the tidal cycle (*i.e.* the flood tide) with fluxes which are both offshore- and onshore-directed.

The temporal variations in the mean cross-shore transport (Figure 7.6), characterised by Flux Term 3 ($\bar{c}\bar{u}$), is largest within the surf zone and directed offshore at the height of the instruments (related to the undertow). Outside the surf zone, however, the steady cross-shore transport component has a magnitude which is generally directed onshore and, therefore, the mean flow-driven transports on either side of the break-point appear to converge.

(b) DEPTH VARIATIONS

Figures 7.7, 7.8 and 7.9 illustrate the changes with depth for the cross-shore flux terms which result from the coupling of cross-shore velocity with suspended sediment concentration, for Tides 164PM, 184PM and 234PM. The relationship of the flux functions to changing depth should allow a direct comparison with the depth-dependent moment 'shape functions'.

Examining Figures 7.8 and 7.9 (Tides 184PM and 234PM, respectively), the tidal asymmetry which is well defined in the previous section is quite pronounced in the depth variations of the suspended sediment fluxes. (Note that the alternating flood/ebb tide flux term values across the beach create the zigzag pattern observed). In general, Cross-Shore Flux Terms 1-3 in Figure 7.8 (18th April) exhibit similar characteristics to those in Figure 7.9 (23rd April). An offshore-directed peak, associated with Term 1 ($c_L u_L$) the long period motion coupling parameter occurs in and just seawards of the breaker zone. The larger offshore-directed peak of Term 2 ($c_S u_S$)

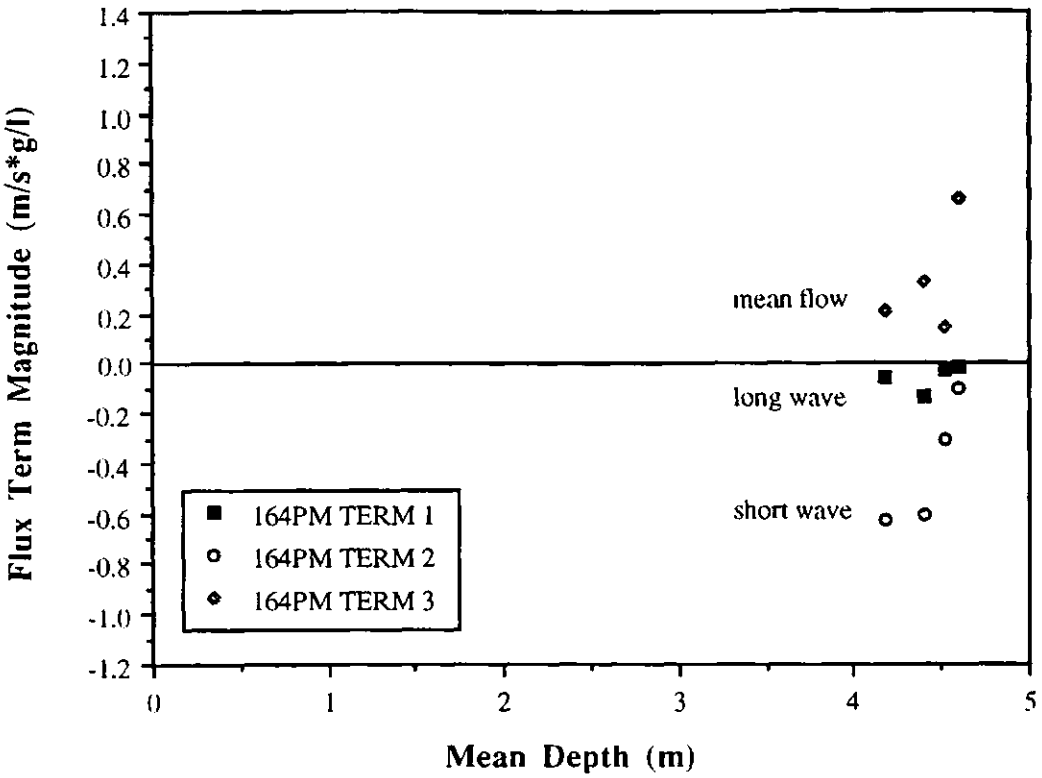

FIGURE 7.7 Variations in Flux Terms 1-3 with depth (April 16, 1991).

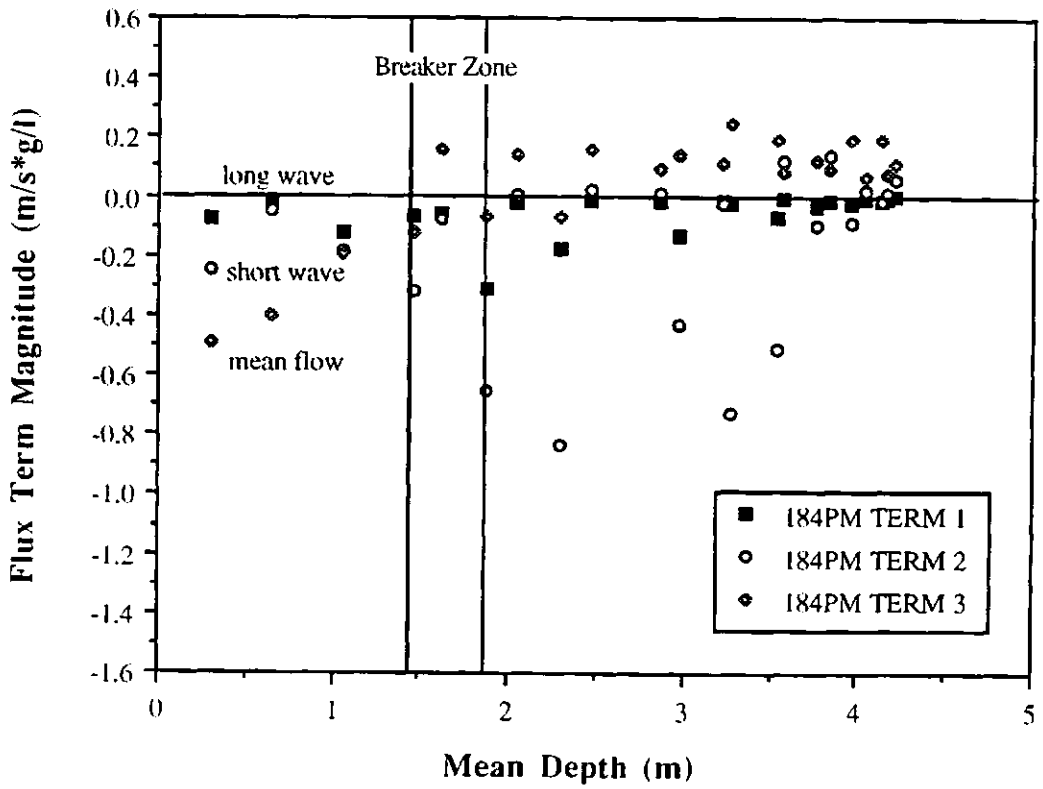

FIGURE 7.8 Variations in Flux Terms 1-3 with depth (April 18, 1991).

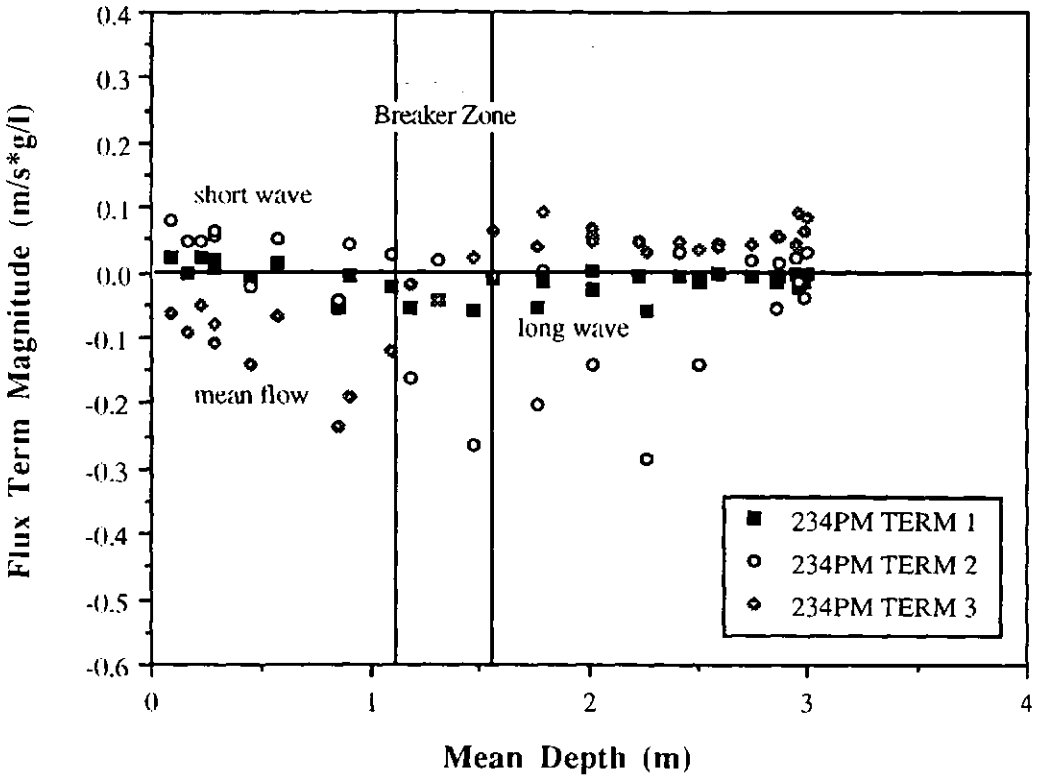

FIGURE 7.9 Variations in Flux Terms 1-3 with depth (April 23, 1991).

similarly arises at and beyond the breaker zone becoming zero at the greater depths offshore. Term 3 ($\bar{c}\bar{u}$) , however, is negative and directed offshore within the surf zone, whilst, seawards of the breakpoint Term 3 is positive in magnitude and, therefore, directed onshore.

Total cross-shore sediment transport rates are illustrated for each of the three selected tidal cycles in Figures 7.10, 7.11 and 7.12, incorporating data from the bottom OBS and EMCM on Rig A2. The relative importance of the cross-shore oscillatory and net components to the total transport rate can be assessed through comparison of Figures 7.4, 7.5 and 7.6 (Flux Terms 1-3 for Tides 164PM, 184PM and 234PM, respectively) with Figures 7.10, 7.11 and 7.12. The mean flow-related parameter, Term 3, dominates the total cross-shore transport rate over the flood tide. From high water and then through the ebb tide, the incident wave-related Term 2 predominates in conjunction with the period of most significant sediment suspension and, furthermore, the most considerable transport rates.

7.2.3 TOTAL CROSS-SHORE SUSPENDED SEDIMENT FLUX

Figures 7.13 and 7.14 show bar chart plots of the three dominant flux term measurements, averaged outside and inside the surf zone. The bar charts describe the temporally- and spatially-averaged transport function variations for Tides 164PM, 184PM and 234PM. These figures provide some indication of the direction and relative magnitude of the cross-shore transport components and, hence, of the various processes driving beach profile change at Spurn Head. Outside the breakpoint (Figure 7.13) the largest parameter, Term 2 ($c_S u_S$), is directed offshore as is Term 1 ($c_L u_L$), whilst Term 3 is conversely directed onshore. Meanwhile, inside the breakpoint (Figure 7.14) the dominant contribution is made by the mean flow transport component, Term 3, which is directed offshore as is, to a lesser extent Term 1, the long period motion coupling function. Term 2, however, describing the transport associated with the gravity band motion, is strongly directed offshore on the 18th April (Tide 184PM) but by the 23rd April (Tide 234PM) the offshore transport has decreased and actually reversed direction, becoming positive and onshore. The magnitude of these

FIGURE 7.10 Variation of net cross-shore transport rate during April 16, 1991.

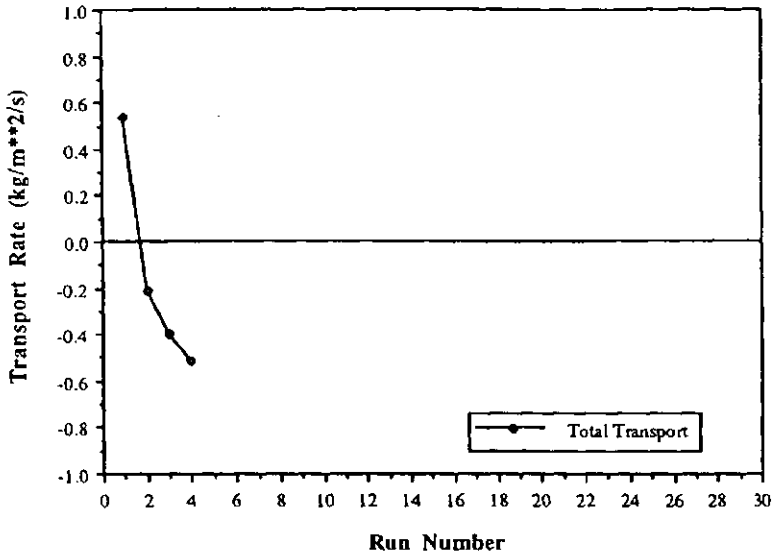

FIGURE 7.11 Variation of net cross-shore transport rate during April 18, 1991.

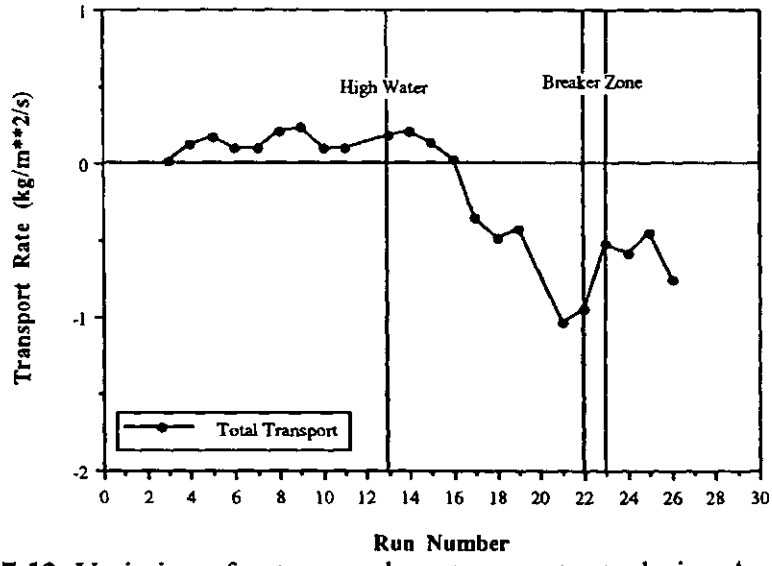

FIGURE 7.12 Variation of net cross-shore transport rate during April 23, 1991.

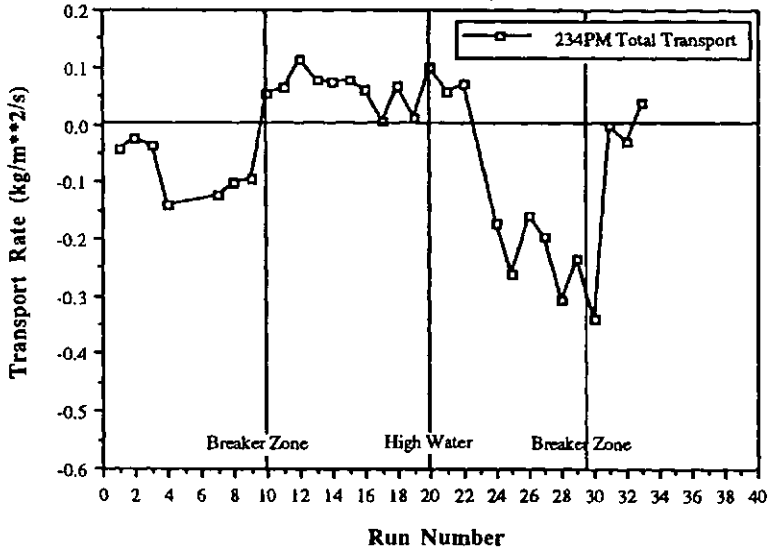

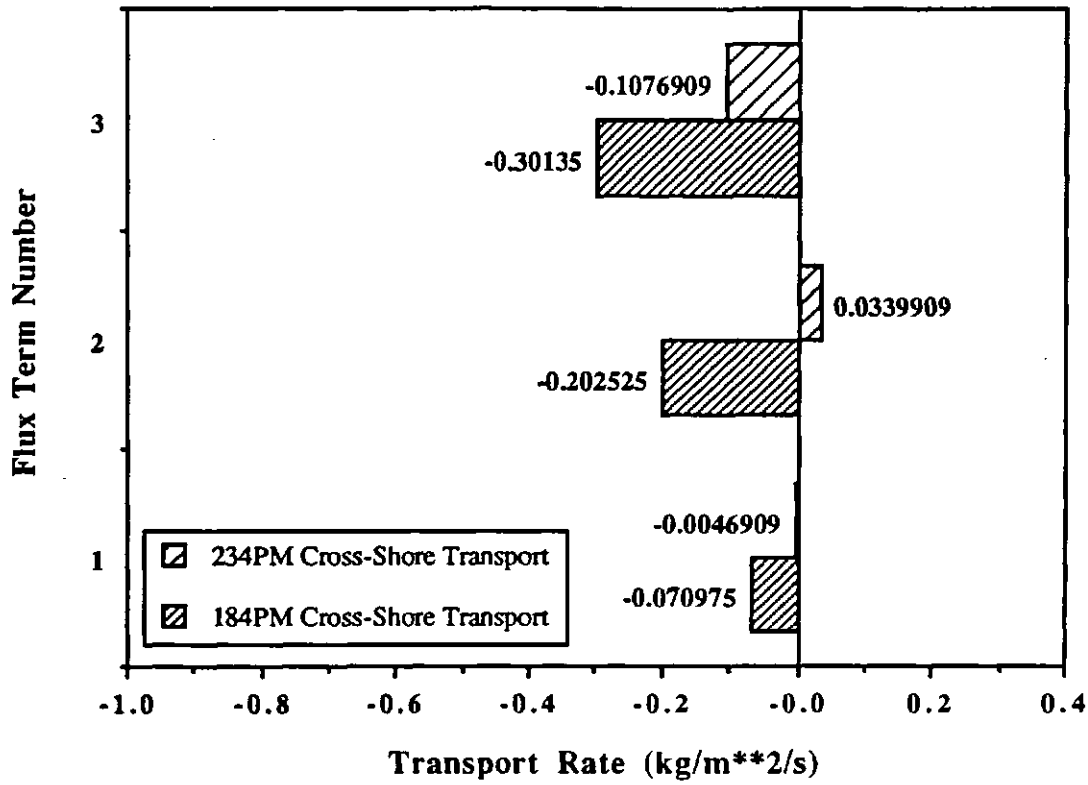

FIGURE 7.13 Cross-shore Flux Terms averaged **inside** the surf zone and per tide for Tides 184PM and 234PM.

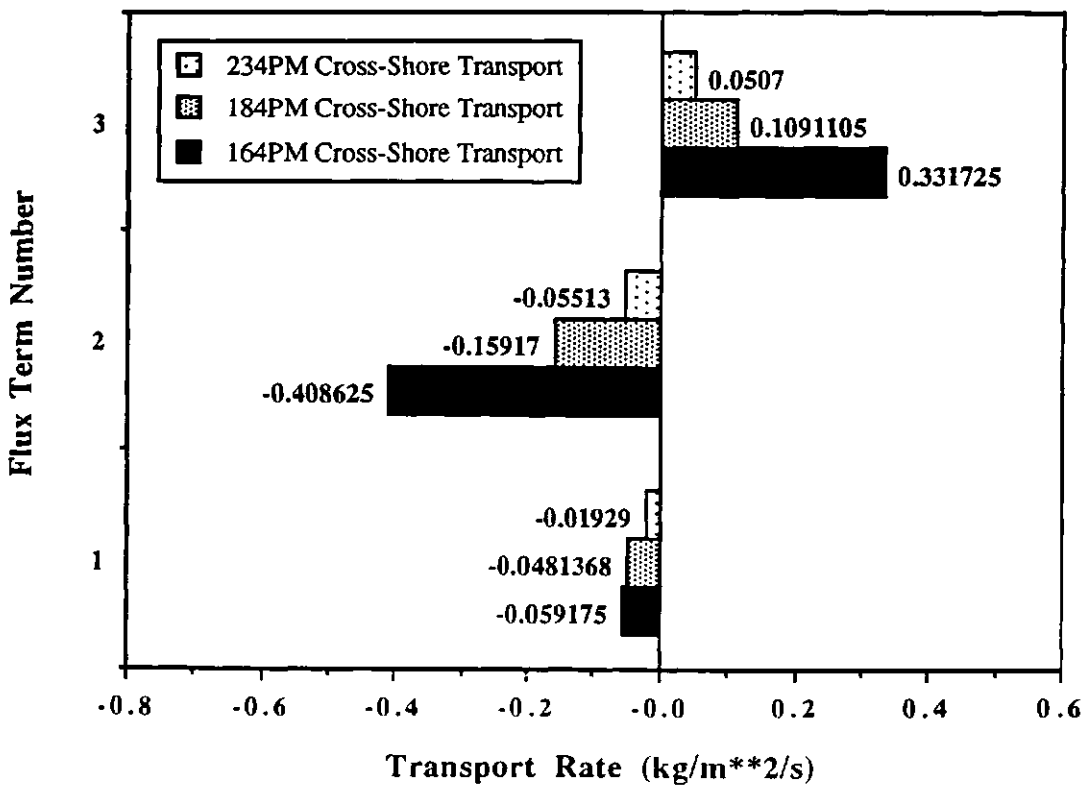

FIGURE 7.14 Cross-shore Flux Terms averaged **outside** the surf zone and per tide for Tides 164PM, 184PM and 234PM.

time- and space-averaged transport functions is generally greater outside the surf zone than inside, which reflects the wave shoaling to breaking profile across the nearshore. It is also true to say that, in Figure 7.14, only Tide 234PM averages over both flood and ebb surf zones, which must explain why the values are smaller.

Examining the three dominant cross-shore transport functions (Terms 1-3) as a function of position within the tidal cycle (*i.e.* flood or ebb tide), it is obvious that the processes driving cross-shore sediment transport in the nearshore zone on a macro-tidal intermediate beach, are highly complicated. The noticeable asymmetry in the magnitude of the cross-shore flux terms between flood and ebb tides, seen in the previous sections, is worth further discussion. In order to clarify this flood/ebb difference, the run-averaged flux term measurements have been divided into those obtained during the flood part of the tidal cycle and those obtained during the ebb. The measurements are then averaged according to their position in the tidal cycle (Figures 7.15 and 7.16) but, once again, these represent very different periods of the tidal cycles.

Sediment transport rates are clearly greater during the *ebb tide* than the flood tide. The magnitudes of the time- and tide-averaged flux terms are several times higher during the retreat of the tide over the instruments and the tidal asymmetry in sediment transport is well defined (Figures 7.15 and 7.16). For this data-set, when the complete tidal cycle is studied, the offshore transport at incident wave frequencies, seaward of the breaker zone and on the ebbing tide, is the dominant cross-shore transport feature (described by Term 2, $c_S u_S$), as seen in Figure 7.16. The greater transport rate, evident over the ebbing tide, is generated through the suspension of large quantities of sediment in response to the incident band motions (Figures 7.2(b) and 7.3(b)). During the flood tide, the mean flow-transport coupling function ($\bar{c}\bar{u}$) is the dominant cross-shore transport parameter for Tide 184PM, whilst the remaining terms in Tide 184PM and all three terms in Tide 234PM, are generally of negligible magnitude (*i.e.* values are near-zero).

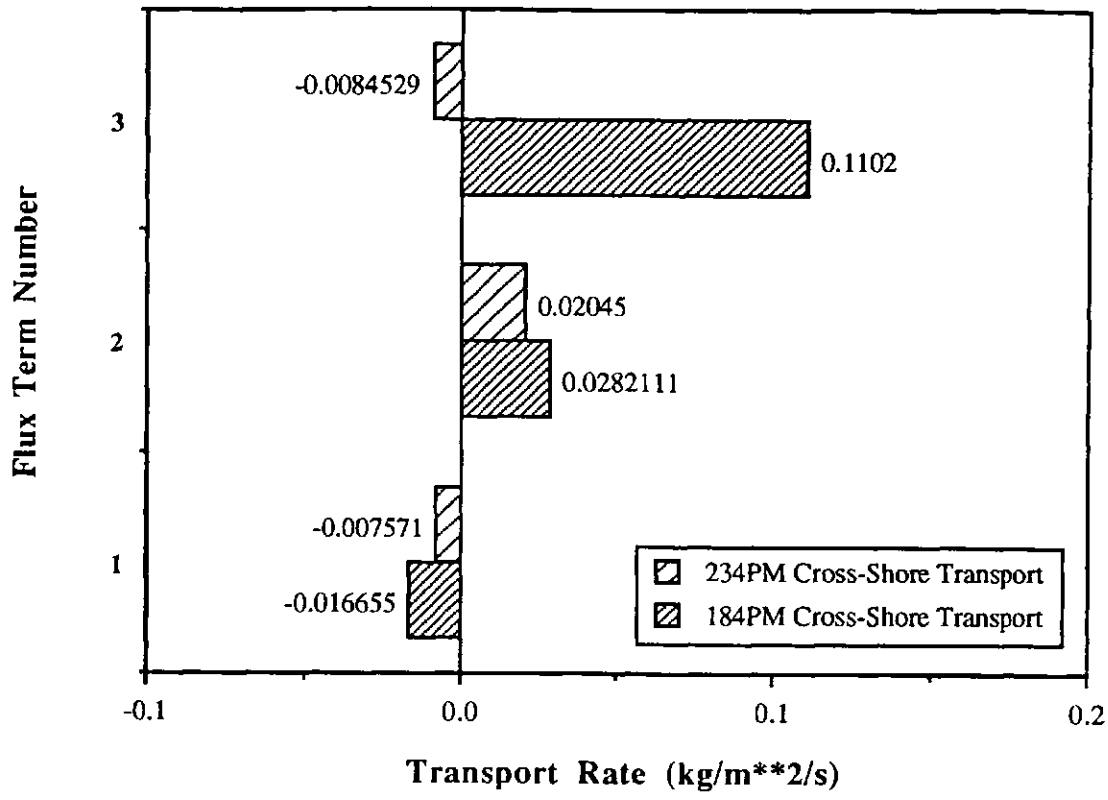

FIGURE 7.15 Cross-shore flux terms averaged over the **flood** tide for Tides 184PM and 234PM.

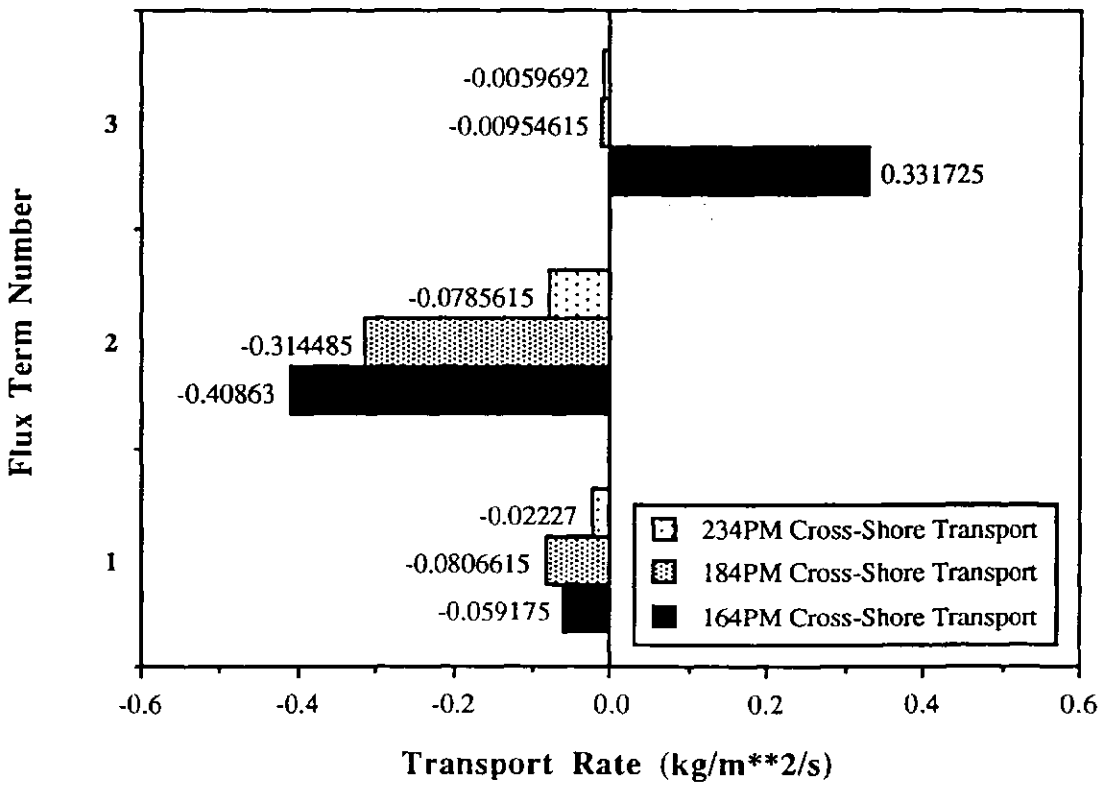

FIGURE 7.16 Cross-shore flux terms averaged over the **ebb** tide for Tides 164PM, 184PM and 234PM.

7.3 DISCUSSION

The analysis described in this chapter reveals some interesting patterns in the cross-shore suspended sediment transport processes which exist on the macro-tidal, intermediate beach at Spurn Head. The usual characterisation of sediment transport parameters involves the frequency analysis of the relative contributions to sediment transport rather than a frequency band approach This study examines the frequency-dependent nature of the cross-shore transport rates using the time series of velocity and suspended sediment concentration.

Whilst many of the results examined in this chapter agree with the findings of other recent work concerning the patterns of sediment transport and the processes driving the transport, the overall picture generated by these flux term results is that the nearshore zone on this macro-tidal intermediate beach is highly complex. The observed behaviour of the various cross-shore sediment transport parameters in this study leads to the suggestion that even the most descriptive and realistic cross-shore transport models that exist at present are a long way from accurately assessing the various factors driving onshore-offshore sediment transport on macro-tidal beaches.

Sediment transport is driven primarily by three of the cross-shore flux terms, Terms 1, 2 and 3. Terms 1-3 describe the coupling between various hydrodynamic forces and the resulting near-bed sediment response, where Term 1 is ($c_L u_L$), Term 2 is ($c_S u_S$) and Term 3 is ($\bar{c}\bar{u}$). Outside the surf zone up to Run 15 (flooding tide) strong onshore transport occurs at the incident wave frequencies, with weaker offshore transport at the infragravity wave frequencies in agreement with Davidson *et al.* (1993). However, after high water (on the ebbing tide) this no longer applies, with a large increase in magnitude in Term 2 now in the offshore direction. In accordance with the incident band component, a noticeable increase in the infragravity-driven transport occurs, remaining directed offshore. The mean flow-driven transport component remains positive (*i.e.* onshore) outside the surf zone with little variability.

Inside the surf zone, transport generated by the residual current contribution (Term 3) predominates, being directed offshore. Immediately following the storm event, during the early part of the field deployment (Tide 184PM), the gravity (Term 2)

and infragravity band (Term 1) parameters remain directed offshore, suggesting the continuation of storm-driven sediment erosion. Conversely, later in the field deployment (Tide 234PM), Terms 1 and 2 are predominantly directed onshore, possibly indicating the initiation of beach replenishment and accretion.

Concentrations of sediment suspension were understandably at their highest during the storm event and tended to decrease with time, through the deployment period. A well-defined peak in the mean near-bed suspended sediment concentration during the latter half of the tidal cycle suggests that an asymmetry exists at Spurn Head between flood and ebb tide transport patterns. Analysis of the cross-shore flux terms replicates the same phenomenon seen in the temporal variations of mean suspended sediment concentrations, with considerably higher magnitudes occurring during the ebb rather than flood part of the tidal cycle.

Davidson *et al.* (1993) examined the same B-BAND data-set but with attention focused primarily upon Tide 234PM, and a co-spectral approach was used to examine the contribution of the gravity, infragravity and mean transport components to the total cross-shore sediment transport, through the tidal cycle. Davidson *et al.* (1993) established the presence of a marked asymmetry in the transport processes between flood and ebb tides, with higher levels of sediment suspension and transport occurring on the ebb tide approximately two hours after high water (and just offshore of the breakpoint). Possible factors which might generate an increased suspension during the ebb tide were discussed by Davidson, including the de-watering of the beach, localised bed-level changes relative to the sensor and destruction of a ripple field which developed during the slack waters of high tide. Whilst the first and second of these causes may influence sediment suspension processes during the tidal cycle, the erosion of a ripple field just subsequent to high water is most likely to have the greatest effect upon the relative magnitudes of flood and ebb tide suspended sediment concentrations (*e.g.* Vincent *et al.*, 1991). Over high water, the oscillatory and mean currents are generally small and in such conditions symmetrical ripples can develop seaward of the surf zone (Davidson *et al.*, 1993). As ebbing begins, current velocities increase and consequently the over-steep ripple bed is destroyed, producing sediment-laden vortices

which are ejected high into the water column. As the ripple bed is removed, the suspended sediment concentrations will gradually decrease. The offshore transport peak on the ebbing tide, associated with the incident band-driving mechanism is, therefore, related to this ripple destruction-sediment ejection mechanism. Inman and Bowen (1963) and Inman and Tunstall (1972) describe how sand can be carried offshore over a rippled bed in association with onshore propagating incident waves. Vortices are generated on either side of the ripples, during the onshore part of the wave cycle sand is trapped in the vortices, as the orbital motion reverses its phase then the sediment-laden vortices are carried in an offshore direction and offshore transport is generated.

7.3.1 COMPARISON BETWEEN VELOCITY MOMENT PREDICTORS AND SAND FLUX TERMS

In order to establish the validity of the velocity moments or spatial 'shape functions', seen in the previous chapter, a direct comparison between the flux terms investigated here, and the velocity moment predictors is necessary. In principle, the moment predictors should be compared with depth-integrated transport rates, but for a first step this examination of sand transport flux at one height above the bed (*i.e.* 0.10m) is sufficient (see Russell, 1993). Figures 7.17(a) to (e) compare the suspended sediment flux terms with their equivalent suspended load transport moment predictors. The values were derived by averaging those measurements which occurred during (i) the flood part of the tidal cycle and inside the surf zone (ii) the flood tide and outside the surf zone (iii) the ebb tide and outside the surf zone and finally, (iv) the ebb tide and inside the surf zone. This time-averaging was carried out for each of the three tidal cycles and allows some consideration of the variation of the terms across the nearshore zone, with respect to the breakpoint, and also takes into account the asymmetry which occurred between flood and ebb tides. Un-normalised velocity moment values are used, as is required for absolute transport predictions. There is no comparison, at this stage, of absolute values of moment and flux estimates; Figure 7.17 is provided purely to compare relative values for the different tidal cycles and different modes of

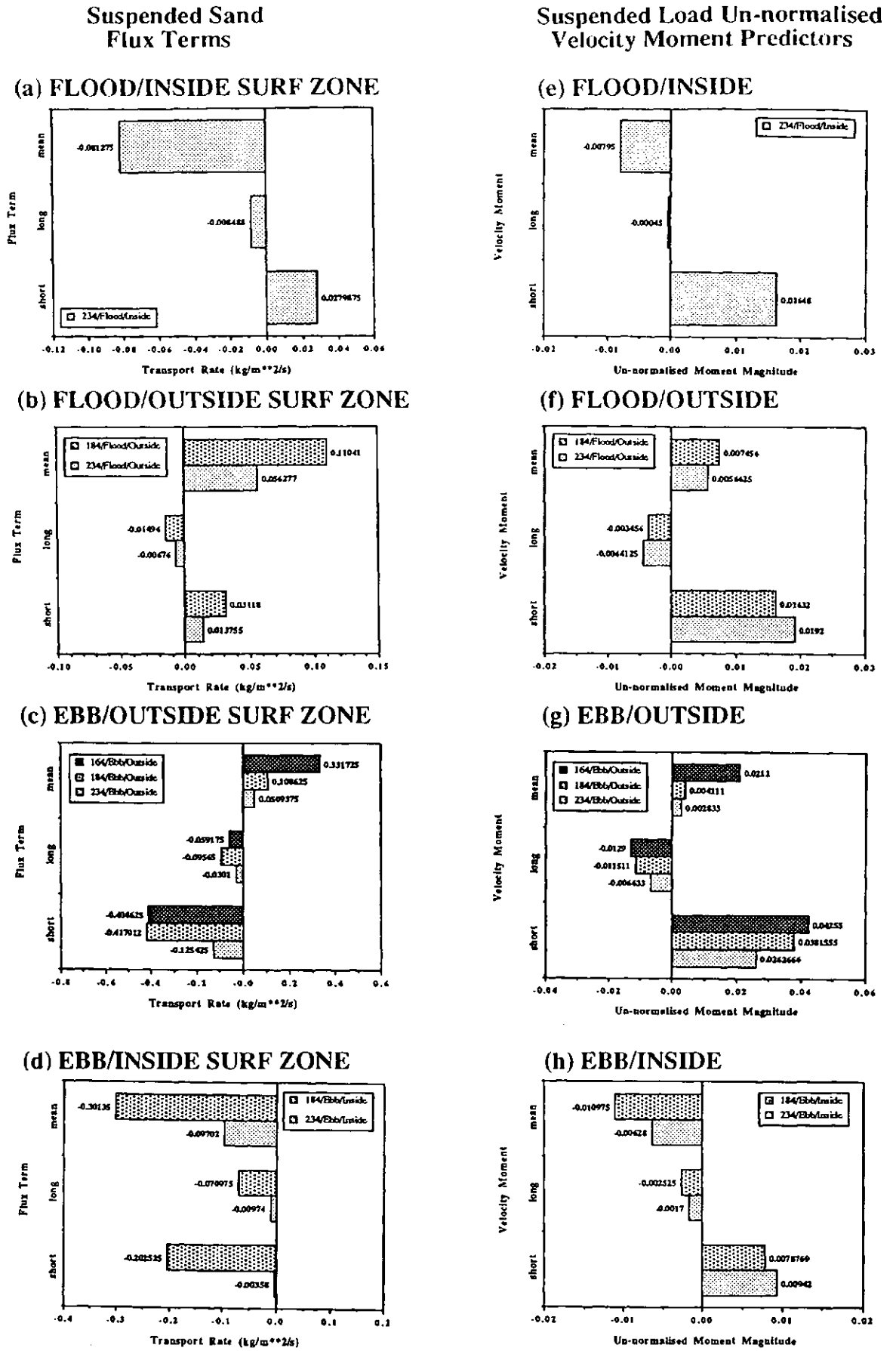

FIGURE 7.17 Suspended sand flux term observations (a) to (d) vs. un-normalised suspended load transport velocity moment predictions (e) to (h). Measurements averaged for flood and ebb stages of the tidal cycle and inside and outside the surf zone.

suspended sand transport.

A number of conclusions can be drawn from Figure 7.17. Inside the surf zone during the flood tide (Figures 7.17(a) and (e)), the sediment flux terms and moment predictions, respectively, compare well for mean, long period and short period flow components. The *sign* of the flux terms are predicted accurately, so that the predicted onshore transport due to the short wave component and the predicted offshore transport due to the long wave and mean flow components agree well with the suspended sand flux observations. The *magnitudes* of the three components do differ, however, with the short wave component having greatest magnitude in the predicted values and the mean flow component having greatest magnitude in the observed suspended sand values. Of course, the flood/inside surf zone diagrams include data from only one tide, Tide 234PM, since the other two tides do not contain any measurements from this region, making any accurate statement of the processes difficult.

Outside the surf zone during the flood tide (Figure 7.17(b) and (f)), there is a similar good agreement in *sign* between the three transport components. Onshore transport is predicted and observed in both the short wave and mean flow components, and offshore transport both predicted and observed in the longer period motion. The relative magnitudes show the same discrepancies as with the flood/inside surf zone case above, predicting the *largest* contribution to be made by the *short wave* component whilst the observations indicate the mean flow transporting agent to be dominant. Figures 7.17(c) and (g) show the case for outside the surf zone during the ebb part of the tidal cycle, these two diagrams are the only ones to include information from all three of the selected tides. It is interesting to see that unlike the previous two cases, it is the *relative magnitudes* of the moment predictions and corresponding suspended sand fluxes which are in agreement here, and it is the sign and inferred transport direction which are not in close agreement. Outside the surf zone during the ebb, observations and predictions show the same pattern with *onshore* transport due to the mean flow component and a smaller *offshore* transport due to the long period flow component. The predicted and observed values for the short wave transporting agent conversely, show the dominant contribution to suspended load

transport to be due to the incident wave contribution. However, the short wave component is estimated to be positive by the velocity moment predictors and, therefore, directed *onshore* outside the surf zone during the ebb, whilst the suspended sand flux terms indicate the transport to be in the opposite direction, driving sediment *offshore*.

In the last case, inside the surf zone during the ebb tide, a similar pattern is seen to the case discussed previously. Both predictions and observations indicate similar *magnitude* and *sign* for the *mean and long period flow* components but do not accurately describe the behaviour of the short wave component. Here, the mean flow is the *dominant* transporting agent with the smallest contribution made by the long period motion, both estimated and measured values indicate negative or *offshore-directed* suspended load transport at the height of the instruments. On the other hand, the significant, although not dominant, contribution made by the short period component is predicted to be *onshore* by the velocity moments and observed to be *offshore* by the flux terms.

It is probable that the lack of agreement between velocity moment predictions and sediment flux observations (*i.e.* the mis-match of predicted/observed values of sign or relative magnitude) is reflecting the complicated pattern of behaviour of suspended sand transport due to wave-current interaction in the presence of bedforms. Davidson *et al.* (1993) discuss the likely influence of bedforms on the incident wave-driven suspended sand transport during a tidal cycle at Spurn Head. Figure 7.3(b), discussed earlier in this chapter, shows a distinct asymmetry of sand suspension concentration on the flood and ebb stages of Tide 234PM which Davidson *et al.* attribute to the presence of degrading ripples on the ebb. Clearly the moment predictors do not provide satisfactory results under the type of conditions found at Spurn Head. A similar investigation of a macro-tidal planar beach would be more likely to yield closer agreement between predictions and observations, since the energetics model was strictly originally designed for flat bed conditions (it has, however, been applied to cases similar to the B-BAND field site by modellers). Further investigation is clearly necessary.

7.4 SUMMARY

The analysis of suspended sediment concentrations in conjunction with current velocity data has generated three non-zero cross-shore suspended sediment flux terms in line with the original work of Jaffe *et al.* (1984). The three terms describe the contribution of the gravity, infragravity and mean flow components to the total transport rate. During the three days examined here, long period wave energy is generally of considerably less significance than the contributions of either the incident band energy or the mean flow component.

Comparison of the suspended sand transport moment predictors with observed sand fluxes reveals that the predictors can provide transport estimates **accurate** in sign for the short wave, long wave and mean flow components for inside and outside the surf zone during the flood stage of the tide, but **inaccurate** in their relative magnitudes. Similarly, the moment predictors can provide transport estimates **accurate** in relative magnitude for the three transport components both inside and outside the surf zone during the ebb part of the tidal cycle, but **inaccurate** for the sign of the short wave contribution. The noticeable asymmetry observed between the flood and ebb stages of the tidal cycle may be a contributory factor to the differences which exist between velocity moment predictions and sand flux observations.

CHAPTER 8
SUMMARY AND CONCLUSIONS

8.1 INTRODUCTION

Instrumentation located across the beach profile at Spurn Head included pressure transducers, electro-magnetic current meters and optical back-scatter sensors which were deployed as four sensor stations in a square configuration, approximately 150m offshore of the high water level. Analysis in this study is concerned with sea-surface elevation, cross-shore current and suspended sediment concentration data recorded at one instrument station over three tidal cycles (16th, 18th and 23rd April, 1991) with conditions ranging from a violent storm event to calm, groupy swell waves.

These high resolution measurements collected over a range of wave and current conditions occurring over a macro-tidal intermediate beach, have enabled a detailed investigation of the processes which drive cross-shore sediment transport in this nearshore environment. In particular, wave groupiness and coupling between the wave envelope/long wave motion across this zone together with cross-shore velocity moments and suspended sediment flux functions, have been examined in this study.

8.2 SUMMARY

8.2.1 WAVE GROUPINESS

Pressure transducer or sea-surface elevation measurements were analysed through time- and frequency-domain techniques which, in turn, produced the incident wave

envelope time series and a wave groupiness factor. This wave groupiness function illustrates the variation of the groupy structure of incoming incident waves across the nearshore. One key result was that wave groupiness persisted throughout the surf zone, and did not decay immediately at the breakpoint as is often assumed. Models describing propagation of wave groups into the surf zone, dissipation by breaking and the effect of long wave velocity and water level fluctuations on wave groupiness, however, do not yet exist (Roelvink, 1993).

The relationship between the incoming wave group and the bound forced long wave was further examined through cross-correlation analysis and the temporal and spatial variation of the cross-correlation function. Cross-correlation between the incident and long wave fields varied systematically across the nearshore. Positive cross-correlation values within the surf zone could be explained by the modulation of short wave breaker heights through the depth variations induced by long period waves (Roelvink and Stive, 1989). However, whether this depth-modulation accompanies forced or free waves, is not certain. Negative correlation coefficient values outside the surf zone are indicative of the incoming wave groups forcing low-frequency motion through the radiation stress gradients of the incident wave envelope. These results agree with other recent field observations (*e.g.* Abdelrahman and Thornton, 1987) where significant direct coupling between the high and low frequency motions is observed.

Near-zero correlation function values, at zero time lag, occurred just onshore of the breaker region possibly associated with a standing long wave nodal point or the competing forced and free long wave energy contributions. It is interesting to note that the cross-correlation and groupiness measurements from three different tidal cycles display similar trends, within the scatter, suggesting that both factors are independent of the offshore wave climate.

8.2.2 SPATIAL SHAPE FUNCTIONS

The two most important velocity moments, based upon Guza and Thornton's (1985a) cross-shore transport equation have been decomposed into mean, gravity and

infragravity band components, generating a number of sub-terms. Despite the occurrence of different wave conditions during each tidal cycle, the results examined in this study, based on field observations, show that both the *bedload* and *suspended load* moments are characterised by consistent patterns. As functions of mean water depth these 'shape functions' are surprisingly insensitive to the different wave conditions for the three tidal cycles examined. The similarity of the normalised values of the moments suggest that the normalisation results in values which are relatively insensitive to wave height variations. There is also some evidence that the scaling with mean water depth is more appropriate than the more intuitive scaling with the ratio of depth to breaking wave depth (*e.g.* Roelvink and Stive, 1989).

The bedload-related functions display a pattern of onshore transport outside the surf zone, due to the dominance of transport associated with gravity wave skewness, and coupling between gravity and infragravity wave variance (stirring) and the mean current. Conversely, there is a smaller offshore-directed transport due to coupling between gravity wave variance and infragravity wave motion. Meanwhile, offshore transport inside the surf zone occurs, due to coupling of gravity and infragravity wave variance with mean currents, in addition to the correlation between the incident wave envelope and infragravity wave motion. These processes predominate over the onshore transport promoted by the incident wave skewness inside the surf zone.

Whilst the suspended load-related derived functions are an order of magnitude greater than the above bedload terms, over the three tides, the results show the same consistent pattern between the various hydrodynamic and sediment transport processes operating in the nearshore zone. It is useful to consider the question : what is the relevance of the spatial shape functions to modelling? Theories such as those by Bailard (1981), Bowen (1980a) and Guza and Thornton (1985a) generate a number of current velocity moments, but their cross-shore shapes, and the relative contributions from different sources, are not well known for field conditions. Naturally, the ability to assign a universal cross-shore shape to these terms for inclusion into nearshore hydrodynamic and sediment transport equations, would greatly ease the process of coastal change prediction. This is perhaps one of the most important implications of

the spatial shape function measurements provided in the present study.

8.2.3 CROSS-SHORE SUSPENDED SEDIMENT FLUX FUNCTIONS

Investigation of the cross-shore sediment fluxes, which arise through a range of wave and current interactions, was conducted through the examination of spatial and temporal variations in the cross-products of sediment concentration and velocity measurements. Cross-shore flux was decomposed into a series of terms describing the relative importance of the mean flow, short wave and long wave contributions, the natural next step was the comparison between these suspended sand fluxes with the moment predictions of suspended sand transport (see also Foote *et al.*, 1993).

Perhaps one of the fundamental criticisms of the research presented here could be the usage of wholly point measurements of the various parameters (including sea-surface elevation, current velocity and suspended sediment concentration measurements) as opposed to the examination of a vertical profile of wave-current interaction and concomitant changes in sediment suspension. Nevertheless, Russell (1993) examined suspended sediment transport on a macro-tidal dissipative beach and suggested that since concentrations of suspended sediment are greatest in the near-bed region, then near-bed sediment transport could perhaps be considered representative of the depth-integrated transport processes. The examination of point measurements of the near-bed sediment transport processes may, therefore, be considered to provide realistic quantification of nearshore sediment behaviour.

Sediment transport is driven, at Spurn Head, by three terms which describe the coupling between the long period motion and the accompanying low-frequency sediment response, incident wave-induced flow linked to a corresponding high-frequency suspension of sediment and the suspended sediment transport due to a mean flow transporting agent. Outside the surf zone, just before high water, strong onshore transport occurred at the incident wave frequencies with weaker offshore transport at the lower frequencies (in agreement with Davidson *et al.*, 1993). After high water, on the ebbing tide, the term coupling a short wave flow and high-frequency sediment response increased in magnitude but in the offshore direction. The subordinate

infragravity-driven transport component, whilst remaining offshore-directed, is only slightly increased in magnitude. The mean flow-related transport is consistently onshore-directed seawards of the breaker region.

Inside the surf zone, the mean flow transport is the dominant component in the offshore direction. Just after the storm at the start of the deployment, the incident and long wave-related transport components remain directed offshore whilst towards the end of the field experiment, these two terms are largely directed onshore. These facts point to storm-related erosion followed by fair-weather beach recovery. Total transport rates through the period of the field deployment agree with the above results, illustrating net offshore transport during the initial storm and post-storm and an increasing quantity of onshore sand transport towards the calmer conditions at the end of the experiment.

One of the most noticeable features in the suspended sediment concentration and transport measurements of the Spurn Head data-set is a prominent asymmetry between flood and ebb tides displaying significantly greater magnitudes over the ebb half of the cycle. The presence of a marked asymmetry in the transport processes, also noted by Davidson *et al.* (1993), is best explained by the location of a ripple field at the instrument location, built up over the slack waters of high tide, then as the increased current velocities pass over an unstable ripple bed as the tide level falls, sediment-laden vortices develop resulting in the ejection of sediment high into the water column (*e.g.* Vincent *et al.*, 1991).

Guza and Thornton's (1985a) adaptation of Bailard's (1981) work for planar beach and uniform bed conditions, established that the terms due to the interaction of the mean field with the oscillating velocity field promoted an offshore sediment flux. In this study, the bedload and suspended load shape functions which relate the mean flow and the oscillatory velocity components indicate a similar offshore sediment transport inside the surf zone. However, outside the surf zone there is a dominant onshore-directed sediment flux.

The present work incorporates a set of terms, split from the original Guza and Thornton moments. Both the suspended load and bedload velocity spatial functions

contain terms describing the coupling of short waves and long wave-induced flow, and the interaction between these oscillatory components promotes an offshore-directed flux across the nearshore. The corresponding cross-shore flux term due to low-frequency wave motion and low-frequency sediment response agrees with these findings with a predominant seawards transport of sediment.

Furthermore, Guza and Thornton (1985a) described terms due wholly to the oscillatory velocity field which appear to promote onshore transport. In this study, both the suspended load and bedload shape functions describing the influence of short incident waves is the most significant oscillatory component and similarly, is directed onshore. The equivalent cross-shore flux term relating to gravity band-driven transport is conversely directed *offshore* for the storm conditions with only a negligible onshore transport occurring during the calmer day.

Comparison between the cross-shore flux terms and the velocity spatial 'shape functions' is interesting and, at the same time, is indicative of the gap that still requires bridging between the available cross-shore sediment transport predictors and field observations of transport. The suspended sediment flux terms were compared with their equivalent suspended load transport moment predictors. Their values were further divided by averaging those measurements which occurred during (i) the flood part of the tidal cycle and inside the surf zone (ii) the flood tide and outside the surf zone (iii) the ebb tide and outside the surf zone and finally, (iv) the ebb tide and inside the surf zone. This time-averaging was carried out for each of the three tidal cycles and allows some consideration of the variation of the terms across the nearshore zone, with respect to the breakpoint, and also takes into account the asymmetry which occurred between flood and ebb tides.

Comparison of the suspended sand transport moment predictors with observed sand fluxes reveals that the predictors can provide transport estimates **accurate** in sign for the short wave, long wave and mean flow components for inside and outside the surf zone during the flood stage of the tide, but **inaccurate** in their relative magnitudes. Similarly, the moment predictors can provide transport estimates **accurate** in relative magnitude for the three transport components both inside and outside the surf zone

during the ebb part of the tidal cycle, but **inaccurate** for the sign of the short wave contribution. The noticeable asymmetry observed between the flood and ebb stages of the tidal cycle may be a contributory factor to the differences which exist between velocity moment predictions and sand flux observations (Davidson *et al.*, 1993).

8.3 CONCLUSIONS

This research has examined the significance of wave groupiness, the relationship between the long period motion and incident wave envelope as nearshore hydrodynamic forces, in addition to the function of current velocity-derived spatial shape functions as predictors of sediment response and to evaluate the relative importance of mean flow, long wave and incident wave contributions. The investigation of cross-shore suspended sediment flux terms to quantify and compare the relative contributions of the mean field, gravity and infragravity components to cross-shore sediment transport, is contrasted with the other findings in order to estimate the suitability of the best physically-based cross-transport equation. On the whole, it could be said that energetics-based predictors for cross-shore sediment transport, do not accurately characterise the driving hydrodynamic forces and subsequent sediment response found at Spurn Head.

The main points to conclude from this work can be summarised as follows :

- Wave groupiness does not decay immediately at the breakpoint, instead a degree of groupiness is maintained through the surf zone up to the shoreline. Modelling the response of sediment in the nearshore should incorporate a wave groupiness factor.
- Outside the surf zone, the cross-correlation between the long period waves and the incident wave envelope has a constant negative value and is relatively insensitive to depth variations. In the wave breaking region the correlation decreases towards zero, whilst within the inner surf zone positive correlation values occur. Interaction between long and short waves changes uniformly over the surf zone.
- Moments of the velocity field relevant to energetics modelling of sand transport rates have been found to vary consistently with mean water depth and are relatively

insensitive to incident wave conditions. There is a dependence on mean water depth rather than a depth-scaled parameter, which requires further investigation. Nevertheless, the suggestion of consistent 'shape functions' for these transport-predicting moments should simplify modelling of sand transport on beaches.

- The terms dominating the bedload spatial shape function inside the surf zone are the skewness of the incident waves, the correlation between the incident wave field and a mean flow and the correlation between the infragravity wave field and a mean flow. Outside the surf zone, the most important bedload shape functions are the skewness of the incident waves, the coupling between incident waves and the mean field, in addition to the contribution of the wave envelope/ long wave coupling term. The suspended load shape functions are described by three terms which comprise mean flow, infragravity and gravity components coupled with the short wave oscillatory skewness parameter.
- Comparison of the suspended sand transport moment predictors with observed sand fluxes reveals that the predictors can provide transport estimates **accurate** in sign for the short wave, long wave and mean flow components for inside and outside the surf zone during the flood stage of the tide, but **inaccurate** in their relative magnitudes. Similarly, the moment predictors can provide transport estimates **accurate** in relative magnitude for the three transport components both inside and outside the surf zone during the ebb part of the tidal cycle, but **inaccurate** for the sign of the short wave contribution. The noticeable asymmetry observed between the flood and ebb stages of the tidal cycle may be a contributory factor to the differences which exist between velocity moment predictions and sand flux observations. The results suggest that the best physically-based energetics models do not accurately predict the conditions which exist on the macro-tidal beach examined at Spurn Head.

8.4 FUTURE RESEARCH

A natural extension to the groupiness and cross-correlation work would be the examination of the incoming and outgoing components of the bound long wave

component. The separation of long waves into onshore and offshore components would show the transformation of the bound long wave.

Since the velocity moment analysis, and sediment flux work has concentrated on the cross-shore aspect of nearshore sediment transport, it would be advantageous to examine the role played by the longshore current in the energetics-based predictors, and the net sand transport rates. Spurn Head is a sand spit characterised by longshore drift it follows, therefore, that examination of the longshore component of sand transport would complement the information provided by this cross-shore sand transport study. According to the study by Davidson *et al.* (1993) this can be achieved by determination of the mean longshore component of transport which dominates the total longshore transport component throughout the tidal cycle. In addition, the examination of both cross- and longshore measurements from different positions across the beach profile and at a number of heights above the seabed, would reveal horizontal and vertical distributions in the dominant processes driving sediment transport.

Comparison of the results discussed here, with measurements from other macro-tidal beach environments would help validate the applicability of the velocity-based predictors of cross-shore sand transport. Similarly, the study of the bedforms over different tidal cycles and for different incident wave conditions would also be very helpful, along with the development of transport predictors appropriate to the different bedform conditions. If these findings prove, to some extent, to have universal application to other coastal environments, then a set of realistic parameterisations would be available for modelling cross-shore sand transport on macro-tidal beaches.

LIST OF REFERENCES

Abdelrahman, S. M. and Thornton, E. B., 1987. Changes in the short wave amplitude and wavenumber due to the presence of infragravity waves. *Proceedings of the Coastal Hydrodynamics Conference*, University of Delaware, 458-478.

Airy, G. B., 1845. Tides and waves. In: *Encyclopedia Metropolitana*, London, p289 (art. 192).

Al-Bakri, D., 1986. Provenance of the sediments in the Humber Estuary and the adjacent coasts, Eastern England. *Marine Geology*, **72**, 171-186.

Aubrey, D. G. and Trowbridge, J. H., 1985. Kinematic and dynamic estimates from electromagnetic current meter data. *Journal of Geophysical Research*, **90** (C5), 9137-9146.

Aubrey, D. G. and Trowbridge, J. H., 1988. Reply to Guza's comment on "Kinematic and dynamic estimates from electromagnetic current meter data" by D. G. Aubrey and J. H. Trowbridge. *Journal of Geophysical Research*, **93** (C2), 1344-1346.

Bagnold, R. A., 1954. Experiments on a gravity-free dispersion of large solid spheres in a Newtonian fluid under shear. *Proceedings of the Royal Society of London, Series A*, **225**, 49-63.

Bagnold, R. A., 1963. Mechanics of marine sedimentation. In : *The Sea, Ideas and Observations*, Volume 3, Wiley-Interscience Publishers, New York, **3**, 507-528.

Bagnold, R. A., 1966. An approach to the sediment transport problem from general physics. *U. S. Geological Survey Professional Paper*, **422-I**, 37pp.

Bailard, J. A., 1981. An energetics total load sediment transport model for a plane sloping beach . *Journal of Geophysical Research*, **86**, 10, 10938-10954.

Bailard, J. A., 1987. Surfzone wave velocity moments. *Proceedings of the Coastal Hydrodynamics Conference*, University of Delaware, 328-342.

Bailard, J. A. and Inman, D. L., 1981. An energetics bedload model for a plane sloping beach : local transport. *Journal of Geophysical Research*, **86 (C3)**, 2035-2043.

Bascom, W., 1964. *Waves and Beaches*. Doubleday Publishing Inc., New York, 267p.

Basinski, T., 1989. Field studies on sand movement in the coastal zone. *Institute of Hydroengineering Report*, Gdansk, 298pp.

Battjes, J. A., 1988. Surf-zone dynamics. *Annual Review of Fluid Mechanics*, **20**, 257-293.

Battjes, J. A. and Van Vledder, G. Ph., 1984. Verification of Kimura's theory for wave group statistics. *Proceedings of the 19th International Conference on Coastal Engineering, Houston*, 642-648.

Battjes, J. A. and Stive, M. J. F., 1985. Calibration and verification of a dissipation model for random breaking waves. *Journal of Geophysical Research*, **90**, 9159-9167.

Bauer, B. O. and Greenwood, B., 1990. Modification of a linear bar trough system by a standing edge wave. *Marine Geology*, **92**, 177-204.

Beach, R. A. and Sternberg, R. W., 1988. Suspended sediment transport in the surf

zone: Response to cross-shore infragravity motion. *Marine Geology*, **80**, 61-79.

Beach, R. A. and Sternberg, R. W., 1991. Infragravity driven suspended sediment transport in the swash, inner and outer-surf zone. *Proceedings of the Coastal Sediments '91 Conference*, Seattle, 114-128.

Beer, T., 1983. *Environmental Oceanography - An Introduction to the Behaviour of Coastal Waters*. Pergamon Press, Oxford, 262p.

Bowen, A. J., 1980a. A simple model of nearshore sedimentation : beach profiles and longshore bars. In : *The Coastline of Canada*. S. B. McCann, editor, Geological Survey of Canada, Ottawa, 1-11.

Bowen, A. J., 1980b. Nearshore velocity measurements and beach equilibrium. *Proceedings of the Canadian Coastal Conference*, Ottawa, 21-30.

Bowen, A. J. and Doering, J. C., 1984. Nearshore sediment transport: Estimates from detailed measurements of the nearshore velocity field. *Proceedings of the 19th International Conference on Coastal Engineering*, Hamburg, 1703-1714.

Bowen, A. J. and Guza, R. T., 1978. Edge waves and surf beat. *Journal of Geophysical Research*, **83** (C4), 1913-1920.

Bowen, A. J. and Holman, R. A., 1989. Shear instabilities of the mean longshore current 1. Theory. *Journal of Geophysical Research*, **94** (C12), 18023-18030.

Bowen, A. J. and Huntley, D. A., 1984. Waves, long waves and nearshore morphology. *Marine Geology*, **60**, 1-13.

Bowen, A. J. and Inman, D. L., 1966. Budget of littoral sands in the vicinity of Point Arguello, California. *U. S. Army Coastal Engineering Research Center Technical Memo.*, Tm-19.

Bowen, A. J. and Inman, D. L., 1969. Rip currents, 2, Laboratory and field observations. *Journal of Geophysical Research*, **74** (23), 5479-5490.

Bowen, A. J. and Inman, D. L., 1971. Edge waves and crescentic bars. *Journal of Geophysical Research*, **76** (36), 8662-8671.

Brenninkmeyer, B., 1976. In situ measurements of rapidly fluctuating, high sediment concentrations. *Marine Geology*, **20**, 117-128.

Brown, J., Colling, A., Park, D., Phillips, J., Rothery, D. and Wright, J., 1989. *Waves, Tides and Shallow-Water Processes*. Prepared by the Open University Course Team, Pergamon Press, Oxford, 171p.

Carrier, G. F. and Greenspan, H. P., 1958. Water waves of finite amplitude on a sloping beach. *Journal of Fluid Mechanics*, Vol. **4**, 97-109.

Carter, G. C. and Ferrie, J. F., 1979. A coherence and cross-spectral estimation program. In : *Programs for Digital Signal Processing*. Edited by the Digital Signal Processing Committee, I.E.E.E. Acoustics, Speech, and Signal Processing Society, New York, 2.3.1-2.3.18.

Chatfield, C., 1984. *The Analysis of Time Series : An Introduction* (Third Edition). Chapman and Hall, London, 268pp.

Church, J. C., Thornton, E. B. and Oltman-Shay, J., 1992. Mixing by shear instabilities of the longshore current. *Proceedings of the 23rd International Conference on Coastal Engineering*, Venice, 2999-3011.

Coastal Engineering Research Center (CERC), 1973. *Shore Protection Manual.* Three volumes. U. S. Army Corps of Engineers (editors), Fort Belvoir, Virginia.

Cooke, R. U. and Doornkamp, J. C., 1974. *Geomorphology in Environmental Management- An Introduction.* Clarendon Press, Oxford, 493p.

Cornaglia, P., 1889. On beaches. Reprinted in: *Beach Processes and Coastal Hydrodynamics.* J. S. Fisher and R. Dolan (editors), 11-26.

Cornish, V., 1898. On sea beaches and sand banks. *Geology*, **2**, 628-674.

D & A Instruments and Engineering, 1988. *Optical Backscatterance Turbidity Monitor.* Instruction Manual, 32p.

Dally, W. R. and Dean, R. G., 1984. Suspended sediment transport and beach profile evolution. *Journal of Waterway, Port, Coastal and Ocean Engineering*, **110** (1), 15-33.

Davidson, M. A., 1990. *Field Investigations of Infragravity Oscillations on a High Energy Dissipative Beach (Llangenith, S. Wales, U.K.).* Unpublished PhD Thesis, University of Wales, 322pp.

Davidson, M. A., 1992. *Implementation of Linear Wave Theory in the Frequency Domain for the Conversion of Sea Bed Pressure to Surface Elevation.* School of Civil and Structural Engineering Internal Report No. 92/008, University of Plymouth, 19p.

Davidson, M. A., Russell, P. E., Huntley, D. A. and Hardisty, J., 1993. Tidal asymmetry in suspended sand transport on a macrotidal intermediate beach. *Marine Geology*, **110**, 333-353.

Dean, R. G., 1974. Evaluation and Development of Water Wave Theories for Engineering Applications. Special Report , No. **1**, U. S. Army Corps of Engineers.

Dean, R. G. and Dalrymple, R. A., 1984. *Water Wave Mechanics for Engineers and Scientists.* Prentice-Hall Inc., New Jersey, 353p.

De Boer, G., 1963. Spurn Point and its predecessors. *The Naturalist*, p113.

De Boer, G., 1964. Spurn Head: Its history and evolution. *The Institute of British Geographers (Transactions and papers)*, **34**, 71-86.

De Boer, G., 1967. Cycles of change at Spurn Head, Yorkshire, England. *Shore and Beach*, **35**, 13-20.

De Boer, G., 1973. Land created by the sea. *Geographical Magazine*, **45**, 377-382.

Doering, J. R. C., 1988. *Wave-Wave Interactions in the Nearshore.* Unpublished PhD Thesis, Dalhousie University, Halifax, Nova Scotia, 139p.

Doering, J. R. C. and Bowen, A. J., 1985. Skewness *et al.* the spatial distribution of the nearshore velocity field. *Proceedings of the Canadian Coastal Conference,* Ottawa Canada, 5-16.

Doering, J. C. and Bowen, A. J., 1987. Skewness in the nearshore zone: A comparison of estimates from Marsh-McBirney current meters and colocated pressure sensors. *Journal of Geophysical Research*, **92**, 13173-13183.

Doering, J. R. C. and Bowen, A. J., 1988. Wave-induced flow and nearshore suspended sediment. *Proceedings of the 21st International Conference on Coastal Engineering*, Malaga, 1452-1463.

Downing, J. P., Sternberg, R. W. and Lister, C. R. B., 1981. New instrumentation for the investigation of sediment suspension processes in the shallow marine environment. *Marine Geology*, **42**, 19-34.

Duxbury, A. C. and Duxbury, A. B., 1991. *An Introduction to the World's Oceans*. Third Edition. Wm. C. Brown Publishers, 446p.

Eckart, C., 1951. Surface waves on water of variable depth. *Wave Report*, **100**, Scripps Institute of Oceanography, University of California, La Jolla, 99p.

Einstein, H. A., 1972. A basic description of sediment transport on beaches. In: *Waves on Beaches and Resulting Sediment Transport*, R. E. Meyer (editor), Academic Press, New York, 462p.

Elgar, S., Freilich, M. H. and Guza, R. T., 1990. Model-data comparisons of moments of nonbreaking shoaling surface gravity waves. *Journal of Geophysical Research*, **95** (C9), 16055-16063.

Elgar, S. and Guza, R. T., 1985. Observations of bispectra of shoaling surface gravity waves. *Journal of Fluid Mechanics*, **161**, 425-448.

Elgar, S., Guza, R. T. and Seymour, R. J., 1984a. Groups of waves in shallow water. *Journal of Geophysical Research*, **89** (C3), 3623-3634.

Elgar, S., Guza, R. T. and Seymour, R. J., 1984b. Prediction of wave group statistics. *Proceedings of the 19th International Conference on Coastal Engineering*, Houston, 770-781.

Elgar, S., Herbers, T. H. C., Okihiro, M., Oltman-Shay, J. and Guza, R. T., 1992. Observations of infragravity waves. *Journal of Geophysical Research*, **97** (C10), 15573-15577.

Foote, Y. L. M. and Huntley, D. A., 1994. Velocity moments on a macro-tidal intermediate beach: Implications for cross-shore sediment transport modelling. *Proceedings of the Coastal Sediments '94 Conference*, Barcelona, (in prep.).

Foote, Y., Huntley, D., Davidson, M., Russell, P, Hardisty, J. and Cramp, A., 1992. Incident wave groups and long waves in the nearshore zone. *Proceedings of the 23rd International Conference on Coastal Engineering*, Venice, 974-989.

Foote, Y., Huntley, D. A. and O'Hare, T., 1993. Sand transport on macrotidal beaches. *Proceedings of the Euromech Conference*, Le Havre, (in press).

Funke, E. R. and Mansard, E. P. D., 1979. *On the Synthesis of Realistic Sea States in a Laboratory Flume*. Natural Research Council of Canada, Hydraulics Laboratory Technical Report No. LTR-HY-66.

Gallagher, B., 1971. Generation of surf beat by non-linear wave interactions. *Journal of Fluid Mechanics*, **49** (1), 1-20.

Gallagher, E. L. and Seymour, R. J., 1992. Oscillatory bedload transport studies by imaging of tracers. *Proceedings of the 23rd International Conference on Coastal Engineering*, Venice, 2084-2094.

Galvin, C. J., 1968. Breaker type classification on three laboratory beaches. *Journal of Geophysical Research*, **73**, 3651-3659.

Goda, Y., 1970. Numerical experiments on wave statistics with spectral simulation. *Report of the Port and Harbour Research Institute*, **9** (3), 3-57.

Goda, Y., 1976. On wave groups. *Proceedings of the International Conference on Behaviour of Offshore Structures*, 115-128.

Green, M. O. and Boon, J. D., 1993. The measurement of constituent concentrations in nonhomogeneous sediment suspensions using optical backscatter sensors. *Marine Geology*, **110**, 73-81.

Greenwood, B. and Osborne, P. D., 1990. Vertical and horizontal structure in cross-shore flows: An example of undertow and wave set-up on a barred beach. *Coastal Engineering*, **14**, 543-580.

Greenwood, B. and Osborne, P. D., 1991. Equilibrium and cross-shore velocity asymmetries in a storm-dominated, barred nearshore system. *Marine Geology*, **96**, 211-235.

Greenwood, B., Osborne, P. D., Bowen, A. J., Hazen, D. G. and Hay, A. E., 1990. C-COAST: The Canadian Coastal Sediment Transport Programme: Suspended sediment transport under waves and currents. *Proceedings of the Canadian Coastal Conference*, Ottawa, Canada, 319-336.

Greenwood, B. and Sherman, D. J., 1984. Waves, currents, sediment flux and morphological response in a barred nearshore system. *Marine Geology*, **60**, 31-61.

Guza, R. T., 1988. Comment on "Kinematic and dynamic estimates from electro-magnetic current meter data" by D. G. Aubrey and J. H. Trowbridge. *Journal of Geophysical Research*, **93**, 1337-1343.

Guza, R. T. and Bowen, A. J., 1976. Finite amplitude edge waves. *Journal of Marine Research*, **34** (1), 269-293.

Guza, R. T. and Davis, R. E., 1974. Excitation of edge waves by waves incident on a beach. *Journal of Geophysical Research*, **79** (9), 1285-1291.

Guza, R. T. and Inman, D. L., 1975. Edge waves and beach cusps. *Journal of Geophysical Research*, **80**, 2997-3012.

Guza, R. T. and Thornton, E. B., 1980. Local and shoaled comparisons of sea surface elevations, pressures, and velocities. *Journal of Geophysical Research*, **85** (C3), 1524-1530.

Guza, R. T. and Thornton, E. B., 1982. Swash oscillations on a natural beach. *Journal of Geophysical Research*, **87** (C1), 483-491.

Guza, R. T. and Thornton, E. B., 1985a. Velocity moments in nearshore. *Journal of Waterway, Port, Coastal and Ocean Engineering*, **111**(2), 235-256.

Guza, R. T. and Thornton, E. B., 1985b. Observations of surf beat. *Journal of Geophysical Research*, **90** (C2), 3161-3172.

Guza, R. T., Thornton, E. B. and Holman, R. T., 1984. Swash on steep and shallow beaches. *Proceedings of the 19th International Conference on Coastal Engineering*, Houston, 708-723.

Hallermeier, R. J., 1982. Oscillatory bedload transport: Data review and simple formulation. *Continental Shelf Research*, **1**, 159-190.

Hamm, L., Madsen, P. A. and Peregrine, D. H., 1993. Wave transformation in the nearshore zone: A review. *Coastal Engineering*, Special Issue, **21**, 5-40.

Hanes, D. M., 1988. Intermittent sediment suspension and its implications to sand tracer dispersal in wave-dominated environments. *Marine Geology*, **81**, 175-183.

Hanes, D. M., 1990. The structure of events of intermittent suspension of sand due to shoaling waves. In: *The Sea : Ocean Engineering Science*, **9**, 941-952.

Hanes, D. M. and Huntley, D. A., 1986. Continuous measurements of suspended sand concentration in a wave dominated nearshore environment. *Coastal Shelf Research*, **6** (4), 585-596.

Hanes, D. M., Vincent, C. E., Huntley, D. A. and Clarke, T. L., 1988. Acoustic measurements of suspended sand concentration in the C^2S^2 experiment at Stanhope Lane, Prince Edward Island. *Marine Geology*, **81**, 185-196.

Hardisty, J., 1987. Higher frequency acoustic measurements of swash processes. *Physical Geography*, **8**, 169-178.

Hardisty, J., 1989. Laboratory and site measurements of nearbed currents and sediment movement beneath waves: A spectral approach. *Advances in Water Modelling and Measurement*, BHRA (Information Services), The Fluid Engineering Centre, Cranfield, 271-289.

Hoad, J., 1991. Monitoring of the response of the inter-tidal beach profile to tidal and wave forcing. *Proceedings of the Coastal Sediments '91 Conference*, Seattle, 385-395.

Holman, R. A., 1981. Infragravity energy in the surf zone. *Journal of Geophysical Research*, **86** (C7), 6442-6450.

Holman, R. A., 1983. Edge waves and the configuration at the shoreline. In: *CRC Handbook of Coastal Processes and Erosion*, P.D. Komar (editor), CRC Press, Inc., Florida, 21-33.

Holman, R. A. and Bowen, A. J., 1982. Bars, bumps, and holes: models for the generation of complex topography. *Journal of Geophysical Research*, **87** (C1), 457-468.

Holman, R. A. and Guza, R. T., 1984. Measuring run-up on a natural beach. *Coastal Engineering*, **8**, 129-140.

Holman, R. A., Huntley, D. A. and Bowen, A. J., 1978. Infragravity waves in storm conditions. *Proceedings of the 16th International Conference on Coastal Engineering*, Hamburg, 268-284.

Holman, R. A. and Sallenger, A. H., 1985. Setup and swash on a natural beach. *Journal of Geophysical Research*, **90** (C1), 945-953.

Holman, R. A. and Sallenger, A. H., 1986. High-energy nearshore processes. *Eos Transactions*, Vol. **67** (49), 1369-1371.

Hom-ma, M. and Horikawa, K., 1963. A laboratory study on suspended sediment due to wave action. *Proceedings of the 10th Congress IAHR*, London, 213-220.

Horikawa, K., 1978. *Coastal Engineering - An Introduction to Ocean Engineering*, University of Tokyo Press.

Howd, P., Bowen, A., Holman, R. and Oltman-Shay, J., 1991. Infragravity waves, longshore currents, and linear sand bar formation. *Proceedings of the Coastal Sediments '91 Conference*, Seattle, 72-83.

Howd, P. A., Bowen, A. J. and Holman, R. A., 1992. Edge waves in the presence of strong longshore currents. *Journal of Geophysical Research*, **97** (C7), 11357-11371.

Huntley, D. A., 1976. Long-period waves on a natural beach. *Journal of Geophysical Research*, **81** (36), 6441-6449.

Huntley, D. A., 1988. Evidence for phase coupling between edge wave modes. *Journal of Geophysical Research*, **93** (C10), 12393-12408.

Huntley, D. A. and Bowen, A. J., 1973. Field observations of edge waves. *Nature*, Vol. **243**, 160-161.

Huntley, D. A. and Bowen, A. J., 1975a. Field observations of edge waves and their effect on beach material. *Journal of the Geological Society*, **131** (68), 69-81.

Huntley, D. A. and Bowen, A. J., 1975b. Comparison of the hydrodynamics of steep and shallow beaches. In: *Nearshore Sediment Dynamics and Sedimentation - An Interdisciplinary Review*. J. Hail and A. Carr (editors), 69-108.

Huntley, D. A., Davidson, M., Russell, P., Foote, Y. and Hardisty, J., 1993. Long waves and sediment movement on beaches: Recent observations and implications for modelling. *Journal of Coastal Research*, Special Issue No. **15**, 215-229.

Huntley, D. A., Guza, R. T. and Bowen, A. J., 1977. A universal form for shoreline run-up spectra? *Journal of Geophysical Research*, **82** (18), 2577-2581.

Huntley, D. A., Guza, R. T. and Thornton, E. B., 1981. Field observations of surf beat, 1. Progressive edge waves. *Journal of Geophysical Research*, **86** (C7), 6451-6466.

Huntley, D. A. and Hanes, D. M., 1987. Direct measurements of suspended sediment transport. *Proceedings of the Coastal Sediments '87 Conference*, New Orleans,723-737.

Huntley, D. H. and Kim, C-S., 1984. Is surf beat forced or free? *Proceedings of the 19th International Conference on Coastal Engineering*, Houston, 1659-1676.

Inman, D. L. and Bagnold, R. A., 1963. Littoral processes. In : *The Sea*, Volume 3, Wiley-Interscience Publishers, New York, **3**, 529-533.

Inman, D. L. and Bowen, A. J., 1963. Flume experiments on sand transport by waves and currents. *Proceedings of the 8th International Conference on Coastal Engineering*, Mexico City, 137-150.

Inman, D. L. and Frautschy, J. D., 1966. Littoral processes and the development of shorelines. *Proceedings of the 10th International Conference on Coastal Engineering*, California, 511-536.

Inman, D. L. and Tunstall, E. B., 1972. Phase dependent roughness control of sand movement. *Proceedings of the 13th International Conference on Coastal Engineering*, Vancouver, 1155-1171.

Jaffe, B. E., Sternberg, R. W. and Sallenger, A. H., 1984. The role of suspended sediment in shore-normal beach profile changes. *Proceedings of the 19th International Conference on Coastal Engineering*, Houston, 1983-1996.

Jenkins, G. M. and Watts, D. G., 1968. *Spectral Analysis and Its Applications*. Holden-Day, San Francisco, 525p.

Johnson, R. R., Mansard, E. P. D. and Ploeg, J., 1978. Effects of wave grouping on breakwater stability. *Proceedings of the 16th International Conference on Coastal*

Engineering, Hamburg, 2228-2243.

Jonsson, I. G., 1966. Wave boundary layer and friction factors. *Proceedings of the 10th International Conference on Coastal Engineering*, California, 127-148.

Kaiser, J. F. and Reed, W. A., 1977. Data smoothing using low-pass filters. *Review of Scientific Instrumentation*, **48**, 1447-1457.

Katoh, K., 1981. Analysis of edge waves by means of empirical eigenfunctions. *Report of the Port and Harbour Research Institute*, **20** (3), Japanese Ministry of Transport, 3p.

Keller, J. B., 1963. Tsunamis - water waves produced by earthquakes. *Int. Union Geod. Geophy. Monogr.*, **24**, Tsunami Hydrodynamics Conference, Honolulu, 154-166.

Kim, C-S., 1985. *Field Observations of Wave Groups and Long Waves on Sloping Beaches.* Unpublished M.Sc. Thesis, Dalhousie University, Halifax, 151p.

Kimura, A., 1980. Statistical properties of random wave groups. *Proceedings of the 17th International Conference on Coastal Engineering*, Sydney, 2955-2973.

King, D. B., 1991. The effect of beach slope on oscillatory flow bedload transport. *Proceedings of the Coastal Sediments '91 Conference*, Seattle, 734-744.

King, D. B., Powell, J. and Seymour, R. J., 1984. A new oscillatory flow tunnel for use in sediment transport experiments. *Proceedings of the 19th International Conference on Coastal Engineering*, Houston, 1559-1570.

Kobayashi, N., 1982. Sediment transport on a gentle slope due to waves. *Journal of Waterway, Port, Coastal and Ocean Division*, **108** (WW3), 254-271.

Kobayashi, N., 1988. Review of wave transformation and cross-shore sediment transport processes in surf zones. *Journal of Coastal Research*, **4** (3), 435-445.

Komar, P. D., 1971. The mechanics of sand transport on beaches. *Journal of Geophysical Research*, **76**, 713-721.

Komar, P. D., 1976. *Beach Processes and Sedimentation.* Prentice-Hall, New Jersey, 429p.

Komar, P. D., 1983. Beach processes and erosion - An introduction. In: *CRC Handbook of Coastal Processes and Erosion.* P. D. Komar (editor), CRC Press Inc., Florida, 1-19.

Kostense, J. K., 1984. Measurements of surf beat and set-down beneath wave groups. *Proceedings of the 19th International Conference on Coastal Engineering*, Houston, 724-739.

Kraus, N. C. and Horikawa, K., 1990. Nearshore sediment transport. In: *The Sea*, Volume **9**, B. Le Mehaute and D. M. Hanes (editors), Wiley-Interscience, New York, 775-813.

Larsen, L. H., 1982. A new mechanism for seaward dispersion of midshelf sediments. *Sedimentology*, **29**, 279-284.

Lau, J. and Travis, B., 1973. Slowly varying Stokes waves and submarine longshore bars. *Journal of Geophysical Research*, **78** (21), 4489-4497.

List, J. H., 1986. Wave groupiness as a source of nearshore long waves. *Proceedings of the 20th International Conference on Coastal Engineering*, Taipei, 497-511.

List, J. H., 1991. Wave groupiness variations in the nearshore. *Coastal Engineering*, **15**, 475-496.

List, J. H., 1992a. A model for the generation of two-dimensional surf beat, *Journal of Geophysical Research*, **97** (C4), 5623-5635.

List, J. H., 1992b. Breakpoint-forced and bound long waves in the nearshore: A model comparison. *Proceedings of the 23rd International Conference on Coastal Engineering*, Venice, 860-873.

Longuet-Higgins, M. S. and Stewart, R.W., 1962. Radiation stress and mass transport in gravity waves, with application to 'surf-beats'. *Journal of Fluid Mechanics*, **13**, 481-504.

Longuet-Higgins, M. S. and Stewart, R. W., 1964. Radiation stress in water waves : a physical discussion, with applications. *Deep Sea Research*, **11**, 529-562.

Madsen, O. S. and Grant, W. D., 1976. Quantitative description of sediment transport by waves. *Proceedings of the 15th International Conference on Coastal Engineering*, Honolulu, 1093-1112.

Mase, H., 1989. Groupiness factor and wave height distribution. *Journal of Waterway, Port, Coastal and Ocean Engineering*, **115**, 105-121.

Mason, S. J., 1985. *Beach Development, Sediment Budget and Coastal Erosion at Holderness*. Unpublished PhD Thesis, University of Sheffield.

Mason, S. J. and Hansom, J. B., 1988. Cliff erosion and its contribution to a sediment budget for part of the Holderness Coast, England. *Shore and Beach*, **56** (4), 30-38.

Mason, S. J. and Hansom, J. B., 1989. A Markov model for beach changes on the Holderness coast of England. *Earth Surface Processes and Landforms*, **14**, 731-743.

Masselink, G. and Short, A. D., 1993. The effect of tide range on beach morphodynamics and morphology: A conceptual beach model. *Journal of Coastal Research*, **9** (3), 785-800.

Medina, J. R. and Hudspeth, R. T., 1990. A review of the analyses of ocean wave groups. *Coastal Engineering*, **14**, 515-542.

Miche, R., 1944. Mouvements ondulatoires de la mer en profondeur constante ou décroissante. *Ann. Ponts Chaussées*, **114**.

Mizuguchi, M., 1987. Experimental study on kinematics and dynamics of wave breaking. *Proceedings of the 20th International Conference on Coastal Engineering*, Taipei, 589-603.

Munk, W. H., 1949. Surf beats. *Eos Transactions*, American Geophysical Union, **30**, 849-854.

Munk, W. H. and Wimbush, M., 1969. A rule of thumb for wave breaking over sloping beaches. *Oceanology*, **6**, 56-59.

Munk, W. H., Snodgrass, F. E. and Gilbert, F., 1964. Long waves on the continental shelf and experiments to separate trapped and leaky modes. *Journal of Fluid Mechanics*, **20**, 529-554.

Nearshore Processes Workshop, 1990. *Report on the State of Nearshore Processes Research*, Report No. OSU-CO-90-6, Oregon State University, 25p.

Nielsen, P., 1979. Some basic concepts of wave sediment transport. *Series Paper 20*, Technical University of Denmark.

Nielsen, P., 1988. Three simple models of wave sediment transport. *Coastal Engineering*, **12**, 43-62.

Nielsen, P., Svendsen, I. A. and Staub, C., 1978. Onshore-offshore sediment movement on a beach. *Proceedings of the 16th International Conference on Coastal Engineering*, Hamburg, 1475-1492.

Nuttal, A. H., 1971. *Spectral Estimation by Means of Overlapped Fast Fourier Transforms of Windowed Data.* NUSC Report, No. **4169**, Department of Navy, USA.

O'Hare, T. J. and Huntley, D. A., 1994. Bar formation due to wave groups and associated long waves. *Marine Geology* (in press).

Okihiro, M., Guza, R. T. and Seymour, R. J., 1992. Bound infragravity waves. *Journal of Geophysical Research*, **97** (C7), 11453-11469.

Oltman-Shay, J. and Guza, R. T., 1987. Infragravity edge wave observations on two Californian beaches. *Journal of Physical Oceanography*, **17**, 644-663.

Oltman-Shay, J. and Howd, P. A., 1993. Edge waves on nonplanar bathymetry and alongshore currents: a model and data comparison. *Journal of Geophysical Research*, **98** (C2), 2495-2507.

Oltman-Shay, J., Howd, P. A. and Birkemeier, W. A., 1989. Shear instabilities of the mean longshore current 2. Field observations. *Journal of Geophysical Research*, **94** (C12), 18031-18042.

Osborne, P. D., 1990. *Suspended Sediment Transport on Barred and Non-barred Beaches.* Unpublished PhD Thesis, University of Toronto, Canada, 196pp.

Osborne, P. D. and Greenwood, B., 1992a. Frequency dependent cross-shore suspended sediment transport. 1. A non-barred shoreface. *Marine Geology*, **106**, 1-24.

Osborne, P. D. and Greenwood, B., 1992b. Frequency dependent cross-shore suspended sediment transport. 1. A barred shoreface. *Marine Geology*, **106**, 25-51.

Osborne, P. D., Greenwood, B. and Bowen, A. J., 1990. Cross-shore suspended sediment transport on a non-barred beach: The role of wind waves, infragravity waves and mean flows. *Proceedings of the Canadian Coastal Conference*, Ottawa, Canada, 349-361.

Otnes, R. K. and Enochson, L., 1972. *Digital Time Series Analysis.* John Wiley and Sons, New York, 467p.

Ottesen Hansen, N-E., 1978. Long period waves in natural wave trains. *Progress Report* **46**, Institute Hydrodync. Hydr. Engng. (ISVA), Technical University of Denmark, 13-24..

Peregrine, D. H., 1983. Breaking waves on beaches. *Annual Review of Fluid Mechanics*, **15**, 149-178.

Pethick, J., 1992. Wave goodbye to Spurn Head. Article written by Corin Hughes Stanton for *New Civil Engineer* (20 February, 1992), 24-25.

Phillips, A. W., 1963. Tracer experiments at Spurn Head, Yorkshire, England. *Shore and Beach*, **31**, 30-35.

Press, F. and Siever, R., 1986. *Earth.* Fourth Edition. W. H. Freeman and Company, New York, 656p.

Priestley, M. B., 1981. *Spectral Analysis and Time Series* (Volumes 1 and 2). Academic Press, London, 890p.

Pringle, A. W., 1985. Holderness coast erosion and the significance of ords. *Earth Surface Processes and Landforms*, **10**, 107-124.

Putrevu, U. and Svendsen, I. A., 1992. Shear instabilities of longshore currents: A numerical study. *Journal of Geophysical Research*, **97** (C5), 7283-7303.

Roelvink, J. A., 1991. Modelling of cross-shore flow and morphology. *Proceedings of the Coastal Sediments '91 Conference*, Seattle, 603-617.

Roelvink, J. A., 1993. *Surf Beat and Its Effect on Cross-shore Profiles.* Delft Hydraulics, Netherlands, 116p.

Roelvink, J. A. and Stive, M. J. F., 1989. Bar-generating cross-shore flow mechanisms on a beach. *Journal of Geophysical Research*, **94**, 4785-4800.

Russell, P. E., 1990. *Field Studies of Suspended Sand Transport on a High Energy Dissipative Beach.* Unpublished Ph.D. Thesis, University of Wales, 318pp.

Russell, P. E., 1993. Mechanisms for beach erosion during storms. *Continental Shelf Research*, **13** (11), 1243-1265.

Russell, P. E., 1994. Simple modelling of sediment suspension processes on natural beaches, (in prep.).

Russell, P., Davidson, M., Huntley, D., Cramp, A., Hardisty, J. and Lloyd, G., 1991. The British Beach And Nearshore Dynamics (B-BAND) programme. *Proceedings of the Coastal Sediments '91 Conference*, Seattle, 371-383.

Rye, H., 1974. Wave group formation among storm waves. *Proceedings of the 15th International Conference on Coastal Engineering*, Honolulu, 164-183.

Sand, S. E., 1982. Wave grouping described by bounded long waves. *Ocean Engineering*, **9**, 567-580.

Sato, S., 1992. Sand transport under grouping waves. *Proceedings of the 23rd International Conference on Coastal Engineering*, Venice, 2411-2425.

Schäffer, H. A., 1993. Infragravity waves induced by short wave groups. *Journal of Fluid Mechanics*, **247**, 551-588.

Schäffer, H. A. and Svendsen, I. A., 1988. Surf beat generation on a mild-slope beach. *Proceedings of the 21st International Conference on Coastal Engineering*, Malaga, 1058-1072.

Shepard, F. P., 1973. *Submarine Geology.* Third Edition. Harper and Row, New York, 517p.

Shi, N. C. and Larsen, L. H., 1984. Reverse sediment transport induced by amplitude modulated waves. *Marine Geology*, **54**, 181-200.

Short, A. D., 1975. Multiple offshore bars and standing waves. *Journal of Geophysical Research*, **80** (27), 3838-3840.

Short, A. D., 1978. Wave power and beach stages: A global model. *Proceedings of*

the 16th International Conference on Coastal Engineering, Hamburg, 1145-1162.

Short, A. D., 1991. Macro-meso tidal beach morphodynamics - An overview. *Journal of Coastal Research*, **7** (2), 417-436.

Skovgaard, O., Svendsen, I. A., Jonsson, I. G. and Brink-Kjœr, O., 1974. *Sinusoidal and Cnoidal Gravity Waves Formulae and Tables*. Institute of Hydrodynamics and Hydraulic Engineering (ISVA), Technical University of Denmark, Lyngby, Denmark, 8pp.

Snodgrass, F. E., Munk, W. H. and Miller, G. R., 1962. Long-period waves over California's continental borderland. Part 1. Background spectra. *Journal of Marine Research*, **20**, 3-30.

Sobey, R. J. and Liang, H-B., 1986. Complex envelope identification of wave groups. *Proceedings of the 20th International Conference on Coastal Engineering*, Taipei, 752-766.

Sonu, C. J., 1972. Field observation of nearshore circulation and meandering currents. *Journal of Geophysical Research*, **77**, 3232-3247.

Sonu, C. J., 1973. Three-dimensional beach changes. *Journal of Geology*, **81**, 42-64.

Sternberg, R. W., Shi, N. C. and Downing, J. P., 1984. Field investigations of suspended sediment transport in the nearshore zone. *Proceedings of the 19th International Conference on Coastal Engineering*, Houston, 1782-1797.

Sternberg, R. W., Kineke, G. C. and Johnson, R., 1990. An instrument for profiling suspended sediment, fluid, and flow conditions in shallow marine environments. *Continental Shelf Research*, **11** (2), 109-122.

Stokes, G. G., 1847. On the theory of oscillatory waves. *Transactions of the Cambridge Philosophical Society*, **8**, 441-473.

Suhayda, J. N., 1974. Standing waves on beaches. *Journal of Geophysical Research*, **79** (21), 3065-3071.

Svendsen, I. A. and Jonsson, I. G., 1980. *Hydrodynamics of Coastal Regions*. Published by Den Private Ingeniørfond, Technical University of Denmark, Lyngby, 285p.

Symonds, G., Huntley, D. A. and Bowen, A. J., 1982. Two-dimensional surf beat: Long wave generation by a time-varying breakpoint. *Journal of Geophysical Research*, **87** (C1), 492-498.

Tang, E. C-S. and Dalrymple, R. A., 1989. Rip currents, nearshore circulation and wave groups. In: *Nearshore Sediment Transport*. R. J. Seymour (editor), Plenum Press, New York, 205-230.

Tatavarti, R. V. S. N., 1989. *The Reflection of Waves on Natural Beaches*. Unpublished PhD Thesis, Dalhousie University, Halifax, Nova Scotia, 175p.

Tatavarti, R. V. S. N., Bowen, A. J. and Huntley, 1988. Incoming and outgoing wave interactions on beaches. *Proceedings of the 21st International Conference on Coastal Engineering*, Malaga, 136-150.

Thorne, P. D., Vincent, C. E., Hardcastle, P. J., Rehman, S. and Pearson, N., 1991. Measuring suspended sediment concentrations using acoustic backscatter devices. *Marine Geology*, **98**, 7-16.

Thorne, P. D., Hardcastle, P.J. and Soulsby, R. L., 1993. Analysis of acoustic measurements of suspended sediments. *Journal of Geophysical Research*, **98** (C1), 899-910.

Thornton, E. B., 1977. Suspended sediments measured within the surf zone. *Proceedings of the Coastal Sediments '77 Conference*, Charleston, 655-668.

Tucker, M. J., 1950. Surf beats: Sea waves of 1 to 5 min. period. *Proceedings of the Royal Society, Series A*, **202**, 565-573.

Ursell, F., 1952. Edge waves on a sloping beach. *Proceedings of the Royal Society of London, Series A*, **214**, 79-97.

Valentin, H., 1954. Der landverlust in Holderness, Ostengland, von 1852 bis 1952. *Die Erde, Berl.*, **6** (3-4), 295-315.

Vincent, C. E., Hanes, D. M. and Bowen, A. J., 1991. Acoustic measurements of suspended sand on the shoreface and the control of concentration by bed roughness. *Marine Geology*, **96**, 1-18.

Vincent, C. E. and Osborne, P. D., 1993. Bedform dimensions and migration rates under shoaling and breaking waves. *Continental Shelf Research*, **13** (11), 1267-1280.

Watson, G. and Peregrine, D. H., 1992. Low frequency waves in the surf zone. *Paper prepared for the 23rd International Conference on Coastal Engineering, Report No. AM-92-11*, University of Bristol, 14p.

Whitehouse, R. J. S. and Hardisty, J., 1988. Experimental assessment of two theories for the effect of bedslope on the threshold of bedload transport. *Marine Geology*, **79**, 135-139.

Winkelmolen, A. M., 1978. Size, shape and density sorting of beach material along the Holderness coast, Yorkshire. *Proceedings of the Yorkshire Geological Society*, **42**, Part 1, No. 6, 109-141.

Wright, L. D., Chappell, J., Thom, B. G., Bradshaw, M. P. and Cowell, P., 1979. Morphodynamics of reflective and dissipative beach and inshore systems: Southeastern Australia. *Marine Geology*, **32**, 105-140.

Wright, L. D., Nielsen, P., Short, A. D. and Green, M. O., 1982. Morphodynamics of a macrotidal beach. *Marine Geology*, **50**, 97-128.

Wright, L. D. and Short, A. D., 1983. Morphodynamics of beaches and surf zones in Australia. In: *CRC Handbook of Coastal Processes and Erosion.* P. D. Komar (editor), CRC Press Inc., Florida, 35-64.

Wright, L. D. and Short, A. D., 1984. Morphodynamic variability of surf zones and beaches: A synthesis. *Marine Geology*, **56**, 93-118.

Wright, L. D., Thom, B. G. and Chappell, J, 1978. Morphodynamic variability of high energy beaches. *Proceedings of the 16th International Conference on Coastal Engineering*, Hamburg, 1180-1194.

Yalin, M. S., 1977. *Mechanics of Sediment Transport.* Second edition. Pergamon Press, Oxford, 290p.

Yasuda, T., Nakashima, N. and Tsuchiya, Y., 1986. Grouping waves and their expression on asymptotic envelope soliton modes. *Proceedings of the 20th International Conference on Coastal Engineering*, Taipei, 864-876.

APPENDIX I

INSTRUMENT DEVELOPMENT COMPANIES

Colnbrook Instrument Development Ltd.,
Poyle Road,
Colnbrook,
Buckinghamshire.

D & A Instruments and
Engineering,
2428 39th Street, N. W.
Washington,
D. C. 20007, USA.

Sensor Technics,
30, Regent Place,
Rugby,
Warwickshire,
CV21 2PN

Valeport Marine Scientific Ltd.,
Unit 7,
Townstal Industrial Estate,
Dartmouth,
Devon,
TQ6 9LX.

APPENDIX II

```
**********************************************************************
**********************************************************************

RINT ver 1.2   Pathname: <STUD3C>R00815>SPURN>SUBROU.F77

**********************************************************************
**********************************************************************

 PROGRAM LOFILT
 DIMENSION BK(150),X(2048),XS(2048),FBK(300),T(2048),Y(2048)
 WRITE (*,*)'INPUT STOPBAND LOSS,dB'
 READ (*,*) AL
 WRITE (*,*)'INPUT RELATIVE LOCATION OF PASSBAND EDGE'
 READ (*,*) BE
 WRITE (*,*) 'INPUT RELATIVE WIDTH OF PASSBAND'
 READ (*,*) DE
 CALL NER (AL,BE,DE,NP,BK)
 DO 20 I=1,NP
) WRITE (*,10) I,BK(I)
) FORMAT (I5,F10.4)
 OPEN (9,FILE='PT1825A2LS.DAT',STATUS='OLD')
 OPEN (11,FILE='LP1825A2PT.DAT',STATUS='NEW')
 OPEN (12,FILE='HP1825A2PT.DAT',STATUS='NEW')
 DO 6 I=1,2048
5 READ (9,*) T(I),X(I)
 FBK (NP)=BK(1)
 DO 30 J=2,NP
 FBK (NP+J-1)=BK(J)
) FBK (NP-J+1)=BK(J)
 NPP=(2*NP)-1
 NMAX=2048-NPP
 DO 50 J=1,NMAX
 XS(J)=0.0
 DO 40 I=1,NPP
 NN=J+I-1
) XS(J)=X(NN)*FBK(I)+XS(J)
 Y(J)=X(J+NP-1)-XS(J)
 WRITE(11,*)T(J),XS(J)
 WRITE(12,*)T(J),Y(J)
 CONTINUE
 STOP
 END


 SUBROUTINE NER (AL,BE,DE,NP,BK)
ROUTINE COMPUTES THE COEFFICIENTS
A NEARLY EQUIRIPPLE LINEAR PHASE
OTHING FILTER WITH AN ODD NUMBER
P+1) OF TERMS AND EVEN SYMMETRY
UT : AL = STOPBAND LOSS IN dB (LAMBDA)
= RELATIVE LOCATION OF IDEAL EDGE OF PASSBAND (BETA)
= RELATIVE WIDTH OF TRANSITION BAND (DELTA)
PUT : NP = NUMBER OF FILTER COEFFICIENT PAIRS (K=0,1,2,...NP)
= ARRAY OF FILTER COEFFICIENTS
(1) = B0,BK(2) = B1, BK(3) = B2,...
(NP+1) = BNP
AL SPAN OF FILTER IS 2*NP INTERVALS
 DIMENSION BK(150)
 PI = 3.141592654
 FK = 1.8445
 IF (AL.GE.21.)FK =0.13927*(AL-7.95)
 ET=0.58417*((AL-21.)**0.4)+0.07886*(AL-21.)
 IF(AL.LT.21.)ET=0
 IF(AL.GT.50.)ET=0.1102*(AL-8.7)
 NP=INT((FK/(2.*DE))+0.75)
T NP AGAINST DIMENSION LIMIT
 IF(NP.GT.149)NP=149
 FNP=NP
 GP=BE*PI
 CALL INO(ET,FIA)
 DO 10 K=1,NP
 FLK=REAL (2*K-1)/2.
```

```
GK=PI*REAL (K)
GE=ET*SQRT(1.-(REAL (K)/FNP)**2)
CALL INO(GE,E)
BK(K)=(SIN(BE*GK)/GK)*(E/FIA)
CONTINUE
BK(NP)=BK(NP)/2.
N=NP+1
DO 20 I=2,N
K=N-I+2
J=K-1
BK(K)=BK(J)
BK(1)=BE
RETURN
END


 SUBROUTINE INO (X,S)
'TINE EVALUATES THE MODIFIED BESSEL
(CTION OF ZEROTH ORDER AT REAL
.UES OF THE ARGUMENT
'UT : X
'PUT : S
 S=1.
 DS=1.
 D=0.
 D=D+2.
 DS=DS*X*X/(D*D)
 S=S+DS
 IF(DS.GT.0.2E-8*S) GOTO 1
 RETURN
 END
```